Simulation Methods for Reliability-Based Design Optimization and Model Updating of Civil Engineering Structures and Systems

Von der Fakultät für Bauingenieurwesen und Geodäsie

der Gottfried Wilhelm Leibniz Universität Hannover

zur Erlangung des Grades

Doktor der Ingenieurwissenschaften

Dr.-Ing.

genehmigte Dissertation

von

Danko José Jerez Urquieta, M.Sc.

Referent:	Prof. Dr.-Ing. Michael Beer
Korreferenten:	Prof. Dr. Costas Papadimitriou
	Prof. Dr.-Ing. Udo Nackenhorst
	Prof. Dr. sc. ETH Elyas Ghafoori
Tag der Promotion:	29. Juni 2023

Erklärung

Ich erkläre hiermit, dass die in dieser Dissertation vorgestellten Ergebnisse auf meiner eigenen Arbeit beruhen und dass ich keine Arbeiten andere Personen vorgelegt habe und dass ich in allen Fällen, in denen ich auf Arbeiten anderer Personen Bezug genommen habe, diese in vollem Umfang und in angemessener Weise angegeben habe.

Danko José Jerez Urquieta

Juni 2023

I dedicate this thesis to my parents, Paola and Abraham,

whose love and sacrifice have always given me strength,

and to my beloved wife, Jocelyn,

for her unfailing support during our journey

Acknowledgments

I would like to express my sincere gratitude to my supervisor and thesis committee chair, Prof. Michael Beer, for his insightful mentoring and support during my studies. I am especially grateful to him for giving me scientific freedom and for providing an excellent working environment.

This endeavor would not have been possible without the invaluable guidance and academic instruction of Prof. Hector Jensen. I am deeply indebted to him for the trust placed in me during all these years, and for his continuous encouragement and perspicacious advice. His motivation, wisdom, knowledge and expertise have been fundamental throughout my learning process.

I would like to extend my sincere thanks to Prof. Costas Papadimitriou, Prof. Udo Nackenhorst and Prof. Elyas Ghafoori for kindly agreeing to serve as members of my thesis defense committee.

I gratefully acknowledge the financial support of ANID (National Agency for Research and Development, Chile) and DAAD (German Agency for Academic Exchange, Germany) under CONICYT-PFCHA/Doctorado Acuerdo Bilateral DAAD Becas Chile/2018-62180007.

Special thanks go to Thomas, Vasilis and George for their kind assistance with the practical aspects of preparing this document.

I would be remiss in not mentioning my wife, Jocelyn, my parents, Abraham and Paola, my siblings, Millaray and Viktor, and my friends for their unwavering support and belief in me. Moreover, every single step in my life finds its foundations on the example set by my grandmother Sonia. May these words serve as a humble tribute to her memory, and to all those who illuminated my path but have already departed.

Shortcomings that remain in this thesis, of whatever kind, are mine alone.

Abstract

This thesis presents a collection of original contributions pertaining to the subjects of reliability-based design optimization (RBDO) and model updating of civil engineering structures and systems. In this regard, probability theory concepts and tools are instrumental in the formulation of the herein reported developments. Firstly, two approaches are devised for the RBDO of structural dynamical systems under stochastic excitation. Namely, a stochastic search technique is proposed for constrained and unconstrained RBDO problems involving continuous, discrete and mixed discrete-continuous design spaces, whereas an efficient sensitivity assessment framework for linear stochastic structures is implemented to identify optimal designs and evaluate their sensitivities. Moreover, two classes of model updating problems are considered. In this context, the Bayesian interpretation of probability theory plays a key role in the proposed solution schemes. Specifically, contaminant source detection in water distribution networks is addressed by resorting to a sampling-based Bayesian model class selection framework. Furthermore, an effective strategy for Bayesian model updating with structural reliability methods is presented to treat identification problems involving structural dynamical systems, measured response data, and high-dimensional parameter spaces. The approaches proposed in this thesis integrate stochastic simulation techniques as an essential part of their formulation, which allows obtaining non-trivial information about the systems of interest as a byproduct of the solution processes. Overall, the findings presented in this thesis suggest that the reported methods can be potentially adopted as supportive tools for a number of practical decision-making processes in civil engineering.

Keywords: Reliability-based design optimization; Bayesian model updating; Structural dynamics; Water distribution networks; Contaminant source detection; Advanced simulation methods

Kurzfassung

Diese Arbeit stellt eine Sammlung von Beiträgen vor, die sich mit der Reliability-based-Design-Optimization (RBDO) und dem Model updating von Strukturen und Systemen im Bauwesen befassen. In diesem Zusammenhang sind wahrscheinlichkeitstheoretische Konzepte für die Formulierung der hier vorgestellten Entwicklungen von entscheidender Bedeutung. Zunächst werden zwei Ansätze für eine RBDO von strukturdynamischen Systemen unter stochastischer Anregung entwickelt. Es wird eine stochastische Suchtechnik für beschränkte und unbeschränkte RBDO-Probleme vorgeschlagen. Diese beziehen kontinuierliche, diskrete und gemischt diskret-kontinuierliche Designräume ein. Gleichzeitig wird ein effizientes Framework zur Bewertung der Sensitivität lineare stochastische Strukturen implementiert, um optimale Designs zu identifizieren und ihre Sensitivitäten zu bewerten. Darüber hinaus werden zwei Klassen von Problem aus dem Model updating betrachtet. Der Fokus wird hierbei auf die Erkennung von Kontaminationsquellen in Wasserverteilungsnetzen mithilfe eines auf Stichproben basierenden Bayesian-Model-Class-selection-Framework gelegt. Ferner wird eine effektive Strategie zur Bearbeitung von Problemen des Bayesian-Model-updating, die strukturdynamischen Systeme, gemessene Systemantwortdaten und hochdimensionale Parameterräume umfassen, vorgestellt. Die beschriebenen Ansätze verwenden stochastische Simulationstechniken als wesentlicher Bestandteil ihrer Formulierung, wodurch nicht-triviale Informationen über betrachtete Systeme als Nebenprodukt der Lösungsprozesse gewonnen werden können. Insgesamt deuten die vorgestellten Ergebnisse dieser Arbeit darauf hin, dass die beschriebenen Methoden potenziell als unterstützende Elemente in praktischen Entscheidungsproblemen im Zusammenhang mit Strukturen und Systemen im Bauwesen eingesetzt werden können.

Keywords: Reliability-based-Design-Optimization; Bayesian-Model-updating; Strukturdynamik; Wasserverteilungsnetze; Kontaminationsquellendetektion; Simulationsmethoden

Table of contents

List of Figures

Chapter 1
Introduction

1.1 Motivation

Civil engineering structures and systems are a crucial component of modern human environments. Bridges, water supply systems, tunnels, buildings, retaining walls, highways, sewage systems, dams, and a plethora of other complex and large-scale engineered systems constitute a fundamental part of the contemporary landscape and, furthermore, play an essential role in enabling societal and economic development. One of the distinctive features of this class of systems is their permanent exposure to natural and anthropogenic actions [1–5]. Thus, the conditions in which they operate and the state of their components are impossible to predict exactly, i.e., they are inherently subject to uncertainty. Such uncertainties must be appropriately considered not only to achieve cost-effective and safe designs but also for the repair, maintenance and enhancement of civil engineering structures and systems over their lifetime [6–10]. This is especially relevant considering the broad implications that the related decision-making processes have from social, economical, technical, and environmental perspectives [11–18].

Diverse uncertainty representation methods have been developed to aid general decision-making processes [19]. In the context of civil engineering, even though non-probabilistic methodologies have been proposed [20, 21], the prevalent uncertainty quantification approach corresponds to the use of probability theory concepts and tools [6, 22–26]. Within this framework, pertinent characteristics of the system of interest are modeled in a probabilistic manner. These comprise, for instance, mechanical properties [27–29], component states [30, 31], operational conditions [32, 33], external excitations [34–39], etc. Such a formulation enables, in turn, a variety of engineering analyses

including probabilistic performance evaluation [40–44], reliability assessment [45–48], stochastic response determination [49–51], probabilistic failure analysis [52], Bayesian model updating [53–57], optimal placement of measurement devices [58, 59], design optimization [60–64], sensitivity analysis [65–68], etc. In this regard, closed-form solutions and approximate analytical techniques can be applied with satisfactory accuracy in certain cases [6, 69–79]. Nevertheless, the implementation of probabilistic approaches often relies on stochastic simulation methods [80, 81] to treat general problems involving complex black-box computational models, such as those usually adopted for the analysis of civil engineering structures and systems.

Direct Monte Carlo simulation (MCS) is perhaps the most well-known stochastic simulation approach [80]. The method relies on the generation of samples of the input random quantities according to their probability distribution. Then, the numerical model under consideration is evaluated for each of them in order to obtain the corresponding realizations of the responses of interest, which are ultimately aggregated to approximate diverse probabilistic measures. Despite its robustness and simplicity, this straightforward approach may face some difficulties in certain cases. For instance, the analysis of rare events can lead to an excessive or even prohibitive number of samples, especially when the numerical cost of a single model evaluation is considerable [82]. Furthermore, if a mechanism to generate independent samples according to the target distribution is not available, the implementation of direct MCS becomes unfeasible [80, 83]. The previous challenges have motivated the development of advanced simulation techniques [84–86] based on, e.g., Markov chain Monte Carlo (MCMC) [81, 87–89]. These specialized strategies can draw samples from complex target distributions for which no closed-form expressions are available. Moreover, they are generally robust to the complexity of the model adopted to represent the system of interest, and usually prove more efficient than direct MCS. In consequence, they have been adopted an efficacious and flexible alternative to address a number of practical applications; see, e.g., [90–100]. Thus, based on the above discussion, it can be argued that advanced simulation techniques offer appealing features for the implementation of probabilistic approaches in the context of civil engineering structures and systems.

Attention is directed to two broad subjects within the previous framework. The first corresponds to reliability-based design optimization (RBDO) [101, 102]. In this setting, reliability is adopted as a probabilistic measure of the system performance when its behavior is characterized as acceptable (safe) or unacceptable (failed) [22]. Such a measure is employed to quantify the plausibility of the system satisfying certain design conditions given the probabilistic characterization of its properties and external loadings. Thus, this class of formulations provides a realistic and rational framework for civil engineering design in which the unavoidable uncertainties arising in the characterization of the system of interest and their effect on performance requirements can be explicitly accounted for during the decision-making process [7]. While this approach has been demonstrated in several applications (see, e.g., [101, 103–110]), one important topic pertains to the RBDO of structural dynamical systems under stochastic excitations [111]. By adopting this perspective, structural design processes are furnished with the versatile framework of stochastic processes to represent uncertain environmental actions [34, 112–114] and to assess their effect on the system response. In addition, the second subject under consideration corresponds to model updating [86], which aims to update the characteristics of a certain computational model based on measurements. The outcomes of this procedure plays an instrumental role in a number of applications including robust response prediction, structural health monitoring, system control, etc. A well-established solution framework to this end corresponds to Bayesian model updating [53, 54]. Instead of obtaining a single updated model, this formulation yields a full probabilistic distribution of models that is consistent with available measurement data and prior engineering knowledge [115]. Such information provides valuable insight for data-driven decision making, which is particularly relevant in view of the contemporary advent and proliferation of sensor technologies [116].

In this thesis, an effort is made to address a number of challenges in the context of RBDO and model updating of civil engineering structures and systems. Specifically, the focus of the herein reported developments is on three topics. The first pertains to the RBDO of structural dynamical systems under stochastic excitation, whose main challenges and solution approaches are presented in Section 1.2. The other two topics are associated with model updating problems in civil engi-

neering, which correspond to the treatment of contaminant detection problems in water distribution networks (WDNs) and the identification of complex structural dynamical models. A concise description of these problems is given in Section 1.3 followed by a brief review of Bayesian model updating procedures. Then, Section 1.4 states the specific objectives of this thesis, while the corresponding developments to achieve them are summarized in Section 1.5. Finally, Section 1.6 outlines the content of the subsequent chapters.

1.2 Reliability-based design optimization

One of the pivotal tasks of civil engineering is to design safe and cost-effective structures not only as part of public infrastructure, but also to satisfy industrial, commercial and private users' needs. Mathematical programming plays an instrumental role to this end, whereby structures are required to be optimum in terms of a given criterion while complying with a set of design requirements related to certain loading conditions [117]. Within this context, it is vital to incorporate all relevant uncertainties into the corresponding optimization problems in an appropriate manner, since neglecting them can be substantially detrimental to the performance of final designs [118]. In this regard, dynamical loads associated with, e.g., wind effects, earthquakes or sea waves [1–3], are particularly relevant due to their significant effect on structural responses and the impossibility of accurately predicting them. To characterize such loads in a probabilistic setting, the use of stochastic excitation models constitutes a well-established and versatile approach [34–36, 39, 114, 119, 120]. Moreover, as already pointed out, RBDO formulations enable a rational and sound theoretical framework in which the system uncertainties and their interaction with performance requirements can be explicitly accounted for during decision-making processes [7, 101, 111].

This thesis focuses on the RBDO of structural dynamical systems under stochastic excitation. Section 1.2.1 formulates the class of problems of interest, while Section 1.2.2 discusses the challenges to solve them. Then, state-of-the-art solution techniques are described in Sections 1.2.3 to 1.2.5. Some additional remarks are given in Section 1.2.6.

1.2.1 Problem formulation

The class of RBDO problems of interest can be stated as

$$\begin{aligned} \min_{\mathbf{x}} \quad & c(\mathbf{x}) \\ \text{s.t.} \quad & r_j(\mathbf{x}) \leq 0, \qquad j = 1, \ldots, n_r \\ & g_j(\mathbf{x}) \leq 0, \qquad j = 1, \ldots, n_g \\ & \mathbf{x} \in \mathbf{X} \subset \mathbb{R}^{n_x} \end{aligned} \tag{1.1}$$

where $\mathbf{x} = [x_1, \ldots, x_{n_x}]^T \in \mathbf{X} \subset \mathbb{R}^{n_x}$ is the vector of n_x design variables (discrete and/or continuous), $c(\mathbf{x})$ is the objective function, $r_j(\mathbf{x}) \leq 0$, $j = 1, \ldots, n_r$, represent n_r requirements on the system reliability, and $g_j(\mathbf{x}) \leq 0$, $j = 1, \ldots, n_g$, constitute n_g standard constraints. The set $\mathbf{X}$ comprises the possible values for the design variables. For each continuous design variable x_i, the side constraints are given by $x_i^L \leq x_i \leq x_i^R$, where x_i^L and x_i^R denote its lower and upper bound, respectively. Further, for each discrete variable x_i a finite set of possible values $\mathbf{X}_i$ is defined such that $x_i \in \mathbf{X}_i$. The objective function $c(\mathbf{x})$ can quantify construction costs, structural performance, users' comfort, expected repair costs, etc. In addition, the reliability constraints $r_j(\mathbf{x}) \leq 0$, $j = 1, \ldots, n_r$, define performance requirements in terms of failure probability measures, whereas the standard constraints $g_j(\mathbf{x}) \leq 0$, $j = 1, \ldots, n_g$, relate to design restrictions for which no structural reliability assessment is needed. Therefore, the evaluation of the latter can be regarded as relatively inexpensive. Finally, it is noted that failure probabilities can be involved in the definition of the objective and/or constraint functions in Eq. (1.1).

Structural dynamical systems under stochastic excitation

The structures of interest can be modeled as a multi-degree-of-freedom system that satisfies

$$\mathbf{M}\ddot{\mathbf{u}}(t) + \mathbf{C}\dot{\mathbf{u}}(t) + \mathbf{K}\mathbf{u}(t) + \mathbf{k}_{NL}\left(\mathbf{u}(t), \dot{\mathbf{u}}(t), \mathbf{y}(t)\right) = \mathbf{f}(t) \tag{1.2}$$

where $\mathbf{u}(t)$ denotes the displacement vector, $\mathbf{k}_{NL}(\mathbf{u}(t), \dot{\mathbf{u}}(t), \mathbf{y}(t))$ the vector of nonlinear restoring forces, $\mathbf{y}(t)$ the state variables of the nonlinear components, and $\mathbf{f}(t)$ the stochastic excitation vector. The matrices $\mathbf{M}$, $\mathbf{C}$, and $\mathbf{K}$ describe the mass, damping, and stiffness of the system, respectively. In addition, the evolution of $\mathbf{y}(t)$ depends on an appropriate nonlinear model. Thus, the equation for the evolution of $\mathbf{y}(t)$ and Eq. (1.2) constitute a coupled system of nonlinear equations whose solution relies, in practice, on complex black-box computational procedures.

Based on Eqs. (1.1) and (1.2), it is seen that the above formulation is quite general in the sense that it allows addressing diverse design problems [101, 104]. In this context, representative applications include the mitigation of seismic pounding risk between buildings [121] and the design of fluid filled tanks [122], wind-excited cable-stayed masts [123], high-rise buildings [124–126], large-scale linear systems [127, 128], and nonlinear devices for seismic protection [110]. Finally, it is noted that the previous formulation can be also extended to a multi-objective optimization framework [129, 130].

First-passage failure probabilities

In the context of structural systems under stochastic excitation, the probability that certain requirements are not fulfilled within a certain reference period, T, constitutes a useful measure of structural performance [85]. This quantity is referred to as first-passage probability and can be construed as a measure of the plausibility of unacceptable structural behavior [71]. In this framework, consider a vector $\mathbf{z} \in \mathbf{Z} \subset \mathbb{R}^{n_z}$ comprising the random variables representing both the stochastic excitation and the uncertain model parameters. The corresponding multivariate probability density function (PDF) is denoted by $q(\mathbf{z}|\mathbf{x})$, that is, $\mathbf{z} \sim q(\mathbf{z}|\mathbf{x})$. It is noted that this PDF can depend on the design variables $\mathbf{x}$; otherwise, the random variables are simply distributed as $\mathbf{z} \sim q(\mathbf{z})$. Then, a first-passage failure event, F, is defined as [131]

$$F = \{d(\mathbf{x}, \mathbf{z}) > 1\} \tag{1.3}$$

$$d(\mathbf{x},\mathbf{z}) = \max_{t\in[0,T]} \max_{\ell=1,\ldots,n_h} \frac{|h_\ell(t;\mathbf{x},\mathbf{z})|}{h_\ell^*} \tag{1.4}$$

where $d(\mathbf{x},\mathbf{z})$ is the so-called normalized demand function. In Eq. (1.4), $h_\ell(t;\mathbf{x},\mathbf{z})$, $\ell = 1,\ldots,n_h$, denote the n_h response functions of interest, whereas $h_\ell^* > 0$, $\ell = 1,\ldots,n_h$, represent the corresponding thresholds. These time-dependent responses are obtained from the solution of Eq. (1.2). Then, the first-passage failure probability function $P_F(\mathbf{x})$ is given by

$$P_F(\mathbf{x}) = \int_{d(\mathbf{x},\mathbf{z})>1} q(\mathbf{z}|\mathbf{x})d\mathbf{z} = \int_{\mathbf{z}\in\mathbf{Z}} I_F(\mathbf{x},\mathbf{z})q(\mathbf{z}|\mathbf{x})d\mathbf{z} \tag{1.5}$$

where $I_F(\mathbf{x},\mathbf{z})$ is the indicator function, with $I_F(\mathbf{x},\mathbf{z}) = 1$ if $d(\mathbf{x},\mathbf{z}) > 1$ and $I_F(\mathbf{x},\mathbf{z}) = 0$ otherwise. For the type of systems of interest, $\mathbf{z}$ usually comprises a large number of components to represent the stochastic excitation. In particular, n_z is often in the order of tens, hundreds, or thousands [34, 114, 120]. Thus, Eq. (1.5) constitutes a high-dimensional integral whose evaluation at each design becomes a computationally challenging task [71, 82, 84].

Reliability assessment techniques

Even though some simplified solution strategies have been proposed to compute first-passage probabilities in certain cases [131, 132], the evaluation of $P_F(\mathbf{x})$ commonly relies on stochastic simulation techniques for realistic and practical applications [82, 84, 85]. Some of these techniques include, e.g., subset simulation [133–136], importance sampling [137], line sampling [138], the domain decomposition method (DDM) [139], directional importance sampling (DIS) [140], and the probability density evolution method (PDEM) [141, 142]. Regardless of their efficiency, the use of these sampling strategies may still require a significant number of system evaluations (in the order of hundreds or thousands) and, in addition, the corresponding estimates present an inherent level of variability [7, 84].

1.2.2 Challenges and classification of solution approaches

Based on the preceding discussion, three main challenges can be identified in the solution of Eq. (1.1). First, failure probability estimation at any given candidate design during the optimization process involves, in principle, a large number of dynamic analyses whose computational efforts can be significant [85]. Second, sampling-based estimates inherently possess a variability level that can be detrimental to the effectiveness of standard optimization routines [143]. Finally, it is generally not straightforward to estimate the sensitivities of failure probability functions in a sufficiently accurate manner [65, 144]. All the previous aspects must be properly addressed by RBDO approaches to obtain meaningful results [111].

Several approaches have been developed for the RBDO of structural dynamical systems under stochastic excitation. These can be classified according to the search strategy and the type of information required during the solution process in three general categories [111], namely, sequential optimization methods (see Section 1.2.3), stochastic search-based techniques (see Section 1.2.4), and schemes based on augmented reliability spaces (see Section 1.2.5).

1.2.3 Sequential optimization methods

Sequential optimization schemes are iterative techniques in which, during each iteration, a suboptimization problem is constructed based on surrogates for the failure probability functions [101]. Such a problem is generally solved by means of standard search techniques to obtain a new candidate solution in a numerically tractable fashion, and the procedure is repeated until a certain convergence criterion is met. In general, these methods require full reliability assessment at relatively few designs during the entire design process. Different choices for the failure probability surrogate have been adopted in this context, which are briefly described in the following.

Exponential-type of approximations

This class of approaches has been demonstrated in RBDO problems where failure probability functions appear only in the constraints. As originally proposed in [145], each sub-optimization problem is constructed using a linear approximation, around the current candidate solution, for the logarithm of the failure probability function in terms of the design variables. That is,

$$P_F(\mathbf{x}) \approx \tilde{P}_F(\mathbf{x};\mathbf{x}^k) = \exp\left(a_0 + \sum_{i=1}^{n_x} a_i(x_i - x_i^k)\right) \tag{1.6}$$

where $\tilde{P}_F(\mathbf{x};\mathbf{x}^k)$ is the current approximation of the failure probability function, $\mathbf{x}^k$ is the current candidate solution and a_i, $i = 0, 1, \ldots, n_x$, are polynomial coefficients. Move limits on the design variables are imposed to control the approximation quality.

Different strategies have been devised to compute the polynomial coefficients. In [145], a scheme based on $n_x + 1$ direct evaluations of $P_F(\mathbf{x})$ around $\mathbf{x}^k$ is considered together with an importance sampling technique [137] for linear structures. This approach is extended in [66] to uncertain linear systems by approximating the modal properties in terms of a convex linearization scheme [146, 147] to evaluate $P_F(\mathbf{x})$. Alternatively, the method introduced in [148] determines the sought coefficients by matching the average and first-order moments of $P_F(\mathbf{x})$ and $\tilde{P}_F(\mathbf{x};\mathbf{x}^k)$ in a region Ω^k around $\mathbf{x}^k$, i.e.,

$$m_{P_F}^{k,0} = \frac{1}{|\Omega^k|}\int_{\Omega^k} \tilde{P}_F(\mathbf{x};\mathbf{x}^k)d\mathbf{x}, \quad m_{P_F}^{k,i} = \frac{1}{|\Omega^k|}\int_{\Omega^k} x_i\tilde{P}_F(\mathbf{x};\mathbf{x}^k)d\mathbf{x}, \quad i = 1, \ldots, n_x \tag{1.7}$$

where $|\Omega^k|$ is the hyper-volume of Ω^k; $m_{P_F}^{k,0}$ is the average of $P_F(\mathbf{x})$ over Ω_k; $m_{P_F}^{k,i}$, $i = 1, \ldots, n_x$, are the first-order moments of $P_F(\mathbf{x})$ over Ω_k; and $\tilde{P}_F(\mathbf{x})$ is given by Eq. (1.6). A single simulation run in the augmented space of random and design variables (see Section 1.2.5) is required to estimate $m_{P_F}^{k,0}$ and $m_{P_F}^{k,i}$, $i = 1, \ldots, n_x$. Lastly, the approach presented in [149] exploits reliability sensitivity information to construct the linear expansion, namely, the coefficients a_i, $i = 0, 1, \ldots, n_x$, are selected to ensure that the estimates of the first-order derivatives of $P_F(\mathbf{x})$ with respect to the

design variables match those of $\tilde{P}_F(\mathbf{x};\mathbf{x}^k)$ in Eq. (1.6).

Convex and conservative approximations

A convex linearization strategy [146] is adopted in [150]. At each iteration, all problem functions are approximated around the current candidate design in terms of direct and reciprocal variables. This leads to simple explicit algebraic sub-optimization problems, which can be efficiently solved using readily available methods [146]. In particular, each function in Eq. (1.1), say $f(\mathbf{x})$, is approximated around the current candidate design $\mathbf{x}^k$ as

$$f(\mathbf{x}) \approx \tilde{f}(\mathbf{x};\mathbf{x}^k) = f(\mathbf{x}^k) + \sum_{(i^+)} \frac{\partial f(\mathbf{x}^k)}{\partial x_i}(x_i - x_i^k) + \sum_{(i^-)} \frac{\partial f(\mathbf{x}^k)}{\partial x_i}\frac{x_i^k}{x_i}(x_i - x_i^k) \tag{1.8}$$

where $\sum_{(i^+)}$ and $\sum_{(i^-)}$ indicate summation over the variables belonging to the groups (i^+) and (i^-), respectively. Group (i^+) contains the variables for which $\partial f/\partial x_i > 0$, and group (i^-) includes the remaining variables. This expansion corresponds to a linearization in terms of the direct variables (x_i) for group (i^+) and of the reciprocal variables $(1/x_i)$ for group (i^-). Some of the attractive features of this scheme pertain to its convexity, separability, and conservatism [146]. Moreover, additional conservatism can be enforced by including second-order terms in Eq. (1.8) [151].

The practical implementation of Eq. (1.8) requires estimating failure probabilities and their derivatives. To this end, linear approximations for the logarithm of the failure probability functions are adopted in [150, 152], whereas a two-level approximation scheme within subset simulation [153, 154] is considered in [151, 155, 156]. Alternatively, the change of probability measure technique [48] together with the PDEM [141, 142] are implemented in [157]. Finally, mixed discrete-continuous RBDO problems are addressed in [151, 152] by resorting to a dual formulation that fully exploits the separability of the corresponding sub-optimization problems.

A threshold-based local approximation

An approach that utilizes some of the advantageous features of subset simulation [133, 134] is proposed in [158]. In this setting, a local approximation of $P_F(\mathbf{x})$ is constructed by reusing the reliability analysis results at the previous candidate solution $\mathbf{x}^k$. First, the normalized demand function is approximated as

$$d(\mathbf{x}, \mathbf{z}) \approx \tilde{d}(\mathbf{x}, \mathbf{z}) = d(\mathbf{x}^k, \mathbf{z}) + \sum_{i=1}^{n_x} \delta_i (x_i - x_i^k) \tag{1.9}$$

where the coefficients δ_i, $i = 1, \ldots n_x$, are computed by means of a least squares fit strategy [158]. Then, the failure probability function is approximated as

$$P_F(\mathbf{x}) = P[d(\mathbf{x}, \mathbf{z}) \geq 1] \approx P\left[d(\mathbf{x}^k, \mathbf{z}) \geq 1 - \sum_{i=1}^{n_x} \delta_i (x_i - x_i^k)\right] \tag{1.10}$$

which is evaluated in terms of the complementary cumulative distribution function estimate at the previous candidate design [134]. In other words, each sub-optimization problem approximates $P_F(\mathbf{x})$ as the failure probability at $\mathbf{x}^k$ associated with the threshold $(1 - \sum_{i=1}^{n_x} \delta_i (x_i - x_i^k))$. To control the quality of the approximations, move limits on the design variables are implemented. Any suitable technique can be adopted to solve the resulting sub-optimization problem.

Line search methods

Line search methods [143] encompass appealing features to address the class of problems of interest. In this regard, as initially suggested in [153, 154], each optimization cycle requires evaluating failure probabilities only along the search direction. Thus, one-dimensional surrogates for the failure probability function can be formulated instead of n_x-dimensional ones. That is,

$$P_F(\mathbf{x}^k + \tau \mathbf{v}^k) \approx \tilde{P}_F(\tau; \mathbf{x}^k) \tag{1.11}$$

where $\tau \geq 0$ is the step size along the search direction $\mathbf{v}^k$. In general, the following steps are carried out during each optimization cycle [159]. First, a search direction is identified using information on the problem functions and their sensitivities [143]. Next, one-dimensional failure probability surrogates are established along the search direction. A surrogate model that uses information on the failure probability functions and their directional derivatives [160] is adopted in [153, 154], although alternative metamodels can be implemented as well. Finally, a new candidate solution is identified by means of a line search procedure. During this process, additional failure probability evaluations are performed, which are utilized to adaptively improve the quality of the surrogates. This approach has been successfully applied in the RBDO of complex structural systems equipped with nonlinear dissipation devices [153, 154, 159], in reliability-based multiobjective problems [161] together with a compromise programming formulation [130], and in design problems incorporating reduced-order models [162] based on substructure coupling for dynamic analysis [163, 164].

Reliability sensitivity assessment is instrumental in the implementation of line search methods. To perform this task, the approaches presented in [153, 154, 161, 165] adopt a two-level approximation scheme [158] that requires a single run of subset simulation [133] plus some additional structural analyses. An alternative strategy is presented in [166] by resorting to the PDEM [141, 142], metamodels at the structural response level, and finite differences. Lastly, a sensitivity assessment framework for linear stochastic structures [140, 167] is implemented in [168] (see Chapter 5).

Multi-level approximation schemes

The optimization techniques proposed in [125, 127, 169, 170], which focus on the RBDO of uncertain linear systems, adopt different surrogate models to approximate, in a simultaneous manner, the peak responses, failure probability functions, and second-order statistics of the system responses. First, the peak responses are approximated either in terms of peak factors [125], the so-called auxiliary variable vector approach [127], or distributions parametrized in terms of second-order statistics [170]. A second approximation level is introduced for cases involving multiple responses of inter-

est, where failure probability is assumed to be proportional to the sum of the component-level failure probabilities [170] or, alternatively, the so-called inverse reliability constraints are approximated using kriging metamodels [169]. The resulting sub-optimization problem explicitly depends on the second-order statistics of the responses of interest. For their evaluation, a third level of approximation is considered by using direct MCS results obtained at the previous candidate design (see, e.g., [169, 170]). In general, these methods have successfully addressed RBDO problems involving high-dimensional design spaces and multiple constraints. Nevertheless, it is noted that their formulation and implementation relies on explicit heuristic approximations for the characteristics of the stochastic system response, and thus, their accuracy cannot be ensured for general cases.

Heuristic approach based on operator norm optimization

Failure probability minimization of linear structural systems subject to Gaussian excitation is addressed in [171, 172] by means of a decoupling strategy. In this case, the system response at any given instant can be expressed as a linear combination of the basic random variables $\mathbf{z}$. Therefore,

$$\tilde{\mathbf{h}}(\mathbf{x}, \mathbf{z}) = \tilde{\mathbf{A}}(\mathbf{x})\mathbf{z} \tag{1.12}$$

where $\tilde{\mathbf{h}}(\mathbf{x}, \mathbf{z}) \in \mathbb{R}^{n_h n_T}$ contains the n_h normalized responses of interest evaluated at n_T discrete time instants, and $\tilde{\mathbf{A}}(\mathbf{x}) \in \mathbb{R}^{n_h n_T \times n_z}$ is a matrix constructed in terms of response thresholds, Karhunen-Loève representations, and the adopted integration rule for the equation of motion. The induced (p_1, p_2)-norm of this matrix is given by

$$\|\tilde{\mathbf{A}}(\mathbf{x})\|_{p_1,p_2} = \sup_{\mathbf{z}\neq\mathbf{0}} \frac{\|\tilde{\mathbf{A}}(\mathbf{x})\mathbf{z}\|_{p_1}}{\|\mathbf{z}\|_{p_2}} = \sup_{\mathbf{z}\neq\mathbf{0}} \frac{\|\tilde{\mathbf{h}}(\mathbf{x}, \mathbf{z})\|_{p_1}}{\|\mathbf{z}\|_{p_2}} \tag{1.13}$$

where $\|\cdot\|_{p_i}$ denotes the L_{p_i}-norm of a vector ($i = 1, 2$). In particular, the values $p_1 = \infty$ and $p_2 = 2$ are adopted. The key idea is to employ the operator norm in Eq. (1.13) as a proxy for the failure probability function, $P_F(\mathbf{x})$. Thus, the design that minimizes $\|\tilde{\mathbf{A}}(\mathbf{x})\|_{\infty,2}$, which can be identified through a standard nonlinear optimization problem, is assumed to minimize $P_F(\mathbf{x})$.

1.2.4 Stochastic search-based techniques

Randomized search in the design space is known to be an effective strategy to escape local optima [173] and, in the context of RBDO, it generally reduces the impact of the variability of failure probability estimates on optimization procedures [7]. Nevertheless, this strategy commonly faces challenges related to the computational efforts required in its application. Several stochastic optimization methods based on advanced simulation techniques have been proposed to solve Eq. (1.1), whose formulation mainly relies on simulated annealing concepts [174].

Asymptotically independent Markov sampling

The asymptotically independent Markov sampling method for global optimization (AIMS-OPT) [175] has been proposed for finding the minimum of the failure probability function, $P_F(\mathbf{x})$. Since such a problem is equivalent to maximizing $\exp(-P_F(\mathbf{x})/T)$ for any given temperature $T > 0$ [174], and artificially treating the design variables as random, an auxiliary (non-normalized) distribution is defined as

$$p_T(\mathbf{x}) \propto \exp\left(-\frac{P_F(\mathbf{x})}{T}\right) U_{\mathbf{X}}(\mathbf{x}), \quad T > 0 \tag{1.14}$$

where $U_{\mathbf{X}}(\mathbf{x})$ is a uniform distribution over the set $\mathbf{X} = \{\mathbf{x} \in \mathbb{R}^{n_x} : x_i^L \leq x_i \leq x_i^U, i = 1, \ldots, n_x\}$. It is noted that the distribution becomes uniform over the search space for arbitrarily high temperatures, i.e., $\lim_{T\to\infty} p_T(\mathbf{x}) = U_{\mathbf{X}}(\mathbf{x})$. Furthermore, as T decreases, more probability mass is concentrated around the designs that maximize $\exp(-P_F(\mathbf{x})/T)$. In the limit case, $\lim_{T\to 0} p_T(\mathbf{x}) = U_{\mathbf{X}^*_{P_F}}(\mathbf{x})$, where $\mathbf{X}^*_{P_F}$ is the optimal solution set. Hence, samples generated according to $p_T(\mathbf{x})$, $T \to 0$, will be in a vicinity of $\mathbf{X}^*_{P_F}$ with very high probability. By sampling from a sequence of tempered distributions $\{p_{T_j}(\mathbf{x}), j = 0, 1, \ldots\}$ with monotonically decreasing temperatures $\infty = T_0 > T_1 > \cdots > T_j > \cdots$, such that $T_j \to 0$ as $j \to \infty$, a transition is established from a uniform distribution over the initial search space to a distribution densely concentrated near the optimal solution set. To perform this task, the MCMC method proposed in [176] is adopted. In general, AIMS-OPT relies on local exploration in neighborhoods of the samples generated at the

previous annealing level, which has attractive parallelization properties [175].

A transitional Markov chain Monte Carlo-based approach

The approach proposed in [177] addresses cost minimization considering a single reliability constraint, i.e., $P_F(\mathbf{x}) \leq P_F^*$, standard constraints, and deterministic linear structural systems under Gaussian excitation. In this case, a (non-normalized) target distribution is defined as

$$p_T(\mathbf{x}) \propto U_{\mathbf{X}_{\text{aux}}}(\mathbf{x}) \exp\left(-\frac{\ln(c(\mathbf{x})/c_0)}{T}\right), \quad T \to 0 \tag{1.15}$$

where c_0 is a scaling factor and $U_{\mathbf{X}_{\text{aux}}}(\mathbf{x})$ is a uniform distribution over the set

$$\mathbf{X}_{\text{aux}} = \{\mathbf{x} \in \mathbf{X} \subset \mathbb{R}^{n_x} : P_F(\mathbf{x}) \leq P_F^* \wedge g_j(\mathbf{x}) \leq 0, j = 1, \ldots, n_g\} \tag{1.16}$$

To generate samples from the target distribution $\lim_{T\to 0} p_T(\mathbf{x})$, the transitional Markov chain Monte Carlo (TMCMC) method [178, 179] is adopted (see Section 1.3.4). A sequence of distributions associated with temperatures $\infty = T_0 > T_1 > \cdots > T_m \to 0$ is introduced. The initial samples, which uniformly populate $\mathbf{X}_{\text{aux}}$, are generated as samples conditional on the auxiliary failure event $\tilde{F} = \{P_F(\mathbf{x}) \leq P_F^*\}$ with the design variables uniformly distributed over the set satisfying the deterministic constraints. To this end, subset simulation [133, 134] is used. For efficient reliability assessment, the DDM [139] is implemented with adaptive sample sizes [177].

Two-phase Bayesian model updating framework

The approach presented in [180–184] addresses constrained and unconstrained RBDO problems involving continuous, discrete, and mixed discrete-continuous design variables (see Chapters 2 to 4). Similar to [175, 177], an auxiliary (non-normalized) distribution is introduced as

$$p_T(\mathbf{x}) \propto U_{\mathbf{X}_{\text{feasible}}}(\mathbf{x}) \ \exp\left(-\frac{c(\mathbf{x})}{T}\right), \quad T > 0 \tag{1.17}$$

where $U_{\mathbf{X}_{\text{feasible}}}(\mathbf{x})$ is a uniform distribution over the feasible design space

$$\mathbf{X}_{\text{feasible}} = \{\mathbf{x} \in \mathbf{X} : r_j(\mathbf{x}) \leq 0, j = 1, \ldots, n_r \wedge g_k(\mathbf{x}) \leq 0, k = 1, \ldots, n_g\} \tag{1.18}$$

It is noted that $\lim_{T\to\infty} p_T(\mathbf{x}) = U_{X_{\text{feasible}}}(\mathbf{x})$, whereas samples following the distribution $p_T(\mathbf{x})$, $T \to 0$, will densely populate a vicinity of the optimal solution set $\mathbf{X}_c^*$. Thus, the original RBDO problem in Eq. (1.1) can be interpreted as a Bayesian model updating problem with prior distribution $U_{\mathbf{X}_{\text{feasible}}}(\mathbf{x})$ and (non-normalized) likelihood function $\lim_{T\to 0} \exp(-c(\mathbf{x})/T)$ [183].

Samples following the target posterior distribution $\lim_{T\to 0} p_T(\mathbf{x})$ are retrieved using the TMCMC method [178, 179] with temperatures $\infty = T_0 > T_1 > \cdots > T_m \to 0$. To obtain the initial set of samples, which follows $U_{X_{\text{feasible}}}(\mathbf{x})$, an auxiliary optimization problem is introduced as

$$\begin{aligned} \min_{\mathbf{x}} \quad & h(\mathbf{x}) = \max\left\{0,\ g_1(\mathbf{x}), \ldots, g_{n_g}(\mathbf{x}),\ r_1(\mathbf{x}), \ldots, r_{n_r}(\mathbf{x})\right\} \\ \text{s.t.} \quad & \mathbf{x} \in \mathbf{X} \end{aligned} \tag{1.19}$$

with corresponding optimal solution set $\mathbf{X}_h^* = \mathbf{X}_{\text{feasible}}$ [180, 183]. Since Eq. (1.19) involves only side constraints on the design variables, the TMCMC method can be directly applied to generate uniformly distributed feasible designs [181]. This leads to a two-phase strategy in which the same sampling technique is implemented to explore the feasible and optimal solution sets in a sequential manner [183]. For improved efficiency, kriging-based adaptive metamodels have been used to approximate the failure probability functions [180, 181, 184].

1.2.5 Schemes based on augmented reliability spaces

An alternative framework for the solution of Eq. (1.1) relies on the so-called augmented reliability problem [67, 185]. In this setting, the design variables $\mathbf{x}$ are artificially treated as random, i.e., $\mathbf{x} \sim p(\mathbf{x})$, where $p(\mathbf{x})$ is usually taken as a uniform distribution over the design space. Then, the

probability of the failure event F in the augmented reliability space $\langle \mathbf{x}, \boldsymbol{\theta} \rangle$ is given by

$$P(F) = \int_{\mathbf{x} \in \mathbb{R}^{n_x}} \int_{\boldsymbol{\theta} \in \mathbb{R}^{n_\theta}} I_F(\mathbf{x}, \boldsymbol{\theta}) q(\boldsymbol{\theta}|\mathbf{x}) p(\mathbf{x}) d\boldsymbol{\theta} d\mathbf{x} \tag{1.20}$$

According to Bayes' theorem [23], the failure probability function $P_F(\mathbf{x})$ can be written as

$$P_F(\mathbf{x}) = P(F|\mathbf{x}) = \frac{P(F)p(\mathbf{x}|F)}{p(\mathbf{x})} \tag{1.21}$$

where $p(\mathbf{x}|F)$ is the marginal distribution of $\mathbf{x}$ conditioned on F. Further, if $p(\mathbf{x}) = U_{\mathbf{X}}(\mathbf{x})$, then $P_F(\mathbf{x}) \propto p(\mathbf{x}|F)$. Based on Eq. (1.21), the failure probability function $P_F(\mathbf{x})$ can be equivalently expressed in terms of the conditional marginal PDF $p(\mathbf{x}|F)$. The approaches reported in this subsection take advantage of this basic relationship to decouple the original RBDO problem.

Stochastic subset optimization

Stochastic subset optimization (SSO) is an iterative approach introduced in [186, 187] for global reliability optimization. In this framework, each iteration shrinks the search domain to reduce its average failure probability value as follows. First, a total of N_T failure samples in the $\langle \mathbf{x}, \boldsymbol{\theta} \rangle$-space are generated using MCMC techniques, where $\mathbf{x}$ is uniformly distributed over the current search space $\hat{\mathbf{X}} \subset \mathbf{X}$. Then, a class $\breve{\mathbf{S}}$ of admissible subsets in $\hat{\mathbf{X}}$ is defined with specified characteristics such as, e.g., size or shape. Finally, the search region is updated as

$$\hat{\mathbf{X}} \leftarrow \underset{\mathbf{S} \in \breve{\mathbf{S}}}{\operatorname{argmin}} \frac{N_S}{V_S} \tag{1.22}$$

where N_S is the number of failure samples in $\mathbf{S}$, and V_S is the volume of $\mathbf{S}$. This non-smooth optimization problem is solved using any suitable method (e.g., [188]). According to [189], the appropriate definition of the admissible subsets remains one of the main challenges in SSO, especially for higher dimensions and disjoint regions. Generally, hyper-rectangles and hyper-ellipses with adjustable ratio between dimensions have been implemented [186, 187]. The SSO method has

been demonstrated in cases involving a relatively small number of design variables [190, 191].

Non-parametric stochastic subset optimization

The non-parametric stochastic subset optimization (NP-SSO) method [192–194] is an extension of SSO to account for reliability constraints. Instead of using parametrized subsets to shrink the search space, NP-SSO focuses on the estimation of the marginal PDF $p(\mathbf{x}|F)$ using boundary-corrected kernel density estimation (KDE) methods [195–198]. Rejection sampling [81] is adopted to generate the independent and identically distributed (i.i.d.) failure samples required by KDE methods. An iterative scheme is implemented in which regions with smaller failure probability values are identified using several soft-computing techniques [199–202]. For constrained RBDO problems, an additional refinement stage is introduced to improve the accuracy of the resulting surrogate for $P_F(\mathbf{x})$ near the boundaries of the feasible design space [194]. Although NP-SSO circumvents some of the difficulties arising in the SSO method, the robustness of KDE approaches for density fitting decreases in high dimensions [203]. Thus, the range of applications of NP-SSO seems to be somewhat limited in terms of the number of design variables.

Approach based on partitioned design space

The iterative approach proposed in [204] aims to obtain a surrogate for the failure probability function in terms of a partitioning of the design space. During each iteration, a number of samples within the current subspace are first obtained. Using these samples, the marginal PDF of the design variables conditioned on failure is approximated in terms of second-order polynomials [205, 206], based on which a new subspace is identified. Ultimately, a failure probability surrogate is obtained for each partition rather than for the entire design space [204]. The method has been demonstrated in reliability-constrained cost minimization problems involving relatively low-dimensional design spaces.

Maximum entropy-based method

A strategy based on the maximum entropy (ME) method (see, e.g., [207, 208]) is proposed in [209] for cost minimization under a single reliability constraint. Specifically, ME estimation under first moment constraints is implemented to approximate $p(\mathbf{x}|F)$ over the entire design space as

$$p(\mathbf{x}|F) \approx \tilde{p}(\mathbf{x}|F) = \exp\left(-\alpha - \boldsymbol{\lambda}^T\mathbf{x}\right) \tag{1.23}$$

where α and $\boldsymbol{\lambda} = \langle\lambda_1, \ldots, \lambda_{n_x}\rangle^T$ are obtained based on available failure samples [209, 210]. Subset simulation [133, 134] is implemented to obtain the required failure samples and to estimate $P(F) \approx \hat{P}(F)$. Based on $\tilde{p}(\mathbf{x}|F)$ and $\hat{P}(F)$, an approximation of $P_F(\mathbf{x})$ is constructed following Eq. (1.21). Further, a three-step strategy is formulated to account for the variability in $\hat{P}(F)$, α and $\boldsymbol{\lambda}$. First, suitable confidence intervals (CIs) are defined for these parameters [209–211]. Then, a set of explicit sub-optimization problems are solved, where each of them corresponds to a realization of $\hat{P}(F)$, α and $\boldsymbol{\lambda}$ drawn from their CIs. Finally, the best design among the resulting solutions is identified using a screening procedure. According to [209], the performance of the approach is expected to decrease for failure probability functions with a strongly nonlinear behavior.

Scheme based on equivalent safety-factor constraints

Equivalent safety-factor constraints are proposed in [212] to replace the original reliability constraints and transform the RBDO problem into a standard nonlinear optimization problem. Such equivalent constraints are given by $\eta_j^*\bar{d}_j(\mathbf{x}) \leq 1$, $j = 1, \ldots, n_r$, where $\eta_j^* \geq 1$ is the designated safety factor and $\bar{d}_j(\mathbf{x}) > 0$ is a user-defined auxiliary demand function. Furthermore, the functional relationship between safety factor and target reliability level is given by [212]

$$P\left[d_j(\mathbf{x}, \boldsymbol{\theta}) - \eta_j^*\bar{d}_j(\mathbf{x}) > 0\right] = P_{F_j}^* \iff P\left[\frac{d_j(\mathbf{x}, \boldsymbol{\theta})}{\bar{d}_j(\mathbf{x})} > \eta_j^*\right] = P_{F_j}^* \tag{1.24}$$

Based on Eq. (1.24), the values of η_j^*, $j = 1, \ldots, n_r$, can be estimated using, e.g., sampling techniques. Direct MCS and parallel subset simulation [213] can be implemented in the augmented reliability space to obtain all safety factors simultaneously [212]. The scheme has been applied to cases involving relatively few design variables.

1.2.6 Remarks

A brief overview of state-of-the-art methods for the RBDO of structural systems under stochastic excitation has been presented in this section. These approaches have been demonstrated in a variety of problems, including complex finite element models and nonlinear structural systems. In this regard, methods for optimal design in stochastic structural dynamics seem to be applicable not only to academic problems, but also to practical engineering design situations.

Following the above presentation, it is noted that the approaches described in this section encompass different advantages and difficulties. Sequential optimization approaches (see Section 1.2.3) are generally more efficient and have been demonstrated in higher-dimensional design spaces, although their usually local nature may not be appropriate for some types of problems. Alternatively, while stochastic search-based techniques (see Section 1.2.4) offer a flexible solution treatment which is suitable for problems involving multiple optima, they may be computationally intensive and may face some challenges in high-dimensional design spaces. Lastly, schemes based on augmented reliability spaces (see Section 1.2.5) allow fully decoupling the RBDO problem, but they have been mostly demonstrated in cases with relatively few design variables. Therefore, the most appropriate method for each particular problem must be carefully chosen. To this end, some relevant aspects that may be considered include the characteristics of the design vector (dimensionality and discrete/continuous nature), possibility of having multiple optima, linearity of the structural system, available computational resources, and the role of the failure probability functions (as objective and/or constraint functions).

The previous discussion suggests that computational aspects play a key role in designing civil engi-

neering structures. In this regard, further developments in certain areas can lead to general advancements in the RBDO of structural dynamical systems under stochastic excitation. These include, indicatively, the implementation of general surrogate modeling techniques for mixed discrete-continuous spaces, the synergetic integration of novel stochastic simulation methods for reliability and sensitivity assessment with suitable optimization procedures, and the formulation of specialized parallelization strategies. Furthermore, specific enhancements can be envisaged for each of the herein described types of RBDO methods in order to extend their applicability and improve their efficiency [111]. By addressing the previous challenges, adequate final designs can be established and, more importantly, valuable insight can be obtained to assist complex decision-making processes in civil engineering practice.

1.3 Model updating

Civil engineering structures and systems are characterized, as previously discussed, by a constant and typically uncontrolled exposure to their environment. Diverse processes such as, e.g., component deterioration, natural hazards and anthropogenic events, can affect the performance of these systems to a significant extent. In this regard, due to the impossibility of accurately predicting such phenomena, assessing the actual state of civil engineering structures and systems based on available data is of paramount importance [18, 214–216]. Moreover, the revolutionary increase in information sharing, data availability and computational capabilities experienced over the last decades has facilitated the collection, transmission and processing of measurements to an unprecedented level [116]. This is evidenced, e.g., by the implementation of supervisory control and data acquisition (SCADA) systems [217, 218] and contemporary structural monitoring procedures [25, 58]. Such scenario provides unique opportunities for the development of effective data-driven strategies towards the lifelong management of civil engineering assets.

Model updating is a particularly attractive tool for system identification based on available data, as it allows integrating engineering models and measurements to gain insight into the actual system

state (e.g., [219]). Nevertheless, modeling and monitoring processes in civil engineering are inherently uncertain due to diverse factors including, for instance, lack of information, complexity of the underlying system physics, potential sensor malfunctioning, inability to forecast environmental processes, and inaccuracies in data processing routines [24, 86, 220]. Taking these uncertainties into account has been widely acknowledged as critical in the formulation and implementation of meaningful model updating procedures [55, 221]. In this regard, Bayesian model updating approaches [7, 24, 53–55, 115, 222] enable a rigorous theoretical framework for model updating with explicit uncertainty treatment. By resorting to the interpretation of probability as a measure of the plausibility of a given hypothesis [23, 223], these procedures ultimately yield an updated probabilistic distribution of models that is consistent with available data and prior knowledge [115].

In this thesis, attention is directed to two classes of model updating problems. These correspond to contaminant source detection in WDNs (see Section 1.3.1) and the identification of complex structural dynamical systems (see Section 1.3.2). Bayesian model updating, which plays an instrumental role in the development of the herein proposed approaches, is concisely formulated in Section 1.3.3. Some pertinent solution techniques for Bayesian model updating problems are briefly described in Section 1.3.4. Finally, Section 1.3.5 provides some general remarks.

1.3.1 Contaminant source detection in water distribution networks

Water distribution networks are regarded as critical infrastructure systems due to the societal and industrial dependence on their performance [16]. Thus, it is pivotal to ensure the efficiency, reliability, and robustness in their operation. Nevertheless, these increasingly interwoven, large-scale and complex hydraulic systems are constantly prone to performance-detrimental disturbances driven by uncontrollable external factors [220]. Examples of these disturbances include leakage [224–226], component failure [30, 227], unauthorized demand [228], sabotage [5], and contamination [229]. In this regard, developing effective data-driven methodologies to identify WDN disturbances constitutes a crucial task from economical, technical, environmental and public health perspectives

[230, 231]. In particular, and given the high susceptibility of public health to the quality of drinking water [231], the accurate and timely identification of contaminant intrusion is a highly relevant goal to ensure water safety in distribution systems. Hence, one of the topics addressed in this thesis corresponds to contaminant source detection [4], which entails characterizing the source of an unwanted substance based on available measurements.

From a broad perspective, available disturbance detection methodologies for WDNs can be categorized in hardware-based, data-driven, and model-based approaches. Hardware-based approaches pinpoint disturbance locations using application-specific techniques [232–234] which, despite a high effectiveness level, may be time-consuming, labor-intensive, and expensive [235]. Alternatively, data-driven and model-based detection approaches use measurements to characterize system perturbations via computational procedures [236, 237]. While data-driven methods focus on distinguishing abnormal behavior directly from sensor records [237], model-based techniques compare available measurements with model predictions to identify network disturbances [238–241]. The latter encompass attractive features pertaining to their ability to integrate historical data records, engineering knowledge and the underlying physics of the WDN in a unified formulation.

Some model updating techniques for contaminant source detection rely on direct optimization procedures [241, 242]. In these methods, the aim is to identify the single contaminant outline that provides the best match between sensor measurements and model predictions [238–240, 243, 244]. Nevertheless, since the underlying physics of contaminant propagation through WDNs usually leads to different contaminant outlines yielding very similar predictions at the measurement points, the solution of the related optimization problem is generally non-unique. Further, the inherent uncertainties involved in the modeling and monitoring processes of WDNs give rise to uncertain data and model predictions [32, 46, 245, 246] which, in turn, commonly yield ill-posed and ill-conditioned inverse problems. By adopting a fully probabilistic treatment of contaminant source detection problems, Bayesian approaches have been recently developed in order to address the previous challenges. These include, indicatively, belief propagation methods [247], the use of beta-

binomial conjugate distributions [75], real-time updating approaches [248], backward probabilistic modeling techniques [73], Bayesian belief network formulations [249, 250], MCMC methods [251–253], and an approach based on Bayesian model class selection [254] (see Chapter 6). Overall, the previous techniques present different scopes, advantages and limitations, and they have been applied to diverse contaminant source detection problems with various levels of effectiveness.

1.3.2 Model updating of complex structural dynamical systems

Current computational capabilities have enabled the use of high-fidelity structural dynamical models in routine engineering analyses, e.g., [219, 255–258]. Moreover, the ever-growing availability of sensors is expected to propel an increase in the overall amount of dynamical response measurements [116]. Thus, it can be argued that the lifelong management of civil engineering assets can be substantially benefitted in the near future by the development of methodologies to evaluate the state of complex structural dynamical systems based on available data [214, 259, 260]. This translates, in practice, to solving high-dimensional inverse problems with inherently uncertain measurements and response predictions. To this end, a fully probabilistic Bayesian formulation constitutes a suitable and flexible framework for the explicit treatment of such uncertainties [24, 261, 262].

Notwithstanding the relevance of high-dimensional Bayesian updating of involved structural dynamical models using measured response data, relatively few contributions have addressed this class of problems. In this regard, the sampling-based techniques presented in [263, 264] rely on auxiliary dynamic systems to establish the transition mechanism in a MCMC framework. That is, fictitious dynamical systems are employed to explore the posterior distribution of the model parameters. These methods have proved quite effective in high-dimensional identification problems, although their implementation faces practical issues associated with the calibration of the algorithm parameters and the need for accurate sensitivity information [265, 266]. Alternative, the approach presented in [267] considers an effective implementation of reliability methods to explore the posterior distribution (see Chapter 7). Additional techniques that have been proposed include subspace

identification methods [268] and Kalman-filtering-based techniques [269]. From a general perspective, the previous approaches have been applied in different types of structural systems with various levels of success, and they offer diverse advantages and limitations. However, it is believed that more developments are needed in this area to improve the effectiveness of identification procedures in the context of complex structural dynamical systems.

1.3.3 Bayesian model updating framework

Following the presentation in Sections 1.3.1 and 1.3.2, it is seen that Bayesian model updating is instrumental in the formulation of the contributions presented in this thesis. Thus, the main aspects of Bayesian model updating are briefly described in the following.

Consider a probabilistic model class M, which comprises a set of models $M(\boldsymbol{\theta})$ parameterized according to the set of random variables $\boldsymbol{\theta} \in \boldsymbol{\Theta} \subset \mathbb{R}^{n_\theta}$, and available measurement data D obtained from the system of interest [115]. In the context of civil engineering structures and systems, the model class allows incorporating assumptions about the underlying physics of the system, a probabilistic measure of the resemblance between measurements and predictions, and a probability distribution that represents the prior state of knowledge about the model parameters $\boldsymbol{\theta}$ [53, 54]. In general, these parameters can be associated with, e.g., physical characteristics of the system, probabilistic properties of the system response, or both [53–55].

Bayesian model updating procedures aim to obtain revised probabilistic information about the system state based on available data [24], which in turn enables updated predictions of, e.g., the system response [263, 267] or its reliability [215, 270]. Specifically, the goal of this class of approaches is to characterize the posterior (updated) PDF of the model parameters $\boldsymbol{\theta}$, which is denoted by $p(\boldsymbol{\theta}|M, D)$. Further, according to Bayes' theorem, this distribution is given by [23, 53]

$$p(\boldsymbol{\theta}|M, D) = \frac{p(D|M, \boldsymbol{\theta})p(\boldsymbol{\theta}|M)}{P(D|M)} \tag{1.25}$$

where $p(\boldsymbol{\theta}|M)$ is the prior PDF, $p(D|M,\boldsymbol{\theta})$ is the likelihood function, and $P(D|M)$ is the so-called evidence for the model class M. In this setting, the prior distribution represents the initial or prior belief about the distribution of $\boldsymbol{\theta}$, whereas the likelihood function quantifies the plausibility of observing the data D given the model $M(\boldsymbol{\theta})$. Moreover, the evidence is given by

$$P(D|M) = E_{p(\boldsymbol{\theta}|M)}\left[p(D|M,\boldsymbol{\theta})\right] = \int_{\boldsymbol{\theta}\in\boldsymbol{\Theta}} p(D|M,\boldsymbol{\theta})p(\boldsymbol{\theta}|M)d\boldsymbol{\theta} \tag{1.26}$$

where $E_{p(\boldsymbol{\theta}|M)}[\cdot]$ denotes expectation with respect to the prior PDF. Thus, from a Bayesian perspective [23], $P(D|M)$ represents the prior robust probability of the hypothesis that measurements D are obtained from the model class M. The evaluation of Eq. (1.26), which is generally not straightforward, is instrumental in the implementation of, e.g., Bayesian model class selection [271] and model averaging [272].

Likelihood function

The definition of the likelihood function is a central element of Bayesian model updating formulations [53, 55, 115]. In general, as already pointed out, the likelihood function $p(D|M,\boldsymbol{\theta})$ can be construed as a measure of the plausibility of obtaining the set of measurements D for a given model $M(\boldsymbol{\theta})$. For civil engineering structures and systems, such a measure is commonly formulated in terms of the so-called prediction errors, that is, the differences between available measurements and model predictions [53]. In this regard, it is assumed that the available data D comprise n_d measurements associated with different channels of measurements and different time instants, which are contained in a vector $\mathbf{d}^* \in \mathbb{R}^{n_d}$. The corresponding predictions associated with the model $M(\boldsymbol{\theta})$ are denoted by $\mathbf{d}(\boldsymbol{\theta}) \in \mathbb{R}^{n_d}$, whose computation often relies on complex black-box computational procedures. Then, the vector $\mathbf{e}(\boldsymbol{\theta}) \in \mathbb{R}^{n_d}$ comprising the prediction errors for all measurement channels and time instants is defined as [53, 221]

$$\mathbf{e}(\boldsymbol{\theta}) = \mathbf{y}^* - \mathbf{y}(\boldsymbol{\theta}) \tag{1.27}$$

In Eq. (1.27), the measurements $\mathbf{y}^*$ deviate from the actual system responses as a result of, e.g., measurement noise, whereas the predictions $\mathbf{y}(\boldsymbol{\theta})$ cannot perfectly reproduce the actual system behavior due to, for instance, modeling assumptions and numerical accuracy. Then, the likelihood function $p(D|M, \boldsymbol{\theta})$ is established by assigning a distribution to the prediction errors in Eq. (1.27). Typically, a zero-mean normal distribution with covariance matrix $\boldsymbol{\Sigma}$ is adopted, that is,

$$p(D|M, \boldsymbol{\theta}) = \det(2\pi\boldsymbol{\Sigma})^{-\frac{1}{2}} \exp\left(-\frac{1}{2}\left[\mathbf{y}^* - \mathbf{y}(\boldsymbol{\theta})\right]^{\mathrm{T}} \boldsymbol{\Sigma}^{-1} \left[\mathbf{y}^* - \mathbf{y}(\boldsymbol{\theta})\right]\right) \tag{1.28}$$

which corresponds to the maximum entropy distribution for a given mean and covariance matrix [23]. A diagonal covariance matrix comprising the prediction error variances is often assumed, although alternative formulations can be used as well [55]. Furthermore, parameters associated with the probabilistic description of the prediction errors can be also included in the set of model parameters. For example, the covariance matrix in Eq. (1.28) can be taken as $\boldsymbol{\Sigma} = \boldsymbol{\Sigma}(\boldsymbol{\theta})$.

Extension to multiple probabilistic model classes

The previous formulation can be extended to consider a set of N_M probabilistic model classes

$$\mathbf{M} = \{M_k, k = 1, \ldots, N_M\} \tag{1.29}$$

where M_k corresponds to the set of parametrized models $M_k(\boldsymbol{\theta}_k)$ with $\boldsymbol{\theta}_k \in \boldsymbol{\Theta}_k \subset \mathbb{R}^{n_{\theta_k}}$ [271]. The corresponding posterior probabilities are given by

$$P\left(M_k|\mathbf{M}, D\right) = \frac{P(D|\mathbf{M}, M_k)P(M_k|\mathbf{M})}{\sum_{l=1}^{N_M} P(D|\mathbf{M}, M_l)P(M_l|\mathbf{M})}, \quad k = 1, \ldots, N_M \tag{1.30}$$

where $P(M_k|\mathbf{M})$ and $P(D|\mathbf{M}, M_k)$ denote, respectively, the prior probability and the evidence of model class M_k. In this setting, $P(M_k|\mathbf{M})$ measures how plausible is the k-th probabilistic model in the absence of data. Often, an uninformative prior state of knowledge is assumed regarding these probabilities and, thus, $P(M_k|\mathbf{M}) = 1/N_M$, $k = 1, \ldots, N_M$. Further, the evidences $P(D|\mathbf{M}, M_k)$,

$k = 1, \ldots, N_M$, are computed according to Eq. (1.26), which constitutes a challenging task in practical applications [178].

The set $\mathbf{M}$ comprises various hypothesis about the system of interest in terms of, e.g., different assumptions about the underlying physics of the system, alternative definitions of the likelihood function, or diverse parametrization schemes. In this setting, Bayesian model class selection [271] aims to identify the most plausible model class based on the available measurement data. Such a model yields the highest posterior probability according to Eq. (1.30) and, therefore, it can be interpreted as the most likely hypothesis about the system of interest based on available data. Alternatively, the entire set of model classes can be employed in a model averaging treatment [272] to make predictions about the system of interest that are consistent with the different hypothesis and available measurements.

1.3.4 Solution methods for Bayesian model updating problems

Closed-form expressions for $p(\boldsymbol{\theta}|M, D)$ in Eq. (1.25) are not generally available for practical problems. Thus, solution schemes for Bayesian model updating problems aim to characterize the posterior distribution either with explicit approximations or in terms of a set of posterior samples.

To construct explicit approximations for the posterior distribution, Laplace's method of asymptotic approximation is usually adopted [53]. In this framework, the posterior distribution is approximated by a multi-dimensional Gaussian distribution centred at the most probable value of the model parameters. This generally requires identifying the point in the model parameter space that yields the maximum likelihood value and, in addition, to evaluate the Hessian matrix of the likelihood function at that point [53, 215, 273]. As a byproduct of these computations, an approximation of the evidence can be also obtained. Such techniques usually yield satisfactory accuracy for large amounts of data and globally identifiable models [215, 245, 271, 273, 274]. Nevertheless, their implementation faces some challenges in problems with insufficient data or in unidentifiable cases [54, 275]. In these scenarios, the posterior PDF tends to be not very peaked, flat, or multimodal,

which in turn makes the validity of asymptotic approximation assumptions doubtful.

A more general approach for Bayesian model updating corresponds to the use of simulation techniques to obtain samples consistent with the posterior distribution. Standard methods, such as direct MCS [80] and rejection sampling [276], are usually not applicable in practical situations. Hence, MCMC methods [81] are commonly adopted to devise sampling-based Bayesian model updating techniques. In this setting, samples are generated by simulating a Markov chain whose stationary state matches a target distribution such as, e.g., the posterior distribution. In the following, pertinent state-of-the-art sampling-based Bayesian model updating methods are briefly summarized.

Metropolis-Hastings algorithm

The Metropolis-Hastings (M-H) algorithm [88, 89] is possibly the most popular MCMC method. In order to generate a Markov chain with stationary distribution equal to, e.g., $p(\boldsymbol{\theta}|M, D)$, the following procedure is considered. To transition from the current state, $\boldsymbol{\theta}^l$, to the next state, $\boldsymbol{\theta}^{l+1}$, a candidate sample $\boldsymbol{\theta}^{\mathrm{c}}$ is first generated from a proposal distribution $\pi^*(\boldsymbol{\theta}^c|\boldsymbol{\theta}^l)$. Then, the next state of the Markov chain is selected as

$$\boldsymbol{\theta}^{l+1} = \begin{cases} \boldsymbol{\theta}^{\mathrm{c}}, & \text{with probability } \alpha \\ \boldsymbol{\theta}^{l}, & \text{with probability } 1-\alpha \end{cases} \tag{1.31}$$

where the acceptance probability α is given by

$$\alpha = \min\left\{1, \frac{p(\boldsymbol{\theta}^{\mathrm{c}}|M)p(D|M,\boldsymbol{\theta}^{\mathrm{c}})}{p(\boldsymbol{\theta}^{l}|M)p(D|M,\boldsymbol{\theta}^{l})}\frac{\pi^*(\boldsymbol{\theta}^{l}|\boldsymbol{\theta}^{c})}{\pi^*(\boldsymbol{\theta}^{c}|\boldsymbol{\theta}^{l})}\right\} \tag{1.32}$$

It can be shown that the above procedure yields the target distribution independent of the choice of the proposal distribution [89, 277]. Nevertheless, the definition of $\pi^*(\cdot|\cdot)$ has a critical impact on the performance of the M-H algorithm. While this method is relatively simple to implement and has been demonstrated in diverse model updating applications [99, 251, 278–281], it can present difficulties in certain cases, including very peaked or multimodal posterior distributions [178, 263].

Furthermore, the evidence in Eq. (1.26) cannot be directly estimated with this approach.

Transitional Markov chain Monte Carlo

The TMCMC method, initially proposed in [178], is a widely used sampling technique for Bayesian model updating. Following some of the ideas presented in [282], a sequential sampling strategy is adopted to achieve a gradual transition from the prior to the posterior distribution. Specifically, a sequence of non-normalized intermediate distributions is defined as

$$p_j(\boldsymbol{\theta}) \propto p(\boldsymbol{\theta}|M)p(D|M,\boldsymbol{\theta})^{\alpha_j}, \quad j = 0, \ldots, m \tag{1.33}$$

where the exponents α_j conform a monotonically increasing sequence such that $0 = \alpha_0 < \cdots < \alpha_m = 1$. Hence, the samples at the initial stage ($j = 0$) follow the prior distribution, whereas posterior samples are obtained at the final stage ($j = m$). During the j-th stage of the method, samples following the intermediate distribution $p_j(\boldsymbol{\theta})$ are generated using MCMC [81]. In particular, a number of independent Markov chains are generated using the traditional M-H algorithm [88, 89], where the corresponding initial states are samples selected from the previous stage using importance sampling and resampling concepts [178]. The exponents α_j, $j = 0, \ldots, m$, are adaptively chosen to achieve a smooth transition between consecutive distributions. In addition, an estimate of the evidence can be obtained as a byproduct of the sampling process [178, 179].

Several applications have demonstrated the effectiveness and robustness of the TMCMC method [93, 95, 283–285]. Further, the annealing nature of the approach [174] and its parallelization features enable efficient implementation strategies [286–288]. Nevertheless, the method may not be suitable to address problems involving high-dimensional parameter spaces [179].

Hamiltonian Monte Carlo

Hamiltonian Monte Carlo (HMC) [265, 289] relies on an auxiliary conservative Hamiltonian system [290] to establish the transition mechanism in a MCMC framework. Specifically, the model

parameters $\boldsymbol{\theta} \in \mathbb{R}^{n_\theta}$ play the role of *position* variables, whereas an auxiliary vector $\mathbf{p} \in \mathbb{R}^{n_\theta}$ of *momentum* variables is introduced. Although alternative formulations have been proposed [291–293], the Hamiltonian $H(\boldsymbol{\theta}, \mathbf{p})$ is typically defined as [265]

$$H(\boldsymbol{\theta}, \mathbf{p}) = -\ln p(\boldsymbol{\theta}|D, M) + \frac{1}{2}\mathbf{p}^{\mathrm{T}}\boldsymbol{\mathcal{M}}^{-1}\mathbf{p} \tag{1.34}$$

where $\boldsymbol{\mathcal{M}} \in \mathbb{R}^{n_\theta \times n_\theta}$ is a symmetric positive-definite matrix. It can be shown that $\boldsymbol{\theta}$ and $\mathbf{p}$ are statistically independent, $\mathbf{p}$ follows a zero-mean Gaussian distribution with covariance matrix $\boldsymbol{\mathcal{M}}$, and $\boldsymbol{\theta} \sim p(\boldsymbol{\theta}|M, D)$ [294]. The trajectory of the auxiliary system $(\boldsymbol{\theta}, \mathbf{p})$ is determined by

$$\frac{d\boldsymbol{\theta}}{dt} = \frac{\partial H}{\partial \mathbf{p}} \tag{1.35}$$

$$\frac{d\mathbf{p}}{dt} = -\frac{\partial H}{\partial \boldsymbol{\theta}} \tag{1.36}$$

The HMC method is implemented as follows. First, an initial system state is defined in terms of the current value of $\boldsymbol{\theta}$ and an independent realization of $\mathbf{p}$. Then, Eqs. (1.35) and (1.36) are solved to determine the system trajectory using, e.g., the leapfrog algorithm [265, 295]. Finally, the system state at a user-defined time instant t_f defines a candidate sample that is either accepted or rejected. Diverse applications, including high-dimensional cases, have demonstrated the capabilities of the HMC method [94, 263, 296, 297]. Nevertheless, some of its implementation challenges relate to the need for sensitivity information and the appropriate definition of the algorithm parameters.

Bayesian model updating with structural reliability methods

Bayesian model updating with structural reliability methods (BUS) relies on the formulation of an equivalent reliability problem [298]. By introducing a uniform random variable $u \in [0, 1]$, a reliability problem can be defined in terms of an auxiliary failure event F_D as

$$F_D = \{u < c\, p(D|M, \boldsymbol{\theta})\}, \quad \boldsymbol{\theta} \sim p(\boldsymbol{\theta}|M) \tag{1.37}$$

where the so-called likelihood multiplier $c > 0$ must satisfy the inequality [276]

$$c \leq L_{\max}^{-1} = \left(\sup_{\boldsymbol{\theta} \in \boldsymbol{\Theta}} p(D|M, \boldsymbol{\theta}) \right)^{-1} \tag{1.38}$$

From Eqs. (1.37) and (1.38), it can be shown that $p(\boldsymbol{\theta}|F_D) = p(\boldsymbol{\theta}|M, D)$ and $P(D) = c^{-1}P(F_D)$, where $P(F_D)$ is the probability of F_D [298]. Thus, sampling from the posterior distribution $p(\boldsymbol{\theta}|M, D)$, which has an unknown shape, is restated as sampling from a distribution with known shape but unknown support, i.e., the conditional marginal distribution $p(\boldsymbol{\theta}|F_D)$. This insight enables, in principle, the entire battery of structural reliability methods as potential solution techniques for Bayesian model updating problems. Furthermore, since dimension sustainability and application robustness are well-recognized features of sampling-based reliability methods [82, 84], BUS can be an attractive choice for complex identification problems involving high-dimensional parameter vectors.

Diverse applications of BUS have demonstrated its effectiveness; see, e.g., [47, 299–302]. In this regard, the choice of the likelihood multiplier is a crucial aspect. While selecting a value such that $c > L_{\max}^{-1}$ leads to a truncated version of the posterior distribution [303], too small values for c can lead to extremely rare failure events. This parameter can be defined a priori [298] and further complemented by post-processing the resulting failure samples [303], or adaptively chosen during the sampling process [267, 304, 305]. Nevertheless, depending on the quality of the available data, the auxiliary failure domain can present a complex geometry or a very small failure probability.

1.3.5 Remarks

Contaminant source detection in WDNs and the identification of complex structural dynamical systems constitute relevant and challenging tasks in the context of civil engineering structures and systems. In this regard, Bayesian model updating represents a suitable methodology, whereby a rigorous probabilistic framework is adopted for characterizing the unavoidable modeling and measurement uncertainties arising in practical scenarios. While sampling-based approaches can be

viewed as versatile and robust solution techniques, the choice of a particular method is problem-dependent. Some of the relevant features to select a sampling technique comprise the quality and amount of measurement data, the need for estimating the evidence, the feasibility of computing sensitivity measures, available computational resources, the possibility of having a multimodal posterior distribution, and the number of model parameters. Thus, it can be argued that further research is needed to furnish effective solution schemes for the herein discussed challenges. Specifically, sound theoretical formulations must be complemented with efficient numerical implementation strategies to yield meaningful identification results in practical scenarios. Developments in this direction can have a beneficial impact on the data-driven management of civil engineering assets over their lifetime, which can subsequently enhance their efficiency, reliability, and robustness.

1.4 Aims and objectives

This thesis aims to develop effective strategies to address a number of challenges pertaining to the fields of RBDO and model updating of civil engineering structures and systems. In particular, the focus is on the specific topics of RBDO of structural dynamical systems under stochastic excitation, contaminant source detection in WDNs, and model updating of involved structural dynamical systems. Due to the complexity of these systems, the extension and synergetic integration of stochastic simulation methods play an instrumental role in the formulation and implementation of the herein presented developments. Following the previous presentation, six specific objectives are formulated.

- Reliability-based design optimization:

    1. To formulate a stochastic search-based method for constrained RBDO problems involving structural dynamical systems under stochastic excitation.

    2. To extend the method developed in Objective No. 1 to general constrained engineering design problems, including mixed discrete-continuous design spaces.

3. To devise efficient implementation strategies of the stochastic search-based technique for constrained and unconstrained RBDO problems involving continuous, discrete, or mixed discrete-continuous design variables and realistic structural dynamical models under stochastic excitation.

4. To develop an efficient reliability sensitivity assessment framework, in the context of linear structural dynamical systems under Gaussian loading, in order to solve constrained RBDO problems and assess the sensitivity of final designs.

- Model updating:

5. To formulate a sampling-based Bayesian model class selection approach for the solution of contaminant source detection problems in WDNs.

6. To develop an effective sampling-based BUS approach for structural dynamical systems involving high-dimensional parameter spaces and measured response data.

1.5 Contributions

This thesis encompasses six original contributions corresponding to the six specific objectives stated in Section 1.4. These contributions are summarized in the following.

1.5.1 Reliability-based design optimization

Two-phase stochastic optimization technique

The first contribution relates to the development of a stochastic optimization approach to address the constrained RBDO of structural dynamical systems under stochastic excitation (see Objective No. 1). Building on the concept of simulated annealing, the constrained optimization problem is restated as an equivalent Bayesian model updating problem. Specifically, a two-phase solution strategy is proposed. Phase I generates uniformly distributed feasible designs, while Phase II ul-

timately populates a vicinity of the optimum solution set. In both phases, the transitional Markov chain Monte Carlo method is implemented. Numerical results indicate that the approach can effectively handle RBDO problems involving complex nonlinear structural models. The key findings of this study are reported in [181] and presented in Chapter 2.

An extension of the first contribution is introduced to address a class of constrained design optimization problems, including mixed discrete-continuous design spaces (see Objective No. 2). The method does not require special constraint-handling techniques, and relatively few user-defined parameters are needed. Numerical results indicate that the approach constitutes a flexible, efficient and competitive optimization technique for the type of problems under consideration, including cases with multiple local optima, complex feasible design spaces, and discontinuous feasible regions. These results are published in [183] and included in Chapter 3.

The third contribution encompasses efficient implementation strategies, in the context of the two-phase optimization method, to address the RBDO of structural dynamical systems under stochastic excitation (see Objective No. 3). Adaptive sampling techniques are implemented for mixed discrete-continuous design variables, and an adaptive surrogate strategy that fully exploits the annealing nature and parallelization features of the method is adopted to approximate first-passage probabilities. Three application examples involving realistic structural models under stochastic excitation, which have been borrowed from [180–182], demonstrate the performance of the optimization method. The key aspects of the development are reported in [184] and in Chapter 4.

Sensitivity assessment of optimum designs

The fourth reported contribution entails the extension of directional importance sampling, a simulation technique tailored to linear structural systems under Gaussian excitation, as a reliability sensitivity assessment framework in the context of RBDO and optimum design sensitivity assessment (see Objective No. 4). Numerical results indicate that the proposed approach provides a potentially useful tool to address a practical class of design optimization problems. The main features of this

approach are presented in [168] and in Chapter 5.

1.5.2 Model updating

Bayesian model class selection for contaminant source detection

The fifth contribution of this thesis proposes a simulation-based Bayesian model class selection framework to address contaminant source detection problems in WDNs (see Objective No. 5). Specifically, each potential source location is represented as a model class whose corresponding parameters characterize the starting time and intensity of the contamination event. To perform the required calculations, the TMCMC method is appropriately integrated with a suitable WDN simulator. Then, the model class with the highest posterior probability is interpreted as the most plausible source location. Numerical results suggest that the method can provide relevant information for decision making even in cases involving relatively scarce and noisy measurements. The key aspects of this development are reported in [254] and included in Chapter 6.

BUS for structural dynamical systems with high-dimensional parameter spaces

In the sixth contribution, an effective implementation of BUS is developed for problems involving structural dynamical systems, measured response data, and relatively high-dimensional parameter spaces (see Objective No. 6). An adaptive strategy to define the equivalent failure event is proposed, which circumvents the need for prior knowledge on the maximum of the likelihood function, whereas parametric reduced-order models are integrated for an efficient numerical implementation. The main outcomes of the study are presented in [267] and in Chapter 7.

1.6 Structure of the thesis

This thesis is composed of eight chapters, including six independent research articles related to the six contributions discussed in Section 1.5. Specifically, the developments reported for RBDO prob-

lems involving structural dynamical systems under stochastic excitation are presented in Chapters 2 to 5, while Chapters 6 and 7 report those pertaining to model updating problems.

Chapter 1 has an introductory role, provides a general description of the problems of interest and briefly summarizes their key aspects. Further, it states the objectives of the thesis and the corresponding contributions reported in the subsequent chapters.

Chapter 2 presents a two-phase stochastic search technique to address RBDO problems involving structural dynamical systems under stochastic excitation, which relies on the formulation of an equivalent Bayesian model updating problem and a pertinent MCMC method.

Chapter 3 generalizes the two-phase optimization method to address a class of constrained engineering design problems, including mixed discrete-continuous design spaces.

Chapter 4 focuses on implementation strategies to improve the numerical efficiency of the two-phase optimization technique towards the solution of RBDO problems involving structural dynamical systems under stochastic excitation.

Chapter 5 presents a strategy for the efficient RBDO and optimum design sensitivity analysis of stochastic linear structures. This relies on the combination of a sensitivity assessment framework enabled by a specialized sampling technique with pertinent gradient-based solution schemes.

Chapter 6 proposes a Bayesian model class selection approach to address contaminant source detection problems in WDNs, which is solved by means of an advanced simulation method.

Chapter 7 addresses Bayesian model updating of complex structural dynamical systems involving high-dimensional parameter spaces and measured response data. An effective implementation of a sampling-based reliability method is formulated to this end.

Chapter 8 provides some concluding remarks and discusses potential topics for future research.

Chapter 2

A general two-phase Markov chain Monte Carlo approach for constrained design optimization: Application to stochastic structural optimization

A general two-phase Markov chain Monte Carlo approach for constrained design optimization: Application to stochastic structural optimization

H. A. Jensen[b,*], D. J. Jerez[a], M. Beer[a,c,d], J. Chen[e]

[a]*Department of Civil Engineering, Federico Santa Maria Technical University, Valparaiso, Chile*

[b]*Institute for Risk and Reliability, Leibniz Universität Hannover, Callinstr. 34, 30167 Hannover, Germany*

[c]*International Joint Research Center for Reliability Engineering and Stochastic Mechanics, Tongji University, Shanghai 200092, China*

[d]*Institute for Risk and Uncertainty and School of Engineering, University of Liverpool, Liverpool L69 7ZF, UK*

Abstract: This contribution presents a general approach for solving structural design problems formulated as a class of nonlinear constrained optimization problems. A Two-Phase approach based on Bayesian model updating is considered for obtaining the optimal designs. Phase I generates samples (designs) uniformly distributed over the feasible design space, while Phase II obtains a set of designs lying in the vicinity of the optimal solution set. The equivalent model updating problem is solved by the transitional Markov chain Monte Carlo method. The proposed constraint-handling approach is direct and does not require special constraint-handling techniques. The population-based stochastic optimization algorithm generates a set of nearly optimal solutions uniformly distributed over the vicinity of the optimal solution set. The set of optimal solutions provides valuable sensitivity information. In addition, the proposed scheme is a useful tool for exploration of complex feasible design spaces. The general approach is applied to an important class of problems. Specifically, reliability-based design optimization of structural dynamical systems under stochastic excitation. Numerical examples are presented to evaluate the effectiveness of the proposed design scheme.

*Corresponding author

E-mail addresses: danko.jerez@irz.uni-hannover.de (D. J. Jerez), hector.jensen@usm.cl (H. A. Jensen), beer@irz.uni-hannover.de (M. Beer).

Keywords: Constrained optimization; Feasible design space; Meta-models; Markov sampling method; Reliability-based design; Stochastic optimization

2.1 Introduction

Structural optimization by means of mathematical programming techniques has been widely accepted as a viable tool for engineering design. The majority of engineering problems involve constrained optimization. The problem is generally that of minimizing a cost function or maximizing a utility function. The constraints are generally those on resources or demand levels. Thus, the optimal design can be regarded as the best feasible design according to a preselected quantitative measure of effectiveness. Due to the practical importance of this class of problems, the development of efficient constrained optimization algorithms has been an important area of research in engineering design [117, 306]. Generally, constrained optimization algorithms are based on standard optimization schemes or stochastic search algorithms. Though, traditional algorithms are well documented in the literature and extensively used in engineering design, final solutions or designs are usually local optima. In this regard, several global optimization algorithms have been devised, including genetic algorithms, simulated annealing, multi-start algorithms, ant colony optimization, particle swarm optimization, annealing evolutionary stochastic approximation Monte Carlo, etc. [174, 307–310]. One important issue associated with constrained optimization is constraint-handling [311–313]. A number of strategies have been suggested in the context of specific stochastic optimization algorithms such as evolutionary algorithms [314], simulated annealing [315], particle swarm optimization [316], and subset simulation-based algorithm [317]. Although the previous stochastic optimization algorithms have been applied in a number of constrained optimization problems, there is still room for further developments in this area, specially when dealing with involved structural models and complex systems.

In the previous context, it is the objective of this contribution to present a framework for solving structural design problems formulated as nonlinear constrained optimization problems. First, the

optimization problem is set into the framework of a Two-Phase Bayesian model updating problem. Phase I generates designs uniformly distributed over the feasible design space, while Phase II obtains a set of designs lying in the vicinity of the optimal solution set. The corresponding Bayesian model updating problem is solved by the transitional Markov chain Monte Carlo method [178, 179]. The methodology can efficiently explore the sensitivity of final designs and constraints with respect to the design variables in the vicinity of the optimal design. The proposed constraint-handling approach is direct and does not require special constraint-handling techniques. Actually, the same framework for obtaining samples in the vicinity of the optimal solution set is used for obtaining samples in the feasible design space. The proposed Two-Phase approach can be viewed as a generalization of the work presented in [180]. In that work, an optimization scheme was proposed for solving unconstrained optimization problems with applications to performance-based design. Moreover, this work can be interpreted as an additional area of application of simulation-based Bayesian model updating techniques. Though the proposed approach can handle general constrained optimization problems, the focus of this contribution is on the reliability-based design optimization of structural dynamical systems under stochastic excitation. It is noted that solving this class of problems involves estimating the system reliability at different designs during the optimization process which is well-known to be very challenging. Then, an efficient and effective solution of this class of problems is important from the practical viewpoint.

The organization of the paper is as follows. Section 2 describes the class of nonlinear constrained optimization problems to be considered in the present contribution. The main ideas of the proposed Two-Phase scheme are discussed in Section 3. Several aspects associated with the implementation of the proposed optimization scheme are addressed in Section 4. Four numerical examples are provided in Section 5. The paper closes with some conclusions and future research efforts.

2.2 Description of the problem

Consider the following inequality-constrained non-linear optimization problem

$$\begin{aligned} \min_{\mathbf{x}} \quad & c(\mathbf{x}) \\ \text{s.t.} \quad & r_i(\mathbf{x}) \leq 1,\ i = 1, \ldots, n_r \\ & \mathbf{x} \in \mathbf{X} \end{aligned} \tag{2.1}$$

where $\mathbf{x} \in \mathbf{X} \subset R^{n_d}$, x_i, $i = 1, \ldots, n_d$, is the vector of design variables with side constraints $x_i^l \leq x_i \leq x_i^u$, $c(\mathbf{x})$ is the objective or cost function, and $r_i(\mathbf{x}) \leq 1$, $i = 1, \ldots, n_r$ are general design constraints. Note that in the present formulation the set of design variables are assumed to be continuous. The objective function $c(\mathbf{x})$ can be defined in terms of initial, construction, repair or downtime costs, structural weight, general cost functions, expected performance measures, etc. Moreover, the constraints may be associated with design requirements such as geometric conditions, material cost components, demand levels, design specifications characterized by means of different performance measures, including reliability measures. Thus, the above formulation is quite general since different optimization formulations can be considered.

2.3 Optimization strategy

2.3.1 Basic background

An approach based on the transitional Markov chain Monte Carlo method (TMCMC) [178, 286] is considered for solving the constrained optimization problem. The TMCMC method, which corresponds to a class of sequential particle filter methods, has proved to be quite effective in a number of Bayesian model updating problems [24, 25, 115, 162, 178]. In fact, this sampling method is capable of populating the region of interest even in challenging model updating problems. In what follows, and for completeness, some of the fundamental ideas of the TMCMC method are

reviewed. In this context, it is assumed that the structural model is characterized in terms of a set of model parameters $\boldsymbol{\theta}$. The objective of Bayesian model updating is to estimate the posterior probability density function of $\boldsymbol{\theta}$, $f_D(\boldsymbol{\theta})$, given some data D. The method relies on the construction of a series of non-normalized intermediate distributions, $f_{D_j}(\boldsymbol{\theta})$, defined as

$$f_{D_j}(\boldsymbol{\theta}) \propto l_D(\boldsymbol{\theta})^{\alpha_j} f(\boldsymbol{\theta}), \qquad j = 0, 1, \ldots, M \tag{2.2}$$

where $l_D(\boldsymbol{\theta})$ represents the likelihood of observing the data D for a given value of the model parameters $\boldsymbol{\theta}$, $f(\boldsymbol{\theta})$ is the prior distribution representing the initial belief or information about the distribution of $\boldsymbol{\theta}$, and α_j is a parameter that increases monotonically with j such that $\alpha_0 = 0$, and $\alpha_M = 1$. In the first step ($j = 0$), the samples are generated from the prior distribution, while in the last stage ($j = M$) the samples are asymptotically distributed as $f_D(\boldsymbol{\theta})$. Due to the nature and annealing property of the TMCMC method, the samples at the last stage of the updating process tend to maximize the likelihood function $l_D(\boldsymbol{\theta})$. This feature of the TMCMC method establishes a connection between Bayesian model updating problems and the solution of the optimization problem defined in Eq. (2.1). In what follows, such connection is discussed in detail.

2.3.2 Preliminary observations

It is noted that finding the minimum of the objective function $c(\mathbf{x})$ is equivalent to find the maximum of the function $\exp(-c(\mathbf{x})/T)$, for any given value of $T > 0$ [174]. In connection with this result, and treating the design variables as random variables uniformly distributed over the feasible design space $\mathbf{X}_{\text{feasible}}$, where

$$\mathbf{X}_{\text{feasible}} = \{\mathbf{x} \in \mathbf{X} : r_i(\mathbf{x}) \leq 1,\ i = 1, \ldots, n_r\}, \tag{2.3}$$

define the non-normalized auxiliary distribution

$$f_T(\mathbf{x}) \propto \exp\left(-\frac{c(\mathbf{x})}{T}\right) \; I_{\mathbf{X}_{\text{feasible}}}(\mathbf{x}) \tag{2.4}$$

where $I_{\mathbf{X}_{\text{feasible}}}(\mathbf{x})$ is the indicator function of the feasible design space $\mathbf{X}_{\text{feasible}}$, that is, $I_{\mathbf{X}_{\text{feasible}}}(\mathbf{x}) = 1$, for $\mathbf{x} \in \mathbf{X}_{\text{feasible}}$, and $I_{\mathbf{X}_{\text{feasible}}}(\mathbf{x}) = 0$, otherwise. It is seen that $f_T(\mathbf{x})$ becomes flatter as the parameter T increases. In fact, $f_T(\mathbf{x})$ is proportional to $I_{\mathbf{X}_{\text{feasible}}}(\mathbf{x})$ as $T \to \infty$. Moreover, as T decreases and tends to zero, the distribution $f_T(\mathbf{x})$ becomes spikier, and it puts more and more of its probability mass into the set that maximizes the function $\exp(-c(\mathbf{x})/T)$, and therefore the corresponding samples minimize the objective function $c(\mathbf{x})$ (optimal solutions set $\mathbf{X}^*$). Thus, a sample drawn from $f_T(\mathbf{x})$ will be in the vicinity of the optimal solutions set $\mathbf{X}^*$ with a very high probability when T converges to zero [175, 177]. Note that in the previous setting, the design variables are artificially treated as random variables as previously pointed out. Such uncertainty is just a tool for setting the optimization problem in the framework of a Bayesian model updating problem.

2.3.3 Approach: General idea

Based on the previous observations, the basic features of the TMCMC method, and some of the ideas suggested in [175, 177, 180], define a sequence of non-normalized intermediate distributions as

$$f_{T_0}(\mathbf{x}) \propto I_{\mathbf{X}_{\text{feasible}}}(\mathbf{x}) \tag{2.5}$$

$$f_{T_j}(\mathbf{x}) \propto \exp\left(-\frac{c(\mathbf{x})}{T_j}\right) \; I_{\mathbf{X}_{\text{feasible}}}(\mathbf{x}), \quad j = 1, 2, \ldots \tag{2.6}$$

where $\infty = T_0 > T_1 > \ldots > T_j > \ldots$ is a sequence of monotonically decreasing parameters with $T_j \to 0$ as $j \to \infty$. In the context of Section 3.1, the design variables $\mathbf{x}$ correspond to the model parameters $\boldsymbol{\theta}$, the function $\exp(-c(\mathbf{x}))$ takes the role of the likelihood function $l_D(\boldsymbol{\theta})$ with $T_j = 1/\alpha_j$, while $I_{\mathbf{X}_{\text{feasible}}}(\mathbf{x})$ represents the non-normalized prior distribution. Note that the

corresponding prior normalized distribution is the uniform distribution, $U_{\mathbf{X}_{\text{feasible}}}(\mathbf{x})$, defined over the feasible design space. In the framework of the TMCMC method, the parameters $T_j, j = 1, 2, \ldots$ are constructed adaptively in such a way that the distributions $f_{T_j}(\mathbf{x})$ and $f_{T_{j+1}}(\mathbf{x})$ be similar by using different criteria [178, 318, 319].

The iteration starts with the generation of samples (designs) $\mathbf{x}_1^0, \ldots, \mathbf{x}_n^0$ from $I_{\mathbf{X}_{\text{feasible}}}(\mathbf{x})$ in order to populate the feasible design space. The samples at stage $j+1$, i.e. $\mathbf{x}_1^{j+1}, \ldots, \mathbf{x}_n^{j+1}$, $j = 0, 1, \ldots$, are obtained by generating Markov chains as in the TMCMC method. The procedure is repeated until a stopping criterion is satisfied. The idea of the method is to iterate until the parameter T_{j+1} is small enough so that the corresponding samples $\mathbf{x}_1^{j+1}, \ldots, \mathbf{x}_n^{j+1}$ are approximately uniformly distributed over the optimal solution set $\mathbf{X}^*$. The samples at the optimal solutions set represent possible designs with similar values of the objective function $c(\mathbf{x})$. If a single optimal solution is needed, a possible choice based on the samples $\mathbf{x}_1^{j+1}, \ldots, \mathbf{x}_n^{j+1}$ is given by $\mathbf{x}^*$, such that $c(\mathbf{x}^*) = \min_{i=1,\ldots,n} c(\mathbf{x}_i^{j+1})$. The reader is referred to [178, 179, 286] for a detailed implementation of the TMCMC method.

2.3.4 Approach: Phase I

It is seen that the proposed approach requires drawing samples uniformly distributed over the feasible design space $\mathbf{X}_{\text{feasible}}$, that is, designs that verify the side constraints, i.e., $\mathbf{x} \in \mathbf{X}$, and the constraints $r_i(\mathbf{x}) \leq 1$, $i = 1, \ldots, n_r$. This is an involved task since the feasible design space, which is not known in advance, could be quite complex. To overcome this difficulty, the following scheme is devised. Consider the following auxiliary unconstrained optimization problem defined in terms of the constraint functions of the original constrained problem given in Eq. (2.1)

$$\begin{aligned} \min_{\mathbf{x}} \quad & h(\mathbf{x}) \\ \text{s.t.} \quad & \mathbf{x} \in \mathbf{X} \end{aligned} \tag{2.7}$$

where $h(\mathbf{x})$ is an auxiliary objective function defined as

$$h(\mathbf{x}) = \begin{cases} \max_i \{r_i(\mathbf{x})\} & \text{if } \exists\ i:\ r_i(\mathbf{x}) > 1 \\ 1 & \text{if } \forall\ i\ ,\ r_i(\mathbf{x}) \leq 1 \end{cases} \tag{2.8}$$

where $i = 1, \ldots, n_r$. Based on the definition of the auxiliary objective function, it is clear that the minimum value of $h(\mathbf{x})$ is equal to 1, while the corresponding optimum solution set, $\mathbf{X}_h^*$, is given by

$$\mathbf{X}_h^* = \{\mathbf{x} \in \mathbf{X} : r_i(\mathbf{x}) \leq 1,\ i = 1, \ldots, n_r\} \tag{2.9}$$

In other words, the optimum solution set of the auxiliary unconstrained optimization problem is equal to the feasible design space, $\mathbf{X}_{\text{feasible}}$, of the original constrained optimization problem (2.1). Then, the solution of the unconstrained optimization problem (2.7) provides a set of designs in the feasible design space. Note that the auxiliary optimization problem can be solved as indicated in Section 2.3.3, with a sequence of non-normalized intermediate distributions defined as

$$f_{T_0}(\mathbf{x}) \propto U_{\mathbf{X}}(\mathbf{x}) \tag{2.10}$$

$$f_{T_j}(\mathbf{x}) \propto \exp\left(-\frac{h(\mathbf{x})}{T_j}\right) U_{\mathbf{X}}(\mathbf{x}), \quad j = 1, 2, \ldots \tag{2.11}$$

where $U_{\mathbf{X}}(\mathbf{x})$ is the uniform distribution defined over $\mathbf{X}$. Recall that $\mathbf{X}$ is the set that defines the side constraints of the design variables. It is easy to show that all feasible samples generated during the different stages of Phase I are uniformly distributed over $\mathbf{X}_{\text{feasible}}$. Then, the sampling process can be stopped if the total number of feasible samples (designs) reaches a certain pre-determined value n_{target}.

2.3.5 Approach: Phase II

The goal of Phase II is to obtain a set of designs lying in the vicinity of the optimal solution set $\mathbf{X}^*$, associated with the constrained optimization problem (2.1). To this end, and in the context

of the approach proposed in Section 2.3.3, the samples at the initial stage of the updating process, which should be uniformly distributed over the feasible design space $\mathbf{X}_{\text{feasible}}$, are the ones obtained from Phase I. Thus, the Two-Phase framework allows the solution of the general constrained design problem formulated in Eq. (2.1). It is noted that the same framework for obtaining samples in the vicinity of the optimal solution set, that is, Phase II, is used for obtaining samples in the feasible design space, i.e., Phase I. Thus, special constraint-handling techniques are not necessary.

2.4 Implementation aspects

2.4.1 Updating process

The actual updating process is performed in an underlying normal space $\mathbf{Y} \subset R^{n_d}$ of independent standard normal variables. The mapping between the spaces $\mathbf{Y}$ and $\mathbf{X}$, i.e., $\mathbf{x} = \mathbf{x}(\mathbf{y})$ is given by $x_i = x_i(y_i) = x_i^l + \Phi(y_i)(x_i^u - x_i^l)$, $i = 1, \ldots, n_d$, where $\Phi(\cdot)$ is the standard normal cumulative univariate distribution function. Validation calculations have shown that performing the updating process in the underlying standard normal space has some numerical advantages due to normalization and boundedness issues [179, 180]. Note that, however, an implementation of the updating process in the physical design space $\mathbf{X}$ is also possible. Once the problem is set into the space of independent standard normal variables, and based on some of the ideas suggested in [175, 177, 180], the Two-Phase scheme is implemented as follows.

2.4.2 Pseudo-code: Phase I

The following steps are involved in Phase I.

1) Initial stage

Set $j = 0$ ($T_0 = \infty$), and generate samples $\{\mathbf{y}_1^0, \ldots, \mathbf{y}_{n_0}^0\}$ in the underlying standard normal space by Monte Carlo simulation. Compute the auxiliary objective function values $\{h(\mathbf{x}(\mathbf{y}_1^0)), \ldots, h(\mathbf{x}(\mathbf{y}_{n_0}^0))\}$.

2) Determination of T_{j+1}

The criterion to select T_{j+1} is based on the effective sample size technique [318, 319]. This technique measures how similar the non-normalized intermediate distribution f_{T_j} is to $f_{T_{j+1}}$. An estimator of the effective sample size, n_{eff}, is given by $\hat{n}_{eff} = 1/\sum_{i=1}^{n_j} \left(\bar{w}_i^j\right)^2$, where n_j is the number of samples at stage j, and $\bar{w}_i^j$ represents the normalized importance weight of the sample $\mathbf{y}_i^j$ (see Step 3). Based on this estimator, it follows that if the distributions are alike, the effective sample size is close to n_j, while n_{eff} is a small number if the distributions are different. The value of T_{j+1} is chosen by imposing the condition $n_{eff} = \nu n_j$ where $\nu \in (0, 1)$ is a user-defined parameter. This condition gives the following nonlinear equation for T_{j+1}

$$\frac{\sum_{i=1}^{n_j} \exp\left(-2h(\mathbf{x}(\mathbf{y}_i^j))\left[\frac{1}{T_{j+1}} - \frac{1}{T_j}\right]\right)}{\left(\sum_{i=1}^{n_j} \exp\left(-h(\mathbf{x}(\mathbf{y}_i^j))\left[\frac{1}{T_{j+1}} - \frac{1}{T_j}\right]\right)\right)^2} = \frac{1}{\nu n_j} \tag{2.12}$$

The previous nonlinear equation can be solved by any suitable numerical technique.

3) Computation of importance weights

Once the parameter T_{j+1} has been determined, compute the importance weights w_i^j of the samples as

$$w_i^j = \frac{f_{T_{j+1}}(\mathbf{x}(\mathbf{y}_i^j))}{f_{T_j}(\mathbf{x}(\mathbf{y}_i^j))} = \exp\left(-h(\mathbf{x}(\mathbf{y}_i^j))\left[\frac{1}{T_{j+1}} - \frac{1}{T_j}\right]\right), \quad i = 1, \ldots, n_j \tag{2.13}$$

and the corresponding normalized importance weights $\bar{w}_i^j = w_i^j / \sum_{p=1}^{n_j} w_p^j, \quad i = 1, \ldots, n_j$.

4) Generation of samples for stage $j + 1$

The samples from $f_{T_{j+1}}$ are based on the samples from f_{T_j}, and according to the TMCMC scheme, they are obtained by generating Markov chains where the lead samples are selected from the distribution f_{T_j}. The lead sample of the Markov chain is a sample from the previous step, e.g. $\mathbf{y}_l^j$, which is selected according to its normalized weight [178]. Each Markov chain is generated by applying the Metropolis-Hastings algorithm [88, 89]. The corresponding proposal probability density func-

tion is a Gaussian distribution centered at the previous sample of the chain and with covariance matrix $\mathbf{\Sigma}_j$ equal to a scaled version of the estimate covariance matrix of the current intermediate distribution f_{T_j}, that is, $\mathbf{\Sigma}_j = \beta^2 \sum_{i=1}^{n_j} \bar{w}_i^j \left(\mathbf{y}_i^j - \bar{\mathbf{y}}^j\right)\left(\mathbf{y}_i^j - \bar{\mathbf{y}}^j\right)^T$, $\bar{\mathbf{y}}^j = \sum_{i=1}^{n_j} \bar{w}_i^j \mathbf{y}_i^j$, where β^2 is a parameter that can be chosen according to different criteria. For example, it can be defined directly by the user or by an adaptive scheme based on the acceptance rate of the sampling process [179, 288].

5) Stopping criterion

At stage $j+1$, identify all samples $\{\mathbf{y}_1, \ldots, \mathbf{y}_m\}$ generated during the previous stages of the updating process, such that $h(\mathbf{x}(\mathbf{y}_i)) = 1, i = 1, \ldots, m$. If $m \geq n_{\text{target}}$ stop the process and continue to Phase II where the samples $\{\mathbf{y}_1, \ldots, \mathbf{y}_m\}$ are used at the initial stage. If $m < n_{\text{target}}$, return to step 2 with $j \leftarrow j+1$.

2.4.3 Pseudo-code: Phase II

The following steps are involved in Phase II.

1) Initial stage

Set $j = 0$ ($T_0 = \infty$). The initial samples of the process, uniformly distributed over the feasible design space $\mathbf{X}_{\text{feasible}}$, are the designs obtained during Phase I. Compute the objective function values $\{c(\mathbf{x}(\mathbf{y}_1^0)), \ldots, c(\mathbf{x}(\mathbf{y}_{n_0}^0))\}$, where $n_0 = m$. Next, compute the corresponding coefficient of variation (c.o.v.) of these samples as

$$\delta_0 = \sqrt{\frac{1}{n_0 - 1} \sum_{i=1}^{n_0} \left[c(\mathbf{x}(\mathbf{y}_i^0)) - \left(\frac{1}{n_0} \sum_{p=1}^{n_0} c(\mathbf{x}(\mathbf{y}_p^0)) \right) \right]^2} \Bigg/ \frac{1}{n_0} \sum_{p=1}^{n_0} c(\mathbf{x}(\mathbf{y}_p^0)) \tag{2.14}$$

2) Initial information for stopping criterion

Set $\delta_{target} = \gamma \delta_0$, where γ is a user-defined parameter, and δ_{target} is the target c.o.v. of the objective function values. Alternatively, the stopping criterion can be defined in terms of a pre-determined maximum number of stages $j_{\max}$.

3) Determination of T_{j+1}

As in Phase I, the criterion to select T_{j+1} is based on the effective sample size technique [318, 319]. Thus, the value of T_{j+1} is chosen to satisfy the nonlinear equation

$$\frac{\sum_{i=1}^{n_j} \exp\left(-2c(\mathbf{x}(\mathbf{y}_i^j))\left[\frac{1}{T_{j+1}}-\frac{1}{T_j}\right]\right)}{\left(\sum_{i=1}^{n_j} \exp\left(-c(\mathbf{x}(\mathbf{y}_i^j))\left[\frac{1}{T_{j+1}}-\frac{1}{T_j}\right]\right)\right)^2} = \frac{1}{\nu n_j} \tag{2.15}$$

where n_j is the number of samples at stage j, and $\nu \in (0,1)$ is as before, a user-defined parameter.

4) Computation of importance weights

The importance weight w_i^j of the sample $\mathbf{y}_i^j$ is defined as

$$w_i^j = \exp\left(-c(\mathbf{x}(\mathbf{y}_i^j))\left[\frac{1}{T_{j+1}}-\frac{1}{T_j}\right]\right), \quad i=1,\ldots,n_j \tag{2.16}$$

with normalized importance weight $\bar{w}_i^j = w_i^j / \sum_{p=1}^{n_j} w_p^j, \quad i=1,\ldots,n_j$.

5) Generation of samples for stage $j+1$

The generation of samples at each step proceeds in a similar manner as in step 4 of Phase I. However, in this case, the candidate sample generated in the context of the Metropolis-Hasting algorithm should belong to the feasible design space $\mathbf{X}_{\text{feasible}}$. If not, the sample is rejected.

6) Stopping criterion

Compute the sample c.o.v. of the objective function values at the $(j+1)$-th stage, δ_{j+1}, as

$$\delta_{j+1} = \sqrt{\frac{1}{n_{j+1}-1}\sum_{i=1}^{n_{j+1}}\left(c(\mathbf{x}(\mathbf{y}_i^{j+1})) - \left[\frac{1}{n_{j+1}}\sum_{p=1}^{n_{j+1}} c(\mathbf{x}(\mathbf{y}_p^{j+1}))\right]\right)^2} \Bigg/ \frac{1}{n_{j+1}}\sum_{p=1}^{n_{j+1}} c(\mathbf{x}(\mathbf{y}_p^{j+1})) \tag{2.17}$$

If $\delta_{j+1} \geq \delta_{target}$, set $j \leftarrow j+1$ and return to Step 3. Otherwise, set $M = j+1$ and stop the process. Obtain the sample-based optimum design $\mathbf{x}^*$, and the corresponding objective function

value as $c(\mathbf{x}^*) = \min_{i=1,\ldots,n_M} c(\mathbf{x}(\mathbf{y}_i^M))$. Alternatively, the optimization process can be stopped if a maximum number of stages $j_{\max}$ has been reached as indicated in step 2. It is noted that other stopping criteria could be also implemented.

2.4.4 Practical observations

As previously pointed out, all feasible samples generated during Phase I are used at the initial stage of Phase II. Additionally, these samples can also be used to explore the feasible design space in a direct manner. This information can give valuable insight into the optimization problem, especially when the design variables exhibit a complex interaction between them. Moreover, the information from the uniformly distributed samples could also be used in connection with other optimization techniques. For example, the best design among the samples generated in Phase I can be used as the initial design in gradient-based optimization schemes such as interior point algorithms. Finally, it is noted that the best solution from Phase I could also be used as an approximation of the solution to the original optimization problem (2.1). In this case, the accuracy of the solution should be studied in detail.

2.4.5 Additional implementation issues

High performance computing (HPC) techniques at the computer hardware level can be considered for increasing the computational efficiency of the proposed Two-Phase approach. In fact, recall that the proposed optimization process, which is based on the TMCMC method, is suitable for a parallel implementation in a HPC environment. The first stage of Phase I, which corresponds to direct Monte Carlo simulation, can be fully scheduled in parallel. In addition, each of the subsequent stages of Phases I and II produces a set of Markov chains that are perfectly parallel. Thus, a number of computer workers can handle the generation of samples corresponding to the different chains [286, 320].

2.4.6 Final remarks

Some of the benefits and advantages of using the proposed optimization scheme can be summarized as follows. First, the proposed optimization scheme is based on a well-developed and widely used updating technique (TMCMC method). Thus, the same framework can be adapted for an effective optimization scheme. Second, the methodology produces a set of nearly optimal solutions instead of a single optimal solution. This feature can be advantageous in many practical cases where additional considerations or alternative criteria can be taken into account to select the appropriate final design. Thus, the approach provides flexibility to the decision-making process. Third, due to the theoretical basis of the approach, it has high chances to reach the vicinity of the global optimum in an effective manner, even in presence of multiple local optima. Fourth, the scheme is a useful tool for exploration of complex feasible design spaces. This is especially useful when design variables exhibit a complex interaction between them. Fifth, the proposed approach provides valuable sensitivity information. In fact, sensitivity of the feasible designs and the final design with respect to the design variables can be obtained directly. Sixth, generally, problems with multiple discontinuous sub-feasible regions can be handled in an effective manner. Seventh, the technique is very-well suited for parallel implementation in a computer cluster. This is extremely important when dealing with optimization problems involving expensive function evaluations such as reliability-based optimization problems. Eight, the proposed constraint-handling technique is direct. Actually, samples in the feasible design space are obtained from the solution of an unconstrained optimization problem which is directly defined in terms of the constraint functions of the original problem. The same framework for obtaining samples in the vicinity of the optimal solution set is used for solving the unconstrained optimization problem. Thus, special constraint-handling techniques are not necessary. This is an advantage from a practical viewpoint. Ninth, due to the generality and flexibility of the formulation, it can handle, in principle, different types of optimization problems. From the structural point of view, these problems may include complex linear and nonlinear systems. Tenth, the proposed framework can handle in a rational and consequent manner problems involving noisy

objective or constraint functions (noisy optimization problems), e.g., general performance-based or reliability-based design optimization problems. Finally, the feasibility of solving general constrained optimization problems in the framework of a Bayesian model updating problem provides an additional technique for solving this type of problems.

2.5 Numerical examples

It is noted that due to the generality of the proposed approach, a number of optimization problems can be considered as potential examples. As previously pointed out, the focus of this contribution is on the application of the proposed optimization scheme to the reliability-based design optimization of structural dynamical systems under stochastic excitation. Solving this class of problems involves estimating the system reliability at different designs during the optimization process which is well-known to be very challenging from a numerical point of view. In addition, complex physical interactions between the design variables can be obtained, and consequently, involved feasible design spaces can be generated. Therefore, this is an ideal scenario to evaluate the performance of the proposed optimization scheme. First, two test problems are presented to illustrate the performance of some of the features of the proposed scheme. Specifically, the efficiency of Phase I in relatively complex feasible design spaces is considered. Then, the effectiveness of the optimization algorithm is demonstrated by two application problems involving the reliability-based optimization of structural dynamical systems under stochastic excitation. The following parameter values of the proposed approach are considered for numerical implementation: $\gamma = 0.05$ (stopping criterion parameter); and $\nu = 0.5$ (effective sample size parameter). In addition, the scaling parameter β is determined by an adaptive scheme that monitors the acceptance rate of the updating process with initial value equal to $\beta = 0.1$ [288]. These values have proved to be adequate in the context of this work.

2.5.1 Test problem 1

The objective of this test problem is to demonstrate the performance of Phase I in generating samples uniformly distributed over the feasible design space. To focus only on this aspect of the proposed implementation, the optimization problem is defined in terms of analytical functions. The constrained optimization problem takes the form

$$\begin{aligned} \min_{\mathbf{x}} \quad & c(\mathbf{x}) \\ \text{s.t.} \quad & r_i(\mathbf{x}) \leq 1, \ i = 1, \ldots, 4 \\ & 2.0 \leq x_1 \leq 7.0 \\ & 0.5 \leq x_2 \leq 5.5 \end{aligned} \tag{2.18}$$

where $c(\mathbf{x})$ is an arbitrary objective function, and

$$\begin{aligned} r_1(\mathbf{x}) &= 2.0 - \frac{x_1^2 x_2}{20} \\ r_2(\mathbf{x}) &= 2.0 - \frac{93.0}{x_1^2 + 8.0x_2 + 5.0} \\ r_3(\mathbf{x}) &= 2.0 - \frac{(x_1 + x_2 - 10.0)^2}{30.0} - \frac{(x_1 - x_2 + 10.0)^2}{120.0} \\ r_4(\mathbf{x}) &= (0.906x_1 + 0.423x_2 - 6.0)^2 + (0.906x_1 + 0.423x_2 - 6.0)^3 - \\ & 0.6(0.906x_1 + 0.423x_2 - 6.0)^4 - (-0.423x_1 + 0.906x_2) \end{aligned} \tag{2.19}$$

Figure 2.1 presents the corresponding feasible design space. The evolution of the samples during the different stages of Phase I is shown in Figure 2.2. At each stage, 1000 samples are considered for illustration purposes. The number of feasible designs generated at the first three stages are 424, 887 and 1000, respectively. Among them, a total of 980 designs are different. Thus, after three stages, almost 1000 different samples uniformly distributed over the feasible design space are obtained. Such samples are shown in Figure 2.3. By comparing Figures 2.1 and 2.3, it is observed that the samples populate the feasible design space in an effective manner.

To get more insight into the updating process of Phase I, the marginal conditional distributions of

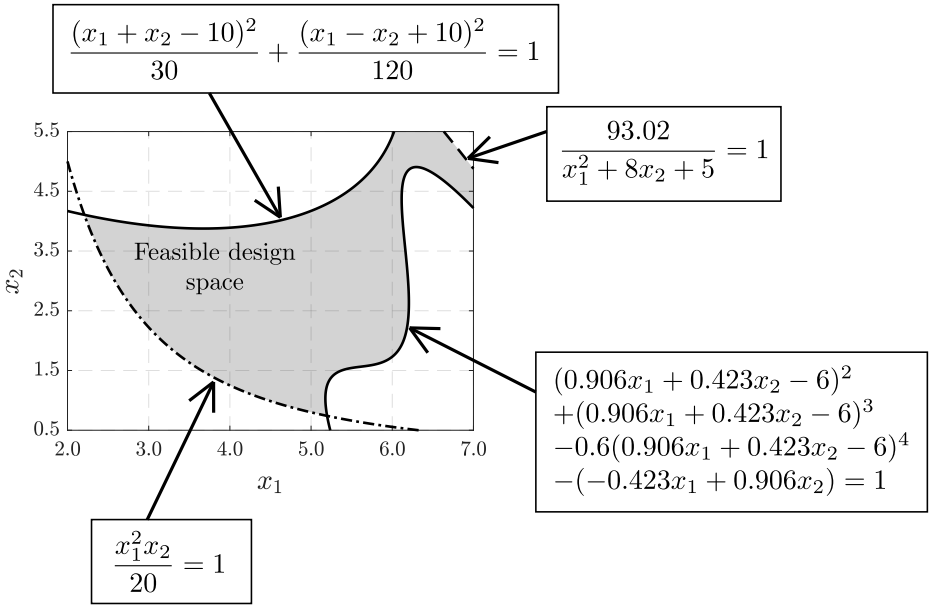

Fig. 2.1: Feasible design space of Test Problem 1.

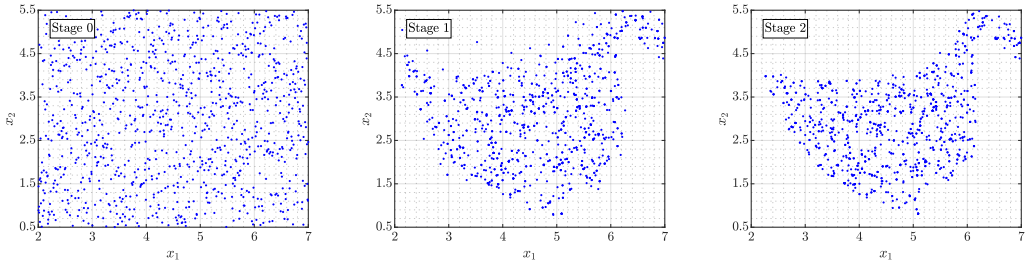

Fig. 2.2: Samples generated at different stages of Phase I. Test Problem 1.

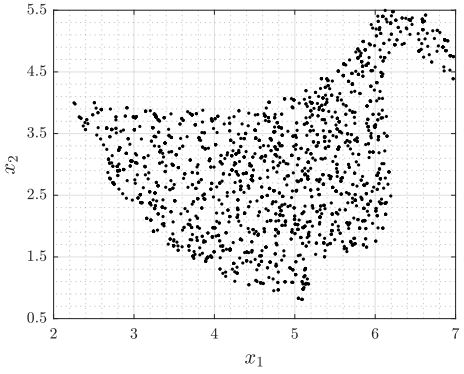

Fig. 2.3: Samples uniformly distributed over the feasible design space. Test Problem 1.

the samples lying in the feasible design space at the final stage of Phase I are shown in Figure 2.4. The histograms are compatible with the distribution of the samples in the feasible design space, as expected. These samples could be used at the initial stage of Phase II for the purpose of solving the

optimization problem formulated in Eq. (2.18), as previously pointed out.

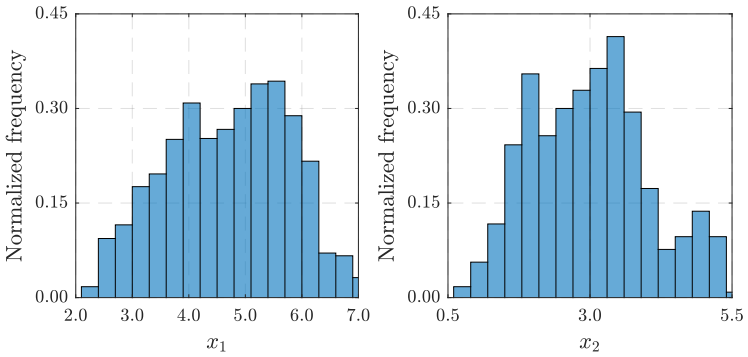

Fig. 2.4: Conditional marginal histograms of the samples obtained at the last stage of Phase I. Test Problem 1.

2.5.2 Test problem 2

As in the first test problem, the objective is to illustrate the performance of Phase I. To this end, consider the constrained optimization problem of the form

$$\begin{aligned} \min_{\mathbf{x}} \quad & c(\mathbf{x}) \\ \text{s.t.} \quad & r(\mathbf{x}) \leq 1 \\ & -3.0 \leq x_1 \leq 3.0 \\ & -3.0 \leq x_2 \leq 3.0 \end{aligned} \tag{2.20}$$

where $c(\mathbf{x})$ is an arbitrary objective function, and the constraint function r is given by the so-called six-hump camel-back function, i.e.,

$$r(x_1, x_2) = 1 + 4.0x_1^2 - 2.1x_1^4 + x_1^6/3.0 + x_1x_2 - 4.0x_2^2 + 4.0x_2^4 \tag{2.21}$$

Figure 2.5 shows the corresponding feasible design space which is a disconnected region. The evolution of the samples during the different stages of Phase I is shown in Figure 2.6. One thousand samples are considered at each stage. After five stages, more than 2000 feasible samples are obtained. Observing the last figure (feasible samples), it is seen that the samples populate the feasible

design space in a rather efficient manner.

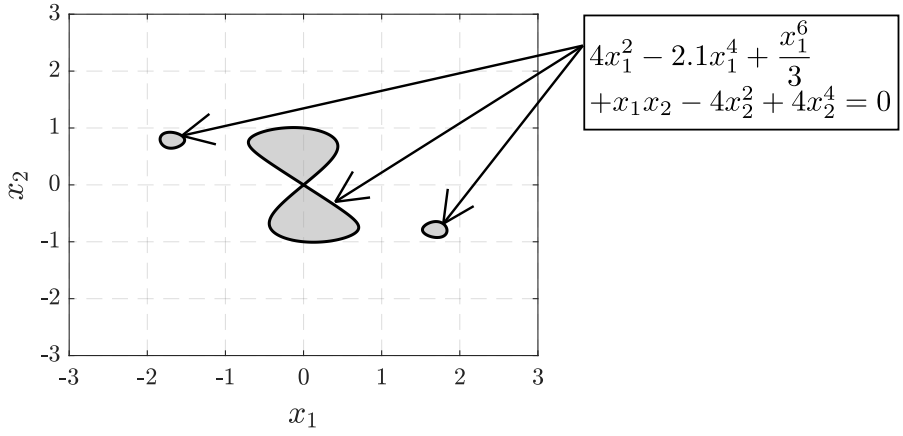

Fig. 2.5: Feasible design space of Test Problem 2. Disconnected region.

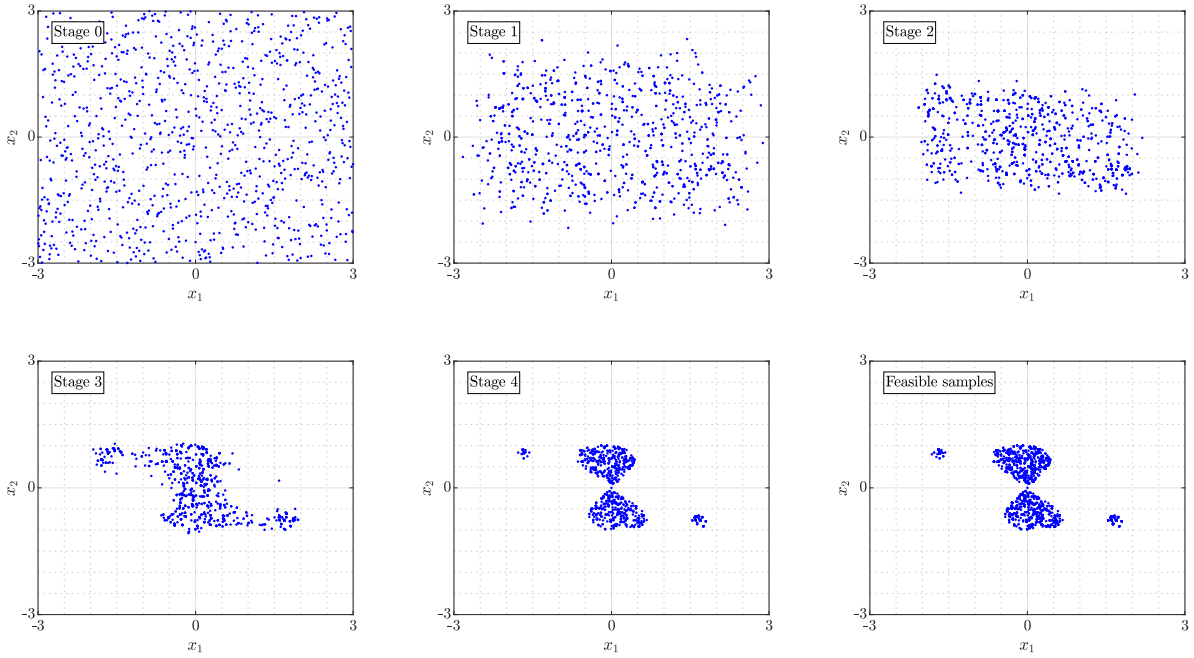

Fig. 2.6: Samples generated at different stages of Phase I. Disconnected region. Test Problem 2.

Another interesting case, where the feasible design space is a region containing interior holes, is

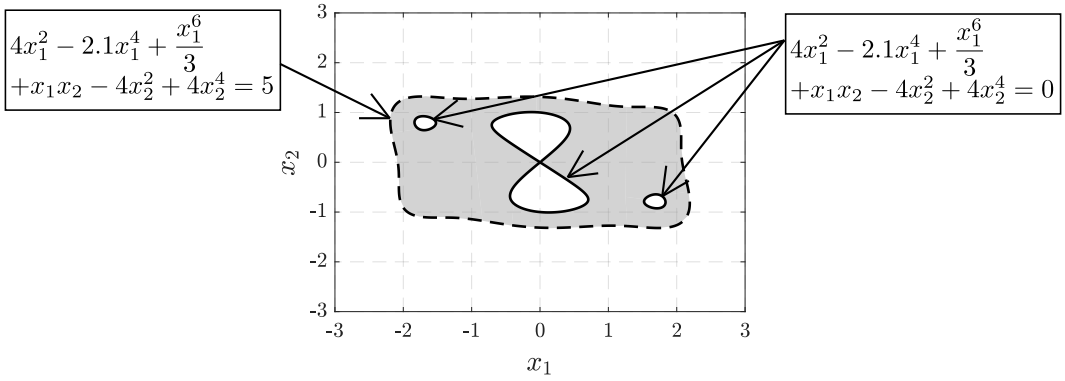

Fig. 2.7: Feasible design space of Test Problem 2. Region with interior holes.

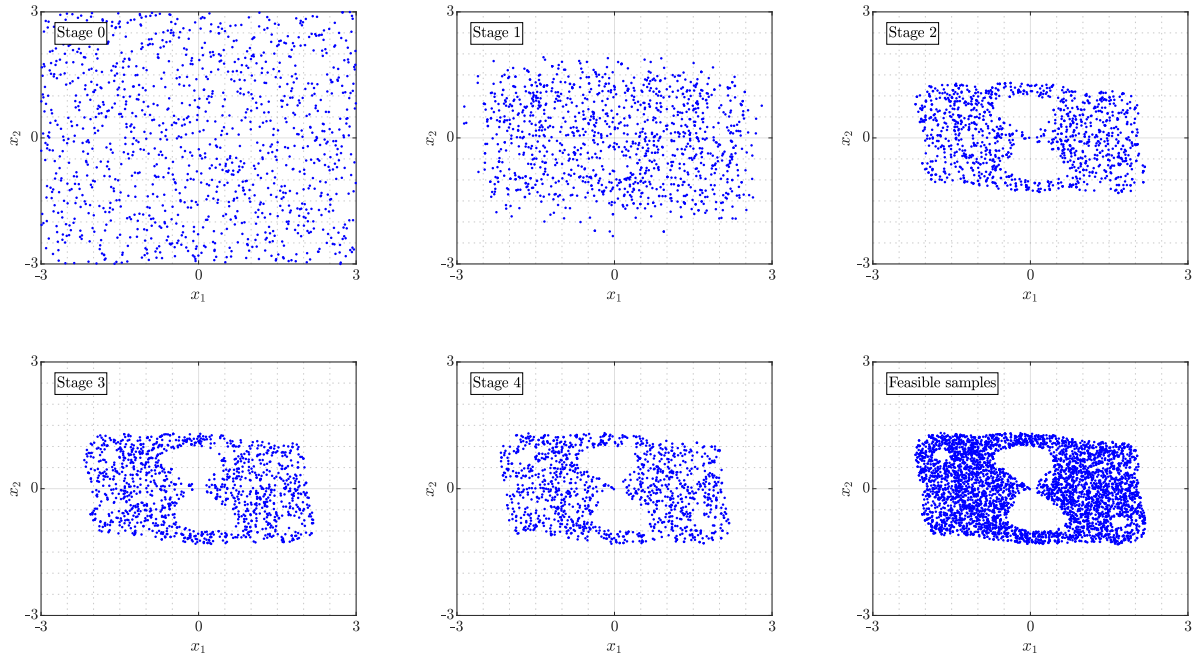

Fig. 2.8: Samples generated at different stages of Phase I. Region with interior holes. Test Problem 2.

given by the problem

$$\begin{aligned} \min_{\mathbf{x}} \quad & c(\mathbf{x}) \\ \text{s.t.} \quad & r_1(\mathbf{x}) \leq 1 \\ & r_2(\mathbf{x}) \leq 1 \\ & -3.0 \leq x_1 \leq 3.0 \\ & -3.0 \leq x_2 \leq 3.0 \end{aligned} \tag{2.22}$$

where $r_1(\mathbf{x}) = 2.0 - r(\mathbf{x})$, and $r_2(\mathbf{x}) = r(\mathbf{x}) - 5.0$. The feasible design space and the evolution of

the samples during the different stages of Phase I are shown in Figures 2.7 and 2.8, respectively. As in the previous cases, it is clear that the samples occupy the feasible design space in an effective way (see feasible samples figure). The previous results, together with additional validation calculations, show the effectiveness of Phase I in populating feasible design spaces, even for complex geometries such as disconnected regions and regions containing interior holes. Finally, it is noted that the different quantities involved in the test problems are analytical functions which are inexpensive to evaluate. Thus, the corresponding numerical effort for populating the feasible design spaces is not relevant in the context of these examples.

2.5.3 Application problem 1

Model description

A simple two degree of freedom system subject to stochastic excitation is considered in this application. The model, which is shown in Figure 2.9, is characterized by normalized masses m_1 and m_2, and normalized stiffnesses k_1 and k_2, which are the parameters to be controlled during the design process. Additionally, 5% of critical damping is added to the model. Though the model is relatively simple from a structural viewpoint, complex interactions between the design variables can be obtained.

The system is subjected to a base acceleration $\ddot{u}_g(t)$, which is modeled as a non-stationary stochastic process. In particular, a stochastic model based on a point-source model is considered [114]. Based on this model, the base acceleration can be expressed as $\ddot{u}_g(t, \mathbf{z})$, where $\mathbf{z} \in \mathbf{Z} \subset R^{n_z}$ is a vector of uncertain parameters involved in the characterization of the excitation. The duration of the excitation is taken as $t_T = 10$s, with a sampling interval equal to $\Delta t = 0.01$s. According to these values, it can be shown that the generation of ground motion samples comprises more than 1000 random variables [114, 133]. A detailed description and implementation of the stochastic excitation model can be found in [34, 114, 321].

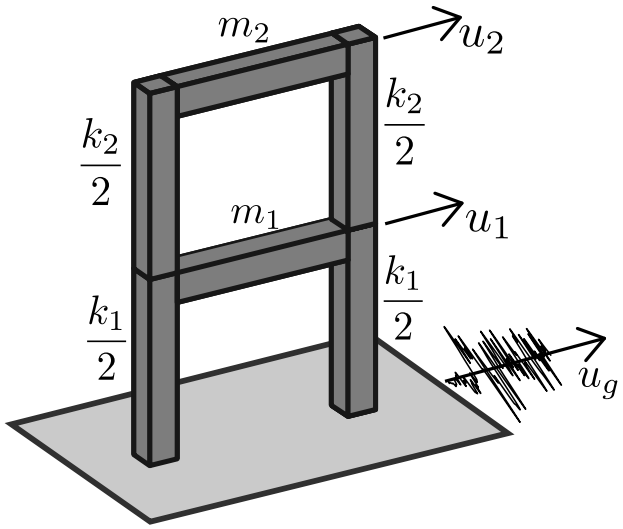

Fig. 2.9: Two-degree-of-freedom system.

Optimization problem

The design problem is written in the form

$$\begin{aligned} \min_{\mathbf{x}} \quad & c(\mathbf{x}) \\ \text{s.t.} \quad & x_2/x_1 \leq 1 \\ & P_F(\mathbf{x})/10^{-2} \leq 1 \\ & 1.0 \leq x_i \leq 5.0,\ i = 1, 2 \end{aligned} \tag{2.23}$$

where $x_i, i = 1, 2$ are the design variables, that is, $x_1 = k_1$ and $x_2 = k_2$, and $P_F(\mathbf{x})$ is the system failure probability evaluated at the design $\mathbf{x}$. For illustration purposes, the objective function is assumed to be proportional to the stiffnesses k_1 and k_2. In particular, $c(\mathbf{x}) = (x_1 + x_2)/10$. The failure probability $P_F(\mathbf{x})$ is defined in terms of a failure event associated with the interstory drifts and the total accelerations at the first and second floor. The characterization of the failure event and the corresponding reliability problem is provided in Appendix A (see Section 2.7). It is noted that the estimation of the probability of failure for a given design, i.e., $P_F(\mathbf{x})$, constitutes a high-dimensional problem which is extremely demanding from a numerical point of view. Such quantity is usually estimated by advanced simulation techniques [133, 138, 141].

Results

The related iso-probability curves are shown in Figure 2.10. These curves are constructed by using a set of failure probability estimates distributed over the design space. The estimates are obtained by Subset simulation [133]. The resulting curves, which are rather rugged because of the variability of the probability estimates, have been smoothed for presentation purposes. The corresponding feasible design space is sketched in Figure 2.11, where some contour curves of the objective function are also shown as well as the optimal design. Due to the responses involved in the definition of the failure event, a highly complex interaction between the design variables is observed.

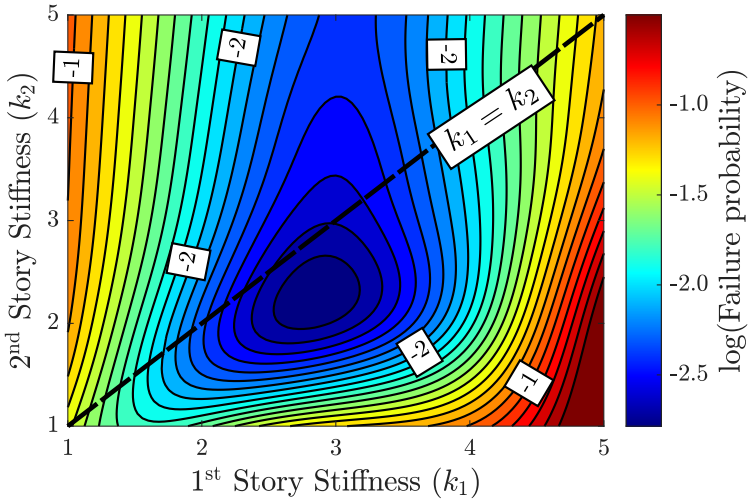

Fig. 2.10: Iso-probability curves. Application Problem 1.

The evolution of the samples during the different stages of Phase I is shown in Figure 2.12. At each stage, 500 samples are considered for illustration purposes. After three stages, more than 500 different feasible designs are generated. These samples, which are uniformly distributed over the feasible design space, are shown in Figure 2.13. Note that the shape generated by these samples shows an excellent agreement with the feasible design space shown in Figure 2.13.

Next, the minimization problem formulated in Eq. (2.23) is solved by the proposed Phase II, where the number of samples per stage is set equal to 500. The samples obtained from the first five

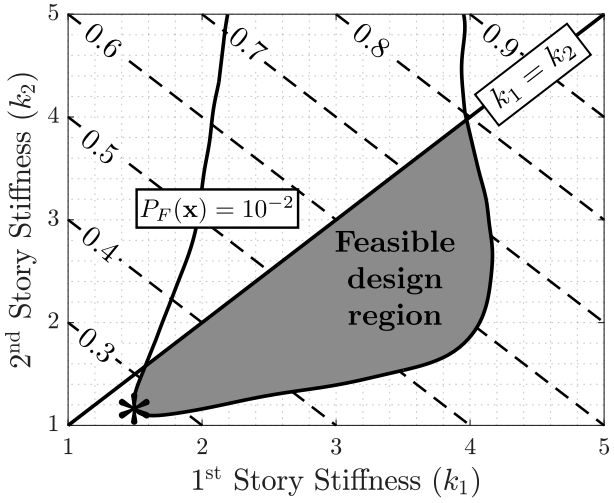

Fig. 2.11: Sketch of the feasible design space, some contour curves of the objective function, and optimal design ($*$). Application Problem 1.

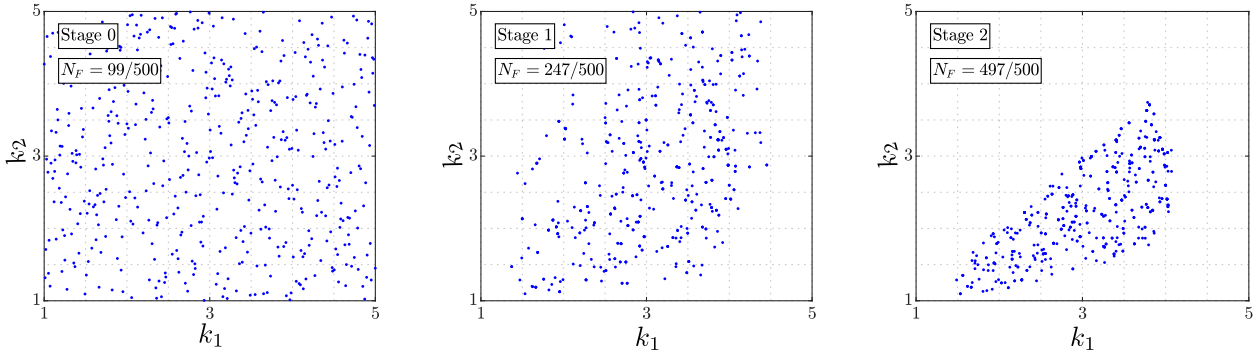

Fig. 2.12: Evolution of samples generated at different stages of Phase I. Application Problem 1.

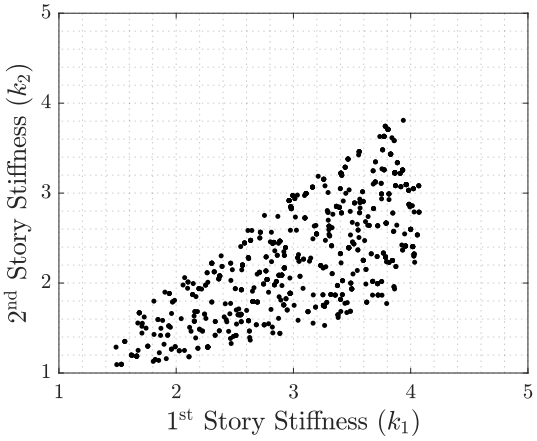

Fig. 2.13: Samples uniformly distributed over the feasible design space. Application Problem 1.

stages are shown in Figure 2.14. At the last stage, the samples populate a vicinity of the optimal solution set, which is consistent with Figure 2.11. The range of the objective function values obtained during the different stages is shown in Figure 2.15. The minimum value obtained during the simulation process (sample-based optimum cost) is equal to 0.25, which is associated with the design $k_1 = 1.43$ and $k_2 = 1.10$, and corresponding reliability constraint value $P_F/10^{-2} = 0.96$, and geometric constraint $x_2/x_1 = 0.74$. Considering the variability involved in the estimation of the probability of failure, the reliability constraint can be considered as active at the final design. Note that this result is compatible with the information provided by Figure 2.11.

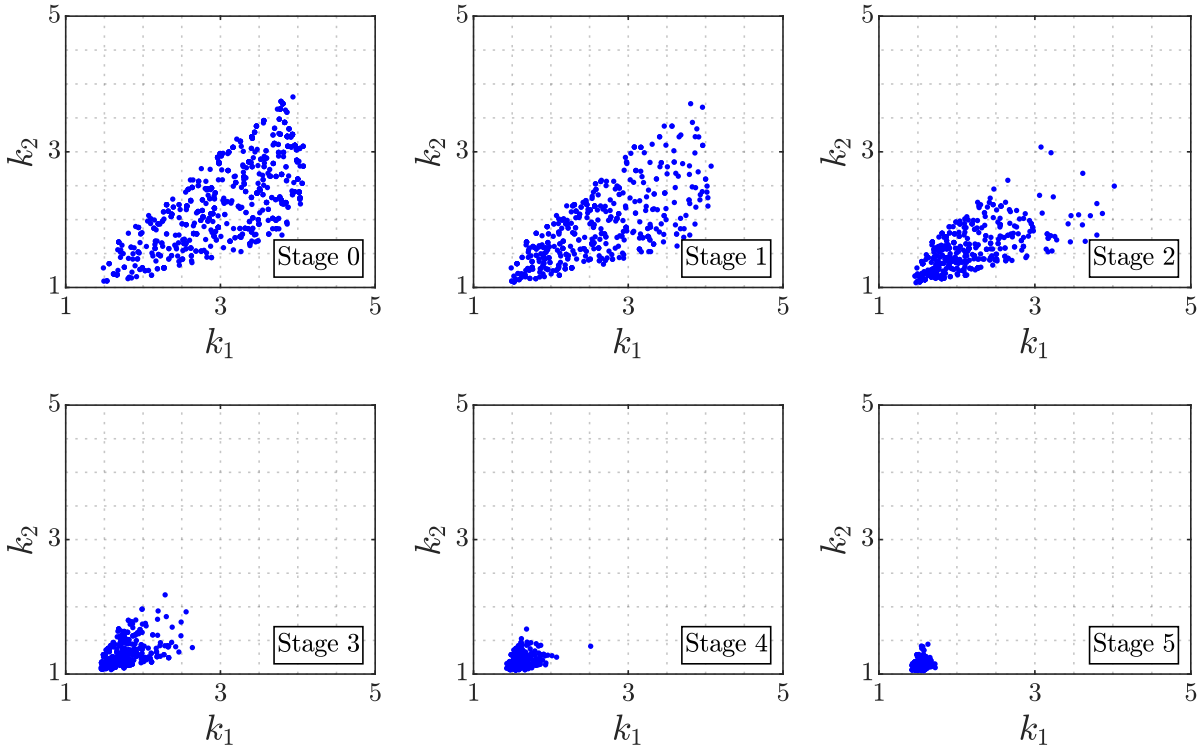

Fig. 2.14: Evolution of samples generated at different stages of Phase II. Application Problem 1.

Finally, observing Figure 2.15, it is seen that the minimum value of the objective function at Stage 0 of Phase II, i.e., at the designs uniformly distributed over the feasible design space, is relatively close to the sample-based optimal cost, i.e., minimum value of the objective function at Stage 5. Thus, the best solution among the samples generated during Phase I gives a good approximation for the value of the objective function at the final design in this case. It is noted that however,

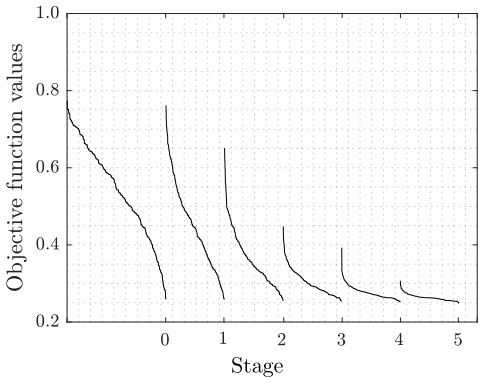

Fig. 2.15: Objective function values at different stages of Phase II. Application Problem 1.

Phase II can provide valuable information about the sensitivity of the final design with respect to the design variables in the vicinity of the final design. This information is quite relevant, specially when dealing with several design variables and complex feasible design spaces.

Numerical effort and comparison

Considering that the total number of sampling stages involved in the optimization process is equal to 8, and that 500 samples are used per stage, the total number of function evaluations is equal to 4000. In this regard, it is noted that a study about the statistical performance of the proposed design scheme in this example problem indicates that the scheme performs in an effective manner even when the number of samples per stage is much smaller than 500. Recall that this number was used only for illustration purposes, as previously pointed out. In other words, the algorithm is capable to obtain the optimal solution set in an effective manner with a relatively small number of samples per stage. Thus, the number of function evaluations (reliability estimates) indicated before overestimates the actually required number.

The comparison of the performance of the proposed optimization scheme with respect to some alternative methods is provided in Table 2.1. In particular, the following stochastic optimization algorithms are considered: genetic algorithm based on dominance-based tournament selection (GAS) [311]; subset simulation-based optimization (SSBO) [317]; co-evolutionary particle swarm optimization (CPSO) [322]; hybrid particle swarm optimization with a feasibility-based rule (HYP-

SOR) [323]; genetic algorithm based on a co-evolution model (GAC) [324]; and harmony search (HS) [325]. The second column of the table corresponds to the function-call factor which is the ratio of the number of function evaluations involved in a given algorithm and the number of function evaluations involved in the proposed scheme. The algorithms were calibrated, in terms of the number of function calls, in such a way that similar final designs were obtained.

Table 2.1: Comparison of numerical efforts with respect to alternative algorithms.

Algorithm	Function-call factor
GAS	6.1
SSBO	6.2
CPSO	14.1
HYPSOR	6.1
GAC	64.1
HS	6.1
Proposed	1.00

It is seen that the proposed algorithm compares very favorably with respect to the other population-based stochastic optimization algorithms for this example problem. The algorithm needs the least number of reliability analyses to solve the problem. In fact, the proposed scheme requires less than one sixth of the function calls involved in the other methods.

2.5.4 Application problem 2

Structural model

A finite element model with about 50000 degrees of freedom is analyzed in the second application problem. The model consists of a non-linear 52-story building under stochastic earthquake excitation. An isometric view of the structural system is shown in Fig. 2.16. The plan view and the dimensions of each floor are shown in Fig. 2.17. The inter-story height is 3.6 m for all floors except the first one which has a height of 14 m.

The building has a reinforced concrete core of shear walls and a reinforced concrete perimeter moment frame as shown in Fig. 2.17. The columns in the perimeter have a circular cross section.

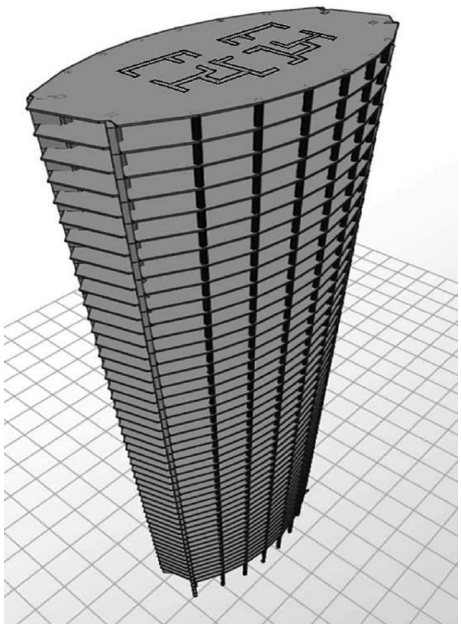

Fig. 2.16: Isometric view of the 52-story building model.

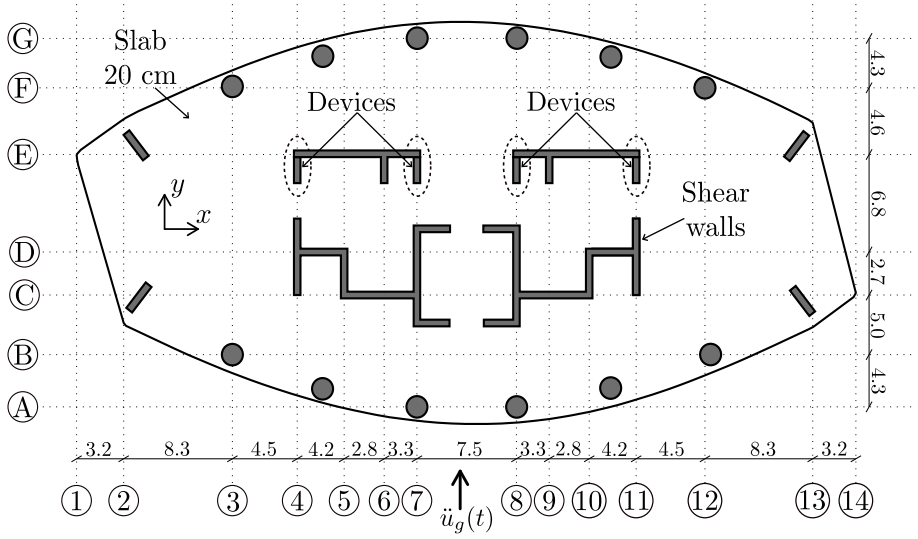

Fig. 2.17: Floor plan of the 52-story building model.

The nominal value for the column's diameter and shear wall's thickness is 0.40 m. In addition, the slab thickness is equal to 0.20 m. Properties of the reinforced concrete have been assumed as follows: Young's modulus $E = 2.45 \times 10^{10}$ N/m^2, Poisson's ratio $\mu = 0.3$, and mass density $\rho = 2500$ kg/m^3. For the dynamic analysis, it is assumed that each floor may be represented as rigid within the plane when compared with the flexibility of the other structural components. Then, the

degrees of freedom of the finite element model are linked to three degrees of freedom per floor (two translational displacements and one rotational displacement) by using condensation techniques. A 5% of critical damping for the modal damping ratios is introduced in the model. The building is excited horizontally by a ground acceleration $\ddot{u}_g(t)$ in the y direction as shown in Fig 2.17. The excitation is modeled as in the previous example problem. The sampling interval is assumed to be $\Delta t = 0.01$s, and the duration of the excitation is $t_T = 15$s.

For aseismic design purposes, the model is reinforced with nonlinear hysteretic devices. At each floor, four devices are implemented as shown on the floor plan of the structure (axes 4, 7, 8, and 11). These elements provide additional resistance and dissipation against relative displacements between floors. Each non-linear device follows the interstory restoring force law $r(t) = k^e(\delta u(t) - q_1(t) + q_2(t))$, where k^e denotes the initial stiffness of the non-linear device, $\delta u(t)$ is the relative displacement between floors at the position of the device in the y direction, and $q_1(t)$ and $q_2(t)$ denote the plastic deformations of the device. The restoring force $r(t)$ acts between adjacent floors with the same orientation as the relative displacement $\delta u(t)$. Using the auxiliary variable $v(t) = \delta u(t) - q_1(t) + q_2(t)$, the plastic elongations are specified by the first-order nonlinear differential equations [326]

$$\begin{aligned}\dot{q}_i(t) \;=\; & (-1)^{i+1}\dot{\delta}u(t)H\Big((-1)^{i+1}\dot{\delta}u(t)\Big)\Big[H\Big((-1)^{i+1}v(t) - v_y\Big)\frac{(-1)^{i+1}v(t) - v_y}{v_p - v_y} \\ & H\Big(v_p - (-1)^{i+1}v(t)\Big) + H\Big((-1)^{i+1}v(t) - v_p\Big)\Big]\;,\; i = 1, 2 \end{aligned} \tag{2.24}$$

where $H(\cdot)$ denotes the Heaviside step function, $\dot{\delta}u(t)$ is the relative velocity between floors at the position of the device in the y direction, v_y is a parameter specifying the onset of yielding, and $k^e v_p$ is the maximum restoring force of the device. All devices have initial stiffness $k^e = 2.8 \times 10^9$ N/m, and model parameters $v_p = 0.006$ m and $v_y = 0.0042$ m. Note that the evaluation of the system response involves the solution of a system of coupled differential equations, that is, the equation of motion of the structural system and the equation for the evolution of the variables describing the plastic deformation of the non-linear devices. The equations are solved by an appropriate step-by-

step integration scheme.

Design problem

The variables to be controlled are the thicknesses of the concrete core of shear walls (t_w) and the diameters of the exterior columns (d_c). The dimensions of these structural components at each floor are linked to one intermediate optimization variable, x, as $t_w = x\ \hat{t}_w$, and $d_c = x\ \hat{d}_c$, where $\hat{t}_w$ and $\hat{d}_c$ are the nominal values of the thickness of the shear walls and the diameter of the exterior columns at each floor, respectively. The intermediate optimization variables are grouped into a number (n_d) of optimization variables. The objective function for the design problem is defined in terms of the intermediate optimization variables. Two reliability constraints are considered in the present example. The constrained optimization problem is formulated as

$$\begin{aligned} \min_{\mathbf{x}} \quad & c(\mathbf{x}) \\ \text{s.t.} \quad & P_{F_1}(\mathbf{x})/10^{-3} \leq 1 \\ & P_{F_2}(\mathbf{x})/10^{-3} \leq 1 \\ & x_{i+1}/x_i \leq 1,\ i = 1, 2, \ldots, n_d - 1 \\ & 0.5 \leq x_i \leq 1.5,\ i = 1, 2, \ldots, n_d \end{aligned} \tag{2.25}$$

where the failure probability $P_{F_1}(\mathbf{x})$ is defined in terms of a failure event associated with the inter-story drift of the first floor, and $P_{F_2}(\mathbf{x})$ is given in terms of a failure event related to the roof displacement. The characterization of the failure events is provided in Appendix B (see Section 2.8). Similarly to the first application problem, the estimation of the probability of failure for a given design requires considerable numerical efforts.

Use of meta-model

It is noted that the proposed Two-Phase approach may require a large number of reliability analyses for populating the region containing the optimal solution set. Clearly, the failure probabilities at the different designs can be estimated directly during the design process, as in the previous

example. However, the numerical demands may become excessive when the computational time for estimating the failure probability functions is significant. To deal with this issue, an adaptive kriging-based meta-model for approximating the failure probability functions is considered in the present example. Information about the meta-model is given in Appendix C (see Section 2.9).

Results: First scenario

In this scenario, two design variables are considered. The first design variable is associated with the lower 26 floors, while the second design variable corresponds to the upper 26 floors of the building. The reliability-based optimal design problem is written in terms of a normalized objective function as

$$\begin{aligned} \min_{\mathbf{x}} \quad & c(\mathbf{x}) \\ \text{s.t.} \quad & P_{F_1}(\mathbf{x})/10^{-3} \leq 1 \\ & P_{F_2}(\mathbf{x})/10^{-3} \leq 1 \\ & x_2/x_1 \leq 1 \\ & 0.5 \leq x_i \leq 1.5,\ i = 1, 2 \end{aligned} \tag{2.26}$$

where $c(\mathbf{x}) = \sum_{i=1}^{2} x_i$. Figure 2.18 shows some iso-probability curves and the corresponding sketch of the feasible design space, including the optimal design. As in the previous example, the curves have been smoothed for presentation purposes. It is observed that the iso-probability curves associated with the interstory drift of the first floor (continuous-lines) show a rather weak interaction between the design variables. In fact, the curves present an important dependence on the design variable related to the thickness of the shear walls and the diameter of the exterior columns at the lower floors (x_1). On the other hand, the iso-probability curves related to the roof displacement (dashed-lines) show a strong interaction between both design variables, as expected. Note that these results give a valuable insight into the interaction and effect of the design variables on the reliability of this complex system.

The set of feasible samples uniformly distributed over the feasible design space is shown in Figure 19 (Stage 0). This information correspond to all feasible designs obtained during Phase I. For

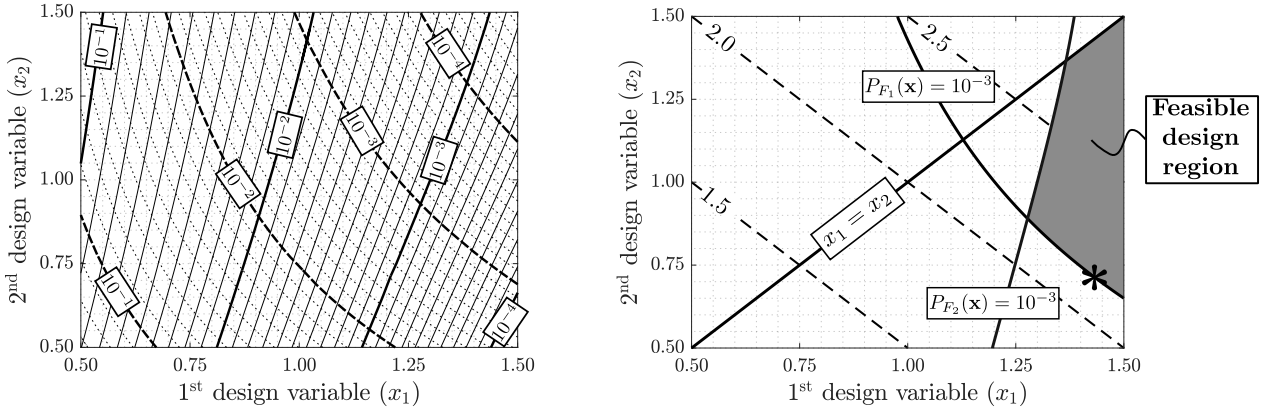

Fig. 2.18: Left figure: Iso-probability curves. P_{F_1}: continuous lines, P_{F_2}: dashed-lines. Right figure: sketch of the feasible design space with the optimal design (asterisk). Application Problem 2. First scenario.

illustration purposes, the algorithm is implemented by considering 500 samples per stage. There are about 500 samples of which more than 200 are different after three stages. The shape generated by these samples agrees very well with the feasible design space shown in Figure 2.18 (right figure). The designs obtained from the first five stages of Phase II are also shown in Figure 2.19. At the last stage, the values of the normalized objective function range from 2.121 to 2.140. The associated optimal design is given by $x_1 = 1.413$ and $x_2 = 0.708$, with corresponding reliability constraint values $P_{F_1}/10^{-3} = 0.999$, and $P_{F_2}/10^{-3} = 0.218$. Thus, the reliability constraint associated with the interstory displacement of the first floor is active at the final design, which is consistent with Figure 2.18 (right figure).

Information about the use of kriging during the different stages of Phase II is shown in Figure 2.20. The number of support points is equal to 12 and an error tolerance level $\epsilon = 0.1$ is selected (see Appendix C in Section 2.9). These values proved to be adequate for the current optimization problem. Once the initial database of support points has been constructed, the surrogate acceptance ratio is almost 100%. Thus, almost all surrogate estimates are accepted from the second stage of Phase II. In this context, the acceptance ratio represents the fraction of failure probability evaluations obtained with the kriging approximation. Overall, that is, considering the generation of the database, more than 87% of the total number of reliability evaluations are performed using the

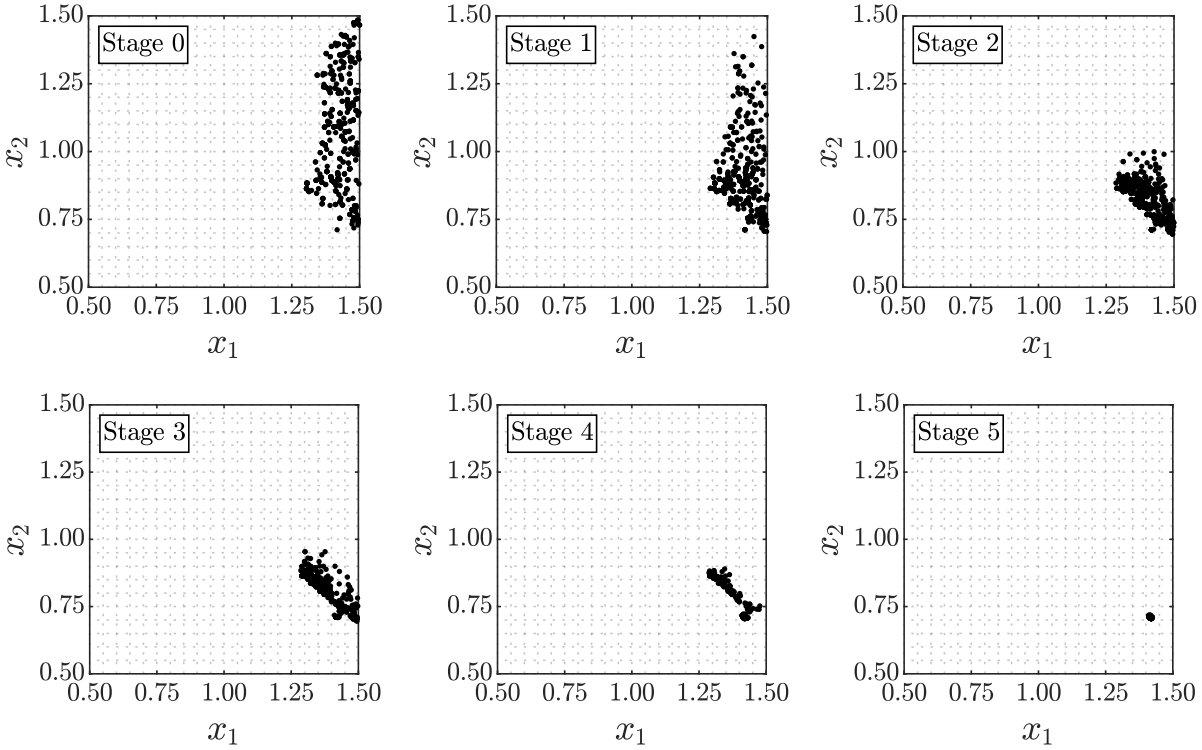

Fig. 2.19: Feasible samples (Stage 0), and the evolution of samples generated at different stages of Phase II. Application Problem 2. First scenario.

meta-model. The previous level of acceptance ratio clearly indicates the efficiency of the proposed adaptive meta-model scheme. This high level of acceptance ratio is due to the fact that the failure probability functions involved in the problem are smoothly varying with respect to the design variables, and thus the surrogate estimates are quite accurate for most of the samples. In terms of accuracy, validation calculations show that the previous results are very similar to those obtained when the reliability constraints are estimated directly, that is, when the meta-model is not used. In fact, the sample-based normalized optimum cost obtained by the proposed approach, i.e., 2.121, is only 0.07% higher than the one obtained without using the kriging approximation. In relation to the computational cost, a speedup close to 10 is obtained by the proposed approach. In this context, the speedup is the ratio of the execution time by solving the design problem directly and the execution time by using the proposed approximation of the failure probabilities during the design process. The actual total number of function evaluations during the entire optimization process is around 500. This small number of function evaluations indicates that use of the proposed meta-model for

approximating the reliability constraints is quite beneficial in terms of computational efficiency.

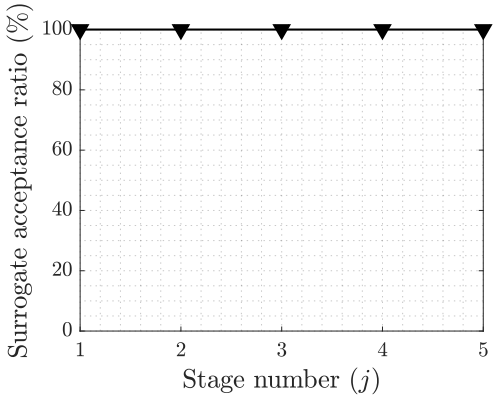

Fig. 2.20: Use of kriging during the different stages of Phase II. Application Problem 2. First scenario.

Results: Second scenario

Under this scenario, the intermediate design variables are grouped into six optimization variables. The definition of these variables is given in Table 2.2.

Table 2.2: Linking detail of intermediate optimization variables.

Design variable	x_1	x_2	x_3	x_4	x_5	x_6
Design elements (floors)	$1-9$	$10-18$	$19-26$	$27-35$	$36-44$	$45-52$

The reliability-based design optimization problem takes the form

$$\begin{aligned} \min_{\mathbf{x}} \quad & c(\mathbf{x}) \\ \text{s.t.} \quad & P_{F_1}(\mathbf{x})/10^{-3} \leq 1 \\ & P_{F_2}(\mathbf{x})/10^{-3} \leq 1 \\ & x_{i+1}/x_i \leq 1,\ i = 1, 2, \ldots, 5 \\ & 0.5 \leq x_i \leq 1.5,\ i = 1, 2, \ldots, 6 \end{aligned} \tag{2.27}$$

where $c(\mathbf{x}) = \sum_{i=1}^{6} x_i$, and the failure events are the ones defined in the first scenario. As in the previous case, the algorithm is implemented by considering 500 samples per stage. The feasible

samples obtained after eight stages of Phase I are shown in Figure 2.21. This figure shows the two-dimensional projections and marginal distributions of the feasible designs obtained after eight steps. A total of 950 feasible samples are obtained, among which 275 are distinct. It is noted that the volume of the feasible design space is very small with respect to the initial design space. In fact, the volume ratio is about 0.01% according to preliminary validation calculations. Then, it is seen that the approach is capable of obtaining samples from the feasible design space even in challenging geometries as in this case.

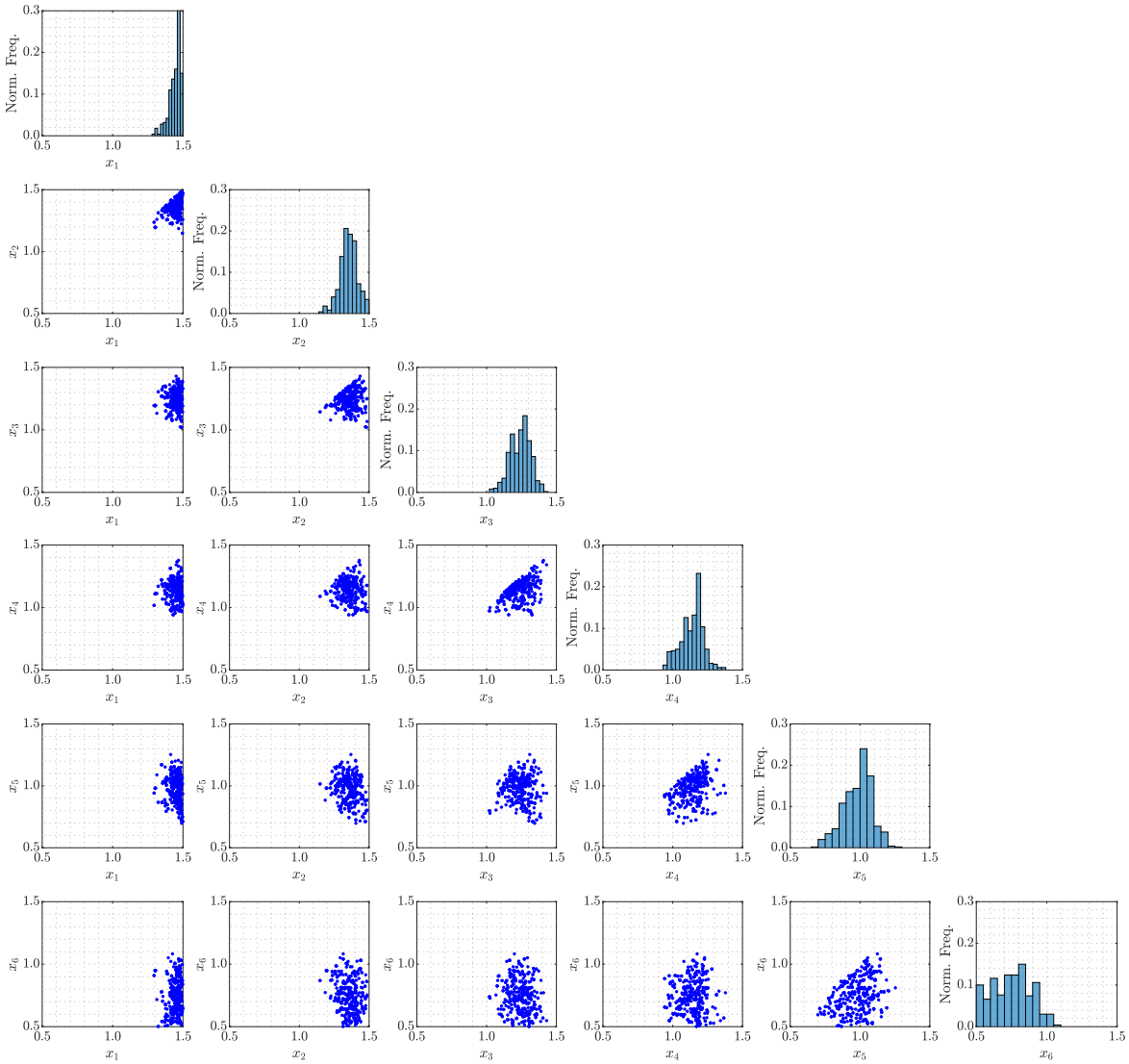

Fig. 2.21: Two-dimensional sample projections and marginal histograms of feasible samples obtained at the last stage of Phase I. Application Problem 2. Second scenario.

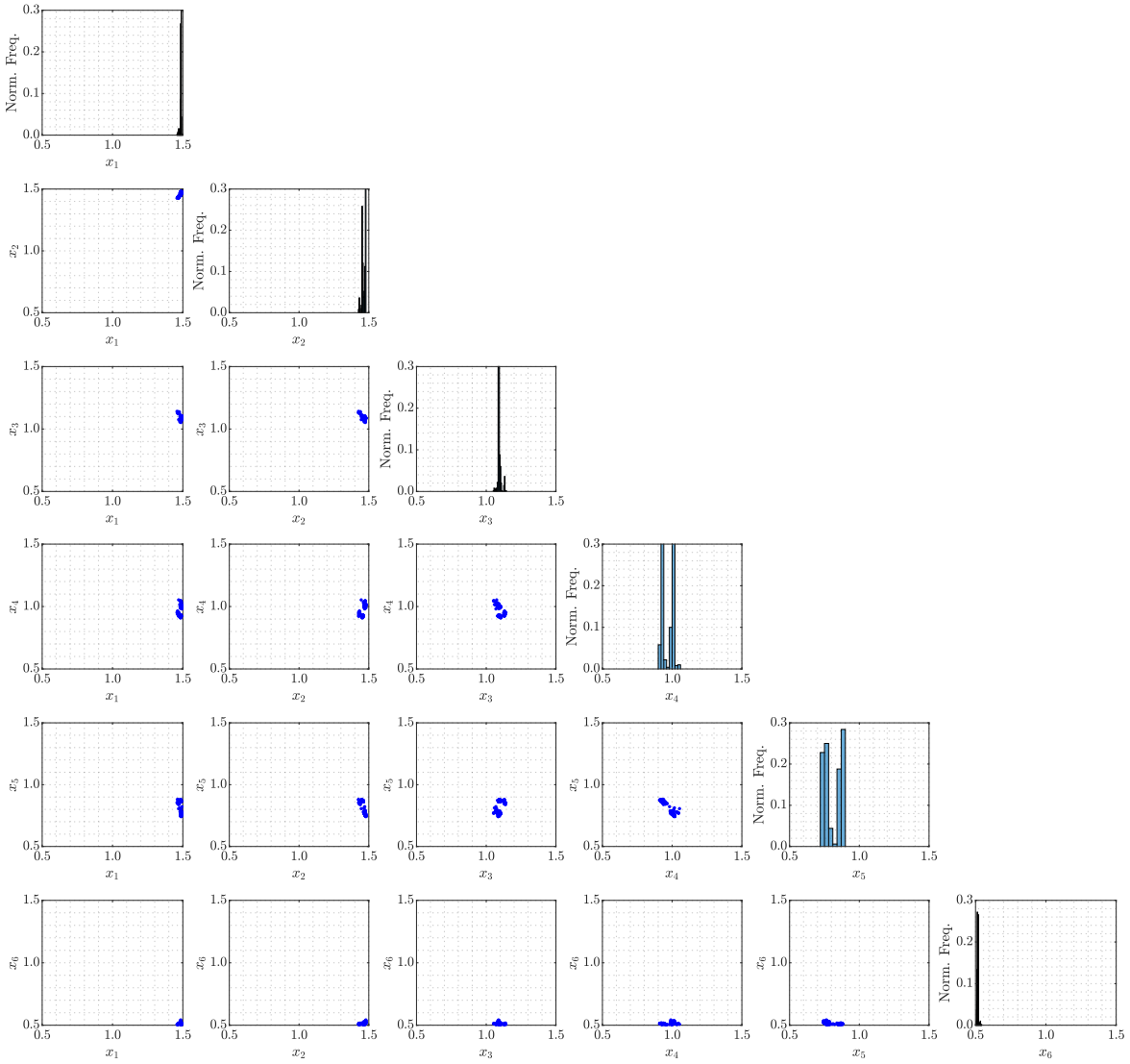

Fig. 2.22: Two-dimensional sample projections and marginal histograms of the design variables obtained at the last stage of Phase II. Application Problem 2. Second scenario.

The set of samples obtained after ten stages of Phase II are shown in Figure 2.22 22. It is observed that the samples are concentrated near a single value. At the last stage, the values of the normalized objective function range from 6.333 to 6.357. Then, the minimum value (sample-based optimal cost) is equal to 6.333, which is associated with the design $\mathbf{x}^T = \langle$ 1.489, 1.476, 1.088, 1.011 ,0.751, 0.515$\rangle$. The corresponding reliability constraint values are $P_{F_1}/10^{-3} = 0.999$, and $P_{F_2}/10^{-3} = 0.169$. Thus, the reliability constraint associated with the interstory displacement of the first floor is active at the final design, which is compatible with the first scenario. On the other hand, the

geometric constraint values are: $x_2/x_1 = 0.991$; $x_3/x_2 = 0.736$; $x_4/x_3 = 0.930$; $x_5/x_4 = 0.743$; and $x_6/x_5 = 0.685$. Based on these results, the first geometric constraint can be considered as active at the final design. It is seen that the final design favors large values of the optimization variables associated with the column diameter and shear wall thickness of the lower floors, which is consistent from the structural point of view. Note that the same feature is exhibited by the final design obtained when considering only two design variables (first scenario). Thus, the final designs obtained from both scenarios are qualitatively similar. However, note that the distribution of the stiffness over the height of the building is more regular in the present scenario, which is reasonable from the optimization point of view (six control or optimization variables instead of two).

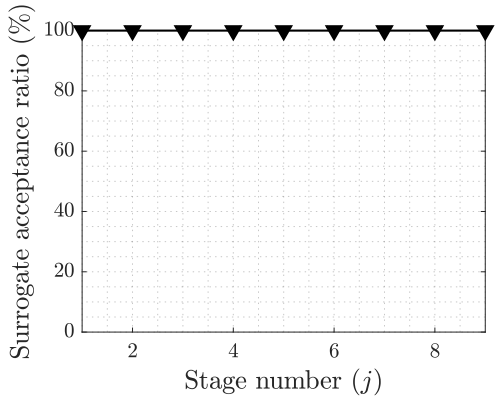

Fig. 2.23: Use of kriging during the different stages of Phase II. Application Problem 2. Second scenario.

The evolution of the surrogate acceptance ratio during the design process is shown in Figure 2.23. In particular, this figure shows the acceptance ratio during Phase II. The number of support points in the context of kriging approximations is equal to 28. This number proved to be adequate for the current scenario. The acceptance rate remains very high during the entire process. Actually, the number of reliability estimates that need to be evaluated directly is less than 6% of the total number of estimates required during the entire optimization process (Phases I and II). Thus, the efficiency of the proposed adaptive scheme is also evident in the context of this scenario. As in the first scenario, the failure probability functions involved in the problem are smoothly varying with respect to the design variables, and thus the surrogate estimates are quite accurate for most of the

samples. Validation calculations show that the previous results are very similar to those obtained when the reliability constraints are estimated directly.

Computational effort

The corresponding speedup factor obtained by the proposed scheme is more than 16 in this case, and the total number of function evaluations (reliability analyses) during the entire optimization process is close to 500. This small number of function calls indicates that the use of the proposed meta-model is very advantageous in terms of computational cost. Note that this significant reduction in computational effort is obtained without compromising the accuracy of the design process. To make a fair comparison of the proposed optimization scheme with other population-based stochastic optimization algorithms it is necessary to develop meta-models in the framework of those algorithms. Clearly, this is beyond the scope of the present contribution. Finally, the results of this application problem show that the use of surrogate modeling techniques together with the proposed optimization scheme can be an efficient and practical choice for solving the class of complex problems considered in the present work.

2.6 Conclusions

A population-based stochastic optimization scheme for solving general constrained optimization problems has been presented. The problem is set into a framework of a Two-Phase Bayesian model updating problem. Phase I generates designs uniformly distributed over the feasible design space, while Phase II obtains a set of designs lying in the vicinity of the optimal solution set. The model updating problem is solved by the transitional Markov chain Monte Carlo method. The proposed constraint-handling approach is direct and does not require special constraint-handling techniques. Actually, the same framework for obtaining samples in the vicinity of the optimal solution set is used for obtaining samples in the feasible design space. In addition, the scheme produces a set of nearly optimal solutions instead of a single optimal solution. This feature can be

advantageous in many practical cases, where additional considerations or alternative criteria can be taken into account to select the appropriate final design. Thus, the approach provides flexibility to the decision-making process. Moreover, due to the generality and flexibility of the formulation, it can handle different types of structural optimization problems involving linear and nonlinear models.

The general approach is applied to an important class of problems. Specifically, reliability-based design optimization of structural dynamical systems under stochastic excitation. The results of the example problems indicate that the samples generated by Phase I populate the feasible design space in an effective manner, even in problems involving challenging geometries. Thus, the proposed scheme is a useful tool for exploration of complex feasible design spaces. Moreover, at the last stage of Phase II, the samples are distributed in the vicinity of the optimal solution set. In terms of computational efficiency, the results indicate that the proposed algorithm compares favorably with respect to other population-based stochastic optimization algorithms.

When dealing with complex reliability-based design optimization problems, the use of meta-models can be very attractive. In fact, the numerical results of application 2 show that high surrogate acceptance rates are obtained during the entire design process. In this manner, a small percentage of direct reliability estimations is required during the procedure allowing substantial savings in computational efforts. Beside, the reduction in computational effort is obtained without compromising the accuracy of the design process. Thus, the use of surrogate modeling techniques together with the proposed optimization scheme may provide an effective numerical tool for dealing with the stochastic optimization of complex structural models.

A future research effort aims to implement the proposed approach to more complex and involved stochastic structural optimization problems. In these cases, the proposed optimization scheme can be combined with parametric reduced-order models. The idea is to perform structural analyses in terms of reduced-order models instead of full finite element models. The extension of the methodology to stochastic optimization problems involving mixed-design variables is an additional topic

for future research. Work in these directions is currently under way.

Acknowledgments

The research reported here was supported in part by CONICYT (National Commission for Scientific and Technological Research) under grant number 1200087. Also, this research has been supported by CONICYT and DAAD under CONICYT-PFCHA/Doctorado Acuerdo Bilateral DAAD Becas Chile/2018-62180007. In addition, this research has been implemented under the PAC (Programa Asistente Cientifico 2017)-UTFSM program. These supports are gratefully acknowledged by the authors.

2.7 Appendix A

The failure event F is characterized as $F(\mathbf{x}, \mathbf{z}) = d(\mathbf{x}, \mathbf{z}) > 1$, where d is a demand function given by

$$d(\mathbf{x}, \mathbf{z}) = \max_{j=1,2} \max_{t \in [0, t_T]} \left\{ \frac{|\delta u_j(t, \mathbf{x}, \mathbf{z})|}{\delta^*}, \frac{|a_j(t, \mathbf{x}, \mathbf{z})|}{a^*} \right\} \tag{2.28}$$

where $\delta u_j(t, \mathbf{x}, \mathbf{z})$, $j = 1, 2$, are the interstory drifts, $a_j(t, \mathbf{x}, \mathbf{z}), j = 1, 2$, are the total accelerations at the first and second floor, respectively, and $\delta^* = 0.42$ and $a^* = 0.84$ are the acceptable response levels. The failure probability function $P_F(\mathbf{x})$ can be written in terms of the demand function as the multidimensional probability integral

$$P_F(\mathbf{x}) = \int_{d(\mathbf{x}, \mathbf{z}) > 1} p(\mathbf{z}) d\mathbf{z} \tag{2.29}$$

where $p(\mathbf{z})$ is the joint probability density function of the uncertain parameters involved in the characterization of the excitation. This function indicates the relative plausibility of the possible values of the uncertain parameters $\mathbf{z} \in \mathbf{Z}$. It is noted that the above multidimensional probability integral involves more than 1000 random variables in this case. Therefore, the reliability estimation for a given design constitutes a high-dimensional problem as previously pointed out [133, 138,

141].

2.8 Appendix B

The failure event associated with the interstory displacement of the first floor is given by

$$F_1(\mathbf{x},\mathbf{z}) = \max_{t\in[0,t_T]} \left\{ \frac{|u_x^1(t,\mathbf{x},\mathbf{z})|}{u^{1^*}}, \frac{|u_y^1(t,\mathbf{x},\mathbf{z})|}{u^{1^*}} \right\} > 1 \tag{2.30}$$

where $u_x^1(t,\mathbf{x},\mathbf{z})$ and $u_y^1(t,\mathbf{x},\mathbf{z})$ are the centroid relative displacements of the first floor along the x and y direction, respectively, and u^{1^*} is the maximum allowable drift equal to 0.08% of the first story height.

The failure event related to the roof displacement is given by

$$F_2(\mathbf{x},\mathbf{z}) = \max_{t\in[0,t_T]} \left\{ \frac{|u_x^2(t,\mathbf{x},\mathbf{z})|}{u^{2^*}}, \frac{|u_y^2(t,\mathbf{x},\mathbf{z})|}{u^{2^*}} \right\} > 1 \tag{2.31}$$

where $u_x^2(t,\mathbf{x},\mathbf{z})$ and $u_y^2(t,\mathbf{x},\mathbf{z})$ are the centroid displacements at the top of the building along the x and y direction, respectively,and u^{2^*} is the maximum allowable roof displacement equal to 0.075% of the building height. As in Application 1, the reliability estimation for a given design constitutes a high-dimensional problem. In fact, more than 1500 random variables are involved in the corresponding multidimensional probability integral in this case.

2.9 Appendix C

A kriging-based model is selected for approximating the failure probability functions [327, 328]. Validation calculations have shown that it is computationally more stable and efficient to perform the kriging interpolation in the physical design space $\mathbf{X}$ rather than in the underlying normal space $\mathbf{Y}$ [180]. Furthermore, it is more convenient, from the numerical point of view, to approximate the logarithm of the failure probability function than the failure probability function itself [101]. In this

framework, the idea is to construct an initial data-base of support points during the first stage of Phase I which is updated during the different stages of the proposed approach. The support points are then used to construct the kriging estimates of the logarithm of the failure probability functions, i.e., $P_{F_i}^{Ln}(\mathbf{x}) = \ln(P_{F_i}(\mathbf{x}))$. The numerical implementation is as follows.

1) The initial set of support points and the corresponding values of $P_{F_i}^{Ln}(\mathbf{x})$ are generated during the first stage of Phase I. This implies a direct evaluation of $P_{F_i}^{Ln}(\mathbf{x})$ at the support points. Define the number of support points n_{su}, and error tolerance level ϵ.

2) For a given candidate sample $\mathbf{x}^{\text{new}}$, find its closest n_{su} support points according to, e.g., the Euclidean distance.

3) Check if $\mathbf{x}^{\text{new}}$ belongs to the n_d-dimensional convex hull of the support points. If not, go to step 6.

4) Estimate the coefficient of variation of the kriging estimate. Check the variability of the estimate. If its coefficient of variation is greater than the error tolerance level ϵ, go to 6.

5) Kriging estimate of $P_{F_i}^{Ln}(\mathbf{x})$ is accepted for the candidate sample $\mathbf{x}^{\text{new}}$. Go to step 7.

6) Evaluate $P_{F_i}^{Ln}(\mathbf{x}^{\text{new}})$ directly from the physical model. Store the values of $\mathbf{x}^{\text{new}}$ and $P_{F_i}^{Ln}(\mathbf{x}^{\text{new}})$ in the database of support points.

7) Continue with the updating process.

This procedure is repeated during the different stages of the proposed Two-Phase method. For more details about the implementation of the meta-model, the reader is referred to [180, 287, 288].

Chapter 3

Asymptotic Bayesian Optimization: A Markov sampling-based framework for design optimization

Asymptotic Bayesian Optimization: A Markov sampling-based framework for design optimization

D. J. Jerez[a], H. A. Jensen[b,*], M. Beer[a,c,d], J. Chen[e]

[a]*Institute for Risk and Reliability, Leibniz Universität Hannover, Callinstr. 34, 30167 Hannover, Germany*

[b]*Departamento de Obras Civiles, Universidad Técnica Federico Santa María, Valparaiso 2390302, Chile*

[c]*International Joint Research Center for Engineering Reliability and Stochastic Mechanics, Tongji University, Shanghai 200092, China*

[d]*Institute for Risk and Uncertainty and School of Engineering, University of Liverpool, Liverpool L69 7ZF, United Kingdom*

[e]*State Key Laboratory of Disaster Reduction in Civil Engineering & College of Civil Engineering, Tongji University, Shanghai 200092, China*

Abstract: This paper presents a Markov sampling-based framework, called Asymptotic Bayesian Optimization, for solving a class of constrained design optimization problems. The optimization problem is converted into a unified two-phase sample generation problem which is solved by an effective Markov chain Monte Carlo simulation scheme. First, an exploration phase generates designs distributed over the feasible design space. Based on this information, an exploitation phase obtains a set of designs lying in the vicinity of the optimal solution set. The proposed formulation can handle continuous, discrete, or mixed discrete-continuous design variables. Appropriate adaptive proposal distributions for the continuous and discrete design variables are suggested. The set of optimal solutions provides valuable sensitivity information of the different quantities involved in the problem with respect to the design variables. Representative examples including an analytical problem involving nonlinear benchmark functions, a classical engineering design problem, and a performance-based design optimization problem of a structural system under stochastic excitation

*Corresponding author
E-mail addresses: danko.jerez@irz.uni-hannover.de (D. J. Jerez), hector.jensen@usm.cl (H. A. Jensen), beer@irz.uni-hannover.de (M. Beer), chenjb@tongji.edu.cn (J. Chen).

are presented to show the effectiveness and potentiality of the proposed optimization scheme. Validation calculations show that the scheme is a flexible, efficient and competitive choice for solving a wide range of classical and complex engineering design problems.

Keywords: Discrete-continuous optimization; Dynamic systems; Metropolis-Hastings algorithm; Markov sampling method; Performance-based design; Stochastic optimization

3.1 Introduction

Constrained optimization problems originate from a large number of involved engineering design processes. The problem is generally formulated in terms of minimizing a cost function or maximizing a utility function subject to multiple inequality constraints. In addition, and due to manufacturing limitations, some design variables cannot be considered as continuous but should be treated as discrete in many cases. Due to the significance of this type of problems, the development of efficient and robust constrained optimization algorithms has been an important area of research in engineering design [117, 151, 306].

One class of optimization schemes for solving constrained optimization problems is based on traditional mathematical optimization algorithms [117, 143, 329, 330]. This type of schemes has been extensively used in a large number of engineering design problems. Recently, stochastic-based search algorithms have been also proposed for constrained optimization. This class of algorithms can be classified into three main groups: evolution-based, physics-based, and swarm-based methods. Evolution-based methods, which are inspired by the laws of natural evolution, include Genetic Algorithms (GA) [307], Evolution Strategies (ES) [331], Genetic Programming (GP) [332], etc. On the other hand, physics-based methods such as Simulated Annealing (SA) [174], Gravitational Search Algorithm (GSA) [333], Subset Simulation-based algorithms (SuS) [133, 317], and Ray Optimization (RO) [334], replicate physical rules. Finally, swarm-based techniques that imitate the social behavior of different groups include Particle Swarm Optimization (PSO) [308], Ant Colony Optimization (ACO) [309], Harmony Search (HS) [335], Artificial Bee Colony (ABC) [336], etc.

Some of the advantages of using stochastic search algorithms include their simplicity, flexibility, and local optima avoidance. In this context, one important issue related to constrained optimization is constraint-handling [312, 313, 324]. In this regard, a number of strategies have been suggested in the context of specific stochastic optimization algorithms such as evolutionary algorithms [314], simulated annealing [315], particle swarm optimization [316, 323], and subset simulation-based algorithm [317]. The previous stochastic optimization algorithms have been applied in a number of constrained optimization problems with different levels of efficiency and robustness.

Considering that design optimization of complex systems is a challenging problem, and the fact that there is no single method capable of solving all types of constrained optimization problems, there is still room for further developments in this area. This motivates the attempt to develop an effective and flexible framework for solving complex constrained optimization problems, including problems with mixed discrete-continuous design variables. In the proposed scheme, which is called Asymptotic Bayesian Optimization (ABO), the optimization problem is converted into a problem of successively generating samples according to a sequence of probability distributions with supports increasingly concentrated in a vicinity of the optimum solution set. The samples are generated by a unified two-phase approach based on an efficient Markov chain Monte Carlo technique [178, 179]. The first phase corresponds to an exploration state which generates designs uniformly distributed over the feasible design space, while the second phase, which is an exploitation state, generates a set of designs lying in the vicinity of the optimal solution set. The proposed constraint-handling approach is direct and does not require special constraint-handling techniques. In fact, the same framework for obtaining samples in the vicinity of the optimal solution set is used for finding designs in the feasible space. The solution scheme can efficiently explore the sensitivity of the objective function and constraints with respect to the design variables in the feasible design space as well as in the neighborhood of the optimal solution set. In this context, appropriate adaptive proposal distributions are suggested for the continuous and discrete design variables. Moreover, the optimization algorithm can be implemented with few control parameters.

In summary, it is the objective of this contribution to propose a unified Markov sampling-based framework for solving a class of constrained optimization problems with application to design optimization. The contribution can be viewed as an extension and generalization of the work presented in [175, 177, 181, 182] in the sense that the same formulation can be used for a wide range of engineering design problems involving continuous, discrete, or mixed discrete-continuous design variables. The structure of the paper is as follows. In Section 3.2, the general formulation of the problem is presented. The relationship between the optimization and the sample generation problem is explained in Section 3.3. Section 3.4 outlines the sample generation scheme to be implemented. The exploration and exploitation phases are discussed in Sections 3.5 and 3.6, respectively. Some advantages of the proposed optimization scheme are highlighted in Section 3.7. The performance and capabilities of the proposed algorithm are demonstrated in Section 3.8 by means of three example problems. The paper closes with some final remarks.

3.2 Problem formulation

Consider the constrained optimization problem formulated as

$$\begin{aligned} \min_{\mathbf{x}} \quad & c(\mathbf{x}) \\ \text{s.t.} \quad & g_j(\mathbf{x}) \leq 0, \quad j = 1, \ldots, n_g \\ & \mathbf{x} \in \mathbf{X} \end{aligned} \tag{3.1}$$

where $c(\mathbf{x})$ is the objective function, $g_j(\mathbf{x})$ is the j^{th} constraint function, n_g is the number of inequality constraints, $\mathbf{x}$ represents the set of design variables, and $\mathbf{X}$ is the search space. The set of design variables is defined as $\mathbf{x} = \langle \mathbf{x}_c^T, \mathbf{x}_d^T \rangle^T \in \mathbf{X} = \mathbf{X}_c \times \mathbf{X}_d \subset R^{n_c+n_d}$, where $\mathbf{x}_c(x_{ci}, i = 1, \ldots, n_c) \in \mathbf{X}_c \subset R^{n_c}$ denotes the set of continuous design variables, n_c is the number of continuous design variables, $\mathbf{x}_d(x_{di}, i = 1, \ldots, n_d) \in \mathbf{X}_d \subset R^{n_d}$ denotes the set of discrete design variables, and n_d is the number of discrete design variables. The side constraints for the continuous design variables are given by $x_{ci}^l \leq x_{ci} \leq x_{ci}^u, i = 1, \ldots, n_c$, where x_{ci}^l and x_{ci}^u are the correspond-

ing lower and upper bounds. Finally, the set of available discrete values $\mathbf{X}_{di}$ for the i^{th} discrete design variable is written as $x_{di} \in \mathbf{X}_{di} = \{x_{di(j)}, j = 1, \ldots, n_{di}\}, i = 1, \ldots, n_d$. For convenience, the available discrete values are listed in an ascending order. The objective function $c(\mathbf{x})$ can be defined in terms of general cost functions, while the design constraints $g_j(\mathbf{x}) \leq 0, j = 1, \ldots, n_g$ can be given in terms of different design specifications.

3.3 Relationship between optimization problem and sample generation problem

Based on the connection between statistical mechanics and combinatorial optimization proposed in [174], with the idea of simulated annealing, the optimization problem in Eq. (3.1) can be converted into a problem of generating sample points or designs according to a specially devised distribution. To examine this connection, it is first observed that finding the minimum of the objective function $c(\mathbf{x})$ is equivalent to find the maximum of the function $\exp(-c(\mathbf{x})/K)$, for any given value of $K > 0$ [174]. The parameter K is usually called *temperature* by analogy with the Boltzmann-Gibbs distribution in statistical mechanics [294]. Next, artificially treating the design variables as random variables distributed over the feasible design space $\mathbf{X}_{\text{feasible}}$, where

$$\mathbf{X}_{\text{feasible}} = \left\{ \mathbf{x} = \langle \mathbf{x}_c^T, \mathbf{x}_d^T \rangle^T : \mathbf{x}_c \in \mathbf{X}_c \wedge \mathbf{x}_d \in \mathbf{X}_d \wedge g_j(\mathbf{x}) \leq 0,\ j = 1, \ldots, n_g \right\}, \tag{3.2}$$

consider the non-normalized distribution

$$f_K(\mathbf{x}) \propto \exp\left(-\frac{c(\mathbf{x})}{K}\right) \ I_{\mathbf{X}_{\text{feasible}}}(\mathbf{x}) \tag{3.3}$$

where $I_{\mathbf{X}_{\text{feasible}}}(\mathbf{x})$ is the indicator function of the feasible design space $\mathbf{X}_{\text{feasible}}$, that is, $I_{\mathbf{X}_{\text{feasible}}}(\mathbf{x}) = 1$, for $\mathbf{x} \in \mathbf{X}_{\text{feasible}}$, and $I_{\mathbf{X}_{\text{feasible}}}(\mathbf{x}) = 0$, otherwise. The distribution $f_K(\mathbf{x})$ becomes proportional to $I_{\mathbf{X}_{\text{feasible}}}(\mathbf{x})$ as $K \to \infty$, and it becomes spikier as $K \to 0$. The previous results correspond to the concept of annealing which indicates that as K decreases, the distribution $f_K(\mathbf{x})$ puts

more and more of its probability mass into the set of feasible designs that maximize the function $\exp(-c(\mathbf{x})/K)$. Thus, a sample or design drawn from $f_K(\mathbf{x})$ will be in a vicinity of the optimal solution set $\mathbf{X}_c^*$ with very high probability when $K \to 0$ [175, 177]. Then, if a number of samples (designs) following the distribution $f_K(\mathbf{x})$ as $K \to 0$ can be generated, the sample points with the smallest value of $c(\mathbf{x})$ among the generated designs can provide a good approximation for the optimal solution set of the problem.

3.4 Sample generation

As previously pointed out, the optimization problem can be converted into a problem of generating sample points (designs) according to the non-normalized distribution $f_K(\mathbf{x})$ with $K \to 0$. The generation of the required samples can be carried out by Markov chain Monte Carlo techniques [81]. This is a family of stochastic simulation algorithms for sampling from arbitrary probability density distributions. They are based on constructing a Markov chain whose state probability distribution converges to any desired target distribution as its stationary distribution. In this context, a number of standard algorithms may be used, including the independent Metropolis-Hastings algorithm [319], the random walk Metropolis-Hastings algorithm [88, 89], the asymptotically independent Markov sampling scheme [176], etc. In the present formulation, a highly effective Markov chain Monte Carlo simulation technique called the transitional Markov chain Monte Carlo (TMCMC) method is employed [178, 179]. It is noted that the treatment of the design variables as random variables is just a tool in the present formulation for setting the optimization problem into a sample generation problem [175, 177, 180]. In the framework of the TMCMC method, define a series of non-normalized intermediate distributions of the form

$$f_{K_0}(\mathbf{x}) \propto I_{\mathbf{X}_{\text{feasible}}}(\mathbf{x}) \quad , \quad f_{K_j}(\mathbf{x}) \propto \exp\left(-\frac{c(\mathbf{x})}{K_j}\right) I_{\mathbf{X}_{\text{feasible}}}(\mathbf{x}) \quad , \quad j = 1, 2, \ldots \tag{3.4}$$

where $\infty = K_0 > K_1 > \ldots > K_j > \ldots$ is a sequence of monotonically decreasing parameters with $K_j \to 0$ as $j \to \infty$. These parameters are constructed adaptively in such a way that the

distributions $f_{K_j}(\mathbf{x})$ and $f_{K_{j+1}}(\mathbf{x})$ be similar [178, 318, 319]. This small change of the shape between consecutive distributions allows to efficiently obtain samples from $f_{K_{j+1}}(\mathbf{x})$ based on the samples from $f_{K_j}(\mathbf{x})$. To this end, different criteria can be used. In particular, a criterion based on the effective sample size technique [318, 319] is considered in the present implementation. According to this criterion, the value of K_{j+1}, given K_j, is chosen to satisfy the equation

$$\frac{\sum_{i=1}^{n} \exp\left(-2c(\mathbf{x}_i^j)\Delta K_j\right)}{\left(\sum_{i=1}^{n} \exp\left(-c(\mathbf{x}_i^j)\Delta K_j\right)\right)^2} = \frac{1}{\nu n} \tag{3.5}$$

where $\Delta K_j = 1/K_{j+1} - 1/K_j$, and $\nu \in (0,1)$ is a user-defined parameter. At the zeroth level, $j = 0$, uniformly distributed samples $\mathbf{x}_1^0, \ldots, \mathbf{x}_n^0$ are generated over the feasible design space $\mathbf{X}_{\text{feasible}}$, where n is the number of samples per stage. The samples at stage $j+1$, i.e., $\mathbf{x}_1^{j+1}, \ldots, \mathbf{x}_n^{j+1}$, $j = 0, 1, \ldots$, which are approximately distributed according to $f_{K_{j+1}}(\mathbf{x})$, are obtained by generating Markov chains using the Metropolis-Hastings algorithm [88, 89]. The lead sample of each chain, $\tilde{\mathbf{x}}^{j+1}$, is a sample from the previous stage, $\mathbf{x}_i^j$, drawn with probability equal to its normalized importance weight, $\bar{w}_i^j, i = 1, \ldots, n$ (see Appendix A). Each candidate design $\mathbf{x}^\star = \langle \mathbf{x}_c^{\star T}, \mathbf{x}_d^{\star T} \rangle^T$ is generated from an adaptive proposal distribution with independent continuous and discrete components [182] as described in appendices B and C, respectively. The candidate design is then accepted or rejected according to the procedure described in Appendix D. The procedure is repeated until the required number of samples has been obtained. It is noted that when the number of samples $n \to \infty$, the samples generated by the previous procedure are actually distributed according to the non-normalized intermediate distributions $f_{K_j}(\mathbf{x}), j = 1, 2, \ldots$ which ultimately are densely concentrated near the optimum solution set. Furthermore, the target non-normalized distribution $f_K(\mathbf{x}) \propto \exp(-c(\mathbf{x})/K) I_{X_{\text{feasible}}}(\mathbf{x}), K \to 0$, can be viewed as the posterior distribution of a Bayesian model updating problem where $\exp(-c(\mathbf{x})/K), K \to 0$, takes the role of the likelihood function and $I_{X_{\text{feasible}}}(\mathbf{x})$ of the prior distribution. These features are the reasons for naming the proposed optimization scheme "Asymptotic Bayesian Optimization". The generation of samples at

stage $j+1$, i.e., $\mathbf{x}_1^{j+1}, \ldots, \mathbf{x}_n^{j+1}$, based on the samples generated at level j, is schematically represented in Fig. 3.1. A detailed implementation of the TMCMC method can be found in [178, 179].

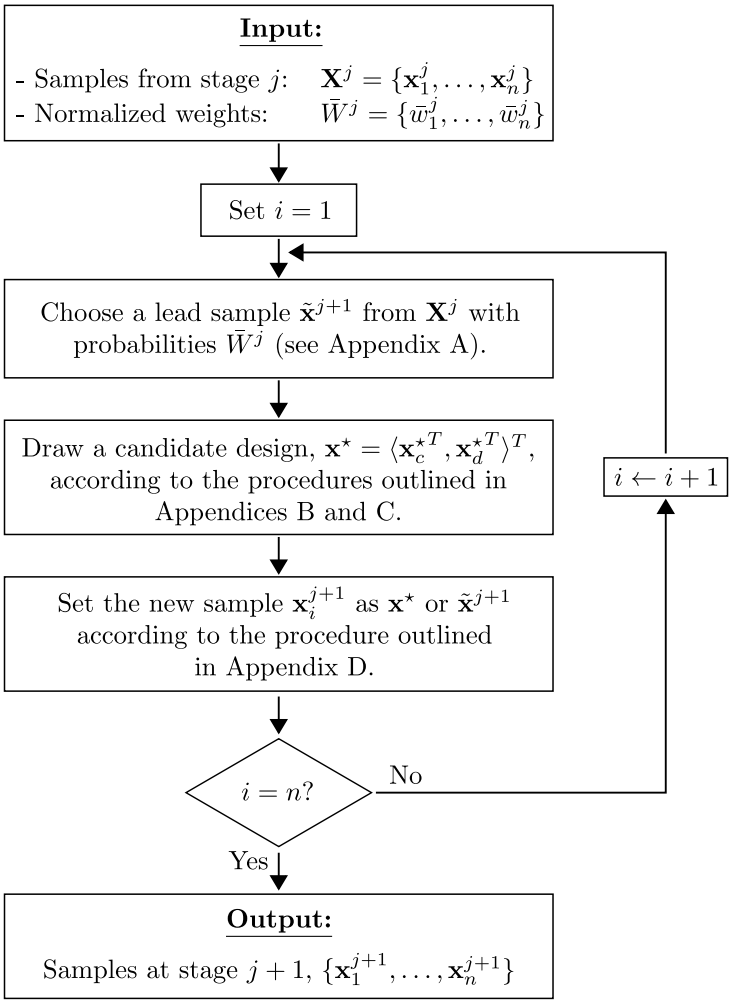

Fig. 3.1: Sample generation process (Flowchart 1).

3.5 Exploration phase

The first step of the proposed solution scheme requires the generation of a set of samples uniformly distributed over the feasible design space $\mathbf{X}_{\text{feasible}}$. To this end, an exploration phase that investigates the feasible domain of the search space is introduced. Following some of the ideas suggested in

[181], define the auxiliary unconstrained optimization problem

$$\begin{aligned} \min_{\mathbf{x}} \quad & h(\mathbf{x}) = \max\left\{0, \max_{j=1,\ldots,n_g} g_j(\mathbf{x})\right\} \\ \text{s.t.} \quad & \mathbf{x} \in \mathbf{X} \end{aligned} \tag{3.6}$$

where all terms have been previously defined. Note that the optimal solution set $\mathbf{X}_h^*$ of the unconstrained optimization problem is given by

$$\mathbf{X}_h^* = \left\{\mathbf{x} = \langle \mathbf{x}_c^T, \mathbf{x}_d^T \rangle^T : \mathbf{x}_c \in \mathbf{X}_c \wedge \mathbf{x}_d \in \mathbf{X}_d \wedge g_j(\mathbf{x}) \leq 0 \ , \ j = 1, \ldots, n_g\right\} \tag{3.7}$$

with minimum objective function value equal to 0. Thus, the optimal solution set $\mathbf{X}_h^*$ of the unconstrained optimization problem given in Eq. (3.6) coincides with the feasible design space defined in Eq. (3.2), i.e., $\mathbf{X}_{\text{feasible}} = \mathbf{X}_h^*$. Note that the problem is unconstrained in the sense that only side constraints on the design variables are considered. The previous optimization problem can be solved as indicated in the previous section, that is, by means of the TMCMC method. In this case, define the sequence of non-normalized intermediate distributions

$$f_{K_0}(\mathbf{x}) = \ U_{\mathbf{X}}(\mathbf{x}) \ \ , \ \ f_{K_j}(\mathbf{x}) \propto \ \exp\left(-\frac{h(\mathbf{x})}{K_j}\right) \ \ U_{\mathbf{X}}(\mathbf{x}) \ \ , \ \ j = 1, 2, \ldots \tag{3.8}$$

where $U_{\mathbf{X}}(\mathbf{x})$ is the uniform distribution defined over the set that characterizes the side constraints, i.e., $\mathbf{X} = \{\mathbf{x} = \langle \mathbf{x}_c^T, \mathbf{x}_d^T \rangle^T : \mathbf{x}_c \in \mathbf{X}_c \wedge \mathbf{x}_d \in \mathbf{X}_d\}$. Therefore, the samples at the first phase ($K_0 = \infty$) can be generated efficiently by direct Monte Carlo simulation. Furthermore, according to the sample generation scheme described in the previous section, the samples at the last stage of the process ($K_j \to 0$) represent designs with objective function value $h(\mathbf{x}) = 0$. In this phase, the parameter K_{j+1} satisfies the equation

$$\frac{\sum_{i=1}^{n} \exp\left(-2h(\mathbf{x}_i^j)\Delta K_j\right)}{\left(\sum_{i=1}^{n} \exp\left(-h(\mathbf{x}_i^j)\Delta K_j\right)\right)^2} = \frac{1}{\nu n} \tag{3.9}$$

according to the effective sample size technique [318, 319]. It can be shown that all feasible designs obtained during the different stages of the exploration phase are uniformly distributed over the set $\mathbf{X}_{\text{feasible}}$ [181]. Therefore, a possible stopping criterion is to obtain a sufficient amount of feasible designs during all stages. In the proposed implementation, the sampling process stops when $m \geq n_{\text{feasible}}$, where m is the total number of feasible designs obtained during the entire simulation process, and n_{feasible} is a user-defined target value. The procedure to generate samples in the feasible design space is schematically shown in Fig. 3.2.

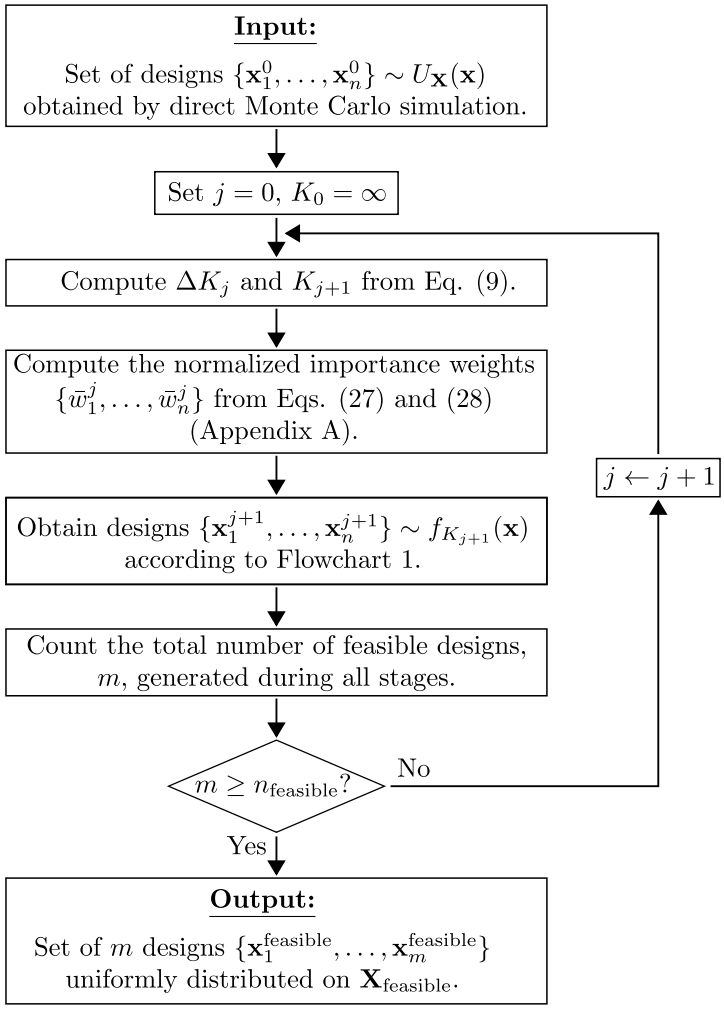

Fig. 3.2: Exploration phase of ABO (Flowchart 2).

3.6 Exploitation phase

3.6.1 Samples in the optimal solution set

The exploitation phase uses the samples generated in the exploration phase to obtain a set of designs lying in the vicinity of the optimal solution set $\mathbf{X}_c^*$. In the context of the approach presented in Section 3.4, the samples uniformly distributed over the feasible design space $\mathbf{X}_{\text{feasible}}$ are the ones obtained from the exploration phase. In addition, as $K_j \to 0$, the distribution $f_{K_j}(\mathbf{x})$ converges to a uniform distribution over the optimal solution set $\mathbf{X}_c^*$ and, therefore, the generated samples become more and more concentrated around $\mathbf{X}_c^*$ as the iterations progress. Clearly, for numerical implementation the algorithm should stop based on any suitable stopping rule. In the present formulation, the sampling procedure stops if a user-defined number of stages, $N_{\max}$, are completed or if the sample coefficient of variation (c.o.v.) of the objective function is below a certain threshold. In particular, the optimization process stops at stage $j = 0, 1, \ldots$ if $j + 1 = N_{\max}$ or, alternatively, $\delta_{j+1} < \gamma\delta_0$, where $\gamma \in (0, 1)$ is a user-defined parameter, and

$$\delta_j = \sqrt{\frac{1}{n-1}\sum_{i=1}^{n}\left(c(\mathbf{x}_i^j) - \left[\frac{1}{n}\sum_{l=1}^{n} c(\mathbf{x}_l^j)\right]\right)^2} \Bigg/ \left(\frac{1}{n}\sum_{l=1}^{n} c(\mathbf{x}_l^j)\right) \quad , \quad j = 0, 1, \ldots \tag{3.10}$$

is the sample c.o.v. of the objective function during stage j. In other words, the algorithm runs until a prescribed number of stages are completed or until δ_{j+1} becomes less than some fraction γ of the initial sample c.o.v. of the objective function, δ_0. Smaller values for γ correspond to better approximations of the optimal solution set. It is noted that alternative stopping criteria can be implemented as well. The corresponding procedure to generate a set of candidate designs is illustrated in Fig. 3.3.

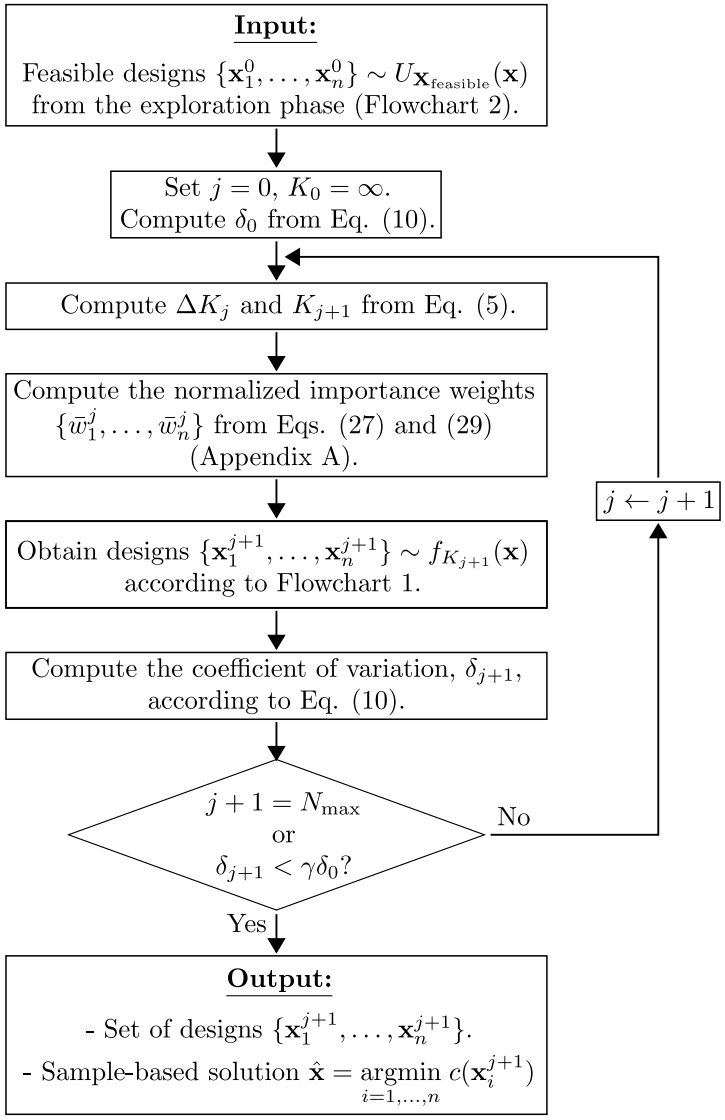

Fig. 3.3: Exploitation phase of ABO (Flowchart 3).

3.6.2 Additional remarks

Due to the annealing property of the approach, candidate designs with objective function values larger than those of the corresponding lead samples can be still accepted during the exploitation phase (see Appendix D). Thus, the probability of accepting a worse candidate solution during the initial stages is not negligible, but it decreases as the temperature parameter approaches zero. In this manner, sub-optimal regions in the feasible design space are potentially visited during the initial stages of the sampling process. The final stages, on the other hand, are almost completely

focused on improving the objective function values of the designs. This feature is beneficial towards avoiding local optima and improving the robustness of the overall optimization scheme.

3.7 Practical observations

Some practical benefits of using the proposed optimization scheme can be summarized as follows.

Adequacy for high performance computing. The sampling simulation technique under consideration, i.e., the TMCMC method, is very-well suited for parallel implementation in a computer cluster. In fact, the first level of the exploration phase, which corresponds to direct Monte Carlo simulation, can be fully scheduled in parallel. In addition, each of the subsequent levels of the exploration and exploitation phases produces a set of Markov chains that are perfectly parallel. Thus, a number of computer workers can handle the generation of samples corresponding to the different chains. This is very important when dealing with optimization problems involving expensive function evaluations.

Improved flexibility for decision making. Asymptotic Bayesian Optimization produces a set of nearly optimal solutions instead of a single optimal solution as well as a number of designs uniformly distributed over the feasible design space. In this manner, sensitivity information about the feasible designs and the final design can be obtained directly. This type of information can be advantageous in many practical cases where additional considerations or alternative criteria can be taken into account to select the appropriate final design. Thus, the approach provides flexibility to the decision-making process.

Robustness and effectiveness. Due to the theoretical basis of the formulation and the properties of the TMCMC method, the Asymptotic Bayesian Optimization scheme has high chances to reach a vicinity of the global optimum in an effective manner, even in presence of multiple local optima, complex feasible design spaces, and problems with multiple discontinuous sub-feasible regions. Moreover, no restrictions are imposed on the number of constraints. Furthermore, due to the gen-

erality and flexibility of the formulation it can handle, in principle, different types of optimization problems. From the structural optimization point of view, these problems may include discrete-continuous design variables, complex linear and nonlinear systems, and performance-based design problems.

Implementation simplicity. Special constraint-handling techniques, such as penalty function methods or other approaches, are not necessary within the context of the proposed two-phase scheme. In fact, the same framework for obtaining samples in the vicinity of the optimal solution set (exploitation phase) is used for finding designs in the feasible set (exploration phase). In addition, the proposed approach requires the definition of few control parameters. These features represent an advantage from a practical viewpoint.

3.8 Examples

Due to the generality of the proposed optimization scheme, a wide range of optimization problems can be considered for evaluating its effectiveness. For clarity and conciseness, three representative numerical examples are chosen and presented in this section. First, a test problem involving highly nonlinear benchmark functions with continuous design variables is examined to illustrate the capabilities of the proposed method in detail and, in addition, to evaluate the effect of the algorithm parameters on its performance. Then, the effectiveness of the Asymptotic Bayesian Optimization scheme is demonstrated by two design optimization problems: a classical engineering design problem including mixed discrete-continuous design variables, and a performance-based discrete-design optimization problem of a structural system under stochastic excitation. As previously pointed out, a number of additional or alternative engineering design problems can be considered as well.

3.8.1 Example No. 1: Benchmark functions

Optimization problem

The constrained optimization problem of interest is stated as

$$\begin{aligned} \min_{\mathbf{x}} \quad & c(x_1, x_2) \\ \text{s.t.} \quad & g(x_1, x_2) \leq 0 \\ & -3.0 \leq x_i \leq 3.0, \quad i = 1, 2 \end{aligned} \tag{3.11}$$

where the objective function $c(x_1, x_2)$ is the so-called *six-hump camel back* function given by

$$c(x_1, x_2) = 4.0x_1^2 - 2.1x_1^4 + x_1^6/3.0 + x_1x_2 - 4.0x_2^2 + 4.0x_2^4 \tag{3.12}$$

and the constraint function $g(x_1, x_2)$ is defined in terms of the *Schaffer function N.2* as

$$g(x_1, x_2) = 0.1 + \frac{\sin^2(x_1^2 - x_2^2) - 0.5}{[1 + 0.001(x_1^2 - x_2^2)]^2} \tag{3.13}$$

where x_1 and x_2 are the design variables which are treated as continuous variables. For illustration purposes, the objective and constraint functions are shown in Fig. 3.4. The left figure shows the objective function in the entire design space, while the right figure depicts the constraint function which is quite involved with abrupt variations in the design space. The corresponding feasible design space is illustrated in Fig. 3.5, where the two optimum solutions and some contours of the objective function are also shown. It is seen that the feasible design space is rather complex, as it involves several disconnected regions and some of them represent a small portion of the search space. In addition, the objective contours indicate that this example problem involves several disconnected sub-optimal regions. The optimal solutions of the optimization problem are given by $\mathbf{x}^* = \langle 0.0898, -0.7126 \rangle^T$ and $\mathbf{x}^* = \langle -0.0898, 0.7126 \rangle^T$, with optimum objective function $c(\mathbf{x}^*) = -1.0316$.

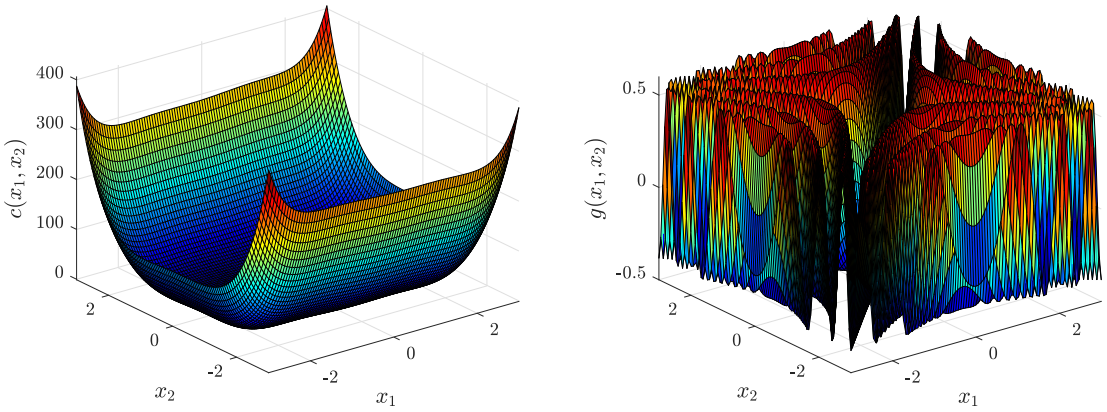

Fig. 3.4: Left: Objective function in the entire design space. Right: Constraint function. Example No. 1.

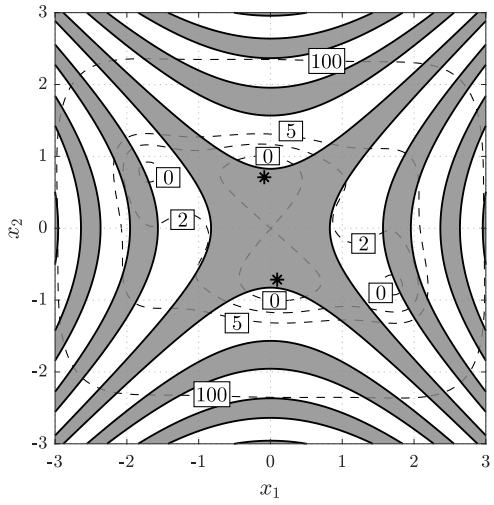

Fig. 3.5: Sketch of the feasible design space (gray area), optimal solutions (*), and contours of the objective function (dashed lines). Example No. 1.

Exploration phase

The following parameter values of the proposed approach are considered for the numerical implementation of the test problem: $\gamma = 0.05$ (stopping criterion parameter); $\nu = 0.5$ (effective sample size parameter); $n = 1000$ (number of samples per stage); and $n_{\text{feasible}} = 5000$ (target feasible sample size). In addition, the scaling parameter β, associated with the proposal distribution (see Appendix B), is determined by an adaptive scheme that monitors the acceptance rate of the updating process [288]. Figure 3.6 shows the evolution of the samples during the different stages of the exploration phase. The process stops at stage $j = 5$. That is, a total of six stages are required

to verify the stopping criterion of the exploration phase. Thus, the samples generated at the final stage correspond to stage 5. It is observed that the samples tend to populate the feasible design space more effectively as the number of stages increases. In fact, the shape of the set of samples at the final stage is very similar to the feasible design space shown in Fig. 3.5. During the different stages, almost 5800 feasible samples are obtained. Thus, it is clear that the method generates a set of samples uniformly distributed over the feasible design space in an effective manner for this example.

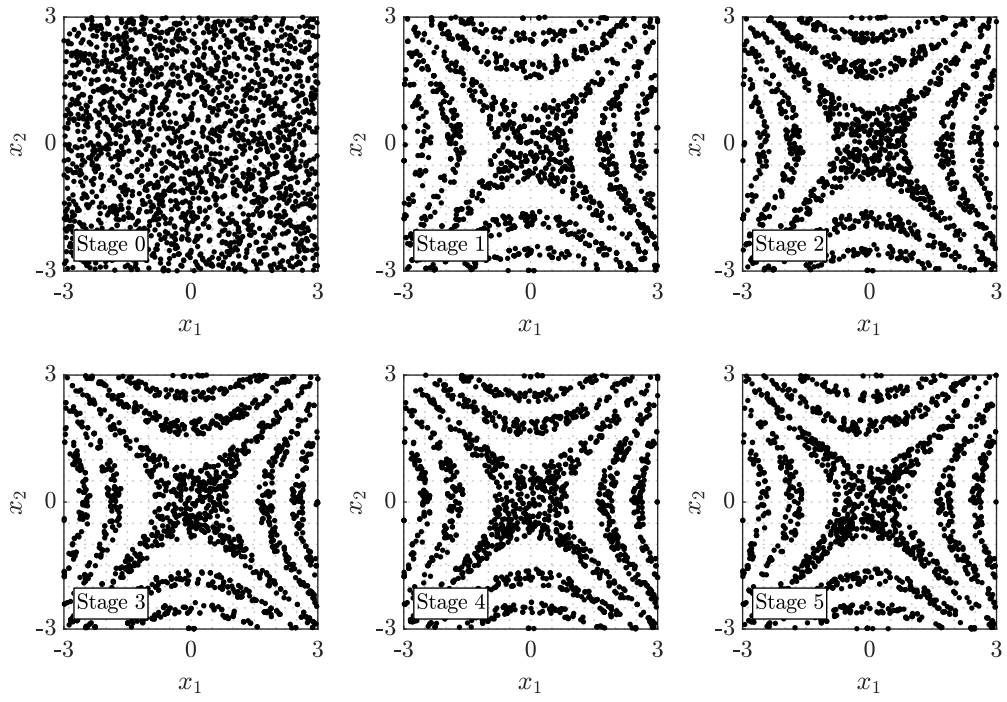

Fig. 3.6: Samples generated during the different stages of the exploration phase. Example No. 1.

Exploitation phase

Based on the set of feasible designs, the exploitation phase aims to obtain samples in a vicinity of the optimal solution set. Figure 3.7 shows the evolution of the samples obtained during the different stages of the exploitation phase. Note that the samples at the initial stage of the exploitation phase (stage 0 in the figure) correspond to the approximately 5800 feasible designs obtained during the exploration phase. It is seen that the intermediate distributions of the samples tend to be more and

more concentrated near the two optimum solutions as the iterations progress. Two clusters can be clearly seen at the last stage of the exploitation phase, whose mean and optimum solutions are given in Table 3.1. The previous results indicate that the method effectively populates a vicinity of the optimal solution set during the final stages for this example, which is consistent with the theoretical foundations of the proposed approach. In summary, the preceding results show the applicability and effectiveness of the proposed approach in a rather complex optimization problem involving a disconnected feasible design space with multiple global optima and several disconnected sub-optimal regions.

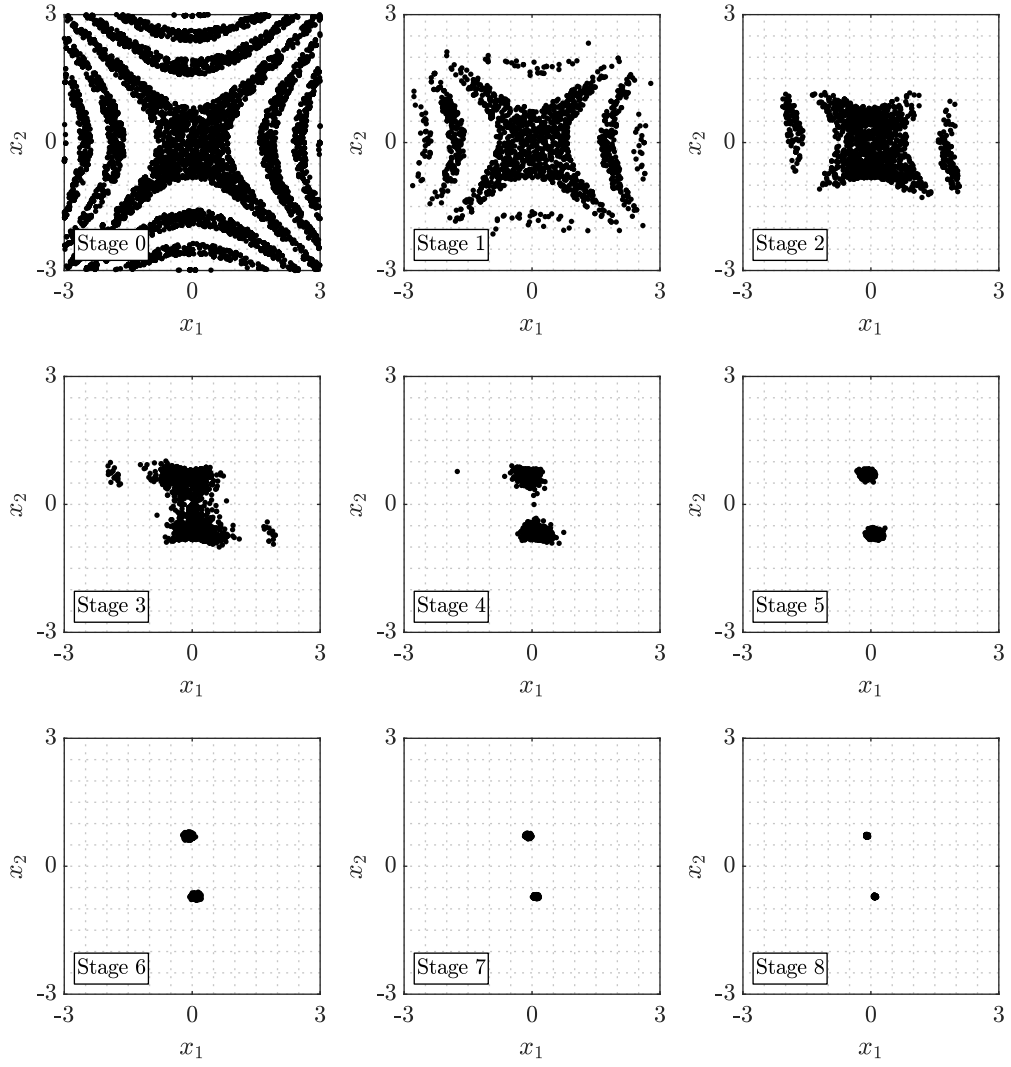

Fig. 3.7: Evolution of samples obtained during the different stages of the exploitation phase. Example No. 1.

Table 3.1: Sample-based mean, sample-based optimum, and actual optimum for each cluster. Example No. 1.

Design	Upper cluster	Lower cluster
Sample-based mean optimum $\bar{\mathbf{x}}$	$\bar{x}_1 = -0.0905$, $\bar{x}_2 = 0.7124$	$\bar{x}_1 = 0.0876$, $\bar{x}_2 = -0.7124$
Objective value $c(\bar{\mathbf{x}})$	-1.0316	-1.0316
Sample-based optimum $\hat{\mathbf{x}}^*$	$\hat{x}_1^* = -0.0901$, $\hat{x}_2^* = 0.7126$	$\hat{x}_1^* = 0.0896$, $\hat{x}_2^* = -0.7126$
Objective value $c(\hat{\mathbf{x}}^*)$	-1.0316	-1.0316
Actual optimum $\mathbf{x}^*$	$x_1^* = -0.0898$, $x_2^* = 0.7126$	$x_1^* = 0.0898$, $x_2^* = -0.7126$
Objective value $c(\mathbf{x}^*)$	-1.0316	-1.0316

Statistical performance

Preliminary validation calculations show that the number of samples per stage, n, plays an important role on the performance of the proposed approach. In this regard, a statistical analysis is carried out to study the influence of this parameter on the quality of the results. In particular, a total of 30 independent optimization runs are conducted for different numbers of samples per stage. They range from 50 to 1000. For comparison purposes, the target number of feasible samples is taken as $n_{\text{feasible}} = 2n$ and the total number of stages during the exploitation phase is limited to 8. The effective sample size parameter is taken as before, that is, $\nu = 0.5$. The statistical analysis is performed as follows. For the r^{th} independent run ($r = 1, \ldots, N_r = 30$), the sample-based optimum cost c_{opt}^r is obtained. In this framework, the optimum cost refers to the smallest objective function value found in each independent run. Based on these values, four statistical parameters are computed, namely, the best optimum cost $c_{\text{opt}}^{\text{best}}$, the worst optimum cost $c_{\text{opt}}^{\text{worst}}$, the average optimum cost $c_{\text{opt}}^{\text{avg}}$, and the coefficient of variation of the optimum cost $c_{\text{opt}}^{\text{c.o.v.}}$. The statistical parameters are formally defined as

$$\begin{aligned} c_{\text{opt}}^{\text{best}} &= \min_{r=1,\ldots,N_r} c_{\text{opt}}^r, \quad c_{\text{opt}}^{\text{worst}} = \max_{r=1,\ldots,N_r} c_{\text{opt}}^r \\ c_{\text{opt}}^{\text{avg}} &= \frac{1}{N_r}\sum_{r=1}^{N_r} c_{\text{opt}}^r, \qquad c_{\text{opt}}^{\text{c.o.v.}} = \frac{\sqrt{\frac{1}{N_r-1}\sum_{r=1}^{N_r}(c_{\text{opt}}^r - c_{\text{opt}}^{\text{avg}})^2}}{\mid c_{\text{opt}}^{\text{avg}} \mid} \end{aligned} \tag{3.14}$$

Table 3.2 shows the performance of the method in terms of the number of samples per stage. It is seen that the best optimum cost coincides with the reference value (-1.03163) even for a small

number of samples per stage. On the other hand, the best, average, and worst optimum costs remain almost invariant, from the practical viewpoint, when the number of samples per stage is greater than 200. Moreover, as expected, the corresponding c.o.v. of the optimum cost reduces as n increases. The previous results indicate that the scheme is able to explore the design space in a very effective manner, even with a relatively small number of samples per stage. Another interpretation of these results is that the proposed method, which is based on Markov chain Monte Carlo simulation, exhibits a good performance in terms of its ergodicity in this particular problem. Although the appropriate value of n is problem-dependent, 200 samples per stage seem to be suitable for this example.

Table 3.2: Statistical performance of the proposed scheme (ABO) in terms of the number of samples per stage (n). Example No. 1.

	optimal cost			
n	best ($c_{\text{opt}}^{\text{best}}$)	mean ($c_{\text{opt}}^{\text{avg}}$)	worst ($c_{\text{opt}}^{\text{worst}}$)	c.o.v. (%) ($c_{\text{opt}}^{\text{c.o.v.}}$)
50	-1.03163	-1.03003	-1.01513	3.5×10^{-3}
100	-1.03163	-1.03154	-1.03103	1.5×10^{-4}
150	-1.03163	-1.03157	-1.03096	1.2×10^{-4}
200	-1.03163	-1.03158	-1.03135	7.0×10^{-5}
500	-1.03163	-1.03162	-1.03158	8.0×10^{-6}
1000	-1.03163	-1.03163	-1.03162	2.0×10^{-6}

Finally, the influence of the effective sample size parameter, ν, on the quality of the optimization results is examined. Table 3.3 shows the best optimum cost, the worst optimum cost, the average optimum cost, and the c.o.v. of the optimum cost for different values of ν. The number of samples per stage is set equal to 200. It is seen that the best and average optimum costs are relatively similar to the reference solution, except for higher values of ν. In addition, the smallest difference between the best and worst optimum costs is obtained for intermediate values of the effective sample size parameter, that is, $\nu = 0.5$. Similarly, the c.o.v. of the optimum cost tends to decrease for intermediate values of ν. These results are reasonable due to the role that ν plays in the optimization process. On the one hand, consecutive intermediate distributions become more similar between

each other for higher values of ν and, as a result, more stages are required to obtain a distribution that is densely concentrated in a vicinity of the optimum solution set. This slower converge leads to a higher variability of the sample-based optimum cost, since the number of stages is limited to eight. On the other hand, smaller values for ν allow more abrupt changes in the shape of consecutive intermediate distributions. This, in turn, can be detrimental to the effectiveness of the Metropolis-Hastings method and, eventually, diminish the accuracy of the sample-based optimum solution. Thus, intermediate values for ν (around 0.5) should be preferred in this example to reduce the variability of the optimum solutions for a fixed computational cost.

Table 3.3: Statistical performance of the proposed scheme (ABO) in terms of the effective sample size parameter (ν). Example No. 1.

	optimal cost			
ν	best ($c_{\text{opt}}^{\text{best}}$)	mean ($c_{\text{opt}}^{\text{avg}}$)	worst ($c_{\text{opt}}^{\text{worst}}$)	c.o.v. (%) ($c_{\text{opt}}^{\text{c.o.v.}}$)
0.3	-1.03163	-1.03160	-1.03124	8.5×10^{-5}
0.5	-1.03163	-1.03158	-1.03135	7.0×10^{-5}
0.7	-1.03163	-1.03124	-1.02899	5.2×10^{-4}
0.9	-1.03091	-1.02093	-0.99980	9.1×10^{-3}

A similar behavior of the method performance with respect to ν is observed for alternative sample sizes. Analogously, the effect of n on the statistical performance of the method remains similar for different values of the effective sample size parameter. Such results are not presented here for conciseness and brevity. As indicated before, a number of samples per stage of around 200 and values for the effective sample size parameter roughly between 0.4 and 0.6 provide a reasonable tradeoff between efficiency and accuracy for this problem.

3.8.2 Example No. 2: A classical engineering design problem

Speed reducer design

The objective of this problem is to minimize the weight of the speed reducer shown in Fig. 3.8. A number of requirements associated with gear and shaft design practices, including bending and

clamp constraints, strength conditions on gear shafts, permissible magnitude of deflection, etc., must be satisfied [337]. Seven design variables are involved in the optimization problem (see Fig. 3.8): width of the gear face (x_1), teeth module (x_2), number of pinion teeth (x_3), length between bearings of shafts 1 and 2 (x_4 and x_5, respectively), and diameter of shafts 1 and 2 (x_6 and x_7, respectively). The problem can be formulated as

$$\begin{aligned} \min_{\mathbf{x}} \quad & c(\mathbf{x}) \\ \text{s.t.} \quad & g_j(\mathbf{x}) \leq 0, \quad j = 1, \ldots, 11 \\ & \mathbf{x} \in \mathbf{X} \end{aligned} \tag{3.15}$$

where the cost function is given by

$$\begin{aligned} c(\mathbf{x}) = {} & 0.7854 x_1 x_2^2 (3.3333 x_3^2 + 14.9334 x_3 - 43.0934) \\ & - 1.508 x_1 (x_6^2 + x_7^2) + 7.4777 (x_6^3 + x_7^3) + 0.7854 (x_4 x_6^2 + x_5 x_7^2), \end{aligned} \tag{3.16}$$

the constraint functions are defined as

$$\begin{aligned} & g_1(\mathbf{x}) = \frac{27}{x_1 x_2^2 x_3} - 1 \;\;,\;\; g_2(\mathbf{x}) = \frac{397.5}{x_1 x_2^2 x_3^2} - 1 \;\;,\;\; g_3(\mathbf{x}) = \frac{1.93 x_4^3}{x_2 x_6^4 x_3} - 1 \\ & g_4(\mathbf{x}) = \frac{1.93 x_5^3}{x_2 x_7^4 x_3} - 1 \;\;,\;\; g_5(\mathbf{x}) = \frac{\sqrt{\left(\frac{745 x_4}{x_2 x_3}\right)^2 + 16.9 \times 10^6}}{110.0 x_6^3} - 1 \\ & g_6(\mathbf{x}) = \frac{\sqrt{\left(\frac{745 x_5}{x_2 x_3}\right)^2 + 157.5 \times 10^6}}{85.0 x_7^3} - 1 \;\;,\;\; g_7(\mathbf{x}) = \frac{x_2 x_3}{40} - 1 \;\;,\;\; g_8(\mathbf{x}) = \frac{5 x_2}{x_1} - 1 \\ & g_9(\mathbf{x}) = \frac{x_1}{12 x_2} - 1 \;\;,\;\; g_{10}(\mathbf{x}) = \frac{1.5 x_6 + 1.9}{x_4} - 1 \;\;,\;\; g_{11}(\mathbf{x}) = \frac{1.1 x_7 + 1.9}{x_5} - 1 \end{aligned} \tag{3.17}$$

and the side constraints on the design variables are $2.6 \leq x_1 \leq 3.6$, $0.7 \leq x_2 \leq 0.8$, $x_3 \in \{17, 18, \ldots, 28\}$, $7.3 \leq x_4 \leq 8.3$, $7.3 \leq x_5 \leq 8.3$, $2.9 \leq x_6 \leq 3.9$, and $5.0 \leq x_7 \leq 5.5$. Note that the number of pinion teeth (x_3) is an integer quantity, whereas the rest of design variables are continuous. Thus, this is a mixed discrete-continuous optimization problem. A thorough description

of the objective and constraint functions can be found in [337].

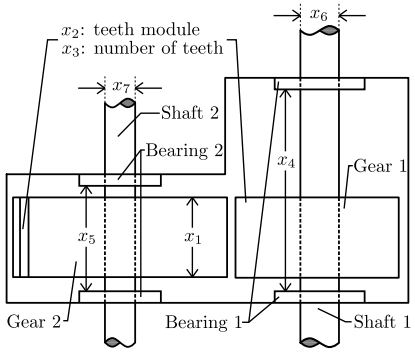

Fig. 3.8: Schematic of the speed reducer design problem. Example No. 2.

The proposed approach is implemented to solve the speed reducer design problem. The effective sample size parameter is taken as $\nu = 0.4$ and $n = 500$ samples per stage are considered. The exploration phase stops after obtaining $n_{\text{feasible}} = 1000$ feasible designs. For illustration purposes, 40 exploitation stages are considered in this case. In addition, the parameters of the discrete proposal distribution (see Appendix C) are defined as $\lambda^* = 2$ and $\tau = 0.05$ for the exploration phase, and as $\lambda^* = 1$ and $\tau = 0$ for the exploitation phase. Note that the parameter λ^* is updated at the beginning of each exploitation stage according to an adaptive scheme that reuses information gathered during previous stages (see Appendix C). Preliminary validation calculations indicate that the previous parameter values are appropriate in the context of this mixed discrete-continuous optimization problem.

First, an exploration phase is performed to generate samples uniformly distributed over the feasible set. After seven stages, a total of 1304 feasible designs are obtained. These designs are shown in Fig. 3.9 by means of two-dimensional projections and marginal histograms. It is noted that the feasible supports of variables x_1 and x_2 present the largest reduction when compared with the initial search space. This gives an insight on the sensitivity of the constraints with respect to the design variables.

The samples shown in Fig. 3.9 are used as the initial set of feasible designs for the exploitation phase. During this phase, samples increasingly concentrated near the set that minimizes the objec-

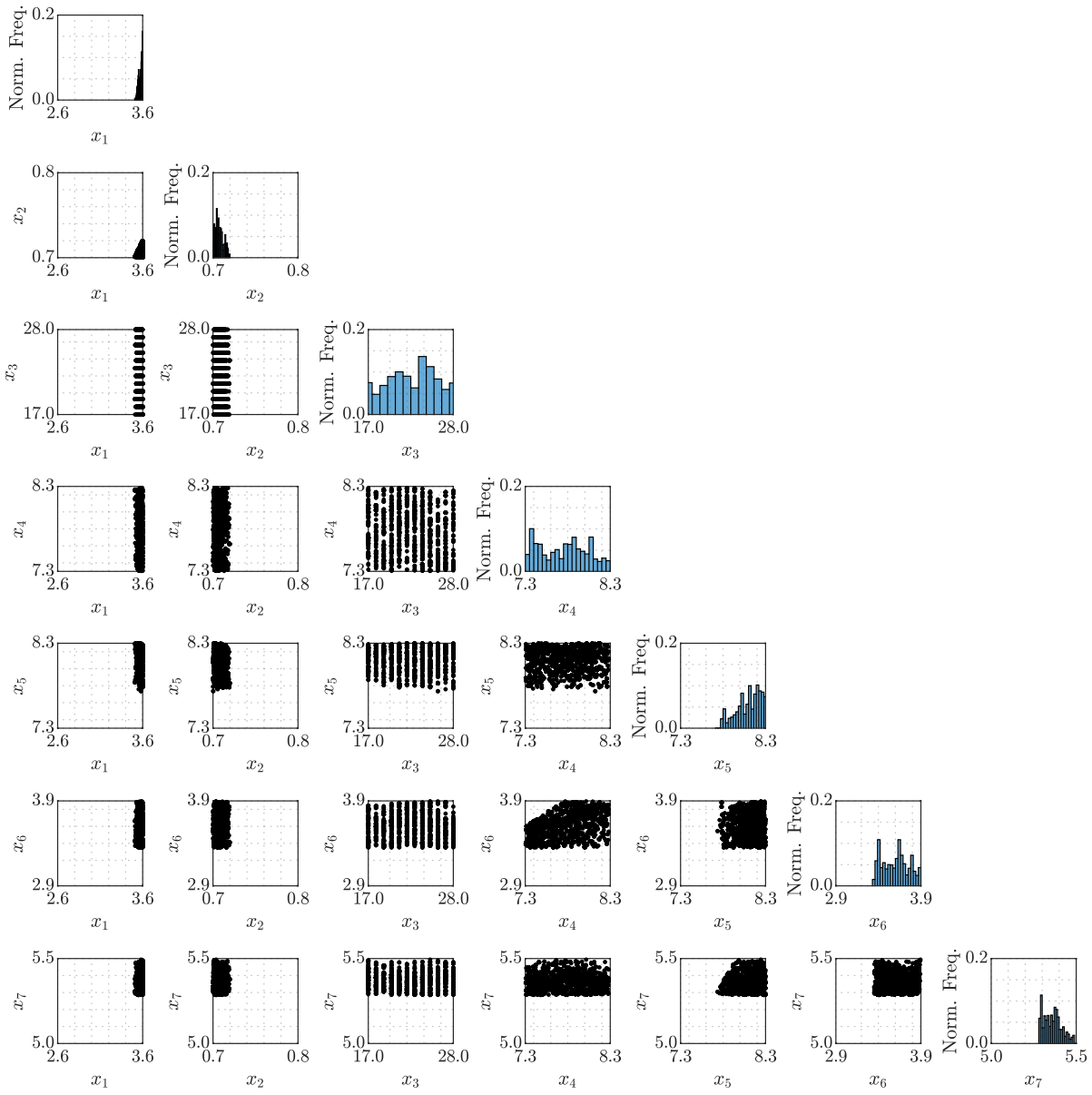

Fig. 3.9: Samples uniformly distributed over the feasible design set. Example No. 2.

tive function are iteratively generated. To illustrate this, Fig.3.10 presents the marginal histograms obtained during stages $j = 0, 5, 10, 15$ and 39 (last stage). Note that the support of x_3 is reduced significantly during the initial stages. In addition, the vicinity of the optimum solution set becomes more densely populated as the optimization process continues, as expected. Correspondingly, the range of the objective function is also reduced during the different stages of the proposed approach. The corresponding sample-based optimum obtained is $\mathbf{x}^* = \langle 3.50000, 0.70000, 17, 7.30001, 7.71533, 3.35022, 5.2$

with $c(\mathbf{x}^*) = 2994.4727$.

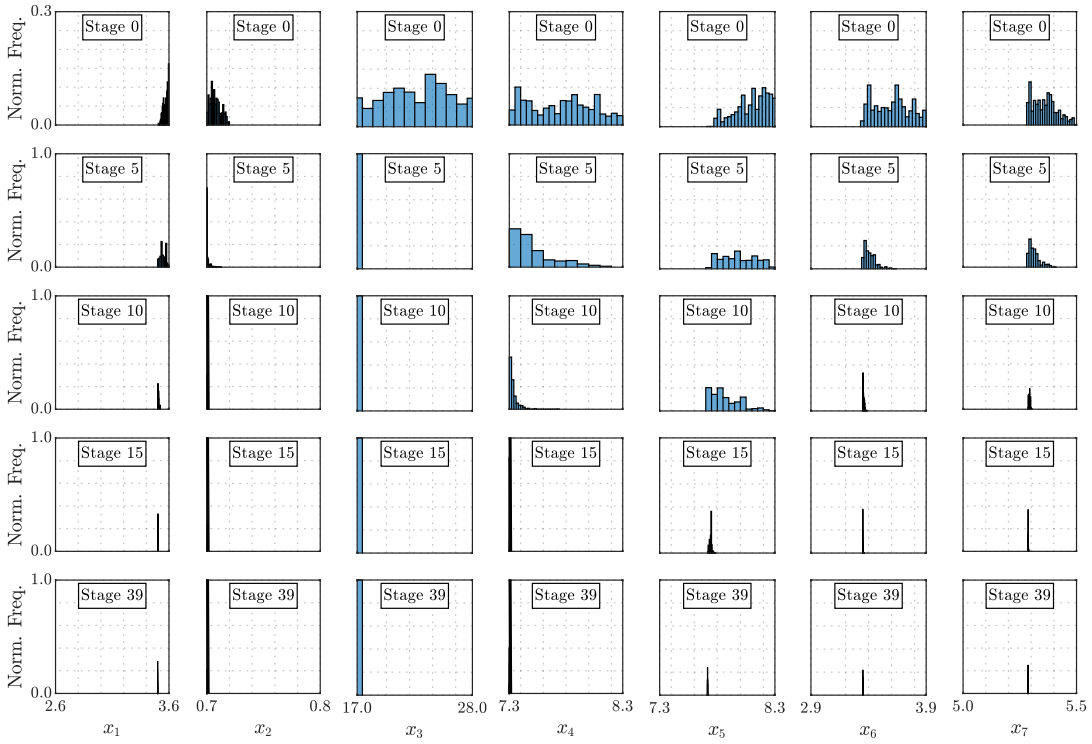

Fig. 3.10: Marginal histograms obtained during different stages of the exploitation phase. Example No. 2.

Finally, Table 3.4 presents the best solution obtained with the proposed approach across 30 independent runs. In addition, the table also shows the solution of this problem obtained by other stochastic search techniques reported in several references. They include Social Behavior inspired Optimization technique (SBO) [338], Particle Swarm Optimization with Differential Evolution (PSO-DE) [339], Differential Evolution with Level Comparison (DELC) [340], and Mine Blast Algorithm (MBA) [341]. For reference purposes, the number of function calls corresponding to each solution is also reported in the table. It is seen that the solution obtained by the proposed approach for this application example is competitive with respect to the ones obtained by other stochastic search techniques. Thus, the proposed framework can be an efficient choice for this problem.

Table 3.4: Best solutions reported by different algorithms. Example No. 2.

Design variables	Optimal values				
	SBO [338]	PSO-DE [339]	DELC [340]	MBA [341]	ABO
x_1	3.500000	3.500000	3.500000	3.500000	3.500000
x_2	0.700000	0.700000	0.700000	0.700000	0.700000
x_3	17	17	17	17	17
x_4	7.300000	7.300000	7.300000	7.300033	7.300004
x_5	7.800000	7.800000	7.715319	7.715772	7.715321
x_6	3.350215	3.350215	3.350240	3.350218	3.350215
x_7	5.286683	5.286683	5.286654	5.286654	5.286655
Weight (lb)	2996.232157	2996.348165	2994.471066	2994.482453	2994.471550
Function calls	70000	54350	30000	25000	24000

3.8.3 Example No. 3: A performance-based optimization problem

Description of the model

The structural model under stochastic excitation shown in Fig. 3.11, which has been borrowed from [182], is considered in this example. Each floor is supported by 48 columns as shown in Fig. 3.11. The columns on axes A, C, D, and F contribute to the horizontal resistance of the floors in the x direction, while those on axes B and E work primarily in the y direction. In addition, a bracing system consisting of tubular steel brace elements is placed in axes A, C, D and F acting in the x direction, and in axes 1, 2, 7 and 8 acting in the y direction. A typical configuration of the brace elements is shown in Fig. 3.12. Thus, a total of 128 brace elements are used in the model, with Young's modulus $E = 2.1 \times 10^{11}$ N/m^2 and weight density $\rho = 7.42$ ton/m^3. All floors have a constant height equal to 3.2 m, leading to a total height of 12.8 m. For a given floor, all columns are assumed to be equal and their specifications are given in Table 3.5 [342]. It is assumed that each floor may be represented with sufficient accuracy as rigid within the $x - y$ plane when compared to the flexibility of the horizontal resistant elements. Hence, each floor can be represented by three degrees of freedom, i.e., two translational displacements along the x and y axes, and a rotational displacement about the z axis. The associated masses $m_x = m_y$ and m_z are taken as constant for all floors and equal to 5.98×10^5 kg and 1.10×10^8 kg m^2, respectively. In addition, a 2% of critical

damping is assumed in the model. It is noted that no attempt has been made to consider a more detailed structural model since the objective of this example is to evaluate the effectiveness of the proposed optimization scheme in a performance-based optimization problem involving a structural dynamical system under stochastic excitation.

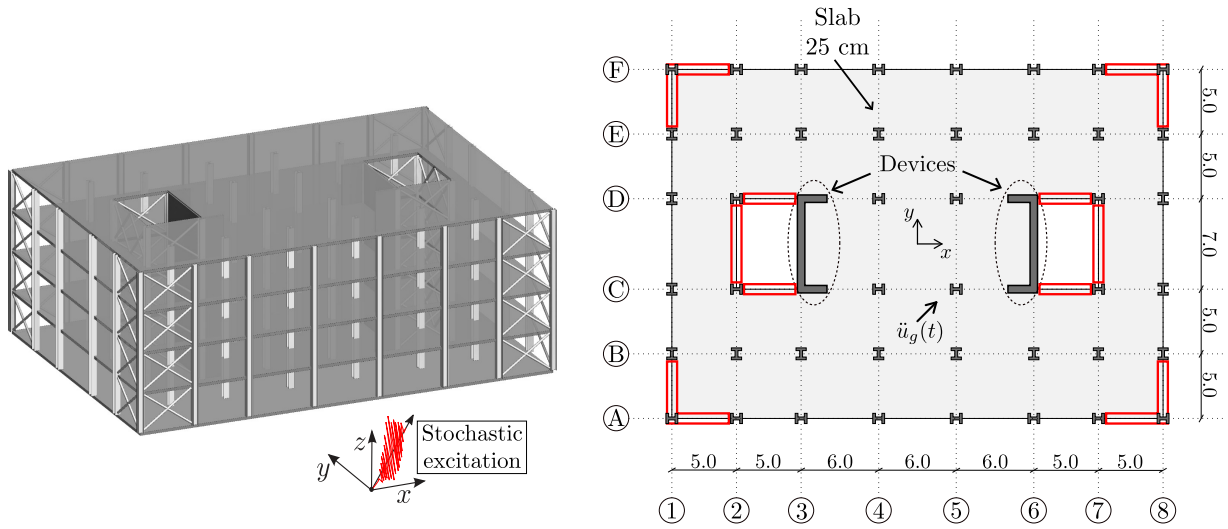

Fig. 3.11: Isometric (left) and plan (right) view of the structural model. Example No. 3.

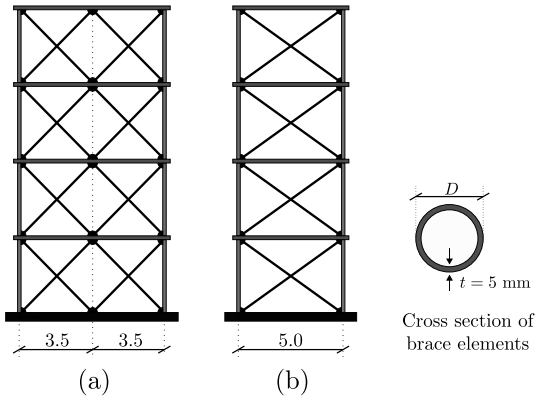

Fig. 3.12: Typical configuration of brace elements. (a) Brace system in axes 2 and 7. (b) Brace system in axes A, C, D, F, 1 and 8. Example No. 3.

The system is subjected to a base acceleration modeled as a non-stationary stochastic process. In particular, a stochastic model based on a point-source model is considered [34, 114]. The model is characterized by a white noise sequence and a series of parameters such as radiation pattern, shear wave velocity in the vicinity of the source, corner frequencies, local site conditions, velocity pulse parameters, and additional seismicity parameters such as the moment magnitude and rupture

Table 3.5: Specification of column elements. Example No. 3.

Floor	Type of section
1	W24 $\times$ 131
2	W24 $\times$ 131
3	W24 $\times$ 104
4	W24 $\times$ 104

distance. Details of the procedure can be found in [34, 114, 321, 343]. The excitation is applied at 45° with respect to the x axis and its duration is taken as $T = 15$ s with a sampling interval equal to $\Delta t = 0.01$ s. Based on these values and according to the stochastic excitation model under consideration, it can be shown that more than 1500 random variables are involved in the generation of base acceleration samples [114]. Thus, a high-dimensional uncertain parameter space is involved in this problem. For illustration purposes, Fig. 3.13 shows a synthetic ground motion sample corresponding to the stochastic point-source model.

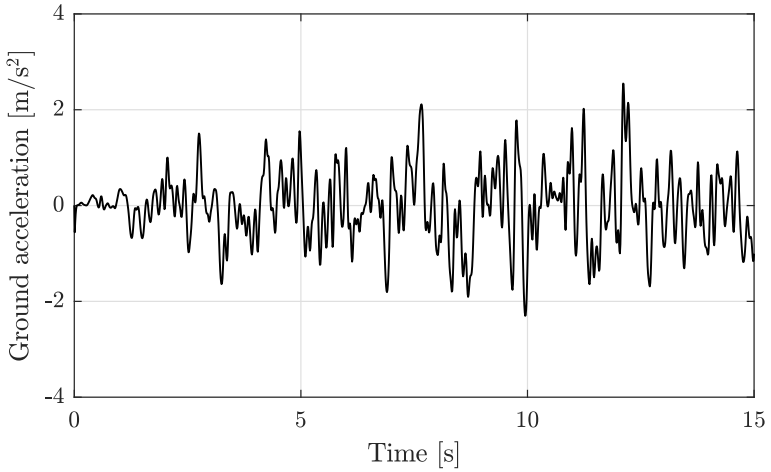

Fig. 3.13: Synthetic ground acceleration sample from the stochastic point-source model. Example No. 3.

For improved seismic behavior, the model is reinforced with nonlinear devices at each floor. At each floor, six devices are implemented as shown in the floor plan of the model (see Fig. 3.11). Specifically, four devices in the x direction and two devices in the y direction are considered. These elements provide additional resistance against relative displacements between floors. The devices

follow the inter-story restoring force law $\kappa(t) = k_d\Big(\delta(t) - \gamma^1(t) + \gamma^2(t)\Big)$, where k_d denotes the initial stiffness of the device, $\delta(t)$ is the relative displacement between floors, and $\gamma^1(t)$ and $\gamma^2(t)$ denote the plastic elongations of the device. Using the auxiliary variable $\mu(t) = \delta(t) - \gamma^1(t) + \gamma^2(t)$, the plastic elongations $\gamma^1(t)$ and $\gamma^2(t)$ are specified by the differential equations [344]

$$\begin{aligned}\dot{\gamma}^i(t) =& \varsigma(i)\dot{\delta}(t)H(\varsigma(i)\dot{\delta}(t))\times \\ & \left[H(\varsigma(i)\mu(t) - \mu_y)\frac{\varsigma(i)\mu(t) - \mu_y}{\mu_p - \mu_y}H(\mu_p - \varsigma(i)\mu(t)) + H(\varsigma(i)\mu(t) - \mu_p)\right] \quad , \quad i = 1, 2\end{aligned} \tag{3.18}$$

where $H(\cdot)$ denotes the Heaviside step function, $\varsigma(1) = 1$, $\varsigma(2) = -1$, μ_y is a parameter specifying the onset of yielding, and k_d μ_p is the maximum restoring force of the device. The values $\mu_p = 6.0 \times 10^{-3}$ m, $\mu_y = 0.7u_p$, and $k_d = 6.0 \times 10^8$ N/m are used for the nonlinear elements. A typical displacement-restoring force curve of the nonlinear devices is shown in Fig. 3.14. Note that, because of yielding, energy dissipation due to hysteresis is introduced in the structural response.

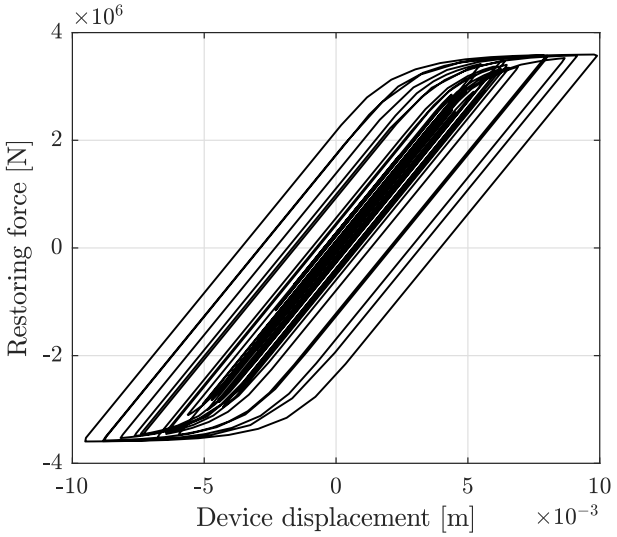

Fig. 3.14: Typical displacement-restoring force curve of the nonlinear device. Example No. 3.

Design problem

The objective function for the optimization problem is defined in terms of the expected value of the root-mean-square (RMS) of the displacement response at the top floor, while the design constraints are given in terms of cost limitations, geometric requirements and availability of section sizes. The vector of design variables $\mathbf{x}$ is defined in terms of the areas of the cross-sections of the steel brace elements. For illustration purposes, the brace elements located every two floors are linked to two design variables, one associated with the x direction and one with the y direction. This leads to four design variables in total. The axes and stories corresponding to each design variable are given in Table 3.6. In this setting, x_1 and x_3 are associated with the brace elements pointing in the x direction, while x_3 and x_4 with those pointing in the y direction. The values for the different design variables (areas of tubular cross-sections) must be selected from the discrete set of available member sizes presented in Table 3.7. Thus, each design variable can be chosen from a discrete set of 48 tubular elements and, therefore, more than 5×10^6 different configurations for the bracing system can be devised.

Table 3.6: Design variables. Example No. 3.

Design variables	Stories	Axes
x_1	1-2	A C D F
x_2	1-2	1 2 7 8
x_3	3-4	A C D F
x_4	3-4	1 2 7 8

The design problem is written as

$$\begin{aligned} \min_{\mathbf{x}} \quad & c(\mathbf{x}) \\ \text{s.t.} \quad & g_1(\mathbf{x}) = \bar{v}(\mathbf{x}) - 1 \leq 0 \\ & g_2(\mathbf{x}) = x_3/x_1 - 1 \leq 0 \\ & g_3(\mathbf{x}) = x_4/x_2 - 1 \leq 0 \\ & x_i \in X,\ i = 1, \ldots, 4 \end{aligned} \tag{3.19}$$

Table 3.7: Available values for the design variables. Example No. 3.

D (in)	A (mm^2)	D (in)	A (mm^2)	D (in)	A (mm^2)
2	719	4	1517	6	2315
2 1/8	769	4 1/8	1567	6 1/8	2365
2 1/4	819	4 1/4	1617	6 1/4	2415
2 3/8	869	4 3/8	1667	6 3/8	2465
2 1/2	919	4 1/2	1717	6 1/2	2515
2 5/8	969	4 5/8	1767	6 5/8	2565
2 3/4	1019	4 3/4	1817	6 3/4	2615
2 7/8	1069	4 7/8	1866	6 7/8	2664
3	1118	5	1916	7	2714
3 1/8	1168	5 1/8	1966	7 1/8	2764
3 1/4	1218	5 1/4	2016	7 1/4	2814
3 3/8	1268	5 3/8	2066	7 3/8	2864
3 1/2	1318	5 1/2	2116	7 1/2	2914
3 5/8	1368	5 5/8	2166	7 5/8	2964
3 3/4	1418	5 3/4	2216	7 3/4	3014
3 7/8	1468	5 7/8	2265	7 7/8	3063

where $\mathbf{x} = \langle x_1, x_2, x_3, x_4 \rangle^T$ is the vector of design variables, $c(\mathbf{x})$ is the objective function, $\bar{v}(\mathbf{x})$ is a normalized cost function associated with the total volume of the bracing system, and X represents the set of available discrete values for the design variables given in Table 3.7. It is noted that $g_1(\mathbf{x})$ is associated with cost limitations, whereas $g_2(\mathbf{x})$ and $g_3(\mathbf{x})$ impose geometric conditions on the final design. As previously pointed out, the objective function corresponds to the expected value of the root-mean-square of the displacement response at the top floor, that is, $c(\mathbf{x}) = E_{\boldsymbol{\theta}}[RMS_d(\mathbf{x}, \boldsymbol{\theta})]$ where $\boldsymbol{\theta}$ is the vector of uncertain parameters involved in the stochastic excitation model, $E_{\boldsymbol{\theta}}(\cdot)$ denotes the expectation with respect to the distribution of $\boldsymbol{\theta}$, and

$$RMS_d(\mathbf{x}, \boldsymbol{\theta}) = \frac{1}{N_T} \sqrt{\sum_{k=1}^{N_T} \{u_x^2(t_k, \mathbf{x}, \boldsymbol{\theta}) + u_y^2(t_k, \mathbf{x}, \boldsymbol{\theta})\}} \tag{3.20}$$

where $u_x(t_k, \mathbf{x}, \boldsymbol{\theta})$ and $u_y(t_k, \mathbf{x}, \boldsymbol{\theta})$ are the x and y components, respectively, of the roof displacement at time instant $t_k, k = 1, \ldots, N_T, N_T = 1500$, for a given realization of $\boldsymbol{\theta}$. The estimate of $c(\mathbf{x})$ is evaluated by means of Monte Carlo simulation [81]. In particular, 2000 samples are

considered, that is, the evaluation of the objective function at each design involves 2000 dynamic analyses in this case. In addition, the normalized cost function is defined as $\bar{v}(\mathbf{x}) = \sum_{i=1}^{4} v_i^* x_i$, with normalized constants $v_1^* = v_3^* = 0.9402 \times 10^{-4}$ and $v_2^* = v_4^* = 1.2363 \times 10^{-4}$.

Results

The proposed optimization framework is implemented to handle this performance-based design problem considering $n = 200$ samples per stage and $\nu = 0.5$ for the effective sample size parameter. In addition, the stopping criteria for the exploration and exploitation phases are to obtain $n_{\text{feasible}} = 400$ feasible designs and to verify $\delta_{j+1} < \gamma\delta_0$ with $\gamma = 0.01$ (see Section 3.6.1), respectively. Moreover, the proposal distributions for the discrete design variables (see Appendix C) are defined by $\lambda_l^* = 3$, $\tau_l = 0.05$, $l = 1, \ldots, 4$, for the exploration phase, and by $\lambda_l^* = 1$, $\tau_l = 0$, $l = 1, \ldots, 4$, for the exploitation phase. As in the previous example, the parameters λ_l^* are updated during the different stages of the exploitation phase according to the strategy presented in Appendix C. Additional validation computations indicate that the previous implementation details are adequate in the context of this application.

Feasible designs are first obtained during an exploration phase. In this case, a total of 544 designs uniformly distributed over the feasible region are obtained after four TMCMC stages, which are shown in Fig. 3.15 by means of two-dimensional projections and marginal histograms. Note that the projections $x_1 - x_3$ and $x_2 - x_4$ show some interaction between the design variables, which is associated with the effect of the geometric constraints. In this regard, the results of the exploration phase provide an insight on the sensitivity of the constraints with respect to the design variables. Starting with this set of feasible designs, an exploitation phase is then carried out to generate a set of designs lying in a vicinity of the optimal solution set. For illustration purposes, Fig. 3.16 shows the minimum and maximum objective function values obtained during the different stages of the exploitation phase. Note that the difference between both values reduces as the optimization process continues, which is consistent with the theoretical foundations of the proposed approach.

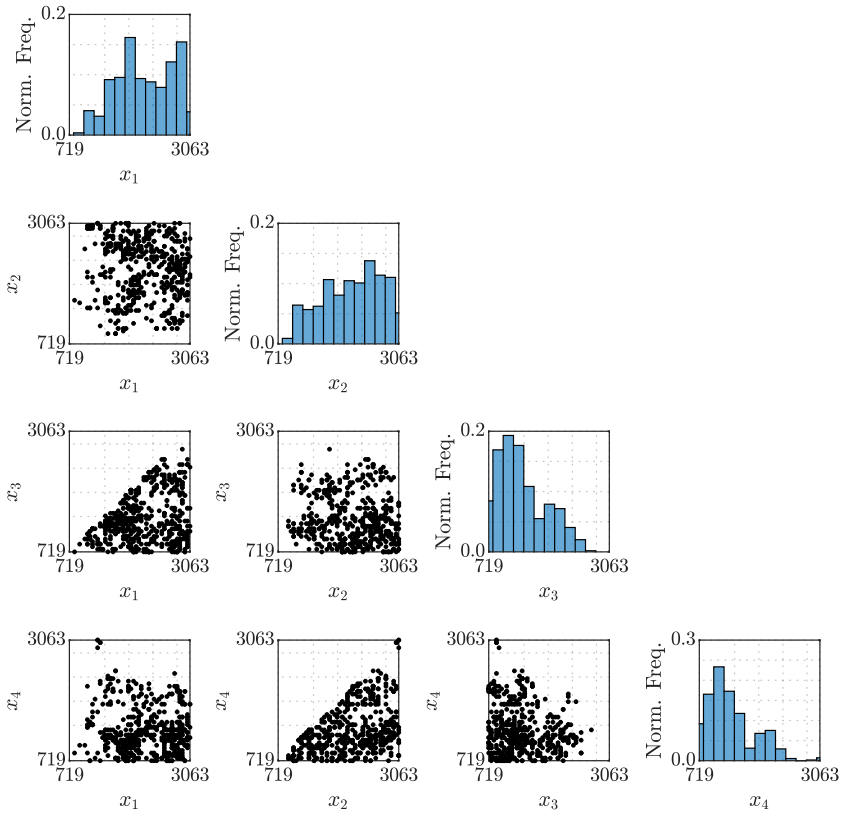

Fig. 3.15: Two-dimensional sample projections and marginal histograms of the feasible samples. Example No. 3.

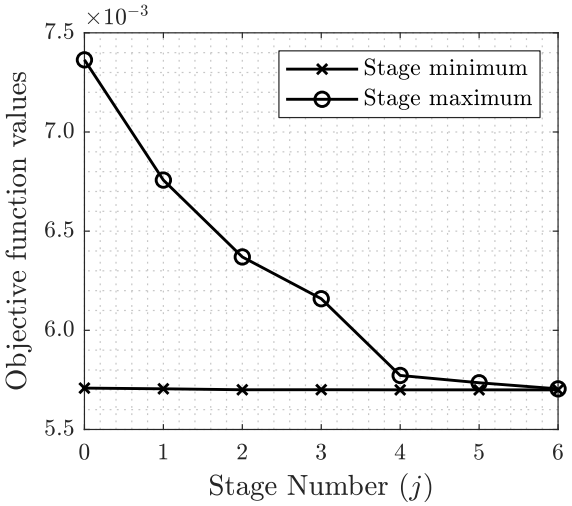

Fig. 3.16: Maximum and minimum objective function values obtained during the different stages of the exploitation phase. Example No. 3.

Figure 3.17 shows the samples, in terms of marginal histograms, obtained during exploitation stages $j = 0$, 2, 4, and 6 (final stage). It is seen that the designs are increasingly concentrated near the set

that minimizes the objective function, as expected. The reduction in the RMS of the displacement at the top floor is attained by selecting higher values for x_1 and x_2, and intermediate values for x_3 and x_4. In other words, larger section sizes are preferred for the braces allocated in the lower stories, which is reasonable from the structural viewpoint. This provides valuable information on the sensitivity of the objective function with respect to the design variables. Furthermore, the last stage of the optimization procedure provides several designs with very similar objective function values (see Fig. 3.16) which, due to the variability in the estimation of this quantity, can be regarded as equivalent from the objective function viewpoint. Therefore, the final design can be selected by considering alternative criteria. This highlights one of the advantages of the proposed optimization framework, that is, a set of candidate designs is obtained instead of a single solution, which provides additional flexibility for the overall decision-making process.

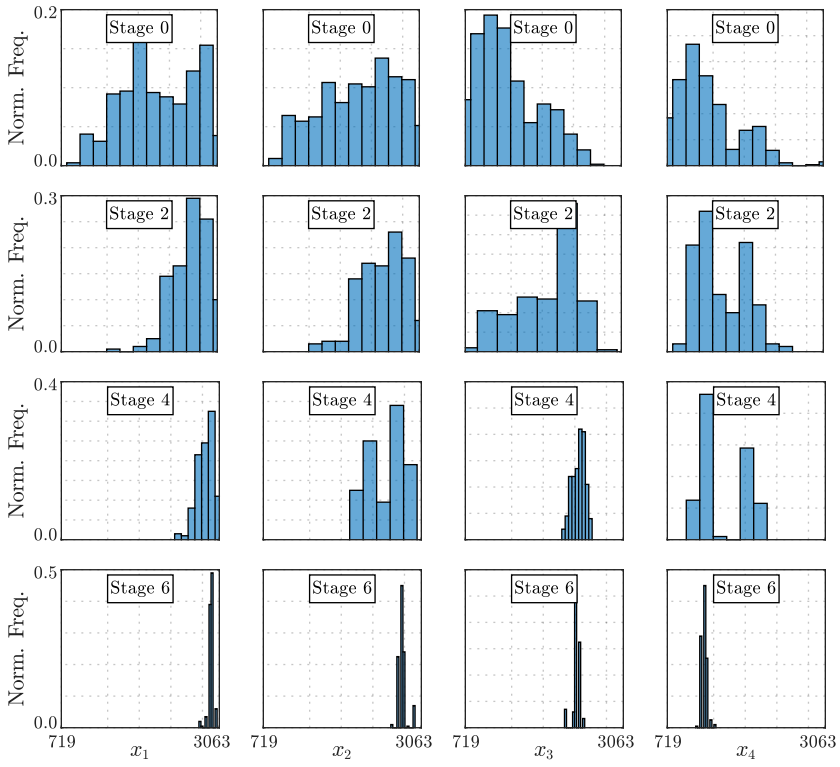

Fig. 3.17: Marginal histograms obtained during different stages of the exploitation phase. Example No. 3.

For reference and comparison purposes, Table 3.8 shows the best solution obtained by the proposed approach. In addition, the optimum design obtained by means of Genetic Algorithms (GA) [307],

which considers a population size of 200 individuals is also reported in the table. It is seen that both solutions are qualitatively similar and, taking into account the variability in the estimation of the objective function value, they can be regarded as equivalent from the optimization viewpoint. However, it is observed that the cost constraint is slightly violated in the GA-based solution. Finally, in terms of numerical efforts, the total number of function calls (expected value of the root-mean-square of the displacement response at the top floor) is in the order of 2000 for both cases.

Table 3.8: Best solutions reported by the proposed method (ABO) and Genetic Algorithms (GA). Example No. 3.

Design variables	Optimal values	
	ABO	GA
x_1	3063	2963
x_2	2714	2864
x_3	2265	2116
x_4	1318	1368
$E_{\boldsymbol{\theta}}[RMS_d(\mathbf{x}, \boldsymbol{\theta})]$	5.70×10^{-3}	5.70×10^{-3}
$g_1(\mathbf{x})$	-5.8×10^{-4}	8.3×10^{-4}
$g_2(\mathbf{x})$	-2.61	-0.37
$g_3(\mathbf{x})$	-0.51	-0.68
Function calls	2000	2138

The results presented in this section and additional validation calculations illustrate that the proposed optimization framework is an effective tool to handle complex constrained optimization problems, such as those involving performance-based measures, nonlinear structural systems under stochastic excitation, and discrete design variables. Thus, the proposed approach is a competitive, general and flexible choice for dealing with a general class of constrained design optimization problems.

3.9 Conclusions

A general Markov sampling-based framework for solving a class of constrained design optimization problems has been presented. The design problem is reformulated as the equivalent task of

obtaining samples uniformly distributed over the optimum solution set. To generate such samples, a sequence of distributions increasingly concentrated around the optimum solution set is introduced. Furthermore, a unified two-phase strategy is developed. An exploration phase generates an initial set of designs uniformly distributed over the feasible domain, and then an exploitation phase generates designs increasingly concentrated in a vicinity of the optimum solution set. The transitional Markov chain Monte Carlo method is adapted to generate the required samples during both phases, and appropriate adaptive proposal distributions are implemented for the continuous and discrete design variables. The capabilities of the proposed approach, which is quite general, have been demonstrated in different types of representative design optimization problems. Numerical results have shown some of the advantages and benefits of the proposed Asymptotic Bayesian Optimization scheme.

- First, the proposed method can handle complex feasible design spaces. In fact, the exploration phase is able to deal with linear and nonlinear constraint functions, and feasible designs can be efficiently generated in cases involving non-trivial geometries for the feasible design space such as disconnected regions.

- Second, the exploitation phase successfully generates designs in a vicinity of the optimum solution set for relatively complex objective functions. Moreover, the method can also handle problems involving single and multiple optima. In general, few stages are required to identify a region that lies close to the optimum solution set.

- Third, the same framework can be used for purely continuous, purely discrete, or mixed discrete-continuous design variables. In this context, suitable adaptive proposal distributions for the continuous and discrete design variables are suggested.

- Fourth, the approach provides benefits from the practical viewpoint. In this regard, relatively few user-defined parameters are involved in the proposed approach. Numerical results indicate that sample sizes in the range of 200-500 and intermediate values for the effective sample size parameter, e.g. 0.5, yield a good tradeoff between efficiency and accuracy for the design

problems investigated in this work. In addition, constraints are handled directly during the sampling process. Therefore, special constraint-handling techniques are not required by the proposed optimization scheme.

- Fifth, information on the sensitivity of the constraint and objective functions with respect to the design variables is provided as a by-product of the sampling process. This feature is particularly valuable in situations where problem functions are not known explicitly. Thus, additional insight for design purposes is obtained without any additional computational effort and, as a result, improved flexibility can be accomplished throughout the overall decision making process.

- Sixth, the same stochastic sampling technique is used to explore the feasible and optimum sets, which is advantageous from the implementation viewpoint.

- Finally, the example problems considered in this contribution and additional validation calculations indicate that the method is very competitive with respect to other state-of-the-art stochastic search techniques. Overall, the proposed Markov sampling-based framework is a valuable tool to deal with a wide range of constrained design optimization problems. In this regard, it is stressed that the proposed Asymptotic Bayesian Optimization scheme is quite general. In other words, it is not customized to a particular class of engineering design problems.

Future research efforts aim to extend the proposed framework to more complex structural optimization problems, including general performance-based design optimization problems. In this context, suitable strategies based on parametric reduced-order models can be integrated to increase the overall efficiency of the optimization procedure. The treatment of multiobjective optimization problems by means of the proposed approach is an additional subject for future work. Another research direction involves the implementation and assessment of alternative sampling schemes within the two-phase framework. Some of these topics are currently under consideration.

3.10 Appendix A

The lead sample in terms of the continuous and discrete design variables, which is denoted as $\tilde{\mathbf{x}}^{j+1} = \langle \tilde{\mathbf{x}}_c^{j+1^T}, \tilde{\mathbf{x}}_d^{j+1^T} \rangle^T$, is a sample from stage j that is selected with probability equal to its normalized importance weight $\bar{w}_i^j, i = 1, \ldots, n$, that is,

$$\bar{w}_i^j = \frac{w_i^j}{\sum_{l=1}^n w_l^j}, \quad w_i^j = \frac{f_{K_{j+1}}(\mathbf{x}_i^j)}{f_{K_j}(\mathbf{x}_i^j)}, \quad i = 1, \ldots, n \tag{3.21}$$

where $w_i^j, i = 1, \ldots, n$ are the importance weights given by

$$w_i^j = \exp\left(-h(\mathbf{x}_i^j)\left[\frac{1}{K_{j+1}} - \frac{1}{K_j}\right]\right) \tag{3.22}$$

for the exploration phase, and

$$w_i^j = \exp\left(-c(\mathbf{x}_i^j)\left[\frac{1}{K_{j+1}} - \frac{1}{K_j}\right]\right) \tag{3.23}$$

for the exploitation phase. If a sample $\mathbf{x}_i^j$ has been already drawn, then the last sample of its corresponding Markov chain is selected as the lead sample.

3.11 Appendix B

A symmetric local proposal distribution p_c is considered for the continuous design variables. The proposal is taken as a Gaussian distribution centered at the lead sample, say $\tilde{\mathbf{x}}_c^{j+1}$, whose covariance matrix $\mathbf{\Sigma}_j$ is equal to a scaled version of the estimate covariance matrix of the continuous design variables following the intermediate distribution $f_{K_j}(\mathbf{x})$. That is,

$$\mathbf{\Sigma}_j = \beta^2 \sum_{i=1}^n \bar{w}_i^j \left(\mathbf{x}_{ci}^j - \bar{\mathbf{x}}_c^j\right)\left(\mathbf{x}_{ci}^j - \bar{\mathbf{x}}_c^j\right)^T \tag{3.24}$$

where β is a scaling parameter, $\mathbf{x}_{ci}^{j}, i = 1, \ldots, n$ are the samples at stage j, $\bar{w}_i^j, i = 1, \ldots, n$ are the normalized importance weights, and $\bar{\mathbf{x}}_c^j = \sum_{i=1}^{n} \bar{w}_i^j \mathbf{x}_{ci}^j$ is the estimate mean of the continuous design variables following $f_{K_{j+1}}(\mathbf{x})$. The scaling parameter β can be defined directly by the user, or it can be determined by an adaptive scheme that monitors the acceptance rate in the context of the Metropolis-Hastings algorithm [179, 288]. It is noted that alternative sampling schemes in the so-called underlying normal space [179] can be also considered in the context of the ABO method.

3.12 Appendix C

The proposal distribution p_d for the vector of discrete design variables $\mathbf{x}_d$ is defined in terms of independent proposal distributions corresponding to each discrete variable, that is,

$$p_d(\mathbf{x}_d^\star | \tilde{\mathbf{x}}_d^{j+1}) = \prod_{l=1}^{n_d} p_{dl}(x_{dl}^\star | \tilde{x}_{dl}^{j+1}) \tag{3.25}$$

where $\mathbf{x}_d^\star = \langle x_{d1}^\star, \ldots, x_{dn_d}^\star \rangle^T$ is the candidate sample, $\tilde{\mathbf{x}}_d^{j+1} = \langle \tilde{x}_{d1}^{j+1}, \ldots, \tilde{x}_{dn_d}^{j+1} \rangle^T$ is the lead sample of the discrete design variables, and $p_{dl}(x_{dl}^\star | \tilde{x}_{dl}^{j+1})$ is the local proposal distribution for the discrete design variable $x_{dl}^\star$. The candidate sample $x_{dl}^\star$ is selected from the set of discrete values adjacent to $\tilde{x}_{dl}^{j+1}$, i.e., $Adj(\tilde{x}_{dl}^{j+1})$, which is defined as

$$Adj(\tilde{x}_{dl}^{j+1}) = \{ x_{dl(i)_{i=1,\ldots,n_{di}}} : \lambda(\tilde{x}_{dl}^{j+1}, x_{dl(i)}) \leq \lambda_l^* \} \tag{3.26}$$

where $\lambda(\tilde{x}_{dl}^{j+1}, x_{dl(i)})$ is the *distance* between the lead sample $\tilde{x}_{dl}^{j+1}$ and the sample $x_{dl(i)}$. For example, if the lead sample corresponds to the s^{th} available value of the discrete variable x_{dl}, that is, $\tilde{x}_{dl}^{j+1} = x_{dl(s)}$, the distance between these two samples is given by $\lambda(\tilde{x}_{dl}^{j+1}, x_{dl(i)}) = \lambda(x_{dl(s)}, x_{dl(i)}) = |s - i|$. The proposal distribution for the l^{th} discrete design variable is defined as [182]

$$p_{dl}(x_{dl}^\star | \tilde{x}_{dl}^{j+1}) = \begin{cases} \frac{1-\tau}{Card(Adj(\tilde{x}_{dl}^{j+1}))}, & \text{if } x_{dl}^\star \in Adj(\tilde{x}_{dl}^{j+1}) \\ \frac{\tau}{Card(Adj^c(\tilde{x}_{dl}^{j+1}))}, & \text{if } x_{dl}^\star \notin Adj(\tilde{x}_{dl}^{j+1}) \end{cases} \tag{3.27}$$

where τ represents a small probability of randomly selecting a nonadjacent value of the lead sample $\tilde{x}_{dl}^{j+1}$, $Adj^c(\tilde{x}_{dl}^{j+1})$ is the complement set of $Adj(\tilde{x}_{dl}^{j+1})$, and $Card(\cdot)$ is the number of discrete available values in the corresponding set.

It is noted that the values for the distribution parameters λ_l^* and τ are problem-dependent. Such parameters can be selected directly by the user or adaptively tuned during the sampling process. In this contribution, an adaptive strategy is implemented. At the beginning of each exploitation stage, the parameter λ_l^* is updated by reusing information obtained during the previous stage. The procedure is carried out as follows. First, the elements of $\mathbf{X}_{dl}$ that were observed during the previous stage are identified. Then, the *maximum number of consecutive values* observed during the previous stage, denoted by η, is obtained. Based on this number, the parameter λ_l^* is updated as

$$\lambda_l^* = \min\{\lambda_l^*, m\} \tag{3.28}$$

where m is the largest integer such that $m \leq (\eta - 1)/2$. The process is repeated for $l = 1, \ldots, n_d$. This scheme tends to decrease the value of λ_l^* for advanced exploitation stages, which can improve the efficiency of the proposed approach. Certainly, alternative strategies can be implemented as well.

3.13 Appendix D

The implementation of the acceptance/rejection test, in the context of the Metropolis-Hastings algorithm, is as follows. The candidate sample $\mathbf{x}^\star = \langle \mathbf{x}_c^{\star T}, \mathbf{x}_d^{\star T} \rangle^T$, is accepted with probability $\rho^\star$, where

$$\rho^\star = \min\left\{1, I_{\mathbf{X}}(\mathbf{x}^\star)\frac{\exp\left(-h(\mathbf{x}^\star)/K_{j+1}\right)}{\exp\left(-h(\tilde{\mathbf{x}}^{j+1})/K_{j+1}\right)}\frac{p_d(\tilde{\mathbf{x}}_d^{j+1}|\mathbf{x}_d^\star)}{p_d(\mathbf{x}_d^\star|\tilde{\mathbf{x}}_d^{j+1})}\right\} \tag{3.29}$$

for the exploration phase, where $I_{\mathbf{X}}(\mathbf{x}^\star) = 1$ if $\mathbf{x}^\star \in \mathbf{X}$ and $I_{\mathbf{X}}(\mathbf{x}^\star) = 0$ otherwise, and

$$\rho^\star = \min\left\{1, I_{\mathbf{X}_{\text{feasible}}}(\mathbf{x}^\star)\frac{\exp\left(-c(\mathbf{x}^\star)/K_{j+1}\right)}{\exp\left(-c(\tilde{\mathbf{x}}^{j+1})/K_{j+1}\right)}\frac{p_d(\tilde{\mathbf{x}}_d^{j+1}|\mathbf{x}_d^\star)}{p_d(\mathbf{x}_d^\star|\tilde{\mathbf{x}}_d^{j+1})}\right\} \tag{3.30}$$

for the exploitation phase. According to the definition of the proposal distribution p_d, the ratio $p_d(\tilde{\mathbf{x}}_d^{j+1}|\mathbf{x}_d^\star)/p_d(\mathbf{x}_d^\star|\tilde{\mathbf{x}}_d^{j+1})$ is given by

$$\frac{p_d(\tilde{\mathbf{x}}_d^{j+1}|\mathbf{x}_d^\star)}{p_d(\mathbf{x}_d^\star|\tilde{\mathbf{x}}_d^{j+1})} = \prod_{l=1}^{n_d} \begin{cases} \frac{Card(Adj(\tilde{x}_{dl}^{j+1}))}{Card(Adj(x_{dl}^\star))} & \text{if } x_{dl}^\star \in Adj(\tilde{x}_{dl}^{j+1}) \\ \frac{Card(Adj^c(\tilde{x}_{dl}^{j+1}))}{Card(Adj^c(x_{dl}^\star))} & \text{if } x_{dl}^\star \notin Adj(\tilde{x}_{dl}^{j+1}) \end{cases} \tag{3.31}$$

If the candidate state $\mathbf{x}^\star$ is rejected, the lead sample $\tilde{\mathbf{x}}^{j+1}$ is repeated. More information about the Metropolis-Hastings algorithm can be found in [88, 89].

Acknowledgments

The research reported here was supported in part by ANID (National Agency for Research and Development, Chile) under grant number 1200087. Also, this research has been supported by ANID and DAAD (German Academic Exchange Service) under CONICYT-PFCHA/Doctorado Acuerdo Bilateral DAAD Becas Chile/2018-62180007. These supports are gratefully acknowledged by the authors.

Chapter 4

A two-phase sampling approach for reliability-based optimization in structural engineering

A two-phase sampling approach for reliability-based optimization in structural engineering

D. J. Jerez[a], H. A. Jensen[b,*], M. Beer[a,c,d]

[a]*Institute for Risk and Reliability, Leibniz Universität Hannover, Callinstr. 34, 30167 Hannover, Germany*

[b]*Department of Civil Engineering, Federico Santa Maria Technical University, Valparaiso 2390123, Chile*

[d]*International Joint Research Center for Resilient Infrastructure & International Joint Research Center for Engineering Reliability and Stochastic Mechanics, Tongji University, Shanghai, China*

[c]*Institute for Risk and Uncertainty and School of Engineering, University of Liverpool, Liverpool L69 7ZF, UK*

Abstract: This work presents a two-phase sampling approach to address reliability-based optimization problems in structural engineering. The constrained optimization problem is converted into a sampling problem, which is solved using Markov chain Monte Carlo methods. First, an exploration phase generates uniformly distributed feasible designs. Then, an exploitation phase is carried out to obtain a set of close-to-optimal designs. The approach is general in the sense that it is not limited to a particular type of system behavior and, in addition, it can handle constrained and unconstrained formulations as well as discrete-continuous design spaces. Three numerical examples involving structural dynamical systems under stochastic excitation are presented to illustrate the capabilities of the approach.

Keywords: Structural engineering; First-passage probability; Stochastic search; Reliability-based optimization; Metamodel.

*Corresponding author

E-mail addresses: danko.jerez@irz.uni-hannover.de (D. J. Jerez), hector.jensen@usm.cl (H. A. Jensen), beer@irz.uni-hannover.de (M. Beer).

4.1 Introduction

Structural engineering practice is inherently related to the design of safe and cost-efficient systems to satisfy private and public needs. Optimization techniques have proved instrumental to this end, whereby suitable design solutions are identified by minimizing a cost function subject to certain constraints [117, 306]. Since the systems of interest are unavoidably exposed to external actions and deterioration processes that are difficult to predict, the treatment of uncertainties is a key aspect to obtain meaningful optimization results. To address this issue, reliability-based optimization (RBO) offers a rational and theoretically sound framework to incorporate the interaction between uncertainties and design requirements into decision-making processes [7, 101, 104]. In this setting, system performance metrics are explicitly included in the objective and/or constraint functions by means of reliability measures.

Structural systems of practical interest are characterized by their exposure to environmental actions, a relatively large scale, and a complex behavior. In this context, the prediction of the system response often relies on complex computational procedures involving, e.g., the numerical solution of nonlinear equations with multiple unknowns. Further, their probabilistic characterization using, e.g., random fields or stochastic processes, requires a relatively large number of random variables, which leads to high-dimensional reliability integrals [82]. These features make reliability assessment a challenging task, which is usually addressed using stochastic simulation [85]. This, in turn, brings challenges to the solution of RBO problems associated with the computational cost, inherent variability, and sensitivity evaluation of the reliability estimates [111].

Several approaches have been reported to address RBO problems involving high-dimensional probability integrals. In general, they can be classified in three groups based on the adopted search strategy [111], namely, sequential optimization approaches, stochastic search-based techniques, and schemes based on augmented reliability spaces. Although the most suitable optimization approach depends on the problem characteristics, the use of stochastic search-based techniques can

be regarded as a general and flexible strategy. These methods do not need sensitivity measures and are not restricted to a specific class of systems. However, they tend to be computationally more intensive than sequential strategies (see, e.g., [150, 159]) or augmented reliability formulations (see, e.g., [204, 345]).

This work presents a stochastic search-based approach for the RBO of structural engineering systems including high-dimensional reliability integrals. The method is based on a two-phase sampling framework [180–183]. An exploration phase is first carried out to obtain feasible designs, which are then used in an exploitation phase that ultimately yields a set of close-to-optimal designs. The method can handle unconstrained, constrained, discrete and continuous formulations [183]. In addition, a suitable metamodel is implemented for improved numerical efficiency [181, 287]. Three examples involving a class of structural systems, namely, structural systems under stochastic excitation, are presented. Overall, the method represents a potentially useful tool to address a practical class of RBO problems in engineering applications.

4.2 Reliability-based optimization

4.2.1 Formulation

The class of problems of interest can be stated as

$$\begin{aligned} \min_{\mathbf{x}} \quad & f(\mathbf{x}) \\ \text{s.t.} \quad & r_j(\mathbf{x}) \leq 0, \quad j = 1, \ldots, n_r \\ & g_k(\mathbf{x}) \leq 0, \quad k = 1, \ldots, n_g \\ & \mathbf{x} \in \mathbf{X} \end{aligned} \tag{4.1}$$

where the vector $\mathbf{x} \in \mathbf{X} \subset \mathbb{R}^{n_x}$ comprises the n_x design variables (continuous and/or discrete), $f(\mathbf{x})$ is a general objective function, $r_j(\mathbf{x}) \leq 0$, $j = 1, \ldots, n_r$, represent n_r constraints in terms of system reliability measures, and $g_k(\mathbf{x}) \leq 0$, $k = 1, \ldots, n_g$, are n_g standard constraints. The

vector of design variables is expressed as $\mathbf{x}^T = \langle \mathbf{x}_c^T, \mathbf{x}_d^T \rangle$ with $\mathbf{x}_c \in \mathbf{X}_c \subset \mathbb{R}^{n_c}$ and $\mathbf{x}_d \in \mathbf{X}_d \subset \mathbb{R}^{n_c}$ containing, respectively, the n_c continuous and n_d discrete design variables. In this formulation, the set $\mathbf{X} = \mathbf{X}_c \times \mathbf{X}_d$ characterizes explicit constraints on the design variables. For the continuous components, side constraints are imposed as

$$\mathbf{X}_c = \left\{ \mathbf{x}_c \in \mathbb{R}^{n_c} : x_i^L \leq x_{ci} \leq x_{ci}^U, i = 1, \ldots, n_c \right\} \tag{4.2}$$

where x_{ci}^L and x_{ci}^U are the lower and upper bounds of the ith continuous design variable, respectively. In addition, the side constraints on the discrete design variables are given by

$$\mathbf{X}_d = \{ \mathbf{x}_d \in \mathbb{R}^{n_d} : x_{di} \in \mathbf{X}_{di}, i = 1, \ldots, n_d \} \tag{4.3}$$

where the set $\mathbf{X}_{di} = \left\{ x_{di(m)}, m = 1, \ldots, \ n_{di} \right\}$ contains the n_{di} allowable values for the ith discrete component of the design vector. For convenience, it is assumed that these values are sorted in an ascending order.

In the previous setting, the objective function $f(\mathbf{x})$ can be related to, e.g., initial construction costs, life-cycle costs, or structural performance measures. Further, the standard constraints $g_k(\mathbf{x}) \leq 0$, $k = 1, \ldots, n_g$, are associated with design requirements such as material availability, budget restrictions, etc., that do not involve system reliability measures. Hence, it is assumed that the functions $g_k(\mathbf{x})$, $k = 1, \ldots, n_g$, are relatively inexpensive to compute. In addition, the reliability constraints represent design conditions expressed in terms of failure probabilities as

$$r_j(\mathbf{x}) = P_{F_j}(\mathbf{x}) - P_{F_j}^* \leq 0, \ j = 1, \ldots, n_r \tag{4.4}$$

where $P_{F_j}(\mathbf{x})$ is the probability of failure event F_j evaluated at design $\mathbf{x}$, and $P_{F_j}^*$ is the corresponding maximum allowable value. The failure events can be defined, e.g., in terms of serviceability conditions, users' comfort requirements, and partial or total collapse. It is noted that, according to this formulation, failure probability measures can be involved in the definition of the objec-

tive function and/or reliability constraints. Thus, the optimization problem stated in Eq. (4.1) is quite general in the sense that it allows the treatment of several RBO formulations. In this regard, indicative applications include the design of wind-excited buildings [126], structural topology optimization [346], and energy harvester optimization [347].

4.2.2 First-passage probabilities

For a general class of complex engineering systems, a suitable reliability measure corresponds to the so-called first-passage probability [71]. This measure quantifies the likelihood of performance requirements not being satisfied at any instant of a reference period. In this framework, consider a vector of basic random variables $\boldsymbol{\theta} \in \mathbb{R}^{n_\theta}$ following the multivariate probability density function $q(\boldsymbol{\theta}|\mathbf{x})$, i.e., $\boldsymbol{\theta} \sim q(\boldsymbol{\theta}|\mathbf{x})$. This distribution can depend, in principle, on the vector of design variables $\mathbf{x}$. If that is not the case, the random variables are simply distributed as $\boldsymbol{\theta} \sim q(\boldsymbol{\theta})$. In general, the vector $\boldsymbol{\theta}$ characterizes the uncertainty in the system properties as well as in the external actions over the system. Then, a first-passage failure event F can be defined as $F = \{d(\mathbf{x}, \boldsymbol{\theta}) > 1\}$ with normalized demand function $d(\mathbf{x}, \boldsymbol{\theta})$ given by

$$d\left(\mathbf{x}, \boldsymbol{\theta}\right) = \max_{t \in [0,T]} \max_{\ell = 1, \ldots, n_\eta} \frac{\eta_\ell(t, \mathbf{x}, \boldsymbol{\theta})}{\eta_\ell^*} \tag{4.5}$$

where $\eta_\ell(t, \mathbf{x}, \boldsymbol{\theta})$, $\ell = 1, \ldots, n_\eta$, are the system response functions of interest with corresponding thresholds $\eta_\ell^* > 0$, and T is the reference period. In general, these functions depend on time, the design variables $\mathbf{x}$, and the basic random variables $\boldsymbol{\theta}$. Hence, from the previous description, failure is defined when any response of interest exceeds its prescribed maximum allowable value at any instant of a reference period. Then, the corresponding first-passage probability can be written as

$$P_F(\mathbf{x}) = \int_{d(\mathbf{x}, \boldsymbol{\theta}) > 1} q(\boldsymbol{\theta}|\mathbf{x}) d\boldsymbol{\theta} \tag{4.6}$$

For most complex engineering systems, the vector of random variables $\boldsymbol{\theta}$ is high-dimensional and, in addition, the responses of interest are only available through involved black-box models. As a result, the evaluation of the previous integral is quite challenging, and its evaluation is usually carried out using stochastic simulation methods [84]. As previously pointed out, this makes the solution of RBO problems a challenging task due to the computational cost, noisy behavior and involved sensitivity estimation of failure probability functions [111].

4.3 Two-phase sampling approach

4.3.1 Underlying idea

Following the ideas of simulated annealing [174], the solution of the optimization problem (4.1) can be equivalently formulated as the generation of designs that follow an appropriate probabilistic distribution. Such a formulation stems from the concept of canonical distribution in statistical mechanics [294] and the fact that finding the minimum of $f(\mathbf{x})$ is equivalent to maximizing the function $\exp(-f(\mathbf{x})/T)$ for any $T > 0$ [174]. Consider the auxiliary distribution

$$p(\mathbf{x}|T) \propto U_{\bar{\mathbf{X}}}(\mathbf{x}) \exp\left(-\frac{f(\mathbf{x})}{T}\right) \tag{4.7}$$

where $T > 0$ is the temperature parameter and $U_{\bar{\mathbf{X}}}(\mathbf{x})$ is a uniform distribution over the feasible set $\bar{\mathbf{X}}$, which is defined as

$$\bar{\mathbf{X}} = \{\mathbf{x} \in \mathbf{X} : r_j(\mathbf{x}) \leq, j = 1, \ldots, n_r \wedge g_k(\mathbf{x}) \leq, k = 1, \ldots, n_g\} \tag{4.8}$$

In Eq. (4.7), the parameter T affects the spread of the distribution $p(\mathbf{x}|T)$. On the one hand, increasing the value of T leads to flatter distributions. In the limit case in which $T \to \infty$, the auxiliary distribution becomes uniform over the feasible set, i.e., $\lim_{T\to\infty} p(\mathbf{x}|T) = U_{\bar{\mathbf{X}}}(\mathbf{x})$. On the other hand, for smaller values of T the distribution in Eq. (4.7) becomes increasingly concentrated

around the feasible designs that minimize $f(\mathbf{x})$. In fact, when $T \to 0$ the probability mass is uniformly distributed over the optimal solution set $\mathbf{X}_f^*$, that is, $\lim_{T\to 0} p(\mathbf{x}|T) = U_{\mathbf{X}_f^*}(\mathbf{x})$. Thus, by generating samples (designs) that follow $p(\mathbf{x}|T)$, $T \to 0$, the optimal solution set corresponding to Eq. (4.1) can be explored. In other words, the solution of the RBO problem can be restated as the generation of samples according to the target distribution $\lim_{T\to 0} p(\mathbf{x}|T)$. It is noted that, in a Bayesian framework, the target distribution can be also interpreted as a posterior distribution where $U_{\bar{\mathbf{X}}}(\mathbf{x})$ plays the role of the prior distribution and $\lim_{T\to\infty} \exp(-f(\mathbf{x})/T)$ of the (unnormalized) likelihood function [183].

4.3.2 Sequence of intermediate distributions

The straightforward generation of samples following $\lim_{T\to 0} p(\mathbf{x}|T)$ with, e.g., direct Monte Carlo simulation is generally unfeasible. To circumvent this issue, a sequential strategy is adopted in this work [175, 177, 178, 282]. Consider the sequence of non-normalized intermediate distributions

$$\begin{aligned} p_0(\mathbf{x}) &= U_{\bar{\mathbf{X}}}(\mathbf{x}) \\ p_j(\mathbf{x}) &\propto U_{\bar{\mathbf{X}}}(\mathbf{x}) \exp\left(-\frac{f(\mathbf{x})}{T_j}\right), \quad j = 1, 2, \ldots \end{aligned} \tag{4.9}$$

where $\infty = T_0 > T_1 > \ldots > T_j > \ldots$ is a sequence of monotonically decreasing temperature parameters, with $T_j \to 0$ as $j \to \infty$. These parameters are adaptively chosen to achieve a smooth transition between distributions. Such strategy has been adopted to address several applications including, e.g., Bayesian model updating [178, 282], structural optimization [175, 177], and structural reliability assessment [348].

Based on the previous setting, it is seen that the initial distribution is uniform over the feasible set, whereas the next distributions in the sequence become increasingly concentrated around the optimal solution set as the temperature parameter decreases. Thus, the main idea is to generate samples (designs) in a sequential manner. In the initial stage ($j = 0$), samples uniformly distributed over the feasible set are obtained. Then, during stage $j = 1, 2, \ldots$, samples following the distribution

$p_j(\mathbf{x})$ are drawn based on the samples from the previous stage. The transitional Markov chain Monte Carlo (TMCMC) method [178] is implemented for the sample generation process. Finally, once a certain stopping criterion is verified, the final designs represent a set of close-to-optimal solutions that follow an approximately uniform distribution over the optimal solution set.

The previous formulation requires an initial set of samples uniformly distributed over the feasible set $\bar{\mathbf{X}}$, which is usually difficult to obtain in a direct manner for practical cases. Thus, a two-phase sampling approach is adopted in this work [181, 183]. First, an exploration phase is carried out to obtain uniformly distributed designs in the feasible set. Then, these designs are used as the initial population of an exploitation phase which ultimately yields a set of close-to-optimal solutions.

4.3.3 Exploration phase

To obtain designs following $U_{\bar{\mathbf{X}}}(\mathbf{x})$, consider the auxiliary optimization problem

$$\begin{aligned} \min_{\mathbf{x}} \quad & h(\mathbf{x}) = \max\left\{0, \max_{j=1,\ldots,n_r} r_j(\mathbf{x}), \max_{k=1,\ldots,n_g} g_j(\mathbf{x})\right\} \\ \text{s.t.} \quad & \mathbf{x} \in \mathbf{X} \end{aligned} \tag{4.10}$$

From the previous definition, the minimum value of the auxiliary objective function $h(\mathbf{x})$ is equal to zero with corresponding optimal solution set [181]

$$\mathbf{X}_h^* = \{\mathbf{x} \in \mathbf{X} : r_j(\mathbf{x}) \leq 0, j = 1, \ldots, n_r \wedge g_k(\mathbf{x}) \leq 0, k = 1, \ldots, n_g\} \tag{4.11}$$

Thus, the optimal solution set in Eq. (4.11) is equal to the feasible design set in Eq. (4.8), i.e., $\mathbf{X}_h^* = \bar{\mathbf{X}}$. In addition, the auxiliary optimization problem in Eq. (4.10) involves only side constraints on the design variables, i.e., $\mathbf{x} \in \mathbf{X}$. Based on these features, consider the sequence of intermediate distributions

$$\begin{aligned} &\bar{p}_0(\mathbf{x}) = U_{\mathbf{X}}(\mathbf{x}) \\ &\bar{p}_j(\mathbf{x}) \propto U_{\mathbf{X}}(\mathbf{x}) \exp\left(-\frac{h(\mathbf{x})}{T_j}\right), \quad j = 1, 2, \ldots \end{aligned} \tag{4.12}$$

where $U_{\mathbf{X}}(\mathbf{x})$ represents a uniform distribution over the set $\mathbf{X}$. In this case, samples at the initial stage ($j = 0$) can be generated directly, while samples at the final stage ($T_j \to 0$) approximately follow a uniform distribution over the feasible set $\bar{\mathbf{X}}$. The TMCMC method [178] is implemented to generate the required samples. To achieve a smooth transition between distributions, the temperature parameter T_{j+1} satisfies the condition [175, 183]

$$\frac{\sum_{\ell=1}^{n} \exp\left(-h\left(\mathbf{x}_j^{(\ell)}\right)\left(T_{j+1}^{-1} - T_j^{-1}\right)\right)}{\left[\sum_{\ell=1}^{n} \exp\left(-h\left(\mathbf{x}_j^{(\ell)}\right)\left(T_{j+1}^{-1} - T_j^{-1}\right)\right)\right]^2} = \frac{1}{\nu n} \tag{4.13}$$

where $\mathbf{x}_j^{(\ell)}$, $\ell = 1, \ldots, n$, are n samples following $\bar{p}_j(\mathbf{x})$ and $\nu \in (0, 1)$ is a user-defined parameter. It is noted that all feasible designs generated during the intermediate stages of the sampling process are uniformly distributed over $\bar{\mathbf{X}}$ [181]. Therefore, the sampling process is stopped when $n_{feasible} \geq n_{target}$, where $n_{feasible}$ is the total number of feasible designs obtained during the different stages and n_{target} is a user-defined target value. At the end of the exploration phase, a total of $n_{feasible}$ designs uniformly distributed over $\bar{\mathbf{X}}$ are available.

4.3.4 Exploitation phase

Starting from the set of feasible designs obtained during the exploration phase, which are distributed according to $p_0(\mathbf{x}) = U_{\bar{\mathbf{X}}}(\mathbf{x})$, the exploitation phase ultimately generates a set of designs lying in the vicinity of the optimal solution set $\mathbf{X}_f^*$. In this setting, samples following the intermediate distributions $p_j(\mathbf{x})$, $j = 1, 2, \ldots$, in Eq. (4.9) are obtained using the TMCMC method. The temperature parameter T_{j+1} verifies the relationship [183]

$$\frac{\sum_{\ell=1}^{n} \exp\left(-f\left(\mathbf{x}_j^{(\ell)}\right)\left(T_{j+1}^{-1} - T_j^{-1}\right)\right)}{\left[\sum_{\ell=1}^{n} \exp\left(-f\left(\mathbf{x}_j^{(\ell)}\right)\left(T_{j+1}^{-1} - T_j^{-1}\right)\right)\right]^2} = \frac{1}{\nu n} \tag{4.14}$$

where $\mathbf{x}_j^{(\ell)}$, $\ell = 1, \ldots, n$, are n samples following the distribution $p_j(\mathbf{x})$, and $\nu \in (0, 1)$ is a user-defined parameter. As already pointed out, the distribution becomes uniform over the optimal

solution set when $T_j \to 0$. For numerical implementation, however, a suitable stopping rule must be imposed. In this regard, the optimization procedure is finished if (i) a prescribed maximum number of stages, N_{max}, are completed, or (ii) the sample coefficient of variation (c.o.v.) of the objective function is sufficiently small. Specifically, the sampling process stops at stage $j = 0, 1, \ldots$, if $j + 1 = N_{max}$ or, alternatively, $\delta_{j+1} < \gamma\delta_0$, where $\gamma \in (0, 1)$ is a user-defined parameter and

$$\delta_j = \frac{\sqrt{\frac{1}{n-1}\sum_{\ell=1}^{n}\left(f\left(\mathbf{x}_j^{(\ell)}\right) - \left[\frac{1}{n}\sum_{m=1}^{n} f\left(\mathbf{x}_j^{(m)}\right)\right]\right)^2}}{\frac{1}{n}\sum_{\ell=1}^{n} f\left(\mathbf{x}_j^{(\ell)}\right)} \tag{4.15}$$

is the sample c.o.v. of the objective function $f(\mathbf{x})$ during stage j. The previous conditions indicate that the algorithm runs until a prescribed number of stages are completed or until δ_{j+1} becomes smaller than some fraction of the initial sample c.o.v. of the objective function, δ_0. It is noted that alternative stopping criteria can be implemented as well. The samples $\left\{\mathbf{x}_{j+1}^{(1)}, \ldots, \mathbf{x}_{j+1}^{(n)}\right\}$ obtained at the final stage of the procedure can be regarded as a set of close-to-optimal designs. Thus, the proposed approach provides, in general, designs which are similar between each other in terms of their objective function value. This is particularly useful, e.g., in cases with multiple sub-optimal regions. Nevertheless, if a single solution is needed, the sample with the smallest objective function value can be selected.

4.3.5 Remarks

According to the previously described procedure, a set of close-to-optimal designs are obtained in a two-phase sampling framework in which the feasible and optimal solution sets are sequentially explored. In this regard, the proposed approach presents several advantageous features. First, due to its theoretical foundations and annealing properties, the procedure has high chances of reaching a vicinity of the optimal solution set. This includes cases involving multiple local optima, multiple discontinuous sub-feasible regions, and complex feasible design spaces [183]. Second, the formulation of the approach does not impose restrictions on the number of constraints or the behavior of

the objective and constraint functions. Moreover, the proposed approach is not limited to a particular type of reliability assessment techniques. Thus, the method is quite general in the sense that, in principle, different classes of RBO problems can be treated with the same formulation. Third, the approach is suitable for practical implementation. In this regard, the same basic framework (i.e., the TMCMC method) is used in the exploration and exploitation phases. In addition, few user-defined parameters are required and, since the treatment of the reliability and standard constraints is direct, no special constraint-handling techniques such as penalty factors are necessary. Fourth, the method produces a set of nearly optimal designs rather than a single final solution. This can introduce additional flexibility to decision-making processes since an appropriate final design can be selected based on alternative considerations. Finally, the sets of designs produced during the different stages of the sampling process allow to assess the sensitivity of the problem functions with respect to the design variables. This information, which is a byproduct of the procedure, gives a valuable insight into the RBO problem at hand.

4.4 Implementation aspects

4.4.1 Transitional Markov chain Monte Carlo method

The TMCMC method [178], which has proved effective in several model updating applications (see, e.g., [24, 25, 115, 270]), is implemented to carry out the exploration and exploitation phases. This technique draws samples at stage $j+1$, i.e., $\left\{\mathbf{x}_{j+1}^{(1)}, \ldots, \mathbf{x}_{j+1}^{(n)}\right\}$, by generating several Markov chains with stationary distribution equal to $\bar{p}_{j+1}$ (exploration phase) or p_{j+1} (exploitation phase). To this end, importance sampling concepts and the Metropolis-Hastings (M-H) algorithm are integrated [178]. In this setting, the ith sample, i.e., $\mathbf{x}_{j+1}^{(i)}$, is generated as follows:

1. Select a lead sample, $\tilde{\mathbf{x}}$, as a design from the previous stage, $\mathbf{x}_j^{(\ell)}$, drawn with probability equal to its normalized importance weight $\bar{w}_j^{(\ell)} = w_j^{(\ell)} / \sum_{k=1}^{n} w_j^{(k)}$, $\ell = 1, \ldots, n$. The weights are given by $w_j^{(\ell)} = \bar{p}_{j+1}\left(\mathbf{x}_j^{(\ell)}\right) / \bar{p}_j\left(\mathbf{x}_j^{(\ell)}\right)$ for the exploration phase and $w_j^{(\ell)} =$

$p_{j+1}\left(\mathbf{x}_j^{(\ell)}\right)/p_j\left(\mathbf{x}_j^{(\ell)}\right)$ for the exploitation phase. If the selected sample, $\mathbf{x}_j^{(\ell)}$, has been previously drawn, then the last state of its corresponding chain is chosen as lead sample $\tilde{\mathbf{x}}$.

2. Draw a candidate design $\mathbf{x}^\star$ from the proposal distribution $p^*(\mathbf{x}|\tilde{\mathbf{x}})$. An adaptive proposal distribution with independent continuous and discrete components is considered [182, 183].

3. Set $\mathbf{x}_{j+1}^{(i)} = \mathbf{x}^\star$ with probability $\rho^* = \min\{1, \alpha\}$, where

$$\alpha = \bar{p}_{j+1}(\mathbf{x}^\star)p^*(\tilde{\mathbf{x}}|\mathbf{x}^\star)/\bar{p}_{j+1}(\tilde{\mathbf{x}})p^*(\mathbf{x}^\star|\tilde{\mathbf{x}}) \tag{4.16}$$

for the exploration phase, and

$$\alpha = p_{j+1}(\mathbf{x}^\star)p^*(\tilde{\mathbf{x}}|\mathbf{x}^\star)/p_{j+1}(\tilde{\mathbf{x}})p^*(\mathbf{x}^\star|\tilde{\mathbf{x}}) \tag{4.17}$$

for the exploitation phase. If the candidate state is rejected, the lead sample is repeated, i.e., set $\mathbf{x}_{j+1}^{(i)} = \tilde{\mathbf{x}}$.

The previous procedure is iteratively carried out until the required number of samples has been obtained. A more detailed description of the TMCMC method, from the theoretical and implementation viewpoints, can be found in [178].

4.4.2 Proposal distribution

The proposed approach requires, in the context of the M-H algorithm, the definition of an appropriate proposal distribution to draw samples from the intermediate distributions. As already pointed out, an adaptive proposal distribution with independent continuous and discrete components is considered in this work [182, 183]. That is, the candidate state is generated from a distribution $p^*(\mathbf{x}|\tilde{\mathbf{x}}) = p_c^*(\mathbf{x}_c|\tilde{\mathbf{x}}_c)p_d^*(\mathbf{x}_d|\tilde{\mathbf{x}}_d)$, where $p_c^*(\mathbf{x}_c|\tilde{\mathbf{x}}_c)$ is the proposal distribution for the continuous design variables and $p_d^*(\mathbf{x}_d|\tilde{\mathbf{x}}_d)$ for the discrete design variables.

Continuous design variables

Following some of the ideas introduced in [178], the proposal distribution for the continuous variables, $p_c^*(\mathbf{x}_c|\tilde{\mathbf{x}}_c)$, is a Gaussian distribution centered at the continuous components of the lead sample. The corresponding covariance matrix, $\tilde{\mathbf{\Sigma}}$, is taken as

$$\tilde{\mathbf{\Sigma}} = \beta^2 \sum_{\ell=1}^{n} \bar{w}_j^{(\ell)} \left(\mathbf{x}_{j,c}^{(\ell)} - \bar{\mathbf{x}}_{j,c}\right) \left(\mathbf{x}_{j,c}^{(\ell)} - \bar{\mathbf{x}}_{j,c}\right)^T \tag{4.18}$$

where β is a scaling parameter, $\mathbf{x}_{j,c}^{(\ell)}$, $\ell = 1, \ldots, n$, are the continuous components of the samples at stage j, $\bar{\mathbf{x}}_{j,c} = \sum_{\ell=1}^{n} \bar{w}_j^{(\ell)} \mathbf{x}_{j,c}^{(\ell)}$, and the normalized weights $\bar{w}_j^{(\ell)}$, $\ell = 1, \ldots, n$, have been previously defined. The scaling parameter β is adaptively tuned according to the observed acceptance rate of the M-H algorithm [179].

Discrete design variables

The discrete proposal distribution, $p_d^*(\mathbf{x}_d|\tilde{\mathbf{x}}_d)$, considers the discrete components to be independent between each other, i.e.,

$$p_d^*(\mathbf{x}_d|\tilde{\mathbf{x}}_d) = \prod_{i=1}^{n_d} p_{di}^*(x_{di}|\tilde{x}_{di}) \tag{4.19}$$

where $\tilde{\mathbf{x}}_d = \langle \tilde{x}_{d1}, \ldots, \tilde{x}_{dn_d} \rangle^T$ contains the discrete components of the lead sample and $p_{di}^*(x_{di}|\tilde{x}_{di})$ is the proposal distribution corresponding to the ith discrete component. The definition of this distribution relies on the set of neighbors of the current lead sample, $\tilde{x}_{di}$, within the corresponding set of available values $\mathbf{X}_{di}$. This set is defined as

$$\text{Adj}(\tilde{x}_{di}) = \left\{ x_{di(m)}, m = 1, \ldots, n_{di} : \lambda(\tilde{x}_{di}, x_{di(m)}) \leq \lambda_i^* \right\} \tag{4.20}$$

where $\lambda(\tilde{x}_{di}, x_{di(m)})$ is the distance between $\tilde{x}_{di}$ and $x_{di(m)}$ within the set $\mathbf{X}_{di}$, and λ_i^* is a user-defined parameter. This distance is defined in terms of the indices of the values within the sorted set $\mathbf{X}_{di}$. For instance, if $\tilde{x}_{di}$ is equal to the sth available value, i.e., $\tilde{x}_{di} = x_{di(s)}$, then the distance

measure becomes $\lambda(\tilde{x}_{di}, x_{di(m)}) = \lambda(x_{di(s)}, x_{di(m)}) = |s - m|$. Based on the previous definitions, the proposal distribution for the ith component is given by

$$p^*_{di}(x_{di}|\tilde{x}_{di} = \begin{cases} \dfrac{1-\tau_i}{\text{Card}[\text{Adj}(\tilde{x}_{di})]}, & \text{if } x_{di} \in \text{Adj}(\tilde{x}_{di}) \\ \dfrac{\tau_i}{n_{di} - \text{Card}[\text{Adj}(\tilde{x}_{di})]}, & \text{otherwise} \end{cases} \tag{4.21}$$

where $\tau_i \in [0, 1]$ represents the probability of randomly selecting a discrete value that does not belong to the set of neighbors of the lead sample $\tilde{x}_{di}$, and Card$[\cdot]$ is the cardinality of the set within square brackets.

In the adopted proposal distribution, the parameters τ_i and λ^*_i jointly characterize its corresponding spread. Such parameters can be directly defined by the user or adaptively modified during the sampling process. In particular, an adaptive strategy is implemented here to update the value of λ^*_i at the beginning of each stage of the exploitation phase. First, the maximum number of consecutive elements of $\mathbf{X}_{di}$ that were observed during the previous stage, denoted by η, is identified. Then, the parameter λ^*_i is defined as

$$\lambda^*_i \leftarrow \min\{\lambda^*_i, L\} \tag{4.22}$$

with L the largest integer such that $L \leq (\eta - 1)/2$. The updating rule is repeated for $i = 1, \ldots, n_d$. This strategy tends to reduce the value of λ^*_i for advanced exploitation stages, which can improve the sampling efficiency. Nonetheless, alternative updating approaches can also be considered.

Acceptance probability

As previously mentioned, the candidate state $\mathbf{x}^\star = \langle \mathbf{x}_c^{\star T}, \mathbf{x}_d^{\star T} \rangle^T$, which is drawn from $p^*(\mathbf{x}|\tilde{\mathbf{x}})$, becomes the next state of the Markov chain with probability $\rho^* = \min\{1, \alpha\}$. For the exploration

phase, the quantity α is given by

$$\alpha = I\left[\mathbf{x}^\star \in \mathbf{X}\right] \frac{\exp\left(-\dfrac{h(\mathbf{x}^\star)}{T_{j+1}}\right)}{\exp\left(-\dfrac{h(\tilde{\mathbf{x}})}{T_{j+1}}\right)} \frac{p_d^*(\tilde{\mathbf{x}}_d|\mathbf{x}_d^\star)}{p_d^*(\mathbf{x}_d^\star|\tilde{\mathbf{x}}_d)} \tag{4.23}$$

where $I\left[\cdot\right] = 1$ if the expression within square brackets is true and $I\left[\cdot\right] = 0$ otherwise. In addition, for the exploration phase the quantity α becomes

$$\alpha = I\left[\mathbf{x}^\star \in \mathbf{X}\right] \frac{\exp\left(-\dfrac{f(\mathbf{x}^\star)}{T_{j+1}}\right)}{\exp\left(-\dfrac{f(\tilde{\mathbf{x}})}{T_{j+1}}\right)} \frac{p_d^*(\tilde{\mathbf{x}}_d|\mathbf{x}_d^\star)}{p_d^*(\mathbf{x}_d^\star|\tilde{\mathbf{x}}_d)} \tag{4.24}$$

In the previous expressions, the ratio $p_d^*(\tilde{\mathbf{x}}_d|\mathbf{x}_d^\star)/p_d^*(\mathbf{x}_d^\star|\tilde{\mathbf{x}}_d)$ is given by

$$\frac{p_d^*(\tilde{\mathbf{x}}_d|\mathbf{x}_d^\star)}{p_d^*(\mathbf{x}_d^\star|\tilde{\mathbf{x}}_d)} = \prod_{i=1}^{n_d} \begin{cases} \dfrac{\text{Card}[\text{Adj}(\tilde{x}_{di})]}{\text{Card}[\text{Adj}(x_{di}^\star)]}, & \text{if } x_{di}^\star \in \text{Adj}(\tilde{x}_{di}) \\ \dfrac{n_{di} - \text{Card}[\text{Adj}(\tilde{x}_{di}))}{n_{di} - \text{Card}(\text{Adj}(x_{di}^\star)]}, & \text{otherwise} \end{cases} \tag{4.25}$$

4.4.3 Adaptive surrogate model

The proposed approach requires the sequential generation of samples. Consequently, a significant number of first-passage probability evaluations may be required by the optimization procedure. To alleviate the corresponding numerical demands, an adaptive surrogate model based on kriging interpolants is implemented [286, 287]. These metamodels approximate the target function using an underlying Gaussian process whose properties depend on the available data points [327, 328]. Some of their advantages are that they do not require a regular grid of support points, the c.o.v. of the kriging prediction can be directly estimated, and they are exact at the support points. Furthermore, given the annealing nature of the proposed approach, the effective support of the current distribution is generally contained in that of prior stages. Thus, data points from previous stages can

be used to construct the metamodel at the current stage. As a result, the previous features enable a local and adaptive surrogate model in which (i) the support points that lie closer to the candidate design are used and (ii) the database is enriched as new designs in the important region of the target distribution are generated.

Specifically, consider a first-passage probability function, $P_F(\mathbf{x})$, involved in the definition of one of the problem functions. A kriging metamodel, $\hat{p}^{kr}(\mathbf{x})$, is implemented to approximate the logarithm of this function, i.e., $\hat{p}_F^{kr}(\mathbf{x}) \approx \ln P_F(\mathbf{x})$. At the beginning of the sampling process, a database corresponding to full model evaluations of $\ln P_F(\mathbf{x})$ is obtained by means of any suitable strategy. Then, the surrogate prediction of a candidate design $\mathbf{x}^\star$ corresponding to a given Markov chain is obtained as follows.

1. Find the N_{sp} points in the database of available values of $\ln P_F(\mathbf{x})$ that are closer to the starting seed of the current Markov chain. The Euclidean distance is considered to this end, although alternative distance metrics can be adopted as well. Construct the kriging metamodel for the current Markov chain, $\hat{p}_F^{kr}(\mathbf{x})$, using this set of designs as the corresponding support points.

2. For a given candidate design, $\mathbf{x}^\star$, verify the following criteria:

   (a) Check if $\mathbf{x}^\star$ belongs to the n_x-dimensional convex hull of the support points. If not, go to step 4.

   (b) Compute the kriging prediction $\hat{p}^{kr}(\mathbf{x}^\star)$. If this value is smaller than the Q-quantile of $\ln P_F(\mathbf{x})$ in the database, go to step 4.

   (c) Compute the c.o.v. of the kriging estimate. If this value is larger than a user-defined tolerance $\epsilon > 0$, go to step 4.

3. If all the criteria in step 2 are verified, the kriging prediction is accepted. Set $P_F(\mathbf{x}) = \exp(\hat{p}_F^{kr}(\mathbf{x}))$ and continue the sampling process.

4. If at least one criterion in step 2 does not hold, the kriging prediction is rejected. An exact evaluation of $P_F(\mathbf{x}^\star)$ is performed and this point is added to the database. Continue the sampling process.

The criteria in step 2 aim to control the quality of the kriging estimate. In addition, the set of support points is kept fixed throughout the generation of a given Markov chain. This is done to avoid potential discontinuities associated with slightly different sets of support points. A more detailed description of the strategy can be found in [180, 286, 287].

4.4.4 Parallelization features

High-performance computing techniques at the computer hardware level can be considered for improved computational efficiency. In this regard, the proposed approach is particularly suitable for parallel implementation due to the properties of the TMCMC method. First, the initial stage of the exploration phase corresponds to direct Monte Carlo simulation and, therefore, it can be fully scheduled in parallel. Thereafter, the method produces Markov chains that can be generated independently. Since the numerical cost of evaluating the reliability at each design is difficult to predict, dynamic scheduling schemes can be beneficial to distribute the function evaluations on a first-come-first-serve basis [286, 287].

Parallelization strategies can also be integrated with the use of adaptive surrogate models to enhance the numerical efficiency of the proposed approach. To this end, a total of n_{par} samples are generated simultaneously, and then the database of support points is updated. This procedure is repeated during each stage until the required sample size is reached. This allows to exploit the parallel features of the TMCMC method while enriching the kriging database on a regular basis. The parameter n_{par} should be relatively small to promote the adaptability of the surrogate model, but not smaller than a certain value beyond which the approach becomes detrimental to the efficaciousness of the parallelization process.

4.5 Application examples

Three application examples involving structural dynamical systems under stochastic excitation are presented, which include unconstrained, constrained, discrete and continuous formulations. In all cases, the structural behavior can be modeled by a multi-degree of freedom system satisfying the equation of motion

$$\mathbf{M}\ddot{\mathbf{y}}(t) + \mathbf{C}\dot{\mathbf{y}}(t) + \mathbf{K}\mathbf{y}(t) + \boldsymbol{\kappa}_{NL}(\mathbf{y}(t), \dot{\mathbf{y}}(t), \mathbf{q}(t)) = \mathbf{f}(t) \tag{4.26}$$

where $\mathbf{y}(t)$ denotes the displacement vector, $\boldsymbol{\kappa}_{NL}(\mathbf{y}(t), \dot{\mathbf{y}}(t), \mathbf{q}(t))$ is the vector of nonlinear restoring forces, $\mathbf{q}(t)$ comprises the state variables of the nonlinear components, and $\mathbf{f}(t)$ represents the excitation vector. The matrices $\mathbf{M}$, $\mathbf{C}$, and $\mathbf{K}$ characterize, respectively, the mass, damping, and stiffness of the system. In addition, the evolution of $\mathbf{q}(t)$ depends on an appropriate nonlinear model. Thus, finding the system response requires, in general, to solve a set of coupled nonlinear equations using suitable time integration schemes. Subset simulation [133, 134] is implemented for reliability assessment in all examples. Nonetheless, alternative simulation methods can also be considered.

4.5.1 Example 1

The reliability-based design of a bridge system subject to stochastic ground excitation is addressed. Figure 4.1 presents an isometric view of the structural model, which has been borrowed from [68, 180]. The bridge is curved in plan and has five spans of lengths equal to 27 m, 25 m, 23 m, 20 m, and 24 m, which give a total length of 119 m. The deck is monolithically supported by four piers of 8 m height, and each pier is founded on an array of four piles of 35 m height. To model the soil-pile interaction, a series of linear translational springs are incorporated along the height of each pile, with stiffness constants increasing linearly from 560 T/m at the surface to 11200 T/m at the base. The piers and piles are modeled as column elements with diameters of 1.6 m and 0.6

m, respectively. In addition, the deck cross section is a box girder modeled with beam and shell elements. Two sliding bearings are included at each abutment to support the bridge deck. These nonlinear devices consist of an upper steel plate with a housing cap for the slider, a bottom plate with a concave semi-spherical stainless-steel surface, and a steel slider [256, 349]. A sketch of the sliding bearing is also shown in Fig. 4.1. Overall, the finite element model of the bridge involves more than 10000 degrees of freedom.

For dynamical analysis purposes, it is assumed that the nonlinearities are localized in the response of the sliding bearings, while the piers, piles, and deck remain linear. In this regard, the linear components are characterized by an elastic modulus equal to 2.94×10^{10} N/m^2, a Poisson ratio equal to 0.2, and a density of 2500 kg/m^3. In addition, a 5% of critical damping ratio is considered. On the other hand, the sliding bearings at the abutments are characterized by an experimentally validated model that incorporates performance degradation effects. These relate to changes in the friction coefficient due to variations in the vertical load, in the relative velocity between plates, and in the sliding surface temperature [256]. For illustration purposes, a representative displacement-restoring force curve of these devices is shown in Fig. 4.2.

As shown in Fig. 4.1, the structural model is subject to a seismic excitation applied at 40° with respect to the y axis. A point-source model [34, 114] is considered to characterize the base excitation as a non-stationary stochastic process. This class of models links available knowledge about the geological site with the uncertainty of future ground motions. To this end, a white noise sequence is considered along with several seismic parameters [34, 114, 321, 343]. The duration of the excitation is $T = 10$ s with a time step of 0.01 s. Thus, more than 1000 random variables are involved in the characterization of the excitation.

In this example, the goal is to minimize the failure probability of the system subject to side constraints on the design variables [180]. Formally, the corresponding RBO problem is formulated

as

$$\begin{aligned} \min_{\mathbf{x}=\langle x_1,x_2\rangle^T} \quad & P_F(\mathbf{x}) \\ \text{s.t.} \quad & 0.5 \leq x_i \leq 1.5, \quad i = 1,2 \end{aligned} \tag{4.27}$$

where x_1 and x_2 are the design variables, and $P_F(\mathbf{x})$ is the probability of $F = \{d(\mathbf{x}, \boldsymbol{\theta}) > 1\}$ evaluated at $\mathbf{x}$. The corresponding demand function is

$$d(\mathbf{x}, \boldsymbol{\theta}) = \max_{\ell=1,2,3} \max_{t\in[0,T]} \frac{|a_\ell(t, \mathbf{x}, \boldsymbol{\theta})|}{a_\ell^*} \tag{4.28}$$

where $a_\ell(t, \mathbf{x}, \boldsymbol{\theta})$ is the absolute acceleration at the ℓth control point and $a_\ell^* = 6.9$ m/s^2. The control points are located at the two abutments and the deck midpoint.

The design variables are associated with two model parameters of the sliding bearings, namely, the initial friction coefficient (μ_0) and the radius of the concave surface (R). For optimization purposes, the intermediate design variables are specified as $x_1 = \mu_0/\bar{\mu}_0$ and $x_2 = R/\bar{R}$ with reference values $\bar{\mu}_0 = 0.106$ and $\bar{R} = 2.235$ m. The initial friction coefficient affects the dissipation capacity of the bearing system, while the radius of the concave surface controls its natural frequency. Thus, it is expected that both parameters will significantly affect the system behavior.

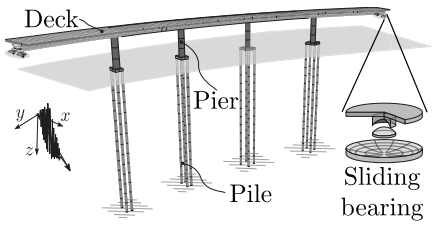

Fig. 4.1: Isometric view of the nonlinear bridge model. Example 1.

To illustrate the effect of the design variables on the objective function, Fig. 4.3 presents contours of $P_F(\mathbf{x})$ in the design space. The results indicate that the failure probability tends to decrease for higher values of the initial friction coefficient and lower values of the radius of the concave surface. Further, a close inspection of the plot shows that the optimal solution set seems to involve a valley near the lower-right corner of the design space. For clarity, this region is highlighted in the figure. Thus, multiple solutions with very similar objective function values can be expected in this case.

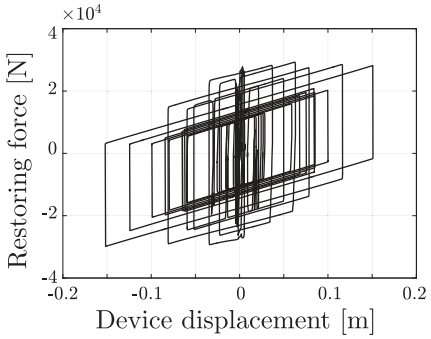

Fig. 4.2: Typical displacement-restoring force curve of the devices. Example 1.

As previously pointed out, the RBO problem in Eq. (4.27) involves only side constraints on the design variables. Hence, uniformly distributed feasible designs can be obtained directly and only the exploitation phase is needed in this case. The proposed approach is implemented with $n = 500$ samples per stage and $\nu = 0.5$. In addition, the adaptive surrogate model is implemented with 20 support points, $\epsilon = 0.1$, and $Q = 0.05$. The database is initialized with all the designs from the initial stage. However, alternative initialization strategies can also be considered.

Figure 4.4 presents the samples obtained at the different stages of the exploitation phase. The initial designs (stage 0) are uniformly distributed over the design space, whereas the samples at the final stage lie in a region near the lower-right corner of the design space. The final set of designs resembles the optimal region identified in Fig. 4.3, which illustrates the effectiveness of the approach. The corresponding failure probability values roughly range between 3×10^{-4} and 7×10^{-4}. The sample-based optimal design is given by $\mathbf{x}^T = \langle 1.32, 0.51 \rangle$ with $P_F(\mathbf{x}) = 3.17 \times 10^{-4}$.

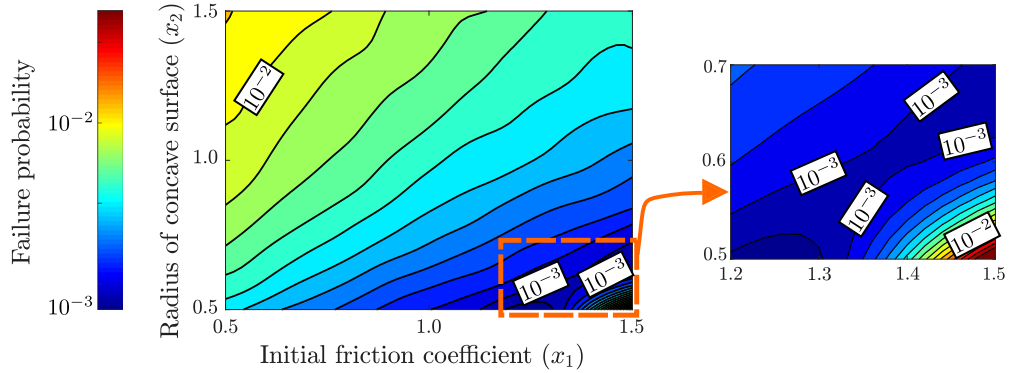

Fig. 4.3: Iso-probability curves in the design space. Example 1.

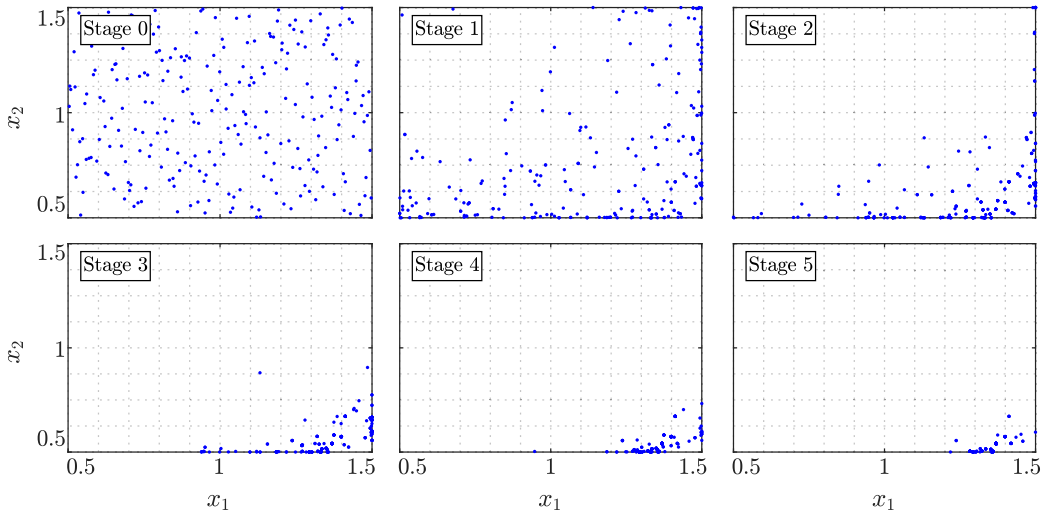

Fig. 4.4: Designs obtained during the different optimization stages. Example 1.

As previously pointed out, an adaptive surrogate model is integrated for improved numerical efficiency. To assess its performance, Fig. 4.5 shows the acceptance rate of the kriging predictions after the initial stage. This quantity corresponds to the fraction of designs that satisfy all acceptance criteria, and it remains above 80% throughout the optimization procedure. Overall, after the initial stage (stage 0), no more than 8% of the total number of design evaluations are performed with full reliability assessment. Thus, the use of kriging greatly improves the numerical efficiency of the method without sacrificing the quality of the optimization results.

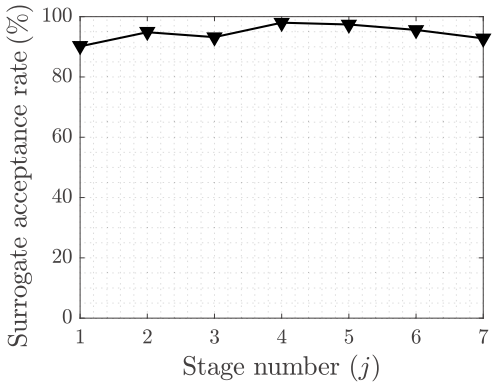

Fig. 4.5: Metamodel acceptance rate during the optimization stages. Example 1.

4.5.2 Example 2

The design of a nonlinear 52-story reinforced concrete building is considered as the second example. The structural model, which has been borrowed from [181], comprises more than 50000 degrees of freedom. For reference purposes, an isometric view of the building and the plan view of each floor are presented in Fig. 4.6. The building includes a core of shear walls and a perimeter of columns with circular cross sections. The nominal value for the corresponding thicknesses and diameters is equal to 0.40 m, whereas the slab thickness is equal to 0.20 m. The same material properties from the previous example are considered. For improved seismic performance, four nonlinear hysteretic devices are placed at each floor to increase the stiffness and dissipation capacity of the system. As indicated in Fig. 4.6, these devices are located along the axes 4, 7, 8 and 11. The restoring force in each device is given by $\kappa(t) = k^e v(t)$ where $k^e = 2.8 \times 10^9$ N/m is the initial stiffness, $v(t) = \delta(t) - q_1(t) + q_2(t)$, $\delta(t)$ denotes the interstory displacement, and $q_1(t)$ and $q_2(t)$ are the plastic elongations of the device. These variables satisfy the first-order nonlinear differential equations [344]

$$\begin{aligned} \dot{q}_1(t) &= \dot{\delta}(t) H(\dot{\delta}(t)) \left[H(v(t) - v_y) \frac{v(t) - v_y}{v_p - v_y} H(v_p - v(t)) + H(v(t) - v_p) \right] \\ \dot{q}_2(t) &= -\dot{\delta}(t) H(-\dot{\delta}(t)) \left[H(-v(t) - v_y) \frac{-v(t) - v_y}{v_p - v_y} H(v_p + v(t)) + H(-v(t) - v_p) \right] \end{aligned} \tag{4.29}$$

where $H(\cdot)$ is the Heaviside step function, $v_y = 0.0042$ m is the yielding onset, and $\kappa_p = k^e v_p$ is the maximum restoring force of the device with $v_p = 0.006$ m.

As illustrated in Fig. 4.6 (right), the building is subject to a horizontal ground excitation, $\ddot{u}_g(t)$, acting along the y axis. This excitation is characterized as a stochastic process using a point-source model, as in the previous example. For dynamic analysis purposes, each floor is regarded as rigid within its plane when compared with the rest of structural components. Thus, by means of appropriate condensation techniques, the degrees of freedom of the entire model are linked to three coordinates per floor (one rotational and two translational displacements). In addition, a 5%

of critical damping ratio at the modal level is considered.

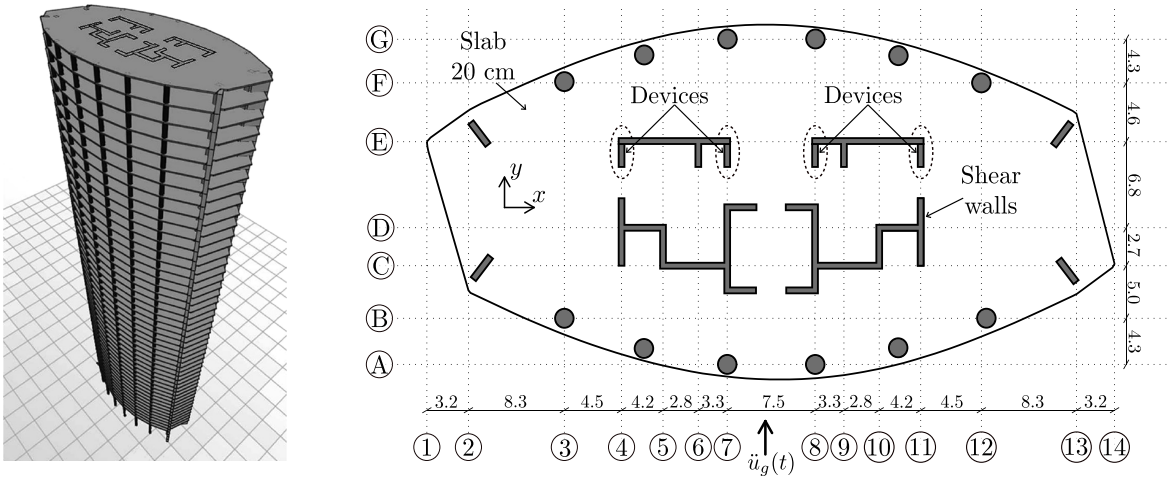

Fig. 4.6: Isometric view (left) and floor plan (right) of the 52-story building model. Example 2.

In this case, the variables to be controlled correspond to the dimensions of the shear walls and exterior columns (see Fig. 4.6). In particular, the wall thickness (t_w) and column diameter (d_c) at each floor are linked to an intermediate optimization variable, x, as $t_w = \bar{t}_w x$ and $d_c = \bar{d}_c x$, respectively, with nominal values $\bar{t}_w = \bar{d}_c = 0.40$ m. For optimization purposes, a total of $n_x = 6$ intermediate variables are considered. These are linked to the design elements of different floors as follows: x_1 is associated with floors 1 to 9, x_2 with floors 10 to 18, x_3 with floors 19 to 26, x_4 with floors 27 to 35, x_5 with floors 36 to 44, and x_6 with floors 45 to 52. Then, a constrained optimization problem is formulated as

$$\begin{aligned} \min_{\mathbf{x}} \quad & f(\mathbf{x}) = \tfrac{1}{6}\textstyle\sum_{i=1}^{6} x_i \\ \text{s.t.} \quad & P_{F_j}(\mathbf{x}) \leq 10^{-3}, \qquad j = 1, 2 \\ & x_{i+1} \leq x_i, \qquad\quad i = 1, \ldots, 5 \\ & 0.5 \leq x_i \leq 1.5, \qquad i = 1, \ldots, 6 \end{aligned} \tag{4.30}$$

where the failure probability functions $P_{F_1}(\mathbf{x})$ and $P_{F_2}(\mathbf{x})$ are associated with the displacement at the first and top floors, respectively, and the standard constraints $x_{i+1} \leq x_i$ impose that the dimensions of upper floor members cannot be larger than those of lower floors. The corresponding

first-passage failure events are defined as $F_j = \{d_j(\mathbf{x}, \boldsymbol{\theta}) > 1\}$, $j = 1, 2$, where

$$d_j(\mathbf{x}, \boldsymbol{\theta}) = \max_{t \in [0,T]} \frac{|u_j^y(t, \mathbf{x}, \boldsymbol{\theta})|}{u_j^*}, \; j = 1, 2 \tag{4.31}$$

with $u_1^y(t, \mathbf{x}, \boldsymbol{\theta})$ and $u_2^y(t, \mathbf{x}, \boldsymbol{\theta})$ denoting the ground-relative displacement along the y direction at the centroid of the first and top floors, respectively. The corresponding thresholds u_1^* and u_2^* are equal to 0.08% of the first story height and 0.075% of the building height, respectively. The reference period is taken as $T = 15$ s with a time step of 0.01 s, which leads to more than 1500 random variables involved in the corresponding multidimensional probability integrals.

The proposed approach is implemented by considering $n = 500$ samples per stage and $\nu = 0.5$ for both phases. The exploration phase considers a target sample size of $n_{target} = 750$ as stopping criterion, whereas $N_{max} = 10$ stages are carried out in the exploitation phase. In addition, the adaptive surrogate model strategy is implemented to approximate the two failure probability functions throughout the entire optimization process. In this regard, the corresponding kriging metamodel considers 28 support points, $\epsilon = 0.1$ and $Q = 0.05$.

First, an exploration phase is carried out. The corresponding final set of samples, which comprises 950 feasible designs, is shown in Fig. 4.7 in terms of two-dimensional projections and marginal histograms. These designs have been retrieved from the eight TMCMC stages carried out during the exploration phase and approximately follow a uniform distribution over the feasible set. The marginal histograms indicate that the effective support of the first design variable is smaller than that of, e.g., the sixth design variable. Thus, the dimensions of the core walls and columns of lower floors seem to be more relevant than of upper floors to determine the feasibility of a given design. Finally, validation calculations indicate that the hypervolume of the feasible set represents less than 0.01% of the initial search space. This illustrates the ability of the proposed approach to explore feasible design spaces with challenging geometries in an effective manner.

Starting from the set of samples in Fig. 4.7, an exploitation phase is carried out to explore the

optimal solution set. The final designs, which are obtained after ten TMCMC stages, are shown in Fig. 4.8. It is seen that they are densely concentrated near a single value in the design space. In fact, the corresponding objective function values range between 6.333 and 6.357 at the final stage. These values represent a relative variation of less than 0.3% and, thus, they can be considered as equivalent from the optimization viewpoint. This illustrates one of the advantages of the proposed approach, as it yields a set of nearly optimal solutions which, in turn, provides additional flexibility for decision-making purposes. Nonetheless, if a single solution is needed, the design with the smallest objective function value can be chosen. Such design is $\mathbf{x}^T = \langle 1.489, 1.476, 1.088, 1.011, 0.751, 0.515 \rangle$, with $f(\mathbf{x}) = 6.333$, $P_{F_1}(\mathbf{x}) = 0.999 \times 10^{-3}$ and $P_{F_2}(\mathbf{x}) = 0.169 \times 10^{-3}$. In addition, the standard constraints verify $x_2/x_1 = 0.991$, $x_3/x_2 = 0.736$, $x_4/x_3 = 0.930$, $x_5/x_4 = 0.743$, and $x_6/x_5 = 0.685$. It is seen that the first reliability constraint, whose response of interest is the first story drift, and the first geometric constraint can be regarded as active at this design from a practical point of view.

4.5.3 Example 3

The design of the bracing system for a 4-story building is considered as the third example. The corresponding structural model, which has been borrowed from [182], is illustrated in Fig. 4.9. Each floor is supported by 48 identical columns. The corresponding cross sections, which are taken from AISC standards [342], are $W24 \times 131$ for the two lower floors and $W24 \times 104$ for the two upper floors. In addition, six nonlinear devices, which follow the same restoring force law from the previous example, are implemented at each floor. Finally, a bracing system consisting of 128 tubular steel elements is incorporated. The braces along axes A, C, D and F act in the x direction, while those along axes 1, 2, 7 and 8 in the y direction. The elastic modulus and density of the bracing elements are taken as 2.1×10^{11} N/m^2 and 7.42 ton/m^3, respectively.

The system is subject to a ground excitation applied at 45 degrees with respect to the x axis (see Fig. 4.9). As in the previous examples, the ground acceleration is represented using a point-source

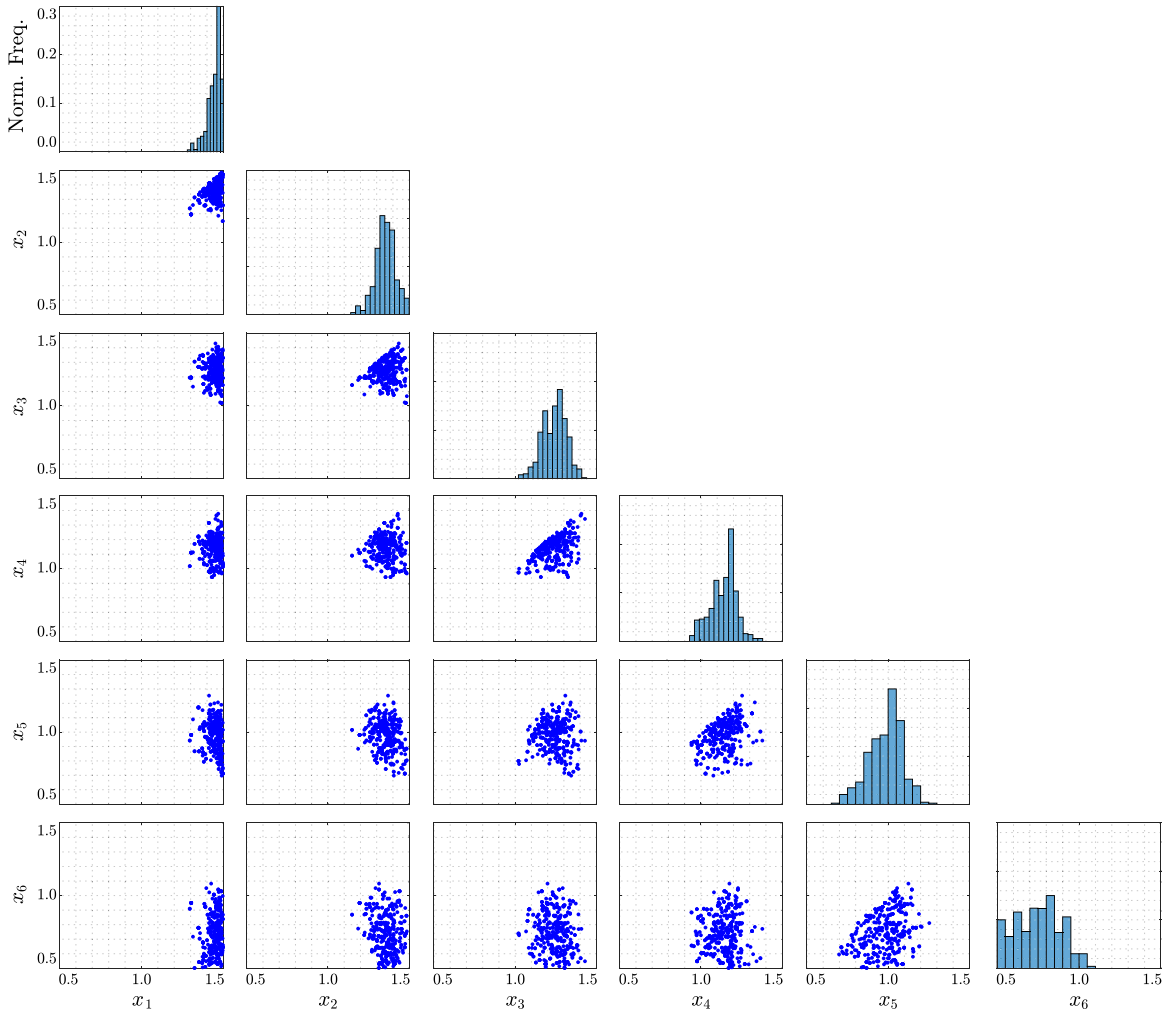

Fig. 4.7: Set of feasible designs obtained in the exploration phase. Example 2.

model. A reference period of $T = 15$ s is considered with a time step of 0.01 s and, therefore, more than 1500 random variables are involved in the characterization of the stochastic process. For dynamic analysis purposes, each floor is assumed as rigid within the $x - y$ plane when compared with the horizontal resistant elements. Using condensation techniques, the global system response can be characterized with three coordinates per floor. The mass and polar inertia of each floor are 5.98×10^5 kg and 1.10×10^8 kg m^2, respectively. Finally, a 2% of critical damping is considered in the model.

In this example, the objective function $f(\mathbf{x})$ is related to the total weight of the brace elements. A total of four design variables are considered to define the areas of the tubular cross sections of

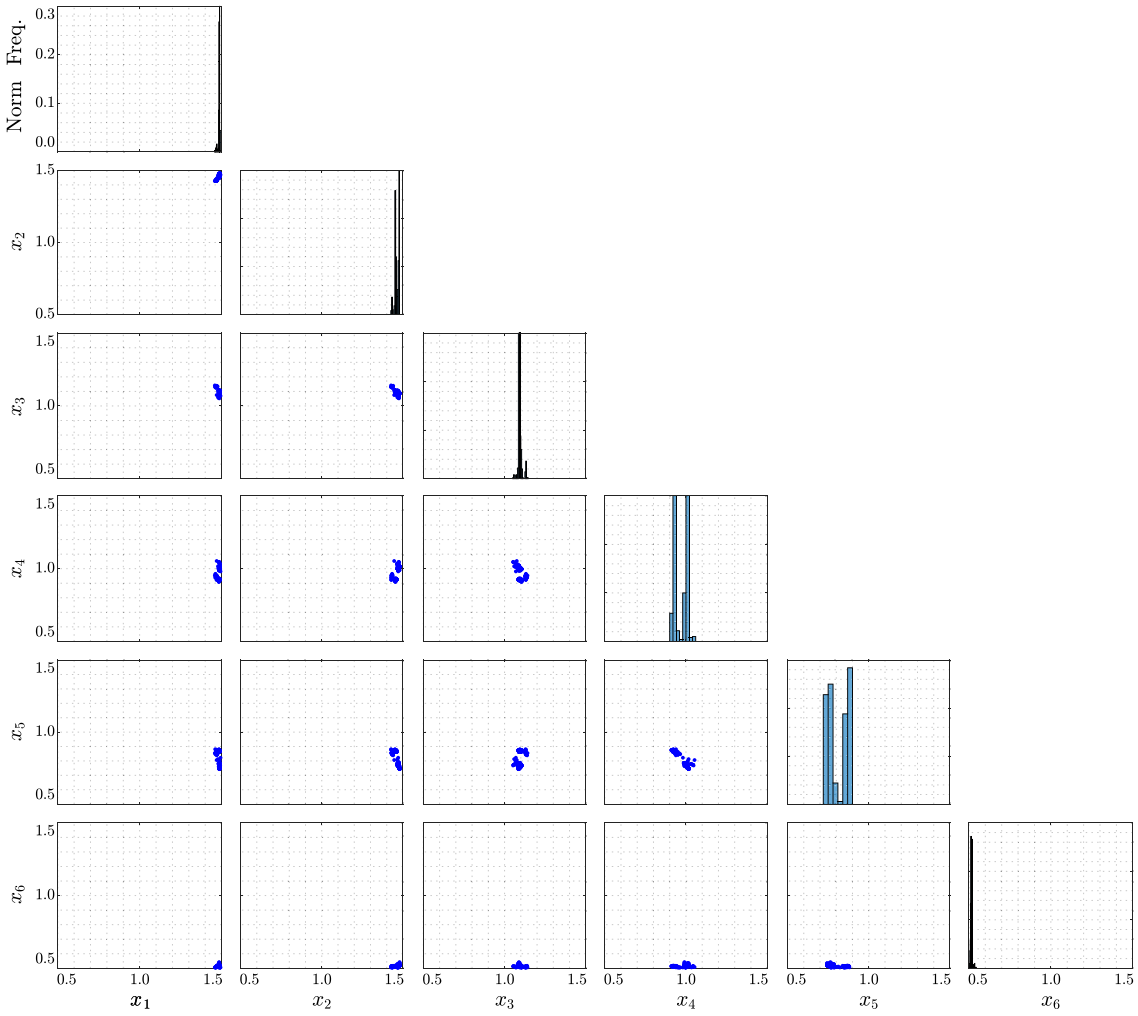

Fig. 4.8: Set of designs at the end of the exploitation phase. Example 2.

the bracing elements. The areas can be chosen from a discrete set of 48 available values ranging from 719 mm^2 to 3063 mm^2 [182]. Each design variable x_i, $i = 1, \ldots, 4$, is linked to the brace elements of two consecutive floors along a certain direction. The variables x_1 and x_2 represent the areas of the bracing elements in the two lower floors along the x and y directions, respectively. For the two upper floors, the areas of the brace elements along the x and y directions are given by x_3 and x_4, respectively. In this setting, the initial search space comprises more than 5×10^6 available

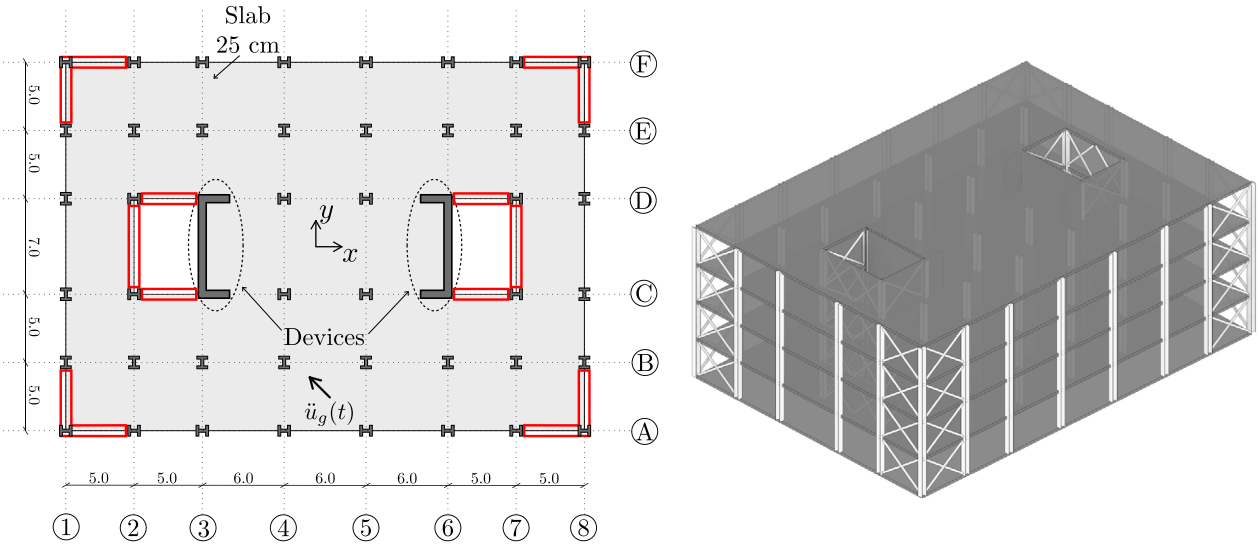

Fig. 4.9: Floor plan (left) and isometric view (right) of the 4-story building. Example 3.

configurations for the bracing system. A constrained RBO problem is formulated as

$$\begin{aligned} \min_{\mathbf{x}} \quad & f(\mathbf{x}) = \textstyle\sum_{i=1}^{4} \bar{f}_i x_i \\ \text{s.t.} \quad & P_{F_j}(\mathbf{x}) \leq 5 \times 10^{-4}, \quad j = 1, 2 \\ & x_i \in \mathbf{X}, \qquad\qquad i = 1, \ldots, 4 \end{aligned} \tag{4.32}$$

where $f(\mathbf{x})$ represents the normalized weight of the bracing system with normalizing constants $\bar{f}_1 = \bar{f}_3 = 8.5 \times 10^{-5}$ and $\bar{f}_2 = \bar{f}_4 = 7.8 \times 10^{-5}$, $P_{F_j}(\mathbf{x})$ is the probability of failure event $F_j = \{d_j(\mathbf{x}, \boldsymbol{\theta}) > 1\}$, and $\mathbf{X}$ comprises the 48 available discrete values for the areas of the bracing elements. The first failure event is defined in terms of the normalized demand function

$$d_1(\mathbf{x}, \boldsymbol{\theta}) = \max_{\upsilon = x,y} \max_{t \in [0,T]} \frac{|u_r^{\upsilon}(t, \mathbf{x}, \boldsymbol{\theta})|}{u_r^*} \tag{4.33}$$

with $u_r^{\upsilon}(t, \mathbf{x}, \boldsymbol{\theta})$ the displacement at the roof centroid along the x or y direction and $u_r^* = 0.033$ m. Similarly, the normalized demand function corresponding to the second failure event is given by

$$d_2(\mathbf{x}, \boldsymbol{\theta}) = \max_{\ell = 1, \ldots, 128} \max_{t \in [0,T]} \frac{|\sigma_\ell(t, \mathbf{x}, \boldsymbol{\theta})|}{\sigma^*} \tag{4.34}$$

where $\sigma_\ell(t, \mathbf{x}, \boldsymbol{\theta})$ is the axial stress of the ℓth brace element and $\sigma^* = 3.31 \times 10^8$ Pa (80% of yield stress).

The proposed approach is implemented considering $n = 100$ samples per stage and $\nu = 0.5$. For illustration purposes, the exploration phase considers a target sample size of 250 feasible designs while the exploitation phase stops after twelve stages. It is noted that, in this case, all design variables are discrete. For the exploration phase the corresponding proposal distribution considers $\lambda_i^* = 5$ and $\tau_i = 0.025$, $i = 1, \ldots, 4$, while for the exploitation phase $\lambda_i^* = 2$ and $\tau_i = 0$. Finally, the adaptive surrogate model strategy is not implemented for this example.

The feasible designs obtained from the exploration space are presented in Fig. 4.10 in terms of two-dimensional projections and marginal histograms. This set is composed of 250 feasible designs obtained in four stages. The results show that the range of the design variables associated with the lower floors (x_1 and x_2) is smaller than of those corresponding to upper floors (x_3 and x_4). Thus, the system performance seems to be more sensitive to the stiffness of lower floors than of upper floors, which is reasonable from the structural viewpoint. This shows some of the advantages of the proposed approach, in the sense that valuable insight about the system behavior can be obtained as a byproduct of the sampling process.

Starting from the designs in Fig. 4.10, an exploitation phase is carried out. After ten stages, the set of samples presented in Fig. 4.11 is obtained. It is seen that these samples densely populate a small portion of the initial search space, i.e., they are almost coincident. To obtain further insight into the optimization procedure, Fig. 4.12 shows the maximum and minimum values of the objective function $f(\mathbf{x})$ observed during the different exploitation stages. It is seen that both values are almost coincident from stage $j = 7$ on. The sample-based minimum objective value is equal to 0.6235, which corresponds to $\mathbf{x}^T = \langle 2615, 2216, 1418, 1368 \rangle$ mm^2. It is noted that this solution imposes larger cross sections for the lower floors, which is consistent from an engineering viewpoint. The corresponding failure probability values satisfy $P_{F_1}(\mathbf{x})/5 \times 10^{-4} = 0.99$ and $P_{F_2}(\mathbf{x})/5 \times 10^{-4} = 0.05$. Thus, the first reliability constraint, which is associated with the maximum roof displacement,

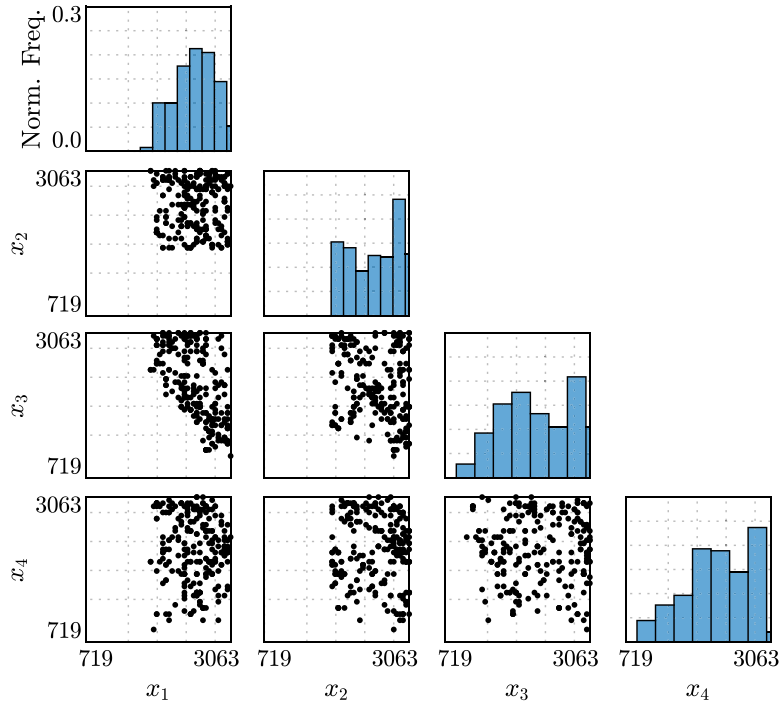

Fig. 4.10: Set of feasible designs obtained in the exploration phase. Example 3.

can be regarded as active at this solution. Finally, in terms of numerical efforts, the total number of designs evaluated in this case is in the order of 1000. That is, the algorithm is capable to explore the optimal solution set of this RBO problem in an effective manner with a relatively small sample size.

4.6 Conclusions

A two-phase sampling approach for the reliability-based optimization of structural engineering systems has been presented. The method relies on the reformulation of the constrained optimization problem as obtaining samples uniformly distributed over the optimal solution set. This task is carried out sequentially. An exploration phase is first carried out to generate feasible designs, which are then used in an exploitation phase to yield a set of close-to-optimal designs. Due to its theoretical foundations, the method has high chances to reach a vicinity of the optimum solution set. Further, it is relatively simple to implement, it provides flexibility for decision-making processes, and it yields sensitivity information as a byproduct of the sampling process. To illustrate the ca-

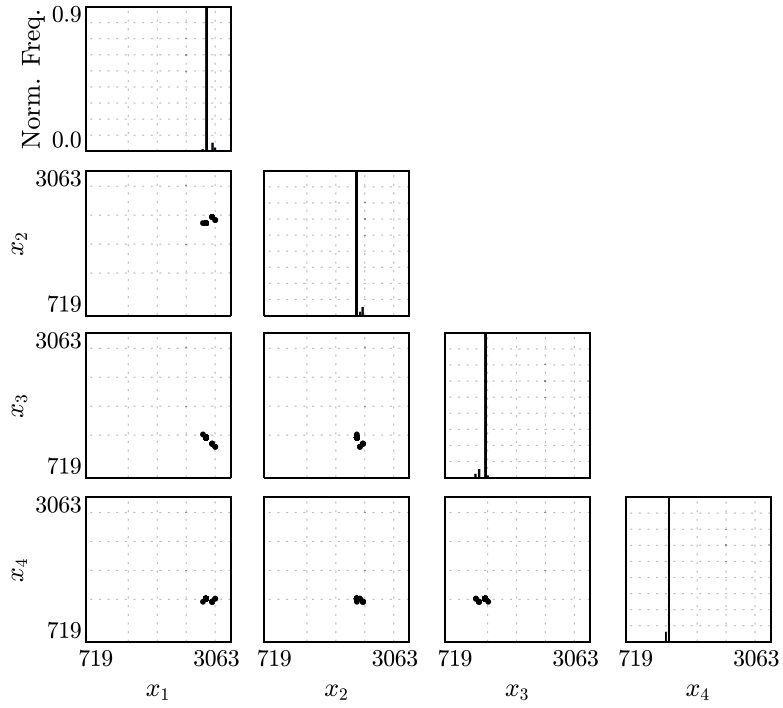

Fig. 4.11: Set of designs at the end of the exploitation phase. Example 3.

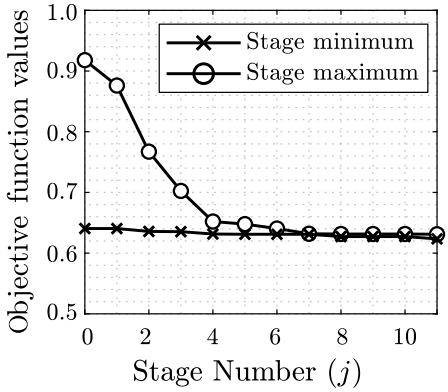

Fig. 4.12: Maximum and minimum objective function values obtained during the exploitation phase. Example 3.

pabilities of the approach, three examples involving nonlinear structural systems under stochastic ground excitation have been presented, which include continuous and discrete design spaces as well as unconstrained and constrained formulations. Overall, the numerical results indicate that the proposed approach is a potentially useful tool for solving a class of practical RBO problems in structural engineering applications.

Chapter 5

On the use of Directional Importance Sampling for reliability-based design optimization and optimum design sensitivity of linear stochastic structures

On the use of Directional Importance Sampling for reliability-based design optimization and optimum design sensitivity of linear stochastic structures

D. J. Jerez[a,*], H. A. Jensen[b], M. A. Valdebenito[c], M. A. Misraji[c], F. Mayorga[d], M. Beer[a,e,f]

[a]*Institute for Risk and Reliability, Leibniz Universität Hannover, Callinstr. 34, 30167 Hannover, Germany*

[b]*Departamento de Obras Civiles, Universidad Técnica Federico Santa María, Avda. España 1680, Valparaíso 2390123, Chile*

[c]*Faculty of Engineering and Sciences, Universidad Adolfo Ibáñez, Av. Padre Hurtado 750, Viña del Mar 2562340, Chile*

[d]*Department of Structural Engineering, University of California San Diego, Gilman Drive 9500, La Jolla 92093, California, United States*

[e]*International Joint Research Center for Engineering Reliability and Stochastic Mechanics, Tongji University, 1239 Siping Road, Shanghai 200092, P.R. China*

[f]*Institute for Risk and Uncertainty and School of Engineering, University of Liverpool, Peach Street, Liverpool L69 7ZF, UK*

Abstract: This contribution focuses on reliability-based design and optimum design sensitivity of linear dynamical structural systems subject to Gaussian excitation. Directional Importance Sampling (DIS) is implemented for reliability assessment, which allows to obtain first-order derivatives of the failure probabilities as a byproduct of the sampling process. Thus, gradient-based solution schemes can be adopted by virtue of this feature. In particular, a class of feasible-direction interior point algorithms are implemented to obtain optimum designs, while a direction-finding approach is considered to obtain optimum design sensitivity measures as a post-processing step of the optimization results. To show the usefulness of the approach, an example involving a building structure is studied. Overall, the reliability sensitivity analysis framework enabled by DIS provides a poten-

*Corresponding author
E-mail address: danko.jerez@irz.uni-hannover.de (D. J. Jerez).

tially useful tool to address a practical class of design optimization problems.

Keywords: Structural design; First excursion probability; Directional Importance Sampling; Optimum design sensitivity; Linear structures; Gaussian loading; Interior point algorithm.

5.1 Introduction

The design of safe and cost-effective structures to satisfy public and private needs is one of the most classical tasks in civil engineering. In this regard, structural systems are usually required to be optimum with respect to a given criterion while complying with a set of design conditions [117]. Moreover, appropriate design procedures must take into account all relevant uncertainties about the system under consideration, as they can significantly affect the expected structural performance of final designs [118]. Especially relevant are uncertainties in environmental dynamical excitations, such as wind effects or earthquakes, which are commonly modeled by means of stochastic processes [34–37, 113, 114, 120, 350, 351]. In this setting, reliability-based optimization (RBO) provides a realistic and rational framework for structural design which explicitly accounts for the uncertainties during the design process [7, 104].

RBO problems are usually formulated as the minimization of an objective function subject to both standard design requirements and reliability constraints. In structural dynamics applications, reliability is measured by means of first-passage probabilities. Some reliability analysis techniques that have been used in this context include, e.g., the Wiener path integral [347], statistical linearization [352], and advanced simulation techniques [110, 149, 175, 177, 204, 209]. In general, the choice of a solution method depends on the particular characteristics of the problem at hand. The reader is referred to [111] for a recent overview on RBO methods for structural dynamical systems under stochastic excitation.

Special attention is directed to the optimal design of linear structures subject to Gaussian excitation under constraints on first-passage probabilities. This type of problems arises, e.g., when require-

ments on serviceability conditions are considered [353, 354]. Several specialized approaches have been reported to address this particular class of problems. A stochastic search method is proposed in [177], which relies on the nested implementation of advanced simulation techniques to explore the design space and evaluate the reliability constraints. An adaptive scheme to allocate computational efforts is integrated for improved numerical efficiency. Alternatively, a sequential optimization approach is presented in [149], where failure probability functions are locally approximated using sensitivity information. It is noted that the previous methods use simulation techniques to evaluate the reliability constraints in a direct manner, without any approximation at the stochastic response level. On the other hand, the sequential optimization approaches presented in [125, 127, 169, 170] mainly rely on approximation schemes for (i) peak responses, (ii) failure probability functions, and (iii) the second-order statistics of the different responses of interest. These methods have proved effective in applications involving uncertain linear systems and high-dimensional design spaces. Approximations of the peak responses are formulated either using peak factors [125], the so-called auxiliary variable vector approach [127], or parametrized distributions [170]. In addition, for demand functions involving more than one response, reliability constraints are approximated with kriging metamodels for the so-called inverse reliability constraints [169], or by assuming the failure probability as proportional to the sum of its corresponding individual component-level failure probabilities [170]. Usually, the computation of the mean values and standard deviations of all responses of interest at any given design is required by these formulations. To this end, surrogates based on direct Monte Carlo simulation results from the previous candidate design are used. Even though all previous approaches have proved effective in a variety of applications, it is believed that there is still room for further developments in this area, particularly in the effective and efficient integration of specialized sampling methods in RBO procedures.

Several stochastic simulation techniques especially tailored to the reliability assessment of linear structures under Gaussian loading have been proposed. These include Efficient Importance Sampling [137], Domain Decomposition Method [139], Multidomain Line Sampling [355], and Directional Importance Sampling (DIS) [140]. These methods exploit the linear relationship between

the structural responses and the set of basic random variables [71] to reduce the variability of failure probability estimates. In this work, DIS [140] is adopted to evaluate the reliability constraints. Further, this method also provides estimates of the first-order derivatives of the failure probability by reusing the sampling results [167]. As a result, sensitivities with respect to design variables and general model parameters can be obtained as a post-processing step of reliability assessment. This feature is particularly advantageous for the treatment of RBO problems, since suitable gradient-based solution schemes can be adopted.

It is the objective of this work to implement DIS as a general reliability and sensitivity assessment framework to treat RBO problems involving linear structural systems under Gaussian excitation. First-order solution schemes are adopted not only to identify optimal designs, but also to assess their sensitivity. On the one hand, a sequential optimization method based on a class of feasible-direction interior point algorithms [159, 356] is adopted to solve the RBO problem. This scheme provides a sequence of feasible designs with improving objective values, which is advantageous for practical purposes. Further, full reliability assessment at only few designs is usually required by this method. On the other hand, a direction-finding technique [357] is implemented to evaluate the sensitivity of optimum designs with respect to model parameter perturbations. This analysis is performed as a post-process of the optimization results, which allows to obtain a deeper understanding of final solutions with reduced computational efforts. Numerical results suggest that DIS represents a potentially useful tool for the treatment of a class of RBO problems.

The structure of this contribution is as follows. Section 5.2 formulates the problems of interest. The main ideas of Directional Importance Sampling are summarized in Section 5.3, whereas Section 5.4 discusses the enabled reliability sensitivity assessment framework. Section 5.5 describes the first-order solution schemes adopted for RBO and optimum design sensitivity assessment. A numerical example is presented in Section 5.6 to illustrate the applicability of the proposed framework. The paper closes with some conclusions and final remarks.

5.2 Formulation of the problem

The class of reliability-based design optimization problems of interest can be stated as

$$\begin{aligned} \min_{\mathbf{x}} \quad & f(\mathbf{x}) \\ \text{s.t.} \quad & r_j(\mathbf{x}) \leq 0, \quad j = 1, \ldots, n_r \\ & g_j(\mathbf{x}) \leq 0, \quad j = 1, \ldots, n_g \end{aligned} \tag{5.1}$$

where $\mathbf{x} \in \mathbb{R}^{n_x}$ denotes a vector of continuous design variables, $f(\mathbf{x})$ is the objective function, $r_j(\mathbf{x}) \leq 0, j = 1, \ldots, n_r$ characterize n_r constraints on structural reliability, and $g_j(\mathbf{x}) \leq 0, j = 1, \ldots, n_g$ represent n_g standard constraints. Typical objective functions include construction or maintenance costs, total weight, etc. Reliability constraints represent design conditions formulated in terms of reliability measures, such as the verification of serviceability limit states. On the other hand, standard constraints are requirements that do not involve structural reliability assessment, including geometric design needs, material availability, etc. Note that the side constraints on the design variables, i.e., $x_i^L \leq x_i \leq x_i^U, i = 1, \ldots, n_x$ with x_i^L and x_i^U the lower and upper bounds on x_i, respectively, are contained in the set of n_g standard constraints. Finally, in the context of this contribution, the objective function does not involve reliability assessment and, therefore, it is assumed that the objective and standard constraint functions are computationally inexpensive to evaluate.

5.2.1 Mechanical modeling

The structural dynamical systems of interest are characterized by means of linear, elastic and classically damped multi-degree-of-freedom models, which satisfy the equation of motion

$$\mathbf{M}(\mathbf{x})\ddot{\mathbf{y}}(t, \mathbf{x}, \boldsymbol{\theta}) + \mathbf{C}(\mathbf{x})\dot{\mathbf{y}}(t, \mathbf{x}, \boldsymbol{\theta}) + \mathbf{K}(\mathbf{x})\mathbf{y}(t, \mathbf{x}, \boldsymbol{\theta}) = \mathbf{q}(\mathbf{x})p(t, \boldsymbol{\theta}) \tag{5.2}$$

where $\ddot{\mathbf{y}}$, $\dot{\mathbf{y}}$, and $\mathbf{y}$ are, respectively, the acceleration, velocity, and displacement vectors of dimension n_y; the matrices $\mathbf{M}$, $\mathbf{C}$, and $\mathbf{K}$ characterize the mass, damping and stiffness properties of the structure; $\mathbf{q}$ is a vector coupling the excitation p with the structural degrees of freedom; and $\boldsymbol{\theta}$ is the vector of basic random variables.

5.2.2 Stochastic Gaussian excitation

The dynamic load p of duration T is characterized as a discrete Gaussian process. This class of stochastic processes can be used to represent uncertain environmental excitations in structural engineering applications; see, e.g., [37, 63, 358–361]. By applying the Karhunen-Loève expansion [8, 91], the discrete Gaussian load can be represented as

$$p(t_k, \boldsymbol{\theta}) = \mu_k + \boldsymbol{\psi}_k^T \boldsymbol{\theta},\ k = 1, \ldots, n_T \tag{5.3}$$

where $p(t_k, \boldsymbol{\theta})$ is the loading at time $t_k = (k-1)\Delta t, k = 1, \ldots, n_T$, Δt is the time step, $n_T = T/\Delta t + 1$ is the number of time instants; $\boldsymbol{\theta}$ is a realization of a standard Gaussian random variable vector of dimension n_θ; μ_k is the expected value of the stochastic process p at time t_k; and $\boldsymbol{\psi}_k$ is a vector of dimension n_θ associated with time instant t_k. The set of vectors $\boldsymbol{\Psi} = [\boldsymbol{\psi}_1, \ldots, \boldsymbol{\psi}_{n_T}]$ is given by $\boldsymbol{\Psi} = \boldsymbol{\Lambda}^{1/2}\boldsymbol{\Xi}^T$, where $\boldsymbol{\Lambda}$ and $\boldsymbol{\Xi}$ comprise, respectively, the n_θ largest eigenvalues and corresponding eigenvectors of the covariance matrix $\boldsymbol{\Sigma}$ of the stochastic load, i.e., $\boldsymbol{\Sigma}\boldsymbol{\Xi} = \boldsymbol{\Xi}\boldsymbol{\Lambda}$. Without loss of generality, a zero-mean stochastic process is assumed as $\mu_k = 0, k = 1, \ldots, n_T$. Finally, it is noted that the characterization of the stochastic load by means of Eq. (5.3) generally involves a large number of basic random variables, i.e., n_θ is usually in the order of hundreds or thousands [71].

5.2.3 Reliability constraints

Requirements on system reliability are usually established using failure probability measures. In this contribution, the reliability constraints are expressed in the form

$$r_j(\mathbf{x}) = \ln\left(P_{F_j}(\mathbf{x})\right) - \ln(P^*_{F_j}) \leq 0, \quad j = 1, \ldots, n_r \tag{5.4}$$

where $\ln(\cdot)$ denotes natural logarithm, $P_{F_j}(\mathbf{x})$ is the probability of failure event F_j evaluated at design $\mathbf{x}$, and $P^*_{F_j}$ is the corresponding maximum allowable value. In the context of structural dynamical systems under stochastic excitation, the probability that certain requirements are not fulfilled within the load duration T is a useful measure of structural performance. Thus, reliability requirements are expressed by means of *first-passage failure events* [82, 84]

$$F_j = \{d_j(\mathbf{x}, \boldsymbol{\theta}) > 1\}, \quad j = 1, \ldots, n_r \tag{5.5}$$

where $d_j(\mathbf{x}, \boldsymbol{\theta})$ is the *normalized demand function* of event F_j given by

$$d_j(\mathbf{x}, \boldsymbol{\theta}) = \max_{t \in [0,T]} \max_{m=1,\ldots,n_{j,h}} \frac{|h_{j,m}(t, \mathbf{x}, \boldsymbol{\theta})|}{h^*_{j,m}} \tag{5.6}$$

where $h_{j,m}(t, \mathbf{x}, \boldsymbol{\theta}), m = 1, \ldots, n_{j,h}$ are the response functions of interest associated with failure event F_j with corresponding threshold levels $h^*_{j,m} > 0$. The response functions are taken as linear combinations of the structural displacements, velocities and/or accelerations. As a result, they are time-dependent and also depend on the design and random variables. Finally, the *first-passage failure probability* associated with the j^{th} reliability constraint is given by

$$P_{F_j}(\mathbf{x}) = \int_{\boldsymbol{\theta} \in \mathbb{R}^{n_\theta}} I_{F_j}(\mathbf{x}, \boldsymbol{\theta}) f_{\boldsymbol{\Theta}}(\boldsymbol{\theta}) d\boldsymbol{\theta} \tag{5.7}$$

where $I_{F_j}(\mathbf{x}, \boldsymbol{\theta})$ is the indicator function with $I_{F_j}(\mathbf{x}, \boldsymbol{\theta}) = 1$ if $d_j(\mathbf{x}, \boldsymbol{\theta}) > 1$ and $I_{F_j}(\mathbf{x}, \boldsymbol{\theta}) = 0$ otherwise, and $f_{\boldsymbol{\Theta}}(\boldsymbol{\theta})$ is the standard multivariate Gaussian probability density function of dimension

n_θ. As already pointed out, $\boldsymbol{\theta}$ may comprise hundreds or thousands of random variables. Therefore, the evaluation of the integral in Eq. (5.7) at each design represents a high-dimensional problem which is extremely demanding from the numerical viewpoint [82, 84]. As already pointed out, DIS [140, 167] is implemented to evaluate the reliability constraints and their first-order derivatives.

5.2.4 Optimum design sensitivity

The formulation of a RBO problem depends a number of parameters to characterize the objective and constraint functions and, therefore, changes in these quantities can affect the final solution [330]. Of particular importance are those involved in the definition of reliability constraints, e.g., excitation model parameters or response thresholds. For a given model parameter, ζ, the rates of change of the optimum objective value, $\frac{df^*}{d\zeta}$, and of the optimum values for the design variables, $\frac{\partial x_i^*}{\partial \zeta}$, $i = 1, \ldots, n_x$, represent suitable sensitivity measures. These derivatives are associated with the greatest feasible improvement of the final solution for small changes in ζ. A direction-finding approach [357] is adopted in this contribution to compute such sensitivities.

5.3 Directional Importance Sampling

Directional Importance Sampling is a stochastic simulation method tailored to linear structural systems subject to Gaussian excitation [140, 167]. Consider a first-passage failure event $F = \{d(\boldsymbol{\theta}) > 1\}$ with normalized demand function $d(\boldsymbol{\theta}) = \max_{k=1,\ldots,n_T} \max_{m=1,\ldots,n_h} |h_m(t_k, \boldsymbol{\theta})|/h_m^*$. For notation simplicity, the explicit dependence of the different quantities on $\mathbf{x}$ has been dropped. Given the system linearity, the m^{th} response of interest evaluated at time t_k can be written as [362]

$$h_m(t_k, \boldsymbol{\theta}) = \mathbf{a}_{m,k}^T \boldsymbol{\theta}, \quad \mathbf{a}_{m,k} = \sum_{q=1}^{k} \epsilon_q \Delta t \eta_m(t_k - t_q) \boldsymbol{\psi}_q \tag{5.8}$$

where ϵ_q depends on the time integration rule [363] and $\eta_m(t)$ is the unit impulse response function computed using modal superposition.

The fundamental ideas of DIS can be summarized as follows. First, the concept of *directional sampling* [364–366] is considered. Instead of using full Cartesian coordinates, the reliability problem is expressed in terms of unit directions $\mathbf{u} \sim f_{\mathbf{U}}(\mathbf{u})$ uniformly distributed over the unit hypersphere $\Omega_{\mathbf{U}} \subset \mathbb{R}^{n_\theta}$. Second, an importance sampling density $f_{\mathbf{U}}^{\text{DIS}}(\mathbf{u})$ is introduced for the unit directions following some of the ideas presented in [137]. Third, the linearity of the responses of interest is exploited to obtain closed-form solutions for the probability of failure conditioned on each sampled direction. As a result, the failure probability can be written as

$$P_F = \int_{\Omega_{\mathbf{u}}} \left[1 - F_{\chi^2}^{n_\theta}\left(c(\mathbf{u})^2\right)\right] \left(\frac{f_{\mathbf{U}}(\mathbf{u})}{f_{\mathbf{U}}^{\text{DIS}}(\mathbf{u})}\right) f_{\mathbf{U}}^{\text{DIS}}(\mathbf{u}) d\mathbf{u} \tag{5.9}$$

where $F_{\chi^2}^{n_\theta}(\cdot)$ is the cumulative distribution function of the Chi-square distribution of n_θ degrees of freedom, and

$$c(\mathbf{u}) = \min_{\substack{m=1,\ldots,n_h \\ k=1,\ldots,n_T}} c_{m,k}(\mathbf{u}) = \min_{\substack{m=1,\ldots,n_h \\ k=1,\ldots,n_T}} \frac{h_m^*}{|\mathbf{a}_{m,k}^T \mathbf{u}|} \tag{5.10}$$

represents the minimum capacity-to-demand ratio across all responses of interest and time instants for the fixed unit vector $\mathbf{u}$. Equivalently, this quantity can be interpreted as the minimum factor by which $\mathbf{u}$ must be amplified to generate failure. Finally, a failure probability estimate is obtained by drawing samples $\mathbf{u}^{(\ell)} \sim f_{\mathbf{U}}^{\text{DIS}}(\mathbf{u})$, $\ell = 1, \ldots, N$, which gives

$$P_F \approx \tilde{P}_F^{\text{DIS}} = \frac{1}{N} \sum_{\ell=1}^{N} \frac{\hat{P}_F \left[1 - F_{\chi^2}^{n_\theta}\left(c(\mathbf{u}^{(\ell)})^2\right)\right]}{\sum_{m=1}^{n_h} \sum_{k=1}^{n_T} \left[1 - F_{\chi^2}^{n_\theta}\left(c_{m,k}(\mathbf{u}^{(\ell)})^2\right)\right]} \tag{5.11}$$

where $\hat{P}_F = 2 \sum_{m=1}^{n_h} \sum_{k=1}^{n_T} \Phi(-h_m^* / \|\mathbf{a}_{m,k}\|)$ with $\Phi(\cdot)$ the standard Gaussian cumulative distribution function. In general, relatively small sample sizes are required to obtain sufficiently accurate reliability estimates [140]. Further, the sample generation process is highly efficient and parallelizable [139]. A detailed description of DIS can be found in [140].

5.4 Reliability sensitivity assessment framework

5.4.1 First-order derivatives with respect to general model parameters

Consider a general model parameter, ν, involved in the definition of the normalized demand function such that $F = \{d(\nu, \boldsymbol{\theta}) > 1\}$. Note that ν can affect the structural properties, the excitation model, or the response thresholds. Following the ideas presented in [167], direct differentiation of the integral in Eq. (5.9) with respect to ν yields

$$\frac{\partial P_F}{\partial \nu} = -\int_{\Omega_{\mathbf{U}}} \left[2c(\nu, \mathbf{u}) \frac{\partial c(\nu, \mathbf{u})}{\partial \nu} f_{\chi^2}^{n_\theta} \left(c(\nu, \mathbf{u})^2 \right) \right] \left(\frac{f_{\mathbf{U}}(\mathbf{u})}{f_{\mathbf{U}}^{\text{DIS}}(\mathbf{u})} \right) f_{\mathbf{U}}^{\text{DIS}}(\mathbf{u}) d\mathbf{u} \tag{5.12}$$

where $f_{\chi^2}^{n_\theta}$ is the probability density function of the Chi-squared distribution of n_θ degrees of freedom. Then, the same set of samples generated to evaluate Eq. (5.11) can be used to estimate the first-order derivatives as

$$\frac{\partial P_F}{\partial \nu} \approx \frac{\partial \tilde{P}_F^{\text{DIS}}}{\partial \nu} = -\frac{1}{N} \sum_{\ell=1}^{N} \frac{2\hat{P}_F(\nu) c(\nu, \mathbf{u}^{(\ell)}) \frac{\partial c(\nu, \mathbf{u}^{(\ell)})}{\partial \nu} f_{\chi^2}^{n_\theta} \left(c(\nu, \mathbf{u}^{(\ell)})^2 \right)}{\sum_{m=1}^{n_h} \sum_{k=1}^{n_T} \left[1 - F_{\chi^2}^{n_\theta} \left(c_{m,k}(\nu, \mathbf{u}^{(\ell)})^2 \right) \right]} \tag{5.13}$$

In the previous equation, the only additional terms that need to be computed are $\frac{\partial c(\nu, \mathbf{u}^{(\ell)})}{\partial \nu}$, $\ell = 1, \ldots, N$. To this end, assume that $c(\nu, \mathbf{u}) = c_{M,K}(\nu, \mathbf{u})$, where (M, K) are the indices that provide the minimum in Eq. (5.10). Then, the sought partial derivative is

$$\frac{\partial c(\nu, \mathbf{u})}{\partial \nu} = \frac{\partial c_{M,K}(\nu, \mathbf{u})}{\partial \nu} = \frac{\partial}{\partial \nu} \left(\frac{h_M^*}{|\mathbf{a}_{M,K}^T \mathbf{u}|} \right) \tag{5.14}$$

Three different scenarios in terms of the type of model parameter can be identified. First, if ν affects structural properties, then the evaluation of Eq. (5.14) simply requires the sensitivities of the spectral properties [367]. Second, when ν represents an excitation model parameter, the derivatives of the vectors associated with the Karhunen-Loève expansion (see Eq. (5.3)) are needed. This can be carried out using any suitable method [147]. Finally, in case ν corresponds to a response threshold,

sensitivity evaluation can be performed with marginal computational efforts. For completeness, Appendix 5.8 provides explicit formulas for the three different scenarios in terms of ν.

5.4.2 Practical advantages

From the practical viewpoint, the adopted reliability sensitivity assessment framework presents two main advantageous features. On the one hand, the formulation presented in this section is quite general in the sense that it can be used to estimate sensitivities with respect to both design variables ($\nu = x_i$) and alternative model parameters ($\nu = \zeta$). On the other hand, the comparison of Eqs. (5.11) and (5.13) reveals that all the information retrieved during reliability assessment is reused to compute the corresponding first-order derivatives. Thus, first-order derivatives of reliability measures can be obtained as a byproduct of reliability assessment. These features are quite beneficial in the context of RBO problems, as they enable effective gradient-based solution schemes to obtain optimum solutions and to evaluate the sensitivity of final designs.

5.5 Implementation of first-order solution methods

5.5.1 Sequential optimization strategy

In order to solve the RBO problem in Eq. (5.1), a first-order sequential optimization approach based on a class of feasible-direction interior point algorithms [159, 356] is adopted. In essence, each optimization cycle requires to identify a feasible-descent direction and to solve a line search problem to find a new candidate along such direction. Several advantages are provided by the adopted optimization strategy. First, the method produces a sequence of feasible designs with consecutively lower objective function values. Hence, the optimization process can be stopped at any iteration to retrieve a feasible solution that is better than the initial one. Second, one-dimensional surrogates for the reliability constraints, instead of multi-dimensional surrogates, can be adaptively generated during each optimization cycle for improved computational efficiency. Finally, relatively few re-

liability analyses are usually required to reach convergence. The reader is referred to [159] for a detailed description of the optimization strategy.

5.5.2 Direction-finding approach for optimum design sensitivity

In this contribution, the framework proposed in [357] is adopted to compute optimum design sensitivities. Consider the augmented design space $\langle x_1, \ldots, x_{n_x}, \zeta \rangle$ of dimension $n_x + 1$, where ζ represents a given model parameter. Then, sensitivity computation can be viewed as finding the *constrained steepest-descent direction* in such augmented space, $\mathbf{s} = [s_1, \ldots, s_{n_x+1}]^T$, which provides the greatest improvement of the objective value while satisfying the problem constraints. This direction is the solution to [357, 368]

$$\begin{aligned} \min_{\mathbf{s}} \quad & \nabla f^T \mathbf{s} \\ \text{s.t.} \quad & \nabla r_j^T \mathbf{s} \leq 0, \quad j \in J_r \\ & \nabla g_j^T \mathbf{s} \leq 0, \quad j \in J_g \\ & \mathbf{s}^T \mathbf{s} - 1 \leq 0 \end{aligned} \tag{5.15}$$

where $\nabla \mathcal{F}^T = \left[\frac{\partial \mathcal{F}(\mathbf{x},\zeta)}{\partial x_1}, \ldots, \frac{\partial \mathcal{F}(\mathbf{x},\zeta)}{\partial x_{n_x}}, \frac{\partial \mathcal{F}(\mathbf{x},\zeta)}{\partial \zeta} \right]\Big|_{\mathbf{x}^*,\zeta^0}$, with $\mathcal{F}$ representing f, r_j, $j \in J_r$, or g_j, $j \in J_g$; ζ^0 is the nominal or actual value of ζ; and J_r and J_g denote the sets of reliability and standard constraints, respectively, that are active at the final design $\mathbf{x}^*$. It is seen that the framework only requires the first-order derivatives of the objective and active constraint functions with respect to x_i, $i = 1, \ldots, n_x$, and ζ. Furthermore, the previous optimization problem can be solved very efficiently, as it involves a linear objective function, linear constraints and a single quadratic constraint [369]. Based on the direction $\mathbf{s}$, the rate of change of the optimum objective is [357]

$$\frac{df^*}{d\zeta} = \frac{\nabla f(\mathbf{x}^*, \zeta^0)^T \mathbf{s}}{|s_{n_x+1}|} \tag{5.16}$$

and the rates of change of the optimum values for the design variables are computed as [357]

$$\frac{\partial x_i^*}{\partial \zeta} = \frac{s_i}{|s_{n_x+1}|},\ i = 1, \ldots, n_x \tag{5.17}$$

If s_{n_x+1} is positive (negative), the previous results are associated with an increase (decrease) in ζ. In case $s_{n_x+1} = 0$, the optimum solution remains unaffected by changes in ζ. If the sign of the change in ζ is specified beforehand, a similar technique can be adopted [357].

Note that all the derivatives of the problem functions with respect to the design variables are readily available from the final optimization cycle. Therefore, only the sensitivities with respect to ζ remain to be evaluated, which is performed by reusing the DIS results at the final design. In other words, optimum design sensitivities are obtained as an effective post-process of the optimization results, which is advantageous for practical purposes.

5.5.3 Remarks

As already pointed out, DIS provides efficient estimation of failure probabilities and their sensitivities for linear structural systems subject to Gaussian excitation. This, in turn, enables first-order solution methods for RBO and optimum design sensitivity analysis. The specific strategies adopted in this work have proved quite effective, as illustrated in Section 5.6. Nonetheless, the use of DIS in RBO problems is not necessarily limited to these particular solution methods. In principle, any suitable method that requires only the gradients of failure probability functions can be integrated with the sensitivity analysis framework described in this contribution. Hence, DIS can be interpreted as a potentially useful and numerically efficient tool to aid informed decision-making processes under uncertainty. Furthermore, this suggests that exploiting particular features of specialized simulation techniques can be quite advantageous for RBO schemes.

5.6 Example problem

In order to illustrate the applicability of the proposed framework, a numerical example involving a realistic building model subject to stochastic loading is presented in this section. The goal of this example is to determine the thicknesses of the core shear walls that minimize structural weight, subject to constraints on serviceability reliability and geometric conditions. Two scenarios in terms of the number of design variables and the number of reliability constraints are addressed. In addition, the sensitivity of the optimum design with respect to response thresholds and excitation model parameters is studied.

5.6.1 Building structure

A three-dimensional finite element model of a 16-story reinforced concrete (RC) building, which has been borrowed from [167], is considered in this section. For illustration purposes, Fig. 5.1 shows a three-dimensional representation of the structural model. The interstory height is equal to 3.25 m, which gives a total height of 52.0 m. In addition, the building is 30 m by 35 m in plan. A perimeter of RC rectangular columns and shear walls plus a core of RC shear walls are considered for the horizontal resistant system. The corresponding material properties are given by Young modulus $E = 2.5 \times 10^{10}$ N/m^2, Poisson ratio equal to 0.3, and mass density equal to 2500 kg/m^3. Shell elements of different thicknesses are considered to model the shear walls and floor slabs. In addition, beam and column elements are also included in the system. As a result, the finite element model involves 29466 degrees of freedom. Since the system is studied for small vibrations, linear elastic behavior is assumed. Finally, 20 modes are kept for dynamic analysis purposes and a 5% of critical damping is considered for all modes.

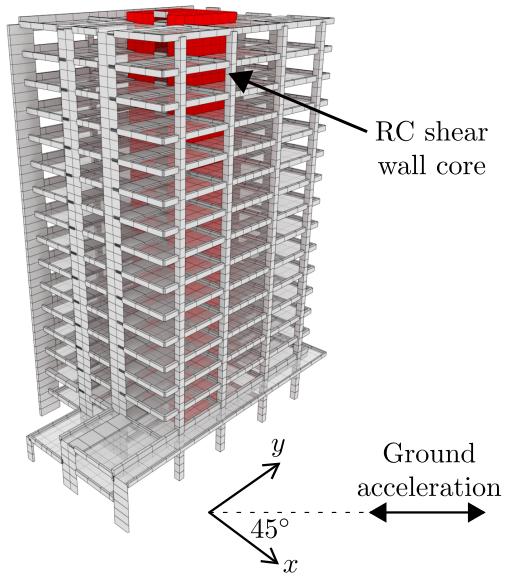

Fig. 5.1: Perspective view of a 16-story reinforced concrete structure under ground excitation.

5.6.2 Stochastic ground excitation

As illustrated in Fig. 5.1, the building is subject to a ground excitation applied at 45° with respect to the x axis. Such loading is modeled as a non-stationary filtered white noise process with duration $T = 10$ s and time step $\Delta t = 0.01$ s. Specifically, a modulated white noise signal passing through a Clough-Penzien filter [370] is considered. Hence, the ground acceleration is given by $\ddot{u}_g(t) = \Omega_1^2 w_1(t) + 2\xi_1\Omega_1\dot{w}_1(t) - \Omega_2^2 w_2(t) - 2\xi_2\Omega_2\dot{w}_2(t)$, where $\Omega_1 = 15.6$ rad/s, $\Omega_2 = 1.0$ rad/s, $\xi_1 = 0.6$ and $\xi_2 = 0.9$ are the filter parameters, and the variables $w_i(t)$, $i = 1, 2$, satisfy the set of coupled differential equations

$$\begin{aligned} \ddot{w}_1(t) + 2\xi_1\Omega_1\dot{w}_1(t) + \Omega_1^2 w_1(t) &= w(t)h(t) \\ \ddot{w}_2(t) + 2\xi_2\Omega_2\dot{w}_2(t) + \Omega_2^2 w_2(t) &= \Omega_1^2 w_1(t) + 2\xi_1\Omega_1\dot{w}_1(t) \end{aligned} \tag{5.18}$$

where $w(t)$ is a white noise process with spectral intensity $S = 1.5 \times 10^{-3}$ m^2/s^3, and $h(t)$ is a time envelope function defined as

$$h(t) = \begin{cases} (t/5)^2 & 0 \leq t \leq 5 \text{ s} \\ 1 & 5 < t \leq 6 \text{ s} \\ e^{-(t-6)^2} & t > 6 \text{ s} \end{cases} \tag{5.19}$$

Finally, for illustration purposes, all the eigenvalues of the covariance matrix of the stochastic process are retained to construct the Karhunen-Lòeve expansion and, as a result, the number of basic random variables is given by $n_\theta = n_T = 1001$. Therefore, the discrete representation of the stochastic ground acceleration involves a large number of basic random variables for this case.

5.6.3 Scenario I: Design problem

For illustration purposes, $n_x = 2$ design variables and a single reliability constraint are considered in this scenario. The thicknesses of the core shear walls of the eight lower stories are linked to the first design variable as $t_{w,s} = \bar{t}_w x_1$, $s = 1, \ldots, 8$, whereas that of the remaining stories is linked to the second design variable as $t_{w,s} = \bar{t}_w x_2$, $s = 9, \ldots, 16$, with $\bar{t}_w = 0.4$ m the reference thickness value. The constrained RBO problem is given by

$$\begin{aligned} \min_{\mathbf{x}=[x_1,x_2]^T} \quad & f(\mathbf{x}) = (x_1 + x_2)/2 \\ \text{s.t.} \quad & r(\mathbf{x}) = \ln(P_F(\mathbf{x})) - \ln(10^{-3}) \leq 0 \\ & g(\mathbf{x}) = x_2 - x_1 \leq 0 \\ & 0.5 \leq x_i \leq 2.0, \quad i = 1, 2 \end{aligned} \tag{5.20}$$

where $f(\mathbf{x})$ is associated with the weight of the core shear walls, $P_F(\mathbf{x})$ is a failure probability function with maximum allowable value $P_F^* = 10^{-3}$, and $g(\mathbf{x}) \geq 0$ is a geometric constraint. Note that this formulation imposes $x_2 \leq x_1$, i.e., walls of lower floors must be thicker than of upper floors. This is a usual consideration in the context of structural design procedures. In addition, the

constraints $0.5 \leq x_i \leq 2.0$, $i = 1, 2$, indicate that the core wall thicknesses lie between 0.2 m and 0.8 m. The failure event F is associated with serviceability conditions, and it is defined as

$$F = \left\{ \max_{m=1,\ldots,16} \max_{k=1,\ldots,1001} \left(\frac{|h_{m,x}(t_k, \mathbf{x}, \boldsymbol{\theta})|}{h_m^*}, \frac{|h_{m,y}(t_k, \mathbf{x}, \boldsymbol{\theta})|}{h_m^*} \right) > 1 \right\} \tag{5.21}$$

where $h_{m,x}(t_k, \mathbf{x}, \boldsymbol{\theta})$ and $h_{m,y}(t_k, \mathbf{x}, \boldsymbol{\theta})$ are the interstory drifts, expressed as a percentage of the floor height, between floors m and $m-1$ along the x and y directions, respectively, and $h_m^* = 0.1\%$, $m = 1, \ldots, 16$, represent the corresponding maximum allowable values. It is assumed that $m = 0$ represents the ground floor. In this setting, failure is defined when any interstory drift along the x or y axes exceeds 0.1% of its corresponding floor height. Such failure criterion can be related, for instance, to the violation of a serviceability limit state of the RC core walls [371]. Finally, it is noted that the evaluation of the failure probability at any given design, $P_F(\mathbf{x})$, represents a challenging problem as it involves a high-dimensional integration domain, a finite element model with thousands of degrees of freedom, and more than 30000 elementary failure domains.

To obtain insight about the design problem, Fig. 5.2 shows the contours of $P_F(\mathbf{x})$. These iso-probability curves have been obtained by considering a set of DIS-based failure probability estimates distributed over the design space. The resulting curves, which are somewhat rugged due to the inherent variability of the estimates, have been smoothed for presentation purposes. From the figure, it is seen that the failure probability seems to be minimized by increasing the core wall thicknesses as much as possible, as expected. In general, the failure probability function depends mainly on x_1 when $x_2 > x_1$, i.e., when the upper core walls are thicker than the lower ones. Meanwhile, a stronger interaction between x_1 and x_2 is observed for $x_2 < x_1$. In this case, an increase in the thickness of the lower core walls can be compensated by a decrease in the thickness of the upper walls to maintain the same reliability level. These results are reasonable from a structural viewpoint. For comparison and reference purposes, Fig. 5.3 shows a sketch of the feasible design set. Some contours of the objective function and a reference location for the optimum design are also presented in the figure. Note that only the reliability constraint is active at the optimum solution.

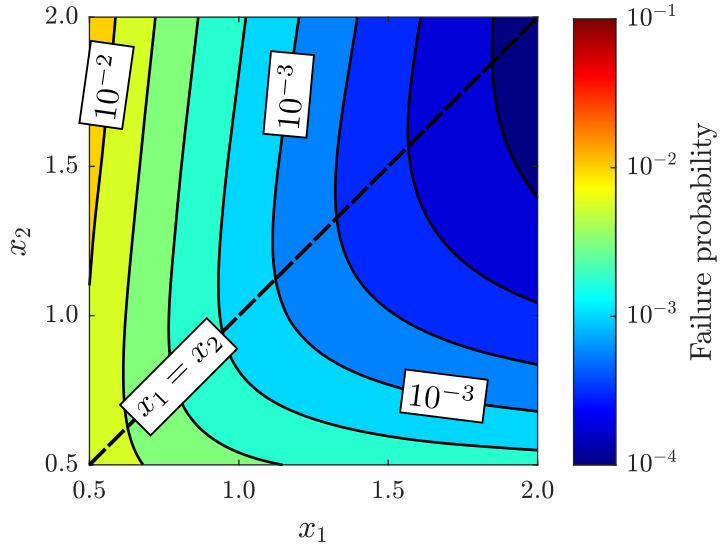

Fig. 5.2: Contours of the failure probability function $P_F(\mathbf{x})$. Scenario I.

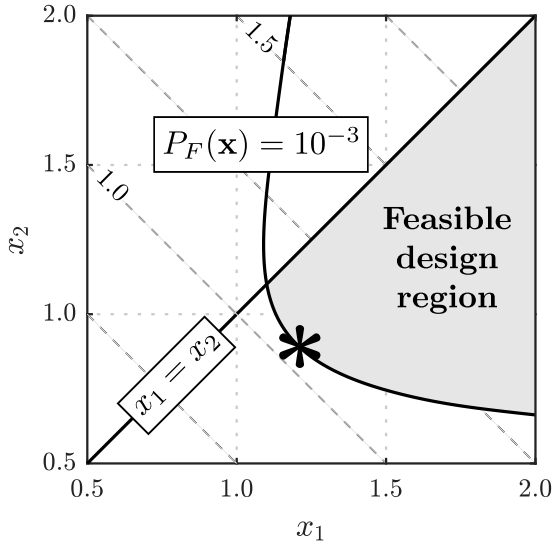

Fig. 5.3: Sketch of the feasible design space, objective contours and optimum design ($*$). Scenario I.

5.6.4 Scenario I: Results

Reliability sensitivity estimates

First-order information on the problem functions is used by the adopted optimization strategy to explore the design space efficiently. Typically, candidate design trajectories tend to move along boundaries of the feasible design set until reaching the optimum region [356]. In this context, poor

quality information about the sensitivity of the active constraints can lead to spurious behavior of the optimization process, since identified search directions might not be actually feasible. Therefore, it is particularly important for the convergence of the algorithm to obtain sufficiently accurate estimates of the gradients of the active reliability constraint functions. For this example, the gradient of the reliability constraint function in Eq. (5.20) is estimated as $\frac{\partial r(\mathbf{x})}{\partial x_i} \approx \frac{1}{\tilde{P}_F^{\mathrm{DIS}}(\mathbf{x})} \frac{\partial \tilde{P}_F^{\mathrm{DIS}}(\mathbf{x})}{\partial x_i}$, $i = 1, 2$. In this regard, the choice of an inadequately small sample size can affect the optimization procedure as such sensitivity estimates might have an unacceptable level of variability. Validation calculations have shown that $N = 2000$ samples provide a reasonable tradeoff between computational cost and quality of the DIS results in this example. For illustration purposes, Fig. 5.4 presents the estimates of $\nabla r(\mathbf{x})$ obtained across 20 independent DIS runs with $N = 2000$ samples. These estimates are evaluated at the design $\mathbf{x} = [1.18, 0.93]^T$, which verifies $P_F(\mathbf{x}) \approx 10^{-3}$. It is seen that the gradient estimates point in a similar direction and, overall, their quality is acceptable in the context of RBO problems involving structural dynamical systems under stochastic excitation.

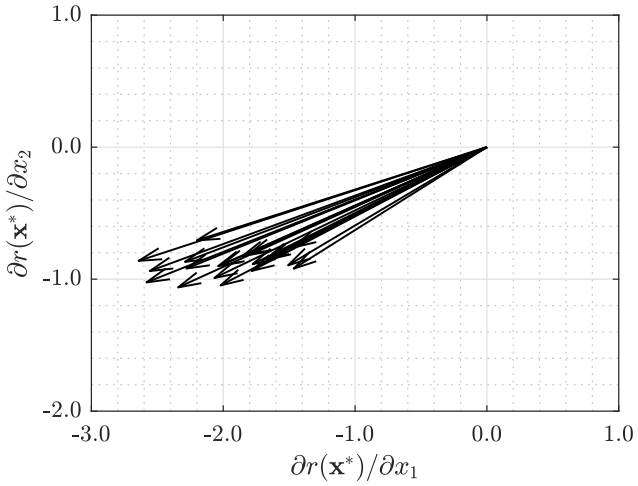

Fig. 5.4: Estimates of the reliability constraint gradient obtained in 20 independent DIS runs. Scenario I.

Optimization process

The sequential optimization strategy presented in Section 5.5.1 is implemented to solve problem (5.20). As already pointed out, this optimization strategy uses sensitivity information provided by

DIS to produce a sequence of feasible designs with decreasing objective function values. The recommendations provided in [159, 356] are considered for numerical implementation. Additionally, a sample size equal to $N = 2000$ is considered for DIS. Furthermore, the customary technique of using common random number streams is implemented, which means that the same sequence of pseudorandom numbers is considered for reliability assessment at each design. Numerical experience indicates that this strategy is quite effective in reducing the effect of the variability of the estimators on RBO procedures [173]. Three different cases in terms of the starting point are studied to evaluate the performance of the optimization scheme. In particular, cases A, B and C correspond to initial designs $\mathbf{x}^{\mathrm{A}} = [1.95, 1.90]^T$, $\mathbf{x}^{\mathrm{B}} = [1.95, 0.80]^T$ and $\mathbf{x}^{\mathrm{C}} = [1.75, 1.00]^T$, respectively. It is noted that the method requires an initial design that is feasible, which can be usually identified using engineering judgment. However, in involved cases where a feasible design is difficult to identify a priori, systematic methods can be implemented to find a starting point [330].

The sequences of candidate designs obtained for the three different starting points under consideration are presented in Fig. 5.5, where the corresponding final solutions are highlighted using dark markers. For reference purposes, some contours of the objective function $f(\mathbf{x})$ are also shown in the figure. In general, the method reaches the active feasible boundary in few optimization cycles. Then, candidate solutions tend to move along that boundary, which in this case is associated with the reliability constraint. Additionally, the three final designs are very similar between each other and they seem to lie along a contour of $f(\mathbf{x})$. To obtain further insight about the optimization process, the objective function values obtained during the different optimization cycles are presented in Fig. 5.6. Note that eight iterations are required in all cases to verify the stopping criterion. From the figure, it is clear that significant improvements in the objective function values are obtained during the initial algorithm iterations, which is beneficial for the type of problems under consideration. In case A, for instance, a relative improvement of approximately 45% is attained after the four initial optimization cycles for case. This behavior is consistent with the large initial displacements in the search space observed in Fig. 5.5. Finally, Table 5.1 presents the optimum designs obtained by the optimization scheme for the three different starting points. For comparison purposes, a ref-

erence solution obtained from a direct double-loop implementation is also presented in the table. This design has been obtained using direct Monte Carlo simulation and genetic algorithms [173] with a population size of 50 individuals. Very similar objective function values are observed for all cases. In fact, the maximum relative difference between the objective values of all the reported solutions is less than 0.5%. Thus, the integration of DIS and suitable gradient-based methods provides optimum designs in an effective manner. Finally, the reliability constraint can be regarded as active while the geometric constraint remains inactive for all the designs reported in the table, as expected.

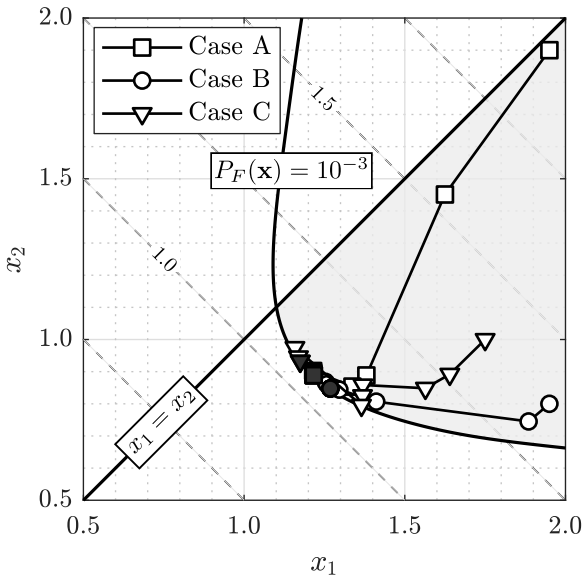

Fig. 5.5: Trajectories of candidate designs corresponding to three different starting points. Scenario I.

Table 5.1: Final designs corresponding to three different starting points and reference solution. Scenario I.

	Case A	Case B	Case C	Reference
x_1^*	1.217	1.268	1.175	1.177
x_2^*	0.889	0.848	0.932	0.928
$P_F(\mathbf{x}^*)/10^{-3}$	0.999	0.999	0.995	0.999
$g(\mathbf{x}^*)$	-0.327	-0.421	-0.242	-0.249
$f(\mathbf{x}^*)$	1.0529	1.0580	1.0536	1.0525

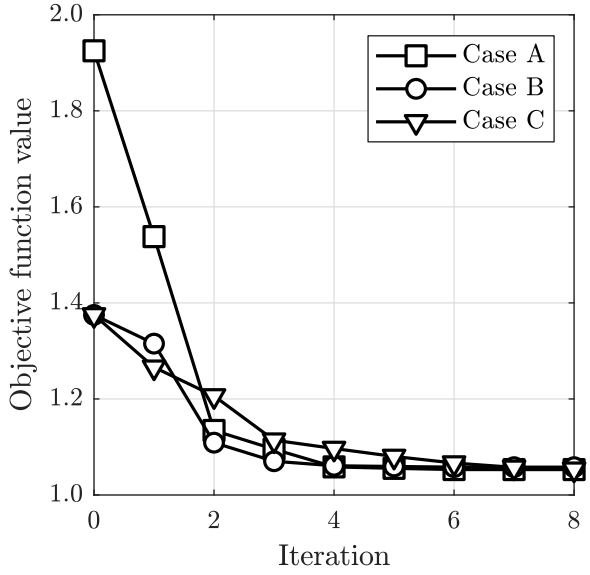

Fig. 5.6: Evolution of candidate objective function values for three different starting points. Scenario I.

Comparison with a finite difference implementation

As discussed in Section 5.4, the sensitivity assessment framework enabled by DIS provides first-order derivatives by post-processing the sampling results. In principle, an alternative means of computing such derivatives is to use finite differences and DIS. To compare the performance of both sensitivity assessment methods, they are integrated with the optimization strategy presented in Section 5.5.1 to solve the RBO problem in Eq. (5.20). Central differences are considered and, therefore, a total of five DIS estimates are required to evaluate the reliability constraint function and its gradient at each design. Validation calculations indicate that a total of $N = 2000$ samples are adequate for both sensitivity assessment techniques.

Table 5.2 summarizes the results obtained by both approaches in terms of the final design, number of optimization cycles (N_{cycles}), and total number of reliability analyses (N_{rel}). For conciseness, only case A is presented in the table. However, validation calculations indicate that similar results are obtained for alternative starting points. Several observations can be made from this table. First, both approaches provide very similar final designs in terms of the objective value. Second, the use of finite differences requires to define an appropriate perturbation step, whereas the framework

described in Section 5.4 circumvents this need. This is an advantage from the practical viewpoint. Third, the proposed approach needs only eight optimization cycles (see Fig. 5.6) whereas the implementation with finite differences requires 12 iterations. Fourth, the number of reliability analyses required by the finite difference implementation is significantly higher than by the proposed approach. In fact, the proposed approach requires 35 reliability analyses, which are associated with the full evaluation of approximately four designs per optimization cycle. Meanwhile, the finite difference implementation requires a total of 640 DIS runs, which is roughly equivalent to the full evaluation of 10 designs per optimization cycle. This behavior can be attributed to the higher variability of sensitivity estimates obtained with finite differences, which tends to reduce the performance of gradient-based optimization methods. For this case, not only such variability affects the choice of the feasible-descent direction in each optimization cycle, but is also detrimental to the convergence of the subsequent line search procedure. Finally, the previous observations indicate that the computational burden of the proposed approach is significantly lower than of using finite differences and, in addition, it provides additional advantages for practical implementation purposes.

Table 5.2: Optimization results obtained with the proposed approach and an implementation based on finite differences. Case A. Scenario I.

	Proposed approach	Finite differences
x_1^*	1.217	1.269
x_2^*	0.889	0.847
$P_F(\mathbf{x}^*)/10^{-3}$	0.999	0.998
$g(\mathbf{x}^*)$	-0.327	-0.422
$f(\mathbf{x}^*)$	1.0529	1.0580
N_{cycles}	8	12
N_{rel}	35	640

Sensitivity of the optimum design with respect to response thresholds

Optimum design sensitivity assessment studies how optimum solutions can change under model parameter perturbations. As described in Section 5.5.2, this is achieved by integrating a direction-

finding approach for optimum design sensitivity analysis with the general sensitivity assessment framework enabled by DIS. For illustration purposes and to show the type of results that can be obtained by the proposed scheme, the sensitivities of the optimum design with respect to the different response thresholds are considered here. Explicit formulas for the computation of these sensitivity measures can be found in Appendix 5.8. Note that, in this case, reliability sensitivity assessment involves negligible computational efforts.

To evaluate the quality of the estimates obtained by the adopted framework, Fig. 5.7 shows the evolution, in terms of the number of samples, of the DIS-based estimates of $\frac{\partial P_F}{\partial h_s^*}$, $s = 7, 9, 10, 11$, evaluated at the final design of case A (see Table 5.1). The rest of the sensitivities are almost zero. From the figure, it is noted that all derivatives are negative. In other words, the failure probability tends to decrease when the maximum allowable values for the different interstory drifts are increased. This is reasonable from an engineering perspective, since higher threshold values correspond to more permissive performance requirements and, as a result, failure becomes less likely in such cases. In addition, it is noted that the estimates become rather stable for $N \geq 2000$ samples. Thus, obtaining first-order derivatives of the failure probability with respect to the response thresholds as a byproduct of the reliability assessment step at the final design, which involves $N = 2000$ samples, is adequate in the context of this example.

Once the first-order derivative of the reliability constraint with respect to each threshold h_s^* is obtained, the approach presented in Section 5.5.2 is implemented to obtain the sought optimum design sensitivity measures. Table 5.3 reports the results corresponding to the final design obtained in case A. However, validation calculations show that similar results are obtained for all final solutions reported in Table 5.1. For presentation purposes, all quantities in the table are normalized by a factor that ensures that the maximum absolute value of the optimum objective sensitivities is equal to one. Several observations can be made from these results. First, the final design is only sensitive to the response thresholds corresponding to stories 7, 9, 10 and 11, which are associated with the non-zero sensitivities reported in Fig. 5.7. Hence, perturbations of the maximum allowable drift

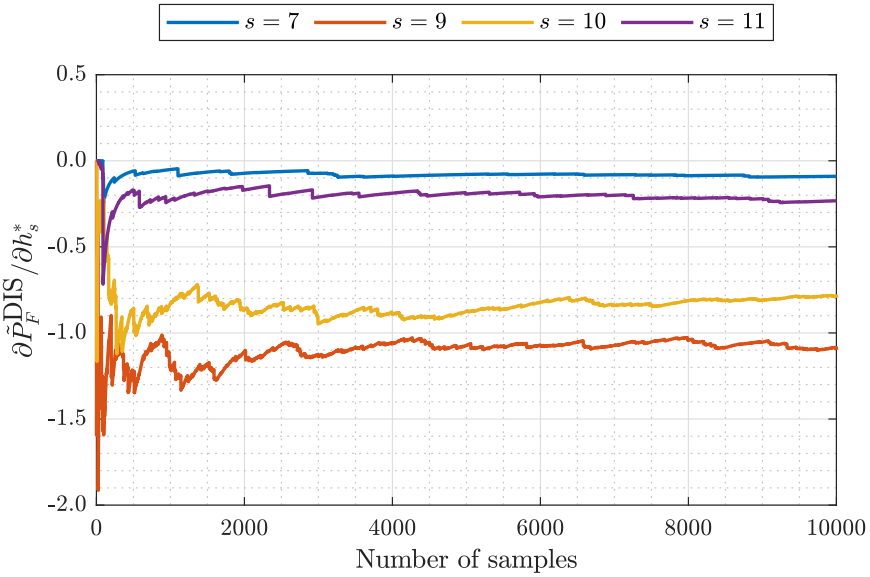

Fig. 5.7: Evolution of the estimator of the partial derivative of the failure probability with respect to different response thresholds (h_s^*) in terms of the number of samples. Scenario I.

values associated with lower and upper stories do not affect the optimum solution in this case. Second, all values presented in the table are negative, i.e., the greatest improvement in the optimum design is obtained by reducing the values of the design variables. Further, the solution of the direction-finding problem in Eq. (5.15) indicates that the results in the table correspond to increases of the different thresholds ($\delta h_s^* > 0$). Note that this behavior is reasonable from the engineering viewpoint since, as already pointed out, higher allowable values for the responses of interest lead to less restrictive design conditions. This highlights one of the advantages of the chosen method for optimum design sensitivity analysis, as it can identify the sign of the perturbation (increase or decrease) that is most beneficial toward improving the final solution. Third, the direction in which the optimum design tends to move is identical for all thresholds and is opposite to the objective function gradient. Fourth, the relative importance of the different parameters with respect to the final solution can be established from the optimum design sensitivity results. In this regard, Table 5.3 indicates that h_9^* and h_{10}^* are the most relevant parameters, h_7^* and h_{11}^* are less important, and the rest of thresholds do not affect the final design. Finally, the previous results illustrate that the implementation of DIS allows to obtain non-trivial information about final designs and their

sensitivities.

Table 5.3: Normalized sensitivities of the optimum objective value and of the optimum values for the design variables with respect to the maximum allowable interstory drifts. Scenario I.

Story (s)	df/dh_s^*	$\partial x_1^*/\partial h_s^*$	$\partial x_2^*/\partial h_s^*$
1–6	0	0	0
7	-0.12	-0.12	-0.12
8	0	0	0
9	-1.00	-1.00	-1.00
10	-0.91	-0.91	-0.91
11	-0.28	-0.28	-0.28
12–16	0	0	0

5.6.5 Scenario II: Design problem

In this scenario, a more complex optimization problem in terms of the number of design variables and the number of constraints is studied. In particular, a total of $n_x = 8$ intermediate design variables are considered. Each design variable is linked to the thickness of the core walls of two consecutive floors as $t_{w,2i-1} = t_{w,2i} = \bar{t}_w x_i$, $i = 1, \ldots, 8$ (see Table 5.4). In addition, seven geometric constraints and 16 reliability constraints are imposed. The resulting optimization problem is stated as

$$\begin{aligned} \min_{\mathbf{x}} \quad & f(\mathbf{x}) = \textstyle\sum_{i=1}^{8} x_i \Big/ 8 \\ \text{s.t.} \quad & r_j(\mathbf{x}) = \ln(P_{F_j}(\mathbf{x})) - \ln(5 \times 10^{-4}) \leq 0, \quad j = 1, \ldots, 16 \\ & g_j(\mathbf{x}) = x_{j+1} - x_j \leq 0, \qquad\qquad\qquad\quad j = 1, \ldots, 7 \\ & 0.5 \leq x_i \leq 2.0, \qquad\qquad\qquad\qquad\quad i = 1, \ldots, 8 \end{aligned} \tag{5.22}$$

where the constraints $g_j(\mathbf{x}) \leq 0$, $j = 1, \ldots, 7$, ensure that walls of lower floors are thicker than of upper floors, and $P_{F_j}(\mathbf{x})$, $j = 1, \ldots, 16$ are failure probability functions with maximum value $P_F^* = 5 \times 10^{-4}$. Note that this value is smaller than the one considered in the previous scenario. The failure events are defined in terms of the normalized interstory drifts as

$$F_j = \left\{ \max_{k=1,\ldots,1001} \left(\frac{|h_{j,x}(t_k, \mathbf{x}, \boldsymbol{\theta})|}{h_j^*}, \frac{|h_{j,y}(t_k, \mathbf{x}, \boldsymbol{\theta})|}{h_j^*} \right) > 1 \right\} \tag{5.23}$$

with $h_j^* = 0.1\%$, $j = 1, \ldots, 16$. Hence, the j^{th} failure probability function is associated with the drift responses, along the x and y directions, of the j^{th} story.

Table 5.4: Linking detail of intermediate design variables. Scenario II.

Design variable	x_1	x_2	x_3	x_4	x_5	x_6	x_7	x_8
Core walls (floors)	1–2	3–4	5–6	7–8	9–10	11–12	13–14	15–16

5.6.6 Scenario II: Results

Optimization results

The sequential optimization strategy presented in Section 5.5.1 is implemented, and a total of $N = 3000$ samples are considered for reliability assessment. To illustrate the effectiveness of the optimization scheme in terms of the starting point, three different initial designs are considered, which are presented in Table 5.5.

Table 5.5: Initial designs corresponding to different cases. Scenario II.

	x_1	x_2	x_3	x_4	x_5	x_6	x_7	x_8
Case A	1.98	1.97	1.96	1.95	1.94	1.93	1.92	1.91
Case B	1.75	1.74	1.73	1.72	1.50	1.49	1.48	1.47
Case C	1.60	1.50	1.40	1.30	1.20	1.10	1.05	1.00

Figure 5.8 shows the candidate objective values obtained throughout the optimization process for the different starting points. From the figure, it is seen that cases A, B and C require 11, 14 and 12 optimization cycles, respectively, to verify the stopping criterion. However, in all cases it is possible to obtain a design that is very similar to the final solution after roughly 10 optimization cycles. This behavior is consistent with the results observed in the previous scenario, since the method is able to reduce significantly the objective values after few optimization cycles. Moreover, the final objective function values obtained in the different cases are very similar between each other. Regarding computational cost, it is noted that each optimization cycle requires the full reliability assessment of a number of designs associated with the identification of the step size along the search direction

[356]. In this context, an average of three designs must be evaluated during each optimization cycle, leading to a total of less than 50 reliability analyses in all cases. This number is relatively small in the context of RBO problems. This highlights some of the benefits of adopting DIS as sensitivity assessment framework, since the use of gradient-based optimization strategies provides greatly improved designs with relatively few reliability analyses. Such a feature represents a significant advantage when compared, e.g., with stochastic search-based methods [111, 139].

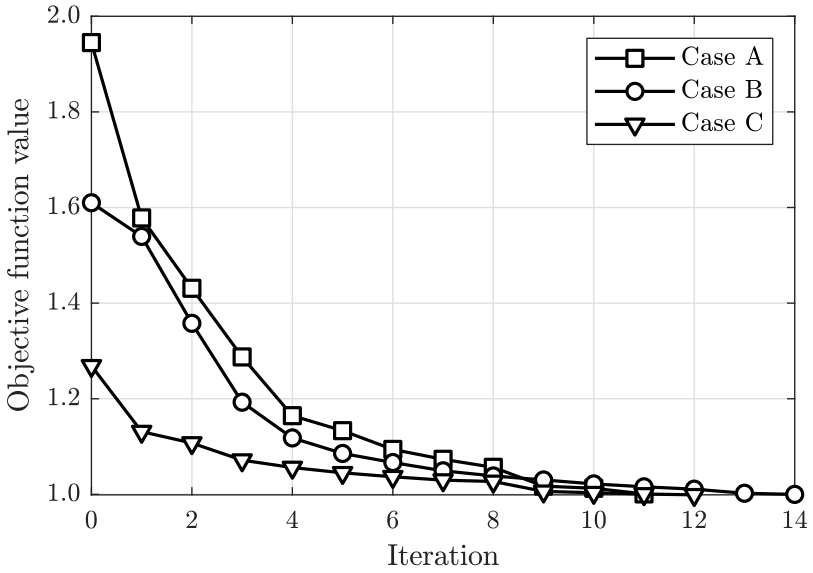

Fig. 5.8: Evolution of candidate objective function values for three different initial designs. Scenario II.

Table 5.6 shows the final designs obtained for the three starting points under consideration. In addition, Table 5.7 reports the corresponding values of the active constraint functions that are regarded as active at the final designs. These correspond to the normalized failure probabilities $P_{F_j}(\mathbf{x})/P_F^*$, $j = 9, 10, 11$, with $P_F^* = 5 \times 10^{-4}$, and $g_j(\mathbf{x})$, $j = 2, 3, 4, 7$. The results indicate that all final designs are quite similar from the objective and constraint viewpoints. In fact, the maximum relative difference between the optimum objective values is about 0.2%. Thus, the first-order method enabled by DIS allows an effective exploration of the design space for this scenario. To gain further insight into the optimization process, Fig. 5.9 presents the evolution of the values of the constraint functions that are active at the final solution for case A. It is seen that the method requires about nine optimization cycles to reach a boundary of the feasible design set where all constraints under

consideration are practically active. Such constraints tend to remain active during the rest of the optimization process. In other words, the search directions identified during the next iterations tend to follow such feasible boundary, which is consistent with the behavior observed in the previous scenario.

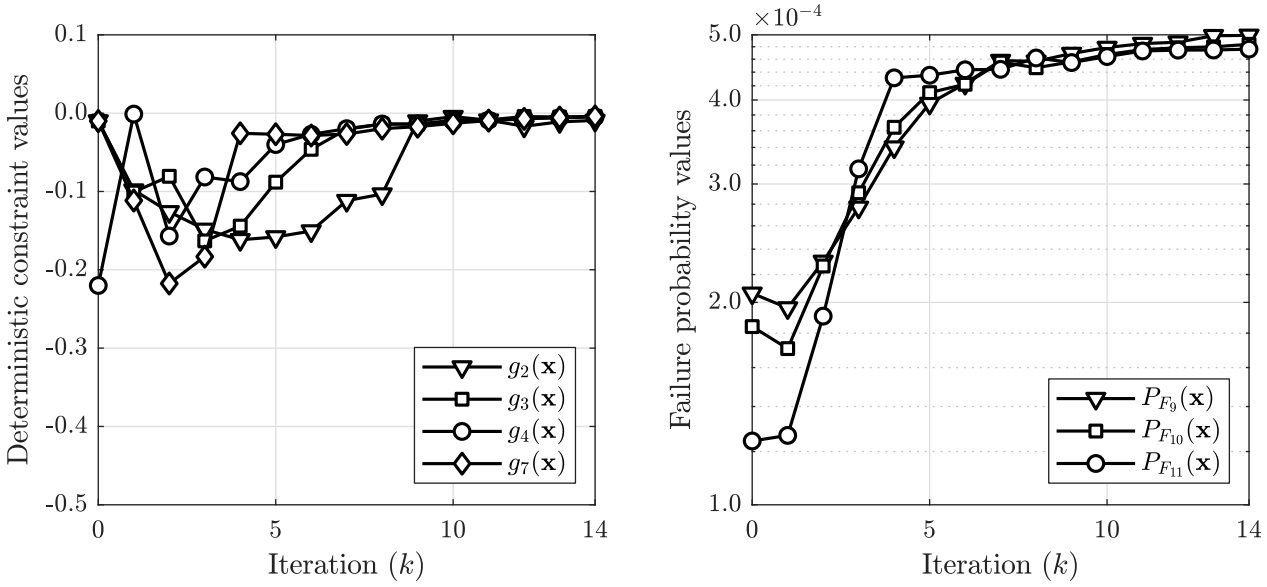

Fig. 5.9: Evolution of active geometric constraints (left) and active failure probability functions (right). Case A. Scenario II.

Table 5.6: Final designs corresponding to three different starting points. Scenario II.

	Case A	Case B	Case C
x_1^*	1.528	1.500	1.498
x_2^*	1.141	1.141	1.141
x_3^*	1.126	1.132	1.130
x_4^*	1.122	1.128	1.129
x_5^*	1.118	1.123	1.125
x_6^*	0.962	0.961	0.959
x_7^*	0.507	0.509	0.507
x_8^*	0.504	0.505	0.504
$f(\mathbf{x}^*)$	1.001	0.999	0.999

Optimum design sensitivity with respect to excitation model parameters

Once a final solution is identified, its sensitivity with respect to the parameters Ω_1 and Ω_2 involved in the definition of the excitation model (see Section 5.6.2) is investigated. The approach described

Table 5.7: Active constraint functions corresponding to three different starting points. Scenario II.

	Case A	Case B	Case C
$P_{F_9}(\mathbf{x}^*)/P_F^*$	0.994	0.998	0.995
$P_{F_{10}}(\mathbf{x}^*)/P_F^*$	0.968	0.968	0.968
$P_{F_{11}}(\mathbf{x}^*)/P_F^*$	0.953	0.952	0.961
$g_2(\mathbf{x}^*)$	-0.015	-0.009	-0.011
$g_3(\mathbf{x}^*)$	-0.004	-0.004	-0.001
$g_4(\mathbf{x}^*)$	-0.004	-0.005	-0.004
$g_7(\mathbf{x}^*)$	-0.003	-0.004	-0.003

in Section 5.5.2 is implemented, which requires the first-order derivatives of the active reliability constraint functions with respect to these parameters. As previously pointed out, such quantities can be computed by post-processing the DIS results. In this context, since Ω_1 and Ω_2 affect the properties of the excitation model, the only additional computations are associated with the sensitivities of the vectors involved in the representation of the stochastic load (see Appendix 5.8). Further, since the same excitation model is considered for all reliability constraints, this analysis needs to be performed once to evaluate the sensitivities of all active constraints. For conciseness, only the results corresponding to the final design of case A are presented here. However, additional calculations indicate that similar results are obtained for cases B and C.

For reference purposes, Figure 5.10 presents the evolution, in terms of the number of samples, of the estimates of $\frac{\partial P_{F_{10}}}{\partial \Omega_1}$ and $\frac{\partial P_{F_{10}}}{\partial \Omega_2}$ evaluated at the final design of Case A (see Table 5.6). Rather stable estimates are obtained for $N \geq 3000$, with $\frac{\partial P_{F_{10}}}{\partial \Omega_1} \approx -1.70 \times 10^{-2}$ and $\frac{\partial P_{F_{10}}}{\partial \Omega_2} \approx -0.03 \times 10^{-2}$. Thus, in this case $P_{F_{10}}(\mathbf{x})$ is much more sensitive to Ω_1 than to Ω_2. Moreover, increasing the values of Ω_1 or Ω_2 tends to decrease the likelihood of exceeding the maximum allowable threshold in the 10$^{\text{th}}$ story. Validation calculations indicate that a similar behavior is also observed for the failure probability functions $P_{F_9}(\mathbf{x})$ and $P_{F_{11}}(\mathbf{x})$, which are associated with the active reliability constraints.

Table 5.8 presents the optimum design sensitivity measures corresponding to perturbations in $\zeta = \Omega_1$ and $\zeta = \Omega_2$, i.e., the sensitivities of the optimum values for the design variable, $\frac{\partial x_i^*}{\partial \zeta}$, $i =$

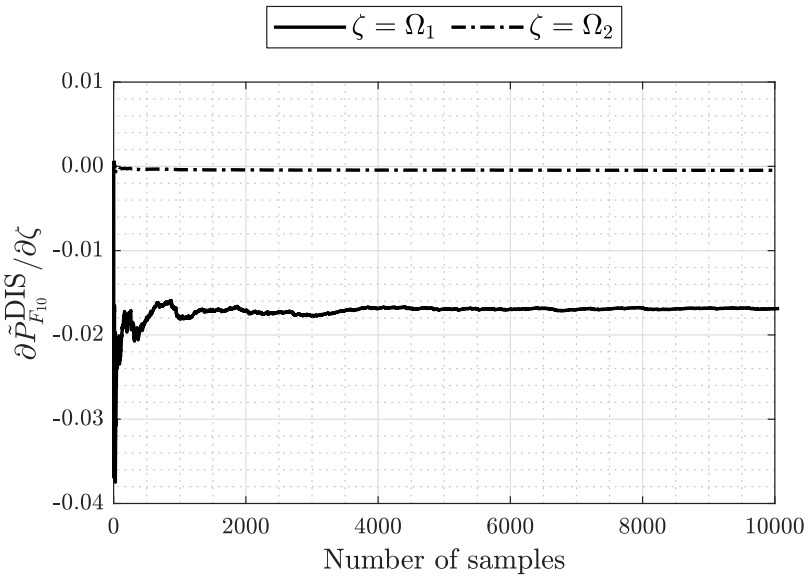

Fig. 5.10: Sensitivity estimates of $P_{F_{10}}$ with respect to Ω_1 and Ω_2 in terms of the number of samples. Scenario II.

$1, \ldots, 8$, and of the optimum objective value, $\frac{df^*}{d\zeta}$. For convenience, all these quantities have been normalized in such a way that the maximum magnitude of the sensitivities of the optimum objective values equals one. From the table, it is seen that the final solution is more sensitive to Ω_1 than to Ω_2, since $\left|\frac{df^*}{d\Omega_1}\right| > \left|\frac{df^*}{d\Omega_2}\right|$. Such behavior, in turn, can be associated with the higher sensitivity of the active reliability constraint functions with respect to this parameter (see Fig. 5.10). Furthermore, the previous results, which are obtained from the solution of Eq. (5.15), correspond to perturbations $\delta\Omega_1 > 0$ and $\delta\Omega_2 > 0$. In other words, improved designs can be obtained for larger values of the filter parameters Ω_1 or Ω_2. This agrees with the results presented in Fig. 5.10. Finally, regarding the rates of change of the optimum values for the design variables with respect to both excitation model parameters, all values in the table are negative. For small changes in Ω_1, the optimum design tends to move almost parallel to the steepest descent direction of the objective function. Meanwhile, a different behavior is observed for perturbations in Ω_2, where core wall thicknesses of upper floors are decreased to a greater extent than the rest. This can be related to the smaller influence of these structural properties on the responses involved in the definition of the active constraint functions, i.e., the drifts of stories 9 to 11.

Table 5.8: Normalized sensitivities of the optimum solution with respect to the excitation model parameters Ω_1 and Ω_2. Case A. Scenario II.

	$\zeta = \Omega_1$	$\zeta = \Omega_2$
$\partial x_1^*/\partial\zeta$	-0.999	-0.038
$\partial x_2^*/\partial\zeta$	-0.999	-0.042
$\partial x_3^*/\partial\zeta$	-1.000	-0.052
$\partial x_4^*/\partial\zeta$	-1.001	-0.052
$\partial x_5^*/\partial\zeta$	-1.001	-0.052
$\partial x_6^*/\partial\zeta$	-0.997	-0.022
$\partial x_7^*/\partial\zeta$	-1.001	-0.170
$\partial x_8^*/\partial\zeta$	-1.003	-0.188
$df^*/d\zeta$	-1.000	-0.077

Based on the previous discussion, it is seen that the optimum design sensitivity approach adopted in this contribution can provide non-trivial information about the effect of model parameter perturbations on final designs. As already pointed out, the required sensitivity measures can be computed as a byproduct of the optimization process by virtue of the reliability sensitivity analysis framework enabled by DIS. Thus, valuable insight for decision-making processes involving linear structural systems subject to Gaussian excitation can be obtained with reduced numerical costs. Overall, the results indicate that the use of DIS allows the implementation of potentially useful tools for a practical and real type of RBO problems.

5.7 Conclusions

This contribution implements Directional Importance Sampling (DIS) as a general reliability and sensitivity assessment framework for reliability-based optimization (RBO) and optimum design sensitivity analysis of linear structural systems under Gaussian excitation. First-order derivatives of the failure probability, with respect to design variables or general model parameters, can be obtained as a byproduct of the sampling process. This enables effective first-order solution methods for the two types of problems under consideration. On the one hand, a first-order sequential optimization strategy based on an efficient feasible-direction interior-point algorithm is adopted

to solve RBO problems. The scheme generates a sequence of feasible designs with improving objective values and, moreover, relatively few optimization cycles are required to obtain greatly improved designs. On the other hand, a direction-finding approach is considered for optimum design sensitivity analysis. In this setting, the rates of change of the optimum objective value and of the optimum values for the design variables with respect to model parameters are computed as a byproduct of the DIS results at the final design. Thus, valuable information on final designs and their sensitivities can be obtained with reduced numerical efforts.

An application example involving a 16-story reinforced concrete building structure subject to ground acceleration modeled as a non-stationary filtered white noise process is addressed to assess the performance of the proposed framework. Structural weight minimization subject to reliability and geometric constraints is studied. In particular, reliability requirements involving serviceability conditions for the interstory drifts are considered. Two alternative scenarios in terms of the number of design variables and reliability constraints are presented. In both cases, the optimization strategy enabled by DIS provides optimum designs in an effective manner. Additionally, significant improvements in the objective values are attained after the initial optimization cycles. Furthermore, numerical results also illustrate the advantages of the adopted framework with respect to a direct finite difference implementation, both in terms of numerical efforts and optimization results. These features are beneficial from a practical viewpoint and highlight the capabilities of DIS in the context of RBO problems. As a byproduct of the optimization results, the sensitivities of the optimum design with respect to response thresholds and excitation model parameters are evaluated. Non-trivial information on how final designs can change under small increases or decreases of model parameters is obtained and, in addition, their relative importance with respect to final solutions can be established. Overall, the results indicate that the general sensitivity analysis framework enabled by DIS provides potentially useful tools for decision-making processes involving linear structural systems subject to Gaussian excitation.

Future research efforts involve the assessment of the framework in more complex structural sys-

tems. In these cases, the computational cost of a single structural analysis can be significant and, therefore, parametric reduced-order model techniques can be integrated to reduce the numerical efforts. Another research direction corresponds to the evaluation of different RBO methods, in terms of efficiency and robustness, for the class of problems addressed in this contribution. Some of these topics are currently under consideration.

5.8 Appendix: Sensitivity of minimum demand-to-capacity ratio

5.8.1 Derivatives with respect to structural parameters

In case ν affects the properties of the structural model, the M^{th} impulse response function in Eq. (5.8) verifies $\eta_M(t) = \eta_M(t,\nu)$ and $\mathbf{a}_{M,K} = \mathbf{a}_{M,K}(\nu)$. Then, from Eq. (5.14) it is seen that

$$\frac{\partial c(\nu,\mathbf{u})}{\partial \nu} = -\frac{h_M^*}{(\mathbf{a}_{M,K}(\nu)^T\mathbf{u})\,|\mathbf{a}_{M,K}(\nu)^T\mathbf{u}|} \times \left(\left(\frac{\partial \mathbf{a}_{M,K}(\nu)}{\partial \nu}\right)^T \mathbf{u}\right) \tag{5.24}$$

with

$$\frac{\partial \mathbf{a}_{M,K}(\nu)}{\partial \nu} = \sum_{q=1}^{K} \varepsilon_q \Delta t \frac{\partial \eta_M(t_K - t_q,\nu)}{\partial \nu} \boldsymbol{\psi}_q \tag{5.25}$$

where $\frac{\partial \eta_M}{\partial \nu}$ can be obtained applying the chain rule due to the use of modal superposition. This requires the derivatives of the mode shapes and natural frequencies, which are computed using the method presented in [367].

5.8.2 Derivatives with respect to excitation model parameters

Assume that ν is involved in the definition of the stochastic excitation model. Hence, $\mathbf{a}_{M,K} = \mathbf{a}_{M,K}(\nu)$ and, therefore, Eq. (5.24) is also valid. However, in this case the first-order derivative of

the linear map $\mathbf{a}_{M,K}$ becomes

$$\frac{\partial \mathbf{a}_{M,K}(\nu)}{\partial \nu} = \sum_{q=1}^{K} \varepsilon_q \Delta t \eta_M (t_K - t_q) \frac{\partial \boldsymbol{\psi}_q(\nu)}{\partial \nu} \tag{5.26}$$

which requires, in turn, the first-order derivatives of the set of vectors $\boldsymbol{\Psi}(\nu) = [\boldsymbol{\psi}_1(\nu), \ldots, \boldsymbol{\psi}_{n_T}(\nu)]$ with respect to ν. From Section 5.2.2, such sensitivities can be computed as

$$\frac{\partial \boldsymbol{\Psi}(\nu)}{\partial \nu} = \frac{1}{2} \boldsymbol{\Lambda}(\nu)^{-1/2} \left[\frac{\partial \boldsymbol{\Lambda}(\nu)}{\partial \nu} \boldsymbol{\Xi}(\nu)^T + 2\boldsymbol{\lambda}(\nu) \frac{\partial \boldsymbol{\Xi}(\nu)}{\partial \nu}^T \right] \tag{5.27}$$

The derivatives of the eigenvalues $\boldsymbol{\Lambda}(\nu)$ and eigenvectors $\boldsymbol{\Xi}(\nu)$ of the covariance matrix of the stochastic load, $\boldsymbol{\Sigma}(\nu)$, can be computed using any suitable method; see, e.g., [147, 372].

5.8.3 Derivatives with respect to response thresholds

Assume that ν corresponds to the s^{th} response threshold, that is, $c(\nu, \mathbf{u}) = c(h_s^*, \mathbf{u})$. Hence, the derivative in Eq. (5.14) can be computed as

$$\frac{\partial c(h_s^*, \mathbf{u})}{\partial h_s^*} = \begin{cases} \dfrac{c_{M,K}(\mathbf{u})}{h_s^*}, & \text{if } s = M \\ 0, & \text{otherwise} \end{cases} \tag{5.28}$$

This means that the required derivative is non-zero only if the s^{th} failure response determines the closest failure boundary along the direction $\mathbf{u}$. Finally, it is noted that Eq. (5.28) involves a single arithmetic operation. Thus, marginal computational efforts are required to evaluate the first-order derivative of the failure probability in this case.

Acknowledgments

This research is partially supported by ANID (National Agency for Research and Development, Chile) under its program FONDECYT, grant numbers 1200087 and 1180271. Also, this research

has been partially supported by ANID and DAAD (German Academic Exchange Service, Germany) under CONICYT-PFCHA/Doctorado Acuerdo Bilateral DAAD Becas Chile/2018-62180007. These supports are gratefully acknowledged by the authors.

Chapter 6

Contaminant source identification in water distribution networks: A Bayesian framework

Contaminant source identification in water distribution networks: A Bayesian framework

D. J. Jerez[a], H. A. Jensen[b,*], M. Beer[a,c,d], M. Broggi[a]

[a]*Institute for Risk and Reliability, Leibniz Universität Hannover, Callinstr. 34, 30167 Hannover, Germany*

[b]*Department of Civil Engineering, Federico Santa Maria Technical University, Valparaiso, Chile*

[c]*International Joint Research Center for Engineering Reliability and Stochastic Mechanics, Tongji University, Shanghai 200092, China*

[d]*Institute for Risk and Uncertainty and School of Engineering, University of Liverpool, Liverpool L69 7ZF, United Kingdom*

Abstract: This work presents a Bayesian model updating approach for handling contaminant source characterization problems in the context of water distribution networks. The problem is formulated in a Bayesian model class selection framework where each model class represents a possible contaminant event. The parameters of each model class characterize the contaminant mass inflow over time in terms of its intensity and starting time. The class with the highest posterior probability is interpreted as the most plausible location for the contaminant injection. The evidences of the model classes are estimated using the transitional Markov chain Monte Carlo (TMCMC) method. The approach provides additional insight into the current network state in terms of posterior samples of the parameters that describe the contaminant event. The effectiveness of the proposed identification framework is illustrated by applying the contaminant source detection approach to a couple of water distribution systems.

Keywords: Bayesian model updating; Contaminant source identification; Model class selection; Water distribution systems.

*Corresponding author

E-mail addresses: danko.jerez@irz.uni-hannover.de (D. J. Jerez), hector.jensen@usm.cl (H. A. Jensen), beer@irz.uni-hannover.de (M. Beer), broggi@irz.uni-hannover.de (M. Broggi).

6.1 Introduction

Water distribution networks are constantly exposed to external events that can negatively affect their performance and the safety of the public. One important type of event is the intrusion, accidental or intentional, of contaminants into the system [4, 231]. The presence of an unwanted substance in the network can be very harmful to users and therefore the identification and characterization of any source of contamination is an important goal in water security [230, 373]. In this context, sensor measurements and available system knowledge must be properly taken into account. However, the use of monitoring data in order to identify and characterize the contamination event remains an open challenge in the security of water distribution systems. Relevant attributes of this type of events include the location of the contaminant source, magnitude of the mass inflow, injection starting time, duration, etc. Certainly, the source location is one of the most relevant features since it allows to take corrective actions in a timely manner. Thus, efforts must be directed towards the effective identification of the contaminant source based on available data from an array of sensors located in the network.

Traditionally, the identification of contaminant sources has been treated as a deterministic inverse problem [241, 242]. Direct optimization approaches, particle backtracking algorithm, data mining and machine learning techniques have been reported in this context [238–240, 243, 244, 374–376]. The main idea is to determine which contaminant outline can result in simulated sensor measurements that best match the real sensor measurements. One of the difficulties of this type of approaches is the non-uniqueness of the solution to the inverse problem. In fact, due to the nature of the problem, different network characterizations may lead to similar behavior at the measurement points. For instance, responses corresponding to a certain injection point with a given starting time and contamination intensity can be similar to the ones of an upstream point with a higher intensity and an earlier starting time.

Modeling and monitoring processes of water distribution networks involve unavoidable uncertain-

ties in hydraulic engineering practice [32, 377]. These uncertainties must be properly taken into account when dealing with identification problems in order to improve the overall security and reliability of these critical infrastructure systems [378]. In the context of contaminant source detection, such uncertainties may include sensor noise, nodal demands, modeling errors, attributes of contaminant events, prior knowledge associated with possible source scenarios, etc. To deal with these issues, Bayesian-type of approaches [23] have been also adopted for solving contaminant source characterization problems. The main idea of these approaches is to obtain revised probabilistic information that allows to decide the most plausible contamination source based on available data. Bayesian techniques, in the context of contaminant source detection problems, include the use of factor graph representation and belief propagation [247], beta-binomial conjugate framework coupled with deterministic backtracking algorithms [75], real-time approaches where the posterior information is updated as new measurements become available [248], backward probabilistic modeling [73], and Bayesian belief networks [249, 250]. These methodologies usually identify a region in the network with relatively high plausibility of containing the true sources, and some of them are limited to steady-state hydraulics. An additional type of Bayesian approaches correspond to sample-based model updating techniques [251–253]. In these contributions, injection location and time profile characteristics are simultaneously considered. Then, a set of posterior samples is obtained and the one that maximizes the posterior probability density function is chosen as the contaminant event. Due to the mixed discrete-continuous nature of the uncertain parameter space, this represents a serious computational challenge in realistic network models. In addition, numerical results reported by the previous contributions have usually identify a broad band of possible sources but they have not been able to single out the true source. Then, it is clear that more research and developments are needed in order to improve the precision, accuracy and efficiency of contaminant source characterization procedures.

In the previous context, this contribution proposes a simulation-based Bayesian model updating framework [24, 53, 54] to deal with contaminant source identification of water distribution systems. In particular, a model class selection problem is formulated where each model class is associated

with a potential source location. In this manner, the most probable source locations are selected taking into account all possible contaminant scenarios for any given injection point and therefore the mixed discrete-continuous nature of the identification parameter space can be circumvented. To solve the model class selection problem a multi-level Markov chain Monte Carlo algorithm, called the transitional Markov chain Monte Carlo (TMCMC) method, is adopted in this work [178]. The method is well-developed and it has been proved in a number of model updating and model class selection applications. Moreover, the approach has been successfully used in resolving some of the difficulties involved in the solution of inverse problems, that is, non-uniqueness, even in presence of limited amount of data and when modeling errors are present. Actually, the TMCMC algorithm can handle globally identifiable cases (set of most probable solutions is a singleton), locally identifiable cases (set of most probable solutions is finite), and unidentifiable cases (set of most probable solutions is uncountable) in an effective manner [178].

Thus, the efforts of this work are focused on the adaptation and implementation of the TMCMC technique into the area of contaminant source characterization with applications to water distribution networks. The approach provides a realistic representation of the uncertainties associated with the hydraulic modeling, water quality behavior, measured data and prior engineering information. The proposed approach is potentially a functional tool for identifying the location of the contaminant sources and estimating the attributes of the contaminant events. In fact, results of the proposed methodology indicate that the location of injection points is clearly identified for practical cases when relatively large model and measurement errors are considered. Thus, the proposed identification process is robust to model and measurement errors for the cases considered in this work. Moreover, the proposed methodology allows to obtain further insight into the contaminant injection profile, in addition to the identification of the contaminant event. This type of information can be useful to assist involved decision making processes in an emergency management framework. The methodology can be considered as an extension of the approach presented in [56] for leakage detection problems.

The organization of the paper is as follows. Section 6.2 presents the contaminant source identification problem in the framework of Bayesian model updating. The proposed approach is introduced in detail in Section 6.3. Section 6.4 discusses some aspects related to the numerical implementation of the proposed method. The effectiveness of the proposed contaminant source identification scheme is demonstrated in Section 6.5 by means of two example problems. The paper closes with some conclusions and final remarks.

6.2 Contaminant source identification

6.2.1 Background and hypotheses

The presence of unwanted substances in a water distribution network can be very harmful to users and, therefore, it is of the utmost importance to take promptly corrective actions. Once the existence of a contaminant event has been confirmed, it needs to be identified. The existence of contamination can be diagnosed by monitoring the changes in concentration over time at certain control points. Then, the basic idea is to update the hydraulic model in order to identify the location of the contaminant event. In other words, the predictions of the updated hydraulic model will match the measured data obtained from an array of sensors located in the network. Although optimal sensor placement is one of the important aspects of an effective contaminant warning system, this work focuses on source identification with the assumption that sensors are located in the network in a somewhat reasonable, sound, or optimal manner.

To simplify and clarify the demonstration of the proposed approach, the following assumptions are considered in this study. First, the array of sensors provides continuous concentration measurements over time rather than a binary signal indicating the presence or absence of the contaminant. Second, the contamination event is modeled as a constant mass flow entering the network at a single node, that is, the same amount of mass per time unit enters the network at a given node and from a certain time instant. In addition, it is assumed that the contaminant is conservative, i.e., it does not

decay as it propagates through the distribution system. Thus, for a given network, the attributes of a contaminant event are determined by three parameters: injection node, contaminant intensity (mass inflow at the injection point), and the starting time. It is noted that, however, multiple sources and alternative injection time profiles can also be considered in the proposed framework. The difference in these cases is that the number of parameters involved in the characterization of the contaminant events may increase. Finally, the analysis of the water distribution network is carried out using the well known hydraulic simulation program EPANET [379, 380]. In this setting, the hydraulic analysis is based on mass conservation equations at all nodes of the network, and energy conservation equations in all network links. On the other hand, the water quality analysis uses a Lagrangian time-based approach to track discrete parcels of water as they move along pipes and mix together at junctions between fixed-length time steps [379]. However, it is noted that different hydraulic simulation packages can be used as well.

6.2.2 Contaminant model classes

Based on the previous information, the contaminant source characterization requires three network parameters, i.e., the injection node N, the contaminant intensity I, and the starting time T. It is noted that N is a discrete quantity, whereas I and T can be regarded as continuous quantities. Thus, the contaminant source characterization problem presents a mixed discrete-continuous nature in terms of the parameters to be identified, that is, the attributes of a contaminant event. In this framework, it is assumed that N_c network nodes have been identified as potential contaminant injection points. The set $\mathbf{N} = \{1, 2, \ldots, N_c\}$ collects the possible injection nodes, that is, $N \in \mathbf{N}$. Clearly, the total number of potential contaminant events N_c is problem-dependent, and it depends on a number of factors such as the layout of the network and additional engineering information. In this regard, appropriate procedures such as particle backtracking algorithms can be used, in principle, to identify the potential contaminant injection points [381, 382]. Since a single contaminant source is assumed, the i^{th} node, $i = 1, 2, \ldots, N_c$, is associated with a class of network models, M_i, that comprises all its feasible contaminant injection profiles. This model class is defined by the

vector of parameters $\boldsymbol{\theta}_i \in \Theta_i \subset R^2$, with $\boldsymbol{\theta}_i = \{T_i, I_i\}$, where T_i represents the starting time of the contaminant event and I_i represents the mass inflow (contaminant intensity). It is noted that if multiple sources or alternative injection time profiles are considered, the only difference in terms of the present formulation is that the number of model classes or the dimension of the parameter space can increase, as previously pointed out. The parameters $\boldsymbol{\theta}_i$ constitute the set of unknowns that parametrize the model class M_i. That is, a particular network model $M_i(\boldsymbol{\theta}_i)$ from the class M_i is selected by specifying the values of the parameter set $\boldsymbol{\theta}_i$. In addition, the set of all model classes is defined in the set $\mathbf{M} = \{M_1, \ldots, M_{N_c}\}$.

It is noted that when multiple sources of contamination are considered, the injection nodes, contaminant intensities and the starting times constitute the set of attributes of the potential contaminant events. The total number of distinct contaminant events, or model classes, may be quite large in the general case, and therefore an exhaustive search for the most probable events could be computationally very expensive or even prohibitive. In this scenario, stochastic search algorithms [173, 174, 307, 383] can be used to effectively provide a near optimal solution for the injection nodes. In this context, it is important to note that in many practical situations the injection nodes are expected to occur only in a certain number of nodes of the network, and therefore the computational complexity of the problem can be significantly reduced. The consideration of multiple sources of contamination and the corresponding assessment of the proposed methodology is subject for future research (see Conclusions).

6.3 Proposed approach

For the purpose of identifying the location of the contamination event, a Bayesian system identification scheme is adopted in this work [115]. The approach is coupled with a hydraulic and water quality behavior simulator for model updating and model class selection of a parametrized class of hydraulic models. It can be regarded as an extension of the methodology introduced in [56, 57] for leakage and connectivity detection problems.

6.3.1 Model class selection

Monitoring data must be gathered and processed to identify the characteristics of the contamination event. The information about the network behavior is denoted by D and it consists of concentration measurements at a number of nodes. The data are used to update the plausibility of all possible injection nodes, i.e., model classes. The most plausible injection node is obtained by solving a Bayesian model class selection problem [178, 271]. To this end, consider the set $\mathbf{M} = \{M_1, M_2, \ldots, M_{N_c}\}$ of the N_c model classes previously defined. Given data D, the posterior probability of each model class, i.e., $P(M_i|\mathbf{M}, \boldsymbol{D}), i = 1, \ldots, N_c$ can be determined as

$$P(M_i|\mathbf{M}, \boldsymbol{D}) = \frac{P(\boldsymbol{D}|M_i)P(M_i|\mathbf{M})}{\sum_{l=1}^{N_c} P(\boldsymbol{D}|M_l)P(M_l|\mathbf{M})} \tag{6.1}$$

where $P(D|M_i)$ is the evidence of the model class M_i, which is a measure of the plausibility of obtaining the measurement data D from M_i. The optimal model class is selected as the one that maximizes $P(M_i|\mathbf{M}, \boldsymbol{D}), i = 1, \ldots, N_c$. Each model class has a prior probability $P(M_i|\mathbf{M}), i = 1, \ldots, N_c$, which measures the plausibility of contamination occurrence at each node before any information is included into the analysis. For the case where no prior information is available, the prior probabilities can be assumed to be equal, that is, $P(M_i|\mathbf{M}) = 1/N_c$. In this case, the selection among the model classes can be based solely on their evidence values.

A procedure to estimate the evidence for the different model classes, which involves a Bayesian model updating problem, is addressed in the following sections. For illustration purposes, a sketch of the proposed Bayesian model class selection approach is provided in Figure 6.1.

6.3.2 Model updating

In order to estimate the evidence of a model class, a Bayesian model updating problem is first considered. To this end, the plausibility of each model $M_i(\boldsymbol{\theta}_i)$, within a class M_i, based on concentration measurements D from the network, is quantified by the updated joint probability density

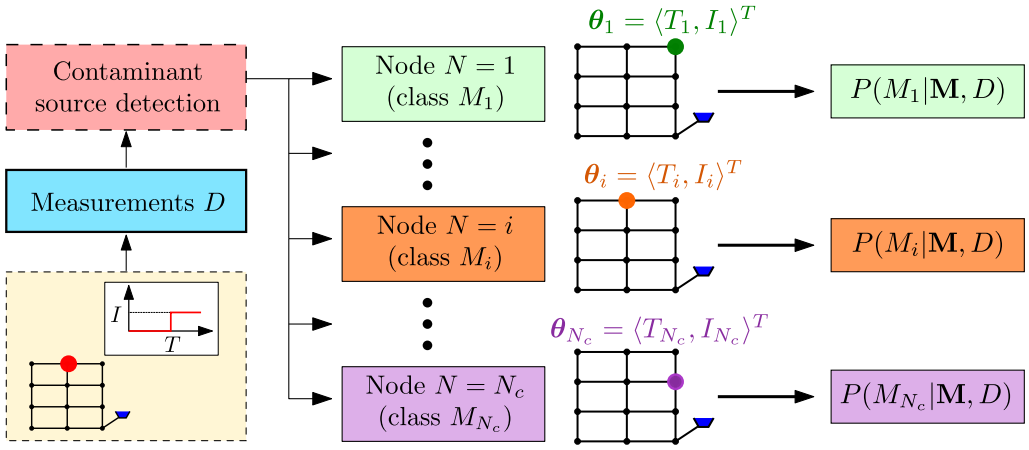

Fig. 6.1: Scheme of the proposed Bayesian model class selection approach.

function $p(\boldsymbol{\theta}_i|M_i, D)$ (posterior probability density function). According to Bayes' Theorem, the posterior probability density function of $\boldsymbol{\theta}_i$ is given by

$$p(\boldsymbol{\theta}_i|M_i, D) = \frac{p(D|M_i, \boldsymbol{\theta}_i)\ p(\boldsymbol{\theta}_i|M_i)}{P(D|M_i)} \tag{6.2}$$

where $p(D|M_i, \boldsymbol{\theta}_i)$ is the likelihood function, $p(\boldsymbol{\theta}_i|M_i)$ is the prior probability density function of $\boldsymbol{\theta}_i$, and $P(D|M_i)$ is the evidence of the model class M_i. The likelihood function expresses the plausibility of observing the data D given a certain $\boldsymbol{\theta}_i$, while the prior probability density function represents the prior or initial belief about the distribution of $\boldsymbol{\theta}_i$. Moreover, the evidence of the model class is written as

$$P(D|M_i) = \int_{\Theta_i} p(D|M_i, \boldsymbol{\theta}_i)\ p(\boldsymbol{\theta}_i|M_i) d\boldsymbol{\theta}_i \tag{6.3}$$

where all terms have been previously defined. In the present formulation, a method that estimates the evidence of the model class as a by-product of the solution to the Bayesian model updating problem is implemented. In particular, the transitional Markov chain Monte Carlo (TMCMC) method is adopted [178]. For completeness and clarity, the basic ideas of the TMCMC method are briefly reviewed in the following sections.

6.3.3 Parameter estimation

The TMCMC method iteratively proceeds from the prior to the posterior distribution of the parameter set $\boldsymbol{\theta}_i$. To this end, a number of non-normalized intermediate distributions $p_j(\boldsymbol{\theta}_i|M_i, \boldsymbol{D}), j = 0, \ldots, m$, are defined as

$$p_j(\boldsymbol{\theta}_i|M_i, \boldsymbol{D}) \propto \; p(\boldsymbol{D}|M_i, \boldsymbol{\theta}_i)^{\alpha_j} p(\boldsymbol{\theta}_i|M_i) \tag{6.4}$$

where the parameter α_j increases monotonically with j such that $\alpha_0 = 0$ and $\alpha_m = 1$. The parameter α_j is chosen in such a way that the change of the shape between two adjacent intermediate distributions be small. In this regard, different criteria can be used [178, 318, 319]. This small change of the shape makes it possible to efficiently obtain samples from $p_j(\boldsymbol{\theta}_i|M_i, \boldsymbol{D})$ based on the samples from the previous distribution. Once the parameter α_j has been computed, the samples at stage j are obtained by generating Markov chains where the lead samples are selected from the distribution $p_{j-1}(\boldsymbol{\theta}_i|M_i, \boldsymbol{D})$. Each sample of the current stage is generated by applying the Metropolis-Hastings algorithm [88, 89]. The lead sample of the Markov chain is a sample from the previous step, i.e., $\boldsymbol{\theta}^k_{i,j-1}, k = 1, \ldots, N_{j-1}$, that is selected according to a probability equal to its normalized weight $\bar{w}(\boldsymbol{\theta}^k_{i,j-1}) = w(\boldsymbol{\theta}^k_{i,j-1}) / \sum_{s=1}^{N_{j-1}} w(\boldsymbol{\theta}^s_{i,j-1})$, where N_{j-1} is the number of samples at the $j-1^{th}$ iteration step, and $w(\boldsymbol{\theta}^k_{i,j-1})$ represents the plausibility weight which is given by $w(\boldsymbol{\theta}^k_{i,j-1}) = p(\boldsymbol{D}|M_i, \boldsymbol{\theta}^k_{i,j-1})^{\alpha_j - \alpha_{j-1}}$.

The proposal probability density function for the Metropolis-Hastings algorithm is chosen as a Gaussian distribution centered at the lead sample of the chain and with a covariance matrix equal to a scaled version of the estimate covariance matrix of the current intermediate distribution, that is, $p_{j-1}(\boldsymbol{\theta}_i|M_i, \boldsymbol{D})$. Then, $\boldsymbol{\Sigma}_{i,j-1} = \beta^2 \sum_{s=1}^{N_{j-1}} \bar{w}(\boldsymbol{\theta}^s_{i,j-1}) \left(\boldsymbol{\theta}^s_{i,j-1} - \bar{\boldsymbol{\theta}}_{i,j-1}\right) \left(\boldsymbol{\theta}^s_{i,j-1} - \bar{\boldsymbol{\theta}}_{i,j-1}\right)^T$, where $\bar{\boldsymbol{\theta}}_{i,j-1} = \sum_{s=1}^{N_{j-1}} \bar{w}(\boldsymbol{\theta}^s_{i,j-1}) \boldsymbol{\theta}^s_{i,j-1}$ and β^2 is a parameter that can be chosen according to different criteria. For example, it can be defined directly by the user or by an adaptive scheme based on the acceptance rate of the sampling process [179, 288]. The procedure is repeated until the parameter α_j is equal to 1 ($j = m$). At the last stage, the samples $\boldsymbol{\theta}^k_{i,m}, k = 1, \ldots, N_m$, are asymptotically distributed as $p(\boldsymbol{\theta}_i|M_i, \boldsymbol{D})$.

6.3.4 Evidence estimation

The estimation of the evidences associated with the different model classes is known to be highly nontrivial. In this regard, the TMCMC method provides a flexible and efficient means to estimate the evidences even in challenging cases such as those involving multi-modal, peaked or flat posterior distributions. In fact, the TMCMC method can estimate the evidences as a by-product and they are given in terms of the mean values of the weights at the different stages, $W_{i,j} = \sum_{k=1}^{N_j} w(\boldsymbol{\theta}_{i,j}^k) \Big/ N_j$, as

$$W_i = \prod_{j=0}^{m-1} W_{i,j} \tag{6.5}$$

where W_i is an asymptotically unbiased estimator of the evidence $P(\boldsymbol{D}|\boldsymbol{M}_i)$ [178]. Note that if only the evidences are required, the process can be stopped at stage $j = m - 1$. The reader is referred to [178, 179] for a detailed description of the TMCMC method. A pseudo-code that illustrates the implementation of the TMCMC method is provided in the Appendix (Section 6.7).

6.4 Implementation aspects

6.4.1 Contaminant data

The likelihood function, $p(\boldsymbol{D}|\boldsymbol{M}_i, \boldsymbol{\theta}_i)$, which measures how plausible is to obtain measurements D from each model $M_i(\boldsymbol{\theta}_i)$ is defined as follows. In the context of the present formulation, it is assumed that the data D are obtained from n_S sensors at n_T time instants. Then, the concentration measurements are contained in a vector $\mathbf{y} \in R^{n_S \times n_T}$ where $\mathbf{y} = \langle {\mathbf{y}_1}^T, \ldots, {\mathbf{y}_{n_S}}^T \rangle^T$, in which $\mathbf{y}_j \in R^{n_T}, j = 1, \ldots, n_S$ is a vector comprising the measurements at the j^{th} sensor and given by $\mathbf{y}_j = \langle y_j(t_1), \ldots, y_j(t_{n_T}) \rangle^T$, where $y_j(t_k)$ represents the concentration level at the j^{th} sensor location at time instant $t_k, k = 1, \ldots, n_T$. Formally, the prediction errors from the model $\boldsymbol{M}_i(\boldsymbol{\theta}_i)$ are written as $e_{jk}(\boldsymbol{\theta}_i) = y_j(t_k) - y_j(t_k, \boldsymbol{\theta}_i)$, $j = 1, \ldots, n_S$, $k = 1, \ldots, n_T$, where $y_j(t_k, \boldsymbol{\theta}_i)$ indicates the concentration level at the j^{th} sensor location at time instant t_k computed from the model class $\boldsymbol{M}_i$,

corresponding to a particular value assigned to the parameter set $\boldsymbol{\theta}_i$. The prediction errors may be due to hydraulic and water quality behavior network modeling and device measurement accuracy that are unavoidable in the modeling and monitoring processes of real water distribution systems, and they are modeled as normally distributed with zero mean and covariance matrix $\mathbf{C}$. Based on the previous conditions, the likelihood function $p(D|M_i, \boldsymbol{\theta}_i)$ is written as [53, 54, 287]

$$p(D|M_i, \boldsymbol{\theta}_i) \quad \propto \quad |\mathbf{C}|^{-1/2} \exp\left[-\frac{1}{2} L(\boldsymbol{\theta}_i, \mathbf{y})\right] \tag{6.6}$$

where $\propto$ indicates proportional, $|\cdot|$ denotes determinant, and $L(\boldsymbol{\theta}_i, \mathbf{y})$ is a weighted measure of fit between the model predictions and the measured data given by

$$L(\boldsymbol{\theta}_i, \mathbf{y}) = [\mathbf{y} - \mathbf{y}(\boldsymbol{\theta}_i)]^T \mathbf{C}^{-1} [\mathbf{y} - \mathbf{y}(\boldsymbol{\theta}_i)] \tag{6.7}$$

where $\mathbf{y}(\boldsymbol{\theta}_i)$ represents the corresponding vector of measurements computed from the model class $M_i(\boldsymbol{\theta}_i)$. For simplicity, the prediction errors are assumed to be independent and, therefore, the covariance matrix $\mathbf{C}$ is a diagonal matrix comprising the prediction error variances. It is noted that, however, different prediction error model classes can be used as well, including models that consider correlation [55, 384]. Finally, it is noted that, in the framework of model updating, parameters associated with the characterization of the covariance matrix can also be included in the parameter set $\boldsymbol{\theta}_i$.

6.4.2 Hydraulic and water quality simulation model

The widely used software EPANET 2.2 is employed in this work for analysis purposes [379, 380]. In other words, measurements computed from the model classes, in the framework of the TMCMC method, are generated by this algorithm. The software allows performing extended period simulation of hydraulic and water quality behavior of water distribution networks. Hydraulic analysis is based on mass conservation equations at all nodes of the network (pipe connection points, tanks

and reservoirs), and energy conservation equations in all network links (pipes, pumps and valves). These two types of relationships lead to a system of nonlinear equations that is solved using a type of Newton iteration scheme. On the other hand, water quality analysis, which simulates the concentration over time of different substances in all network components, uses a Lagrangian time-based approach to track discrete parcels of water as they move along pipes and mix together at junctions between fixed-length time steps [379]. Water quality analysis uses information gathered from a previous hydraulic simulation of the network in order to propagate the substance across the network. Hence, water quality results do not affect the hydraulic behavior of the system under analysis. Validation calculations have shown the efficiency and flexibility of this simulation model in a large number of water distribution networks.

6.4.3 Computational efficiency

The proposed approach presents several advantages for implementation in a high-performance computing (HPC) environment. In fact, all model classes are perfectly independent from each other. Thus, the estimation of the evidences of the different model classes is perfectly parallel and the analyses can be carried out simultaneously taking advantage of available parallelization techniques. Moreover, the first stage of the TMCMC method corresponds to direct Monte Carlo simulation and, therefore, it can be completely scheduled in parallel. In addition, subsequent stages involve the generation of a number of Markov chains that are perfectly parallel. Hence, the corresponding sampling process can also be scheduled in a parallel setting. The load balance in the computer workers can be based on a static or dynamic job-scheduling scheme [320]. Clearly, if a high-performance computing environment is not available, the evidences for each potential contaminant event need to be estimated in a sequential manner. Although such estimation may be computationally expensive and could represent a possible limitation of the methodology, in many practical situations the injection nodes are expected to occur only in a certain number of nodes of the network. For instance, available pre-screening techniques [381, 382] as well as engineering knowledge about the network can be used to rule out unfeasible nodes before the identification

process is carried out. In addition, surrogate models can be integrated, in principle, to reduce the computational efforts associated with the evaluation of the likelihood function [287, 288]. Thus, the computational complexity of the problem can be significantly reduced, even for the case when a HPC environment is not accessible. The implementation and evaluation of the previous techniques within the proposed approach represent a future research effort.

6.5 Numerical examples

6.5.1 Simplified network model

The objective of this example is to study in detail some of the capabilities of the proposed contaminant source identification scheme. In particular, the effect of increasing the amount of available data and the effect of model and measurement uncertainties on the performance of the approach are explored. To this end, two cases are analysed in terms of the uncertainty included in the identification process. Case A considers uncertainty in the hydraulic model properties, whereas case B considers both, modeling and measurement errors. In addition, two scenarios in terms of the amount of measurements are studied in each case.

Network description

A simple network subject to a contamination event is considered in the test problem. The network is shown in Figure 6.2 and comprises 17 nodes, 21 pipes and a single reservoir. The distances between the nodes are also indicated in the figure. All nodes are located at the same level, whereas the reservoir has a relative height of 15 m. The water enters to the distribution system through node 1. The head-losses in pipes are modeled using the Darcy-Weisbach equation. All pipes are of diameter 110 mm, with roughness coefficient $\varepsilon = 0.0046$ mm. The nodes have a maximum demand of 0.5 l/s and follow a typical demand pattern which is shown in Figure 6.3. An extended period of 36 hours is shown in the figure.

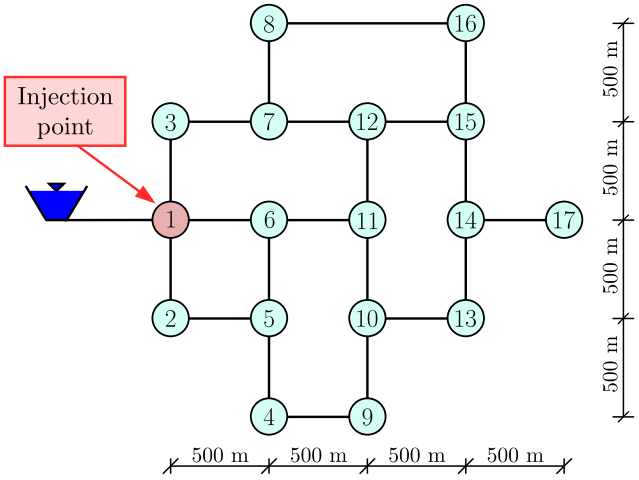

Fig. 6.2: Water distribution network. Test problem.

For illustration purposes, it is assumed that the injection point is node 1, as indicated in Figure 6.2. The substance can propagate to all network nodes and a periodic behavior of the contaminant concentration response can be eventually reached at every point of the network. The injection of the substance starts two hours after the beginning of the simulation period. A constant intensity of 100 mg/min is considered. The hydraulic and water quality time step, in the context of EPANET, is 5 min.

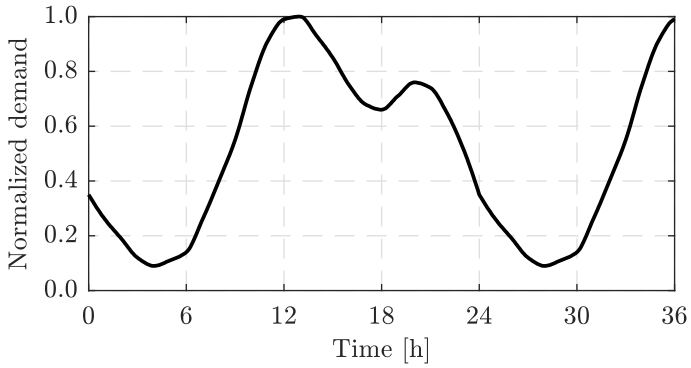

Fig. 6.3: Normalized demand pattern.

Synthetic measurements

The performance of the proposed identification process is evaluated considering synthetic measurements. The data considered for identification purposes are concentration levels over time obtained

at nodes 10 and 17, whose location is shown in Figure 6.4. The corresponding time history of the contaminant injection is also shown in the figure. As previously mentioned, continue-valued sensors are considered for the identification process. Measurement and modeling errors are accounted explicitly in the analysis in order to consider a realistic setting [56, 57, 245]. In order to include measurement noise in the sensors, an error term is added to the predictions of the actual network. Simulated data are generated as

$$y_j(t_k) = y_j^{\text{actual}}(t_k) + y_j^{\text{noise}}(t_k) \ , \ j = 1, \ldots, n_S \ , \ k = 1, \ldots, n_T \tag{6.8}$$

where $y_j^{\text{actual}}(t_k)$ represents the concentration level in the actual system and $y_j^{\text{noise}}(t_k)$ accounts for the measurement error. The quantities $y_j^{\text{actual}}(t_k)$ are obtained from an EPANET model that is representative of the actual system and it is referred to as the actual network. This model has hydraulic properties that deviate from the ones considered for identification purposes. The particular characteristics that are perturbed from their nominal values are the pipe roughness coefficients and peak nodal demands. The roughness coefficient of the l^{th} pipe at the actual network is given by $\varepsilon_l^{\text{actual}} = \varepsilon_l^{\text{nominal}}(1+\alpha u_l)$, where $\varepsilon_l^{\text{nominal}}$ is the roughness coefficient of the l^{th} pipe in the model class used for identification, u_l is a random number uniformly distributed over $[-1, 1]$ and $\alpha \in [0, 1]$ represents the intensity of the uncertainty expressed as a percentage of the nominal value. Similarly, the peak demand of the l^{th} node is written as $\delta_l^{\text{actual}} = \delta_l^{\text{nominal}}(1 + \beta u_l)$, where $\delta_l^{\text{nominal}}$ is the peak demand of the l^{th} node in the model class used for identification, u_l is a random number uniformly distributed over $[-1, 1]$ and $\beta \in [0, 1]$ represents the intensity of the uncertainty expressed as a percentage of the nominal value. Thus, it is clear that the model classes used for identification are not capable to represent the behavior of the actual network exactly.

Moreover, the measurement error $y_j^{\text{noise}}(t_k)$ is generated as $y_j^{\text{noise}}(t_k) = y_j^{\text{actual}}(t_k) \ \gamma \ u_{j,k}$, where $u_{j,k}$ is a random number uniformly distributed over $[-1, 1]$ and $\gamma \in [0, 1]$ represents the measurement noise intensity expressed as a percentage of the response obtained from the actual network.

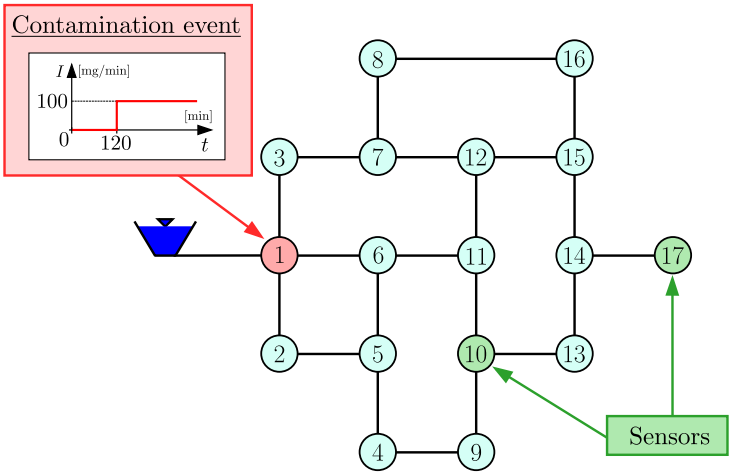

Fig. 6.4: Location of sensors in the network.

Definition of probabilistic model classes

The set of probabilistic model classes comprises all feasible contaminant source locations based on prior engineering information. All network nodes are considered as potential injection points with the same plausibility. Thus, the posterior probability of $N_c = 17$ model classes must be evaluated. As previously pointed out, appropriate techniques such as particle backtracking algorithms can be used, in principle, to reduce the number of potential contaminant injection points [381, 382]. As discussed in Section 6.2, each model class involves a constant mass flow into a given node starting at a given time instant. Hence, the i^{th} model class, M_i, is parametrized by $\boldsymbol{\theta}_i = \langle T_i, I_i \rangle^T$, where T_i is the injection's starting time and I_i is the contaminant intensity. A uniform prior distribution for the uncertain parameters $\boldsymbol{\theta}_i$ is considered for each model class. They are defined in the intervals $T_i \in [0, 540]$ min, and $I_i \in [0, 1000]$ mg/min. The upper bound for the starting time is associated with the first arrival of the contaminant to the sensors.

In this regard, Figure 6.5 shows the measurements obtained at the sensors when no errors are considered in the analysis, that is, $\alpha = \beta = \gamma = 0$ (idealized network). It can be observed that the contaminant arrives at node 10 about seven hours after the injection starts. On the other hand, the contaminant arrives at node 17 about ten hours after the start of the injection. Then, it is observed that the source start time can be anytime from 9 hours before the time of first detection up to the

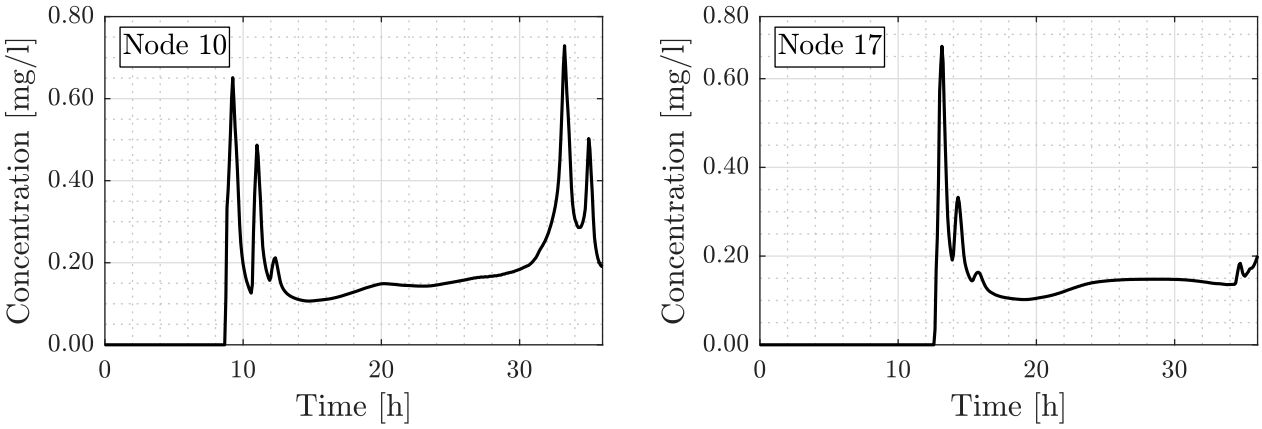

Fig. 6.5: Measurements of nodal concentration over time. Idealized network.

time of detection. Similar arrival times are obtained when model and measurement uncertainties are considered. Based on the previous information, the upper bound of the starting time is set equal to 540 min (9 hours). For reference purposes, recall that the actual contaminant source location is node 1, with starting time $T_1 = 120$ min, and intensity $I_1 = 100$ mg/min. In terms of the TMCMC method, 100 samples per stage are considered in its implementation.

Results of Case A: Hydraulic model uncertainty

Model errors are imposed by perturbing the values of all pipe roughness coefficients and peak nodal demands, as previously pointed out. For illustration purposes, relatively large perturbations are introduced simultaneously for the pipe roughness coefficients and peak nodal demands. In particular, $\alpha = \beta = 10\%$. In terms of the proposed framework, it is assumed that all probabilistic model classes present the same prior probability, since there is no particular preference to any possible injection node based on previous information. Then, the model class selection problem can be addressed considering only the evidence values. In addition, two scenarios are considered regarding the data-set size used in the analysis. The first scenario considers measurements up to the time of first detection of the contaminant (5 min after the first detection), while the second scenario contemplates measurements up to 60 min after the first arrival of the contaminant to any sensor (about 10 hours).

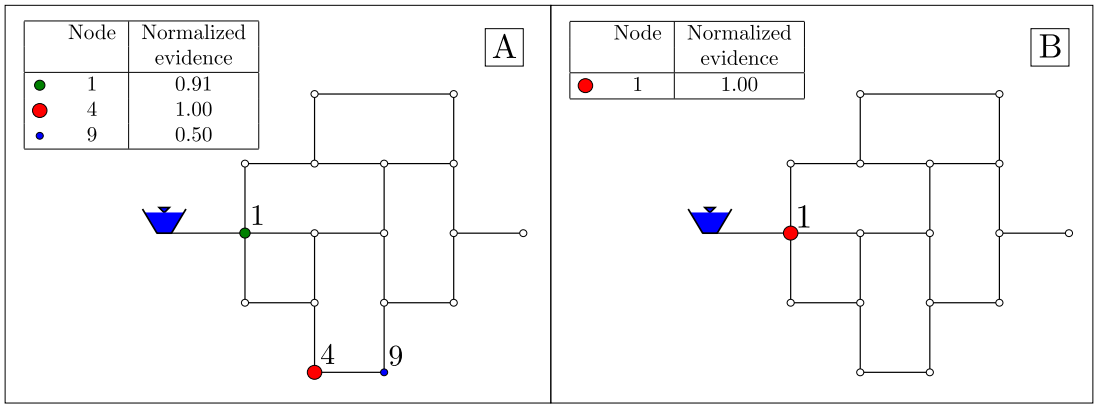

Fig. 6.6: Normalized evidences of all model classes. A) Scenario 1. B) Scenario 2. Hydraulic model uncertainty.

Figure 6.6 shows the normalized evidences of the model classes associated with the different injection nodes obtained for both scenarios. The normalized evidences are such that their maximum value is equal to one. It is observed that the injection node is correctly identified in the second scenario (Figure 6.6-B), where the normalized evidence of model class 1, which considers node 1 as the injection point, is equal to one, and the evidences of the other model classes are almost equal to zero. However, the actual injection node is not identified correctly in the first scenario (Figure 6.6-A). In fact, the most probable contaminant event identified corresponds to injection node 4. Additionally, contaminant injection in nodes 1 and 9 also leads to model classes with evidences different to zero. It is noted that nodes 1, 4 and 9 are upstream from node 10, which is consistent from the physical point of view. Thus, although the actual injection node is not identified correctly, the results still provide important information about the network behavior. When more data are available, the contaminant event is properly determined as indicated from the results associated with Scenario 2, where the location of the injection point is clearly identified even when relatively large model errors are included in the model that generates the data.

To obtain further insight into the contaminant source identification process, Figure 6.7 shows the corresponding identification process when using model class M_1, that is, the most probable model class. This figure shows how the samples in the $T_1 - I_1$ space converge for the actual contaminant event during the different TMCMC stages when the second scenario is considered. Note that both,

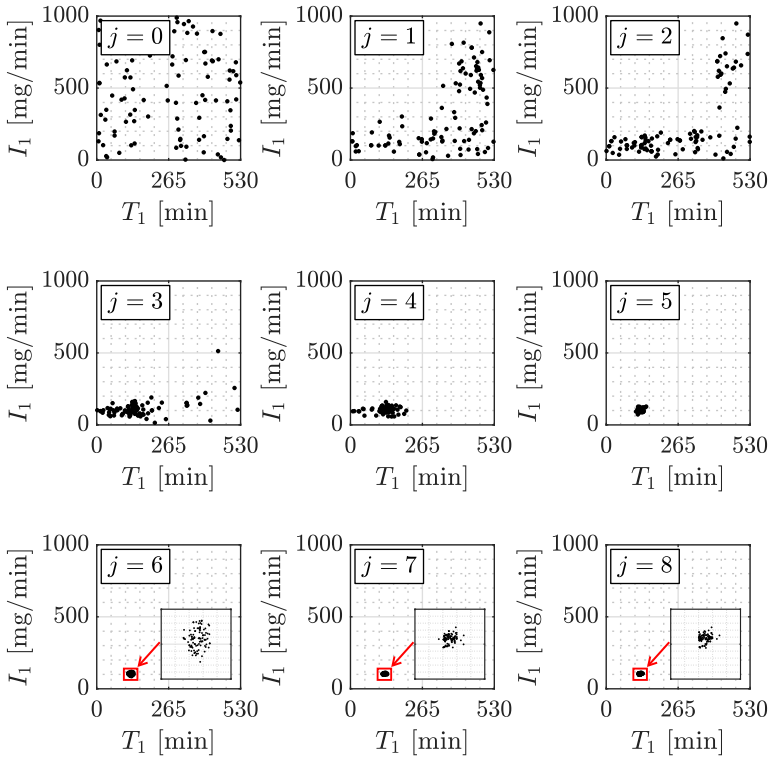

Fig. 6.7: Plot of samples in the $T_1 - I_1$ space generated at different steps of the transitional Markov chain Monte Carlo method when updating model class M_1. Hydraulic model uncertainties.

the contaminant intensity and the starting time are correctly identified. The starting time ranges from 120 to 135 min, whereas the contaminant intensity values range from 97.3 to 112.0 mg/min. The posterior mean estimate of the model parameters is $\boldsymbol{\theta}_1 = \langle T_1, I_1 \rangle^T = \langle 124.9, 104.1 \rangle^T$. From the different steps of the identification process, it is clear that the prior uncertainty of the contaminant intensity value and the starting time is significantly reduced due to the available data.

Results of Case B: Hydraulic model and measurement errors

To consider a more practical and realistic situation, it is assumed that model and measurement errors are present in the analysis. To this end, the perturbation levels for the pipe roughness coefficients, peak nodal demands, and measurement noise intensities are taken equal to $\alpha = \beta = \gamma = 10\%$. Figure 6.8 shows the normalized evidences obtained for scenarios 1 and 2. Under this case, the actual contaminant event is not correctly identified in the first scenario (Figure 6.8-A), but the most probable injection points are located across the flow paths from the actual injection location (node

1) to the sensor recording non-zero concentrations (node 10), as in Case A where only model uncertainties are considered. Thus, although the correct node is not identified, the proposed approach still provides relevant information about the current state of the network.

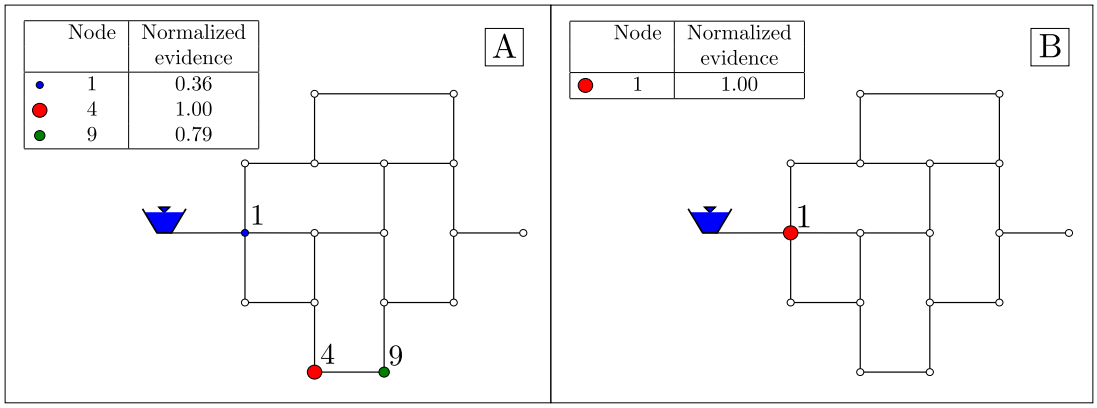

Fig. 6.8: Normalized evidences of all model classes. A) Scenario 1. B) Scenario 2. Hydraulic model and measurement errors.

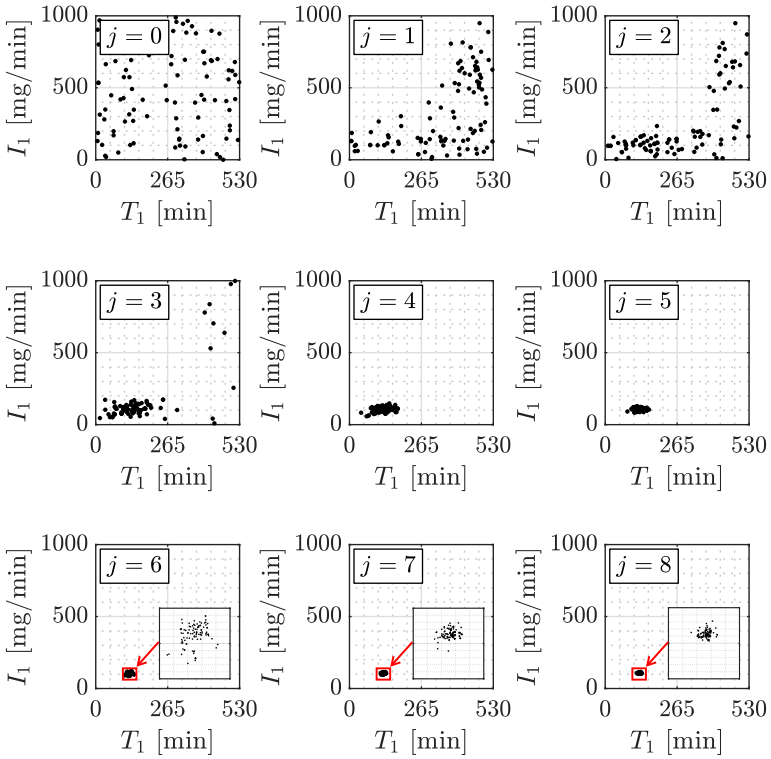

Fig. 6.9: Plot of samples in the $T_1 - I_1$ space generated at different steps of the transitional Markov chain Monte Carlo method when updating model class M_1. Hydraulic model and measurement errors.

If more information is available, i.e., Scenario 2 (Figure 6.8-B), the injection node is properly de-

termined. In fact, among all model classes, the proposed identification scheme clearly favors model class M_1. Thus, it is clear that increasing the amount of available data is highly beneficial towards the identification process, which is reasonable from the practical point of view. The corresponding identification process when using model class M_1 is shown in Figure 6.10. This figure shows the evolution of samples in the $T_1 - I_1$ space during the different TMCMC stages. At the final stage of the identification process, the starting time ranges from 116 to 134 min, whereas the contaminant intensity values range from 101.6 to 115.5 mg/min. The posterior mean estimate of the model parameters is $\boldsymbol{\theta}_1 = \langle T_1, I_1 \rangle^T = \langle 126.4, 106.6 \rangle^T$. Then, the samples of the model parameters $\boldsymbol{\theta}_1$ are distributed around the actual value, as for the case where only model uncertainties are considered. Note that the model parameters (contaminant intensity and starting time) are globally identifiable since the set of posterior samples (most probable model parameters) populates a vicinity of the target values. Based on the previous results, it is concluded that the identification of the contaminant event is quite robust to model and measurement errors for this particular network.

6.5.2 Application problem

The objective of this example is to evaluate the capabilities of the proposed approach in a more realistic network model. Two different events are considered in terms of the location of the contaminant source. For each event, two different scenarios in terms of the amount of measurements are contemplated. In all cases, modeling and measurement uncertainties are included in the data generation process.

Description of the network

The water distribution network considered as an application problem corresponds to Example Network 3 provided as a tutorial in EPANET 2.2 [379]. This system has been studied in the context of contaminant source detection by other researchers in previous contributions [75, 177, 248, 251, 252]. It consists of 92 nodes, 117 pipes, two reservoirs, three fully-mixed tanks and two pumps. The layout of the network and some of its elements are shown in Figure 6.10. Transient flows are

developed in the pipeline system due to the varying operational conditions, demand requirements, and the filling and draining of the storage tanks during the network operation. In this context, most nodes follow the normalized demand pattern shown in Figure 6.11 during the analysis period. In addition, a total of 65.75 km of pipelines are allocated to distribute water to the different nodes. The pipe distributions in terms of Hazen-Williams coefficients and diameters are shown in Tables 6.1 and 6.2, respectively. A simulation period of 24 h is considered for analysis purposes. The corresponding hydraulic simulation step and water quality step are equal to 5 min.

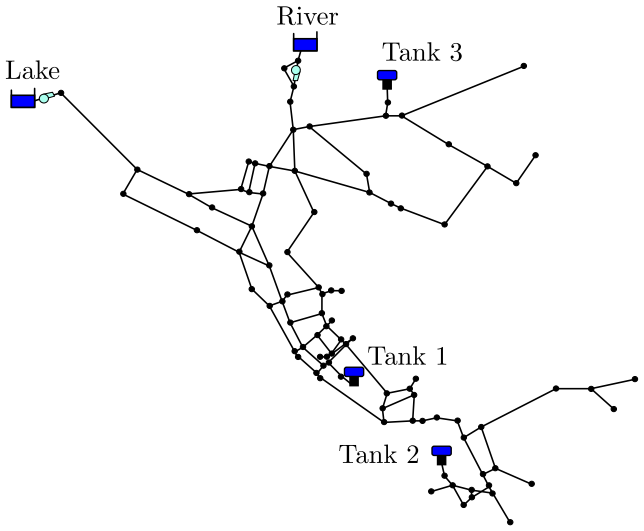

Fig. 6.10: Water distribution network. Application problem.

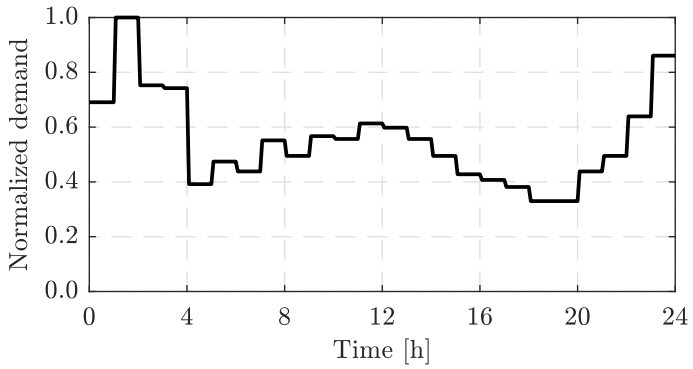

Fig. 6.11: Normalized demand pattern. Application problem.

Table 6.1: Distribution of pipes in terms of their roughness coefficients. Application problem.

Hazen-Williams coefficient	Number of pipes	Total length (km)
110	1	4.33
130	97	41.40
140	4	14.24
141	12	5.69
199	3	0.09

Table 6.2: Distribution of pipes in terms of their diameters. Application problem.

Diameter (mm)	Number of pipes	Total length (km)
203.2	25	10.97
254.0	4	1.18
304.8	50	20.22
355.6	3	0.82
406.4	7	6.07
457.2	1	4.33
508.0	1	0.24
609.6	10	3.69
762.0	13	18.15
2514.6	3	0.09

Contamination events

Two different contamination events are studied in order to explore the capabilities of the proposed approach. In each event, a conservative chemical is injected at a single node with a constant mass inflow of 0.2 kg/min. The location of these two events within the network is illustrated in Figure 6.12. Event 1 is associated with a contaminant inflow at node 101, starting 2 h after the beginning of the simulation. On the other hand, Event 2 corresponds to a contaminant injection into node 157, starting 5 h after the beginning of the simulation. Note that compared with Event 1, a more complex contaminant propagation pattern can be expected in Event 2 since node 157 is located in an intermediate sector of the network. The attributes of each event under consideration are summarized in Table 6.3.

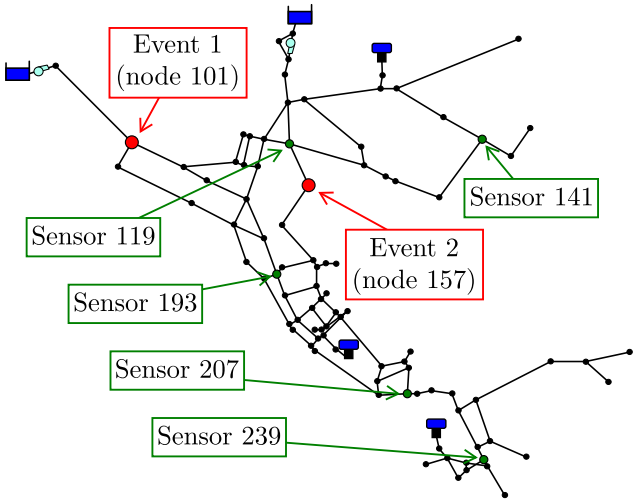

Fig. 6.12: Location of contaminant sources and array of sensors. Application problem.

Concentration measurements at given network nodes are considered for identification purposes. In this context, five fixed sensors recording contaminant concentration every 5 min are allocated in the network according to Figure 6.12. This array of measuring devices is the one reported in [75], which is based on the example provided in the threat ensemble vulnerability assessment and sensor placement optimization tool (TEVA-SPOT) toolkit [75, 385]. The same sensor configuration is considered for both contaminant events. Finally, the corresponding concentration measurements are obtained as in the previous example. Modeling and measurement uncertainties have been simultaneously considered in the data generation processes for both events. In this manner, a more realistic scenario in terms of the available information about the actual network condition is addressed. As in the test problem, 100 samples per stage are considered in the framework of the TMCMC method.

Table 6.3: Attributes of the contaminant events. Application problem.

	Event 1	Event 2
Source node	101	157
Intensity I (kg/min)	0.2	0.2
Starting time T (min)	120.0	300.0

Results: Event 1

This event is associated with a contaminant injection at node 101, that is, close to one of the water sources (see Figure 6.12). For illustration purposes, Figure 6.13 shows the corresponding concentration measurements at the sensors during the entire simulation period when no uncertainties are taken into account, that is, $\alpha = \beta = \gamma = 0$. It is noted that the contaminant arrives first to node 193 about 60 min after the injection starts, and the concentrations tend to decrease at the end of the analysis period. This is attributed to the varying operational conditions of the system under analysis. For reference purposes, the actual values of the contamination parameters for Event 1 are $T = 120$ min and $I = 0.2$ kg/min.

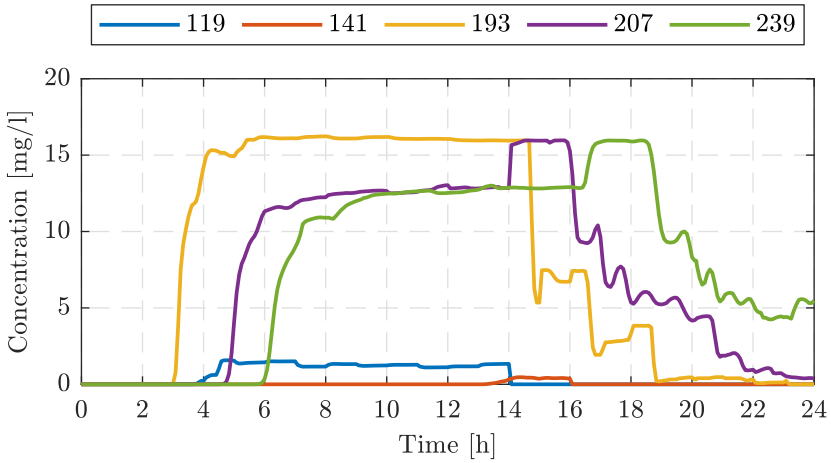

Fig. 6.13: Measurements of nodal concentration over time. Application problem. Event 1.

The synthetic measurements considered for identification purposes are obtained considering model and measurement errors as previously pointed out. In particular, the uncertainty levels are given by $\alpha = \beta = \gamma = 10\%$. The Bayesian model class selection problem considers all network nodes as potential injection points with the same degree of plausibility. This leads to a total of $N_c = 92$ model classes whose posterior probability needs to be estimated. The parameters of each model class M_i are given by $\boldsymbol{\theta}_i = \langle T_i, I_i \rangle^T$ where T_i is the injection's starting time and I_i is the constant mass inflow (contaminant intensity). The prior distribution for the model parameters is taken as uniform with $I_i \in [0, 1]$ kg/min and $T_i \in [0, 180]$ min. It is noted that the upper bound for the

starting time corresponds to the instant in which the contaminant arrives to the sensors for the first time.

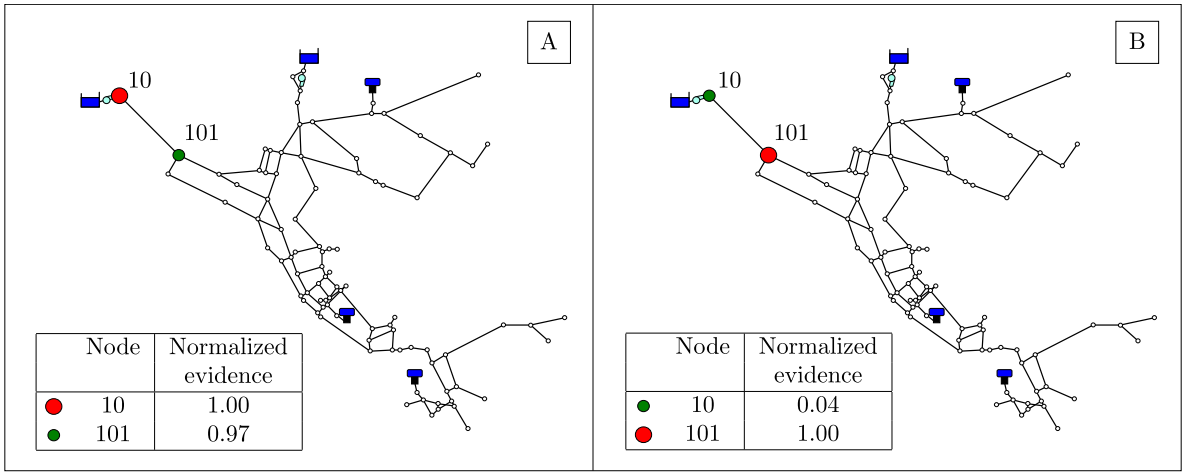

Fig. 6.14: Normalized evidences of all model classes. Application problem. Event 1. A) Scenario 1. B) Scenario 2.

The contaminant source characterization process is carried out considering two cases in terms of the amount of available measurements. Scenario 1 considers measurements from the beginning of the simulation up to 60 min after the contaminant arrives to two sensors (about 5 hours), whereas Scenario 2 considers measurements during the entire analysis period (24 hours). Since all injection points have the same prior probability, the model class selection process can be performed solely based on their evidences. Figure 6.14 illustrates the normalized evidences obtained for all model classes, where nodes with normalized evidence close to zero have been depicted with small white circles. For Scenario 1 (see Figure 6.14-A), two nodes have similar evidence values. In fact, the evidence of node 10 is slightly larger than of the actual contamination source (node 101). Validation calculations show similar results when considering measurements up to 60 min after the initial contaminant detection (about 4 hours). It is observed that nodes 10 and 110 are adjacent, that is, they belong to the same pipeline. Thus, even when the actual injection point is not identified as the most probable one, the results still provide information that can be useful to decision makers. When the measured data consider the entire simulation period, i.e., Scenario 2, (see Figure 6.14-B), the actual injection point is properly identified. Moreover, the evidence of node 10 represents about

4% of the evidence of node 101 in this case. This illustrates that the system identifiability seems to improve as the amount of available measurements increases.

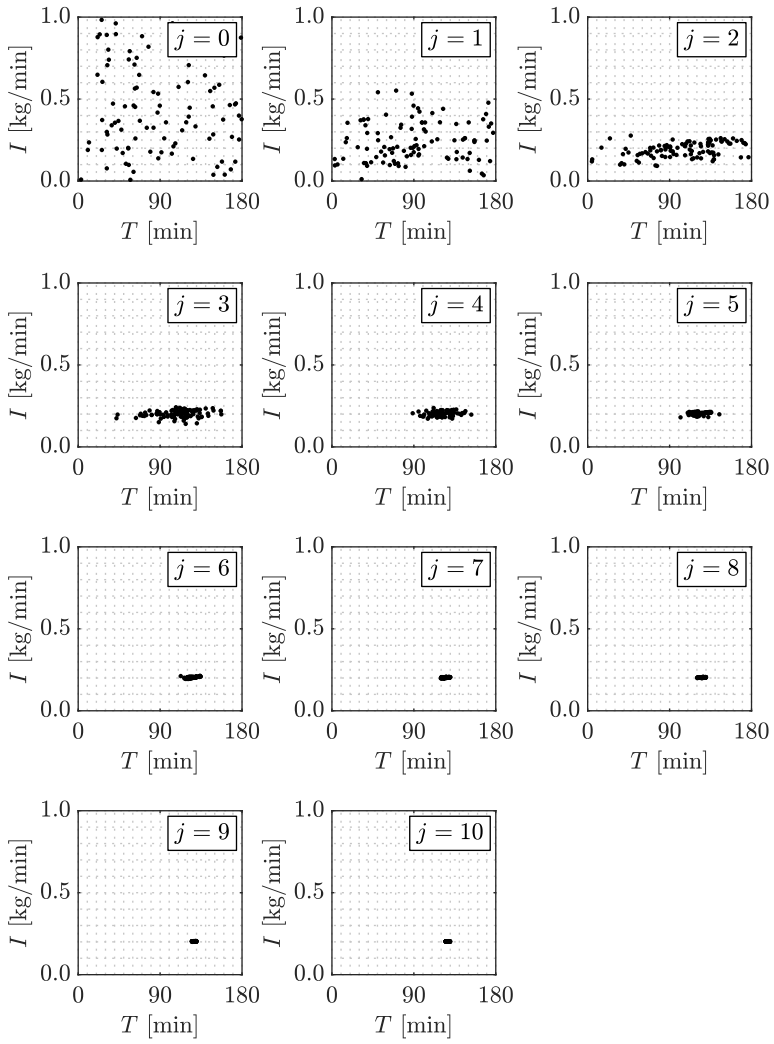

Fig. 6.15: Plot of samples in the $T - I$ space generated at different steps of the transitional Markov chain Monte Carlo method when updating the model class associated with node 101. Application problem. Event 1.

The proposed methodology can provide additional insight into the contaminant event in terms of posterior samples of the model parameters. To illustrate this, Figure 6.15 shows the evolution of samples obtained during the different stages of the TMCMC method when Scenario 2 is considered. It is noted how the samples converge from the prior distribution (stage $j = 0$) to the posterior distribution (stage $j = 10$). The posterior samples are concentrated near the actual values for the

contamination parameters. Thus, the model parameters are globally identifiable in this case. At the last stage, the starting time ranges from 125 to 130 min, while the contaminant intensity from 0.201 to 0.204 kg/min. The corresponding posterior mean estimate of the model parameters is given by $\boldsymbol{\theta} = \langle T, I \rangle^T = \langle 127.3, 0.203 \rangle^T$. The slight differences with respect to the target values are explained due to the presence of measurement noise and modeling errors. Note that, however, these values can be considered as the actual values from a practical point of view.

Results: Event 2

The contaminant is injected at node 157 in this event. This node is located in an intermediate sector of the network (see Figure 6.12). The corresponding target values of the contaminant source parameters are $T = 300$ min for the starting time and $I = 0.2$ kg/min for the contaminant intensity. The concentration measurements reported in Figure 6.16 are associated with Event 2 when no uncertainties are taken into account, i.e., $\alpha = \beta = \gamma = 0$. In this case, the contaminant arrives first to sensor 207 after 135 min of continuous injection, that is, 435 min since the beginning of the simulation period. On the other hand, sensors 119 and 141 do not receive contaminant influence during that period of time. This is attributed to the location of the contaminant source as well as to the flow patterns developed during the simulation period.

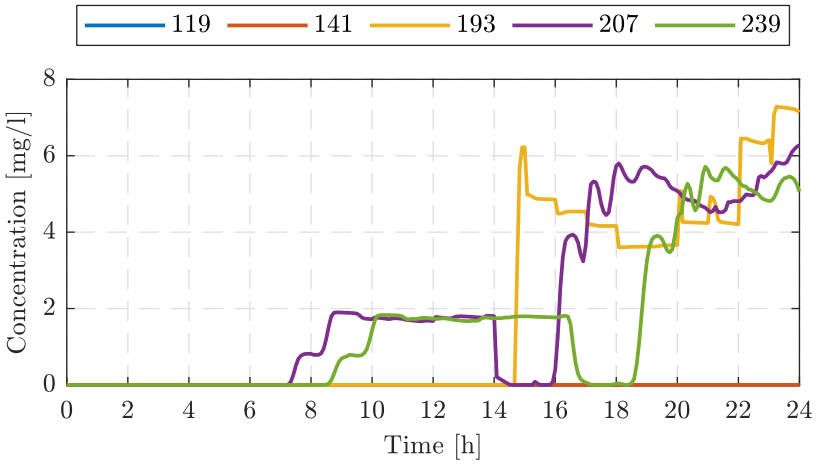

Fig. 6.16: Measurements of nodal concentration over time. Application problem. Event 2.

Model and measurement uncertainties are considered in this event. The uncertainty levels in

roughness coefficients, peak nodal demands and concentration measurements are given by $\alpha = \beta = \gamma = 10\%$. As for the previous event, $N_c = 92$ model classes are considered with parameters $\boldsymbol{\theta}_i = \langle T_i, I_i \rangle^T$ for each model class. A uniform prior distribution is considered with $I_i \in [0, 1]$ kg/min and $T_i \in [0, 435]$ min. The upper limit for T_i coincides with the arrival time of the contaminant to the sensors.

Two scenarios in terms of the time-span for measurements are addressed, as in Event 1. Scenario 1 involves measurements from the beginning of the simulation up to 60 min after the contaminant arrives to two sensors (about 10 hours), whereas Scenario 2 considers measurements over the entire simulation period (24 hours). As in the previous event, the source identification can be performed based on the evidence values only. In this context, Figure 6.17 presents the normalized evidences of all potential injection locations. Normalized evidences close to zero are depicted with small white circles. It is seen that only node 195 presents a normalized evidence different from zero in Scenario 1 (see Figure 6.17-A), that is, the contaminant source is not properly identified when considering measurements up to 60 min after the detection in a second sensor. On the other hand, the identification results improve when more data are incorporated in the identification process. In fact, the actual contamination source (node 157) is identified as the most plausible in Scenario 2 (see Figure 6.17-B), although nodes 159 and 161 present similar evidence values. It is noted that validation calculations show similar results when considering measurements up to 60 min after the contaminant arrives to three sensors (about 16 hours). These results are reasonable from the hydraulic viewpoint since these three nodes are part of a single flow path and, therefore, contaminant injection in any of these locations generates similar propagation patterns through the water distribution network.

Figure 6.18 shows the samples obtained during the different stages of the TMCMC method for the model class associated with node 157 and considering measurements over the entire simulation period. The samples at the initial stage ($j = 0$) are drawn from the prior distribution whereas the last stage ($j = 7$) generates samples from the posterior distribution. It is seen how measurement data

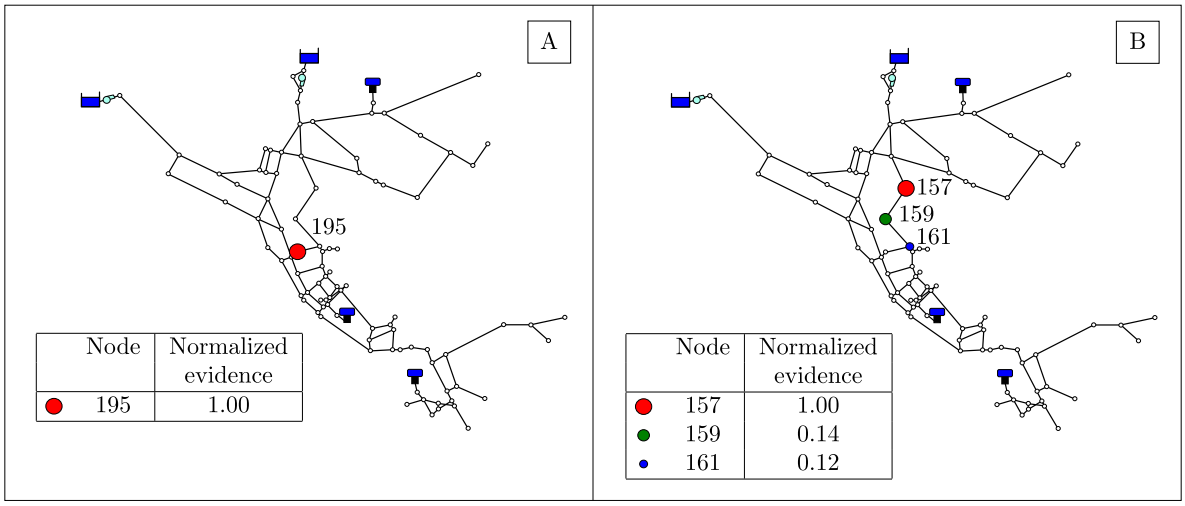

Fig. 6.17: Normalized evidences of all model classes. Application problem. Event 2. A) Scenario 1. B) Scenario 2.

significantly reduce the uncertainty in the model parameters. Note that the posterior samples populate a vicinity of the target values for the model parameters, and therefore the model parameters are globally identifiable as in Event 1. In fact, the starting time ranges from 279.8 to 311.4 min and the contaminant intensity from 0.198 to 0.207 kg/min at the last stage. Moreover, the corresponding posterior mean estimate is $\boldsymbol{\theta} = \langle T, I \rangle^T = \langle 297.7, 0.203 \rangle^T$. These results illustrate one of the advantages of the proposed methodology, which allows to obtain further insight into the contaminant injection profile in addition to the solution to the model class selection problem. This type of information can be potentially useful to assist involved decision making processes in an emergency management framework.

Computational cost

The proposed approach presents advantageous features for implementation in a high performance computing environment. As previously pointed out, the computational burden is almost entirely associated with the water quality analyses of the water distribution network. The number of network simulation runs for each model class depends, among other things, on the amount of samples per stage and the number of TMCMC stages needed. In Event 2, the computational effort for obtaining one water network solution is approximately 0.43 s and the average time spent to obtain posterior

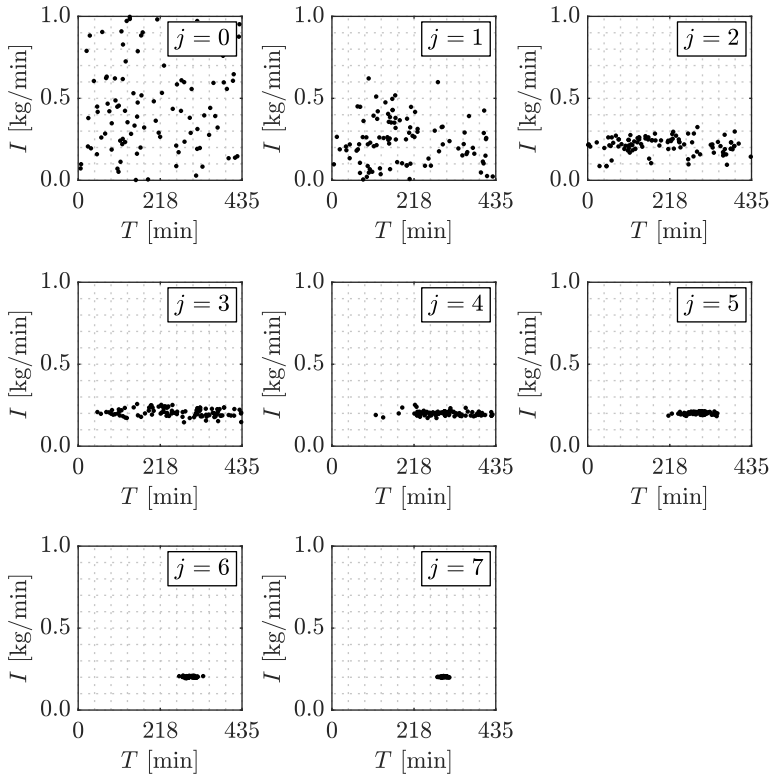

Fig. 6.18: Plot of samples in the $T - I$ space generated at different steps of the transitional Markov chain Monte Carlo method when updating the model class associated with node 157. Application problem. Event 2.

samples of a given model class is about 6.4 min. Considering a parallel implementation to evaluate the evidences of the model classes and neglecting the generation of posterior samples, which are not required by the evidence estimate provided by the TMCMC method, the entire model class selection process takes about 1.3 hrs. The previous computational efforts are based on the implementation of the identification process in available twelve-core multi-threaded computer units. Of course, if more advanced computer power is available, the time to solve the contaminant source characterization problem can be significantly reduced.

6.6 Conclusions

A Bayesian model class selection framework for handling contaminant source characterization problems in the context of water distribution networks has been presented. The parameters of each

model class characterize the contaminant mass inflow over time in terms of its intensity and starting time. The class with the highest posterior probability is interpreted as the most plausible location for the contaminant injection. The evidences of the model classes are estimated as a by-product of the model updating technique, i.e., the transitional Markov chain Monte Carlo method. The model updating technique is combined with a multi-purpose hydraulic and water quality simulation model in order to obtain the quantities of interest, including concentration measurements at a number of nodes. In addition, the proposed methodology presents advantageous features for its implementation in a high performance computing environment.

The effectiveness and capabilities of the proposed methodology are demonstrated with a couple of water distribution systems. Results indicate that overall, the proposed method is potentially a useful tool to address contaminant source detection problems. The proposed approach can provide relevant information for decision making processes even when relatively scarce and noisy data are available. In addition, it can provide additional insight into the actual system state in terms of the characteristics of the injection process. Generally, the scenarios where the actual injection node was not identified are associated with high levels of uncertainty and relatively short measurements periods. However, in these cases, the method is still able to identify nodes that are close to the actual source. The results also show the importance of an appropriate selection of the sensors configuration in order to improve the accuracy of contaminant source detection and therefore the safety of water utility networks.

Future research efforts involve the assessment of the proposed technique in more complex water distribution networks and the consideration of field data as well as multiple sources of contamination and alternative injection profiles. The implementation of optimal sensor location strategies to improve the predictive capability of the proposed approach in the framework of utility networks is an additional subject for future research. Another research direction is the treatment of binary or fuzzy sensors as well as the integration of pre-screening techniques and surrogate models within the proposed framework. Finally, the consideration of stochastic models such as water-demand

models within the proposed identification scheme is also one topic for further research. Some of these issues are currently under consideration.

6.7 Appendix

The following pseudo-code illustrates the implementation of the transitional Markov chain Monte Carlo method [178] to obtain posterior samples associated with the i^{th} model class M_i. It is assumed that the corresponding log-likelihood function $\mathcal{L}_i(\boldsymbol{\theta}_i) = \ln\left(p(D|M_i, \boldsymbol{\theta}_i)\right)$ is available (see Eq. (6.6)).

1. Define β^2. Set $j = 0$ and $\alpha_0 = 0$. Obtain samples $\boldsymbol{\theta}_{i,j}^k, k = 1, \ldots, N_0$, distributed according to the prior distribution $p(\boldsymbol{\theta}_i|M_i)$. Compute the corresponding log-likelihood values $\mathcal{L}_{i,j}^k = \mathcal{L}_i(\boldsymbol{\theta}_{i,j}^k), k = 1, \ldots, N_0$. Note that this step is equivalent to perform direct Monte Carlo simulation.

2. Define $\mathcal{L}^* = \max_{k=1,\ldots,N_j} \mathcal{L}_{i,j}^k$. Compute α^* such that

$$\frac{\sigma_w}{\mu_w} = 1 \tag{6.9}$$

where

$$\mu_w = \frac{1}{N_j} \sum_{k=1}^{N_j} \exp\left\{(\alpha^* - \alpha_j)(\mathcal{L}_{i,j}^k - \mathcal{L}^*)\right\} \tag{6.10}$$

$$\sigma_w = \sqrt{\frac{1}{N_j - 1} \sum_{k=1}^{N_j} \left(\exp\left\{(\alpha^* - \alpha_j)(\mathcal{L}_{i,j}^k - \mathcal{L}^*)\right\} - \mu_w\right)^2} \tag{6.11}$$

3. Set $\alpha_{j+1} = \min(1, \alpha^*)$ and compute

$$\hat{w}_{i,j}^k = \exp\left\{(\alpha_{j+1} - \alpha_j)(\mathcal{L}_{i,j}^k - \mathcal{L}^*)\right\} \tag{6.12}$$

$$\bar{w}_{i,j}^k = \frac{\hat{w}_{i,j}^k}{\sum_{\iota=1}^{N_j} \hat{w}_{i,j}^\iota} \tag{6.13}$$

$$\ln(W_{i,j}) = \ln\left(\frac{1}{N_j}\sum_{k=1}^{N_j}\hat{w}_{i,j}^{k}\right) + (\alpha_{j+1} - \alpha_j)\mathcal{L}^{*} \tag{6.14}$$

4. If $\alpha_{j+1} = 1$ and no posterior samples are required, go to step 8. Otherwise, continue with step 5.

5. Obtain the parameters of the proposal distribution

$$\bar{\boldsymbol{\theta}}_{i,j} = \sum_{k=1}^{N_j}\bar{w}_{i,j}^{k}\boldsymbol{\theta}_{i,j}^{k} \tag{6.15}$$

$$\boldsymbol{\Sigma}_{i,j} = \beta^2\sum_{k=1}^{N_j}\bar{w}_{i,j}^{k}\left(\boldsymbol{\theta}_{i,j}^{k} - \bar{\boldsymbol{\theta}}_{i,j}\right)\left(\boldsymbol{\theta}_{i,j}^{k} - \bar{\boldsymbol{\theta}}_{i,j}\right)^{T} \tag{6.16}$$

and define $\boldsymbol{\theta}_{i,j}^{k(\text{loc})} = \boldsymbol{\theta}_{i,j}^{k}, k = 1,\ldots,N_j$, and $\mathcal{L}_{j,k}^{k(\text{loc})} = \mathcal{L}_{i,j}^{k}, k = 1,\ldots,N_j$. These variables are used to track the evolution of each Markov chain.

6. Apply the Metropolis-Hastings algorithm [88, 89] to generate N_{j+1} samples distributed according to $p_{j+1}(\boldsymbol{\theta}_i) \propto p(\boldsymbol{\theta}_i|M_i)p(D|M_i,\boldsymbol{\theta}_i)^{\alpha_{j+1}}$. For $k = 1$ to N_{j+1}:

   (a) Draw ν from the set $\{1,2,\ldots,N_j\}$ with probabilities equal to the normalized weights $\bar{w}_{i,j}^{\iota}, \iota = 1,\ldots,N_j$. Set the lead sample as $\boldsymbol{\theta}_i^{\text{lead}} = \boldsymbol{\theta}_{i,j}^{\nu(\text{loc})}$ with $\mathcal{L}_i^{\text{lead}} = \mathcal{L}_{i,j}^{\nu(\text{loc})}$.

   (b) Generate a candidate sample $\boldsymbol{\theta}_i^{\text{cand}}$ from a multivariate normal distribution with covariance matrix $\boldsymbol{\Sigma}_{i,j}$ and centred at $\boldsymbol{\theta}_i^{\text{lead}}$. If $p(\boldsymbol{\theta}_i^{\text{cand}}|M_i) = 0$, set $\Upsilon = 1$ and go to Step 5-(c). Otherwise, compute $\mathcal{L}_i^{\text{cand}} = \mathcal{L}_i(\boldsymbol{\theta}_i^{\text{cand}})$ and

$$\ln(\Upsilon) = \alpha_{j+1}\left(\mathcal{L}_i^{\text{cand}} - \mathcal{L}_i^{\text{lead}}\right) + \ln\left(p(\boldsymbol{\theta}_i^{\text{cand}}|M_i)\right) - \ln\left(p(\boldsymbol{\theta}_i^{\text{lead}}|M_i)\right) \tag{6.17}$$

   (c) Generate ξ uniformly distributed on $[0,1]$. If $\ln(\xi) \leq \min\{\ln(\Upsilon), 0\}$, set $\boldsymbol{\theta}_{i,j+1}^{k} = \boldsymbol{\theta}_i^{\text{cand}}$, $\mathcal{L}_{i,j+1}^{k} = \mathcal{L}_i^{\text{cand}}$ and update the last element of the current Markov chain as $\boldsymbol{\theta}_{i,j}^{\nu(\text{loc})} = \boldsymbol{\theta}_i^{\text{cand}}$ and $\mathcal{L}_{i,j}^{\nu(\text{loc})} = \mathcal{L}_i^{\text{cand}}$. Otherwise, set $\boldsymbol{\theta}_{i,j+1}^{k} = \boldsymbol{\theta}_i^{\text{lead}}$ and $\mathcal{L}_{i,j+1}^{k} = \mathcal{L}_i^{\text{lead}}$.

7. If $\alpha_{j+1} < 1$, set $j \leftarrow j+1$ and go back to step 2. Otherwise, continue with step 8.

8. Stop the sampling process, set $m = j + 1$, and compute the evidence estimate as

$$P(D|M_i) \approx W_i = \exp\left(\sum_{j=0}^{m-1} \ln(W_{i,j})\right) \tag{6.18}$$

Acknowledgments

The research reported here was supported in part by CONICYT (National Commission for Scientific and Technological Research) under grant number 1200087. Also, this research has been supported by CONICYT and DAAD under CONICYT-PFCHA/Doctorado Acuerdo Bilateral DAAD Becas Chile/2018-62180007. In addition, this research has been partially supported by DFG (German Research Foundation) under Grant No. BE 2570/3-1 and BR 5446/1-1. These supports are gratefully acknowledged by the authors.

Chapter 7

An effective implementation of reliability methods for Bayesian model updating of structural dynamic models with multiple uncertain parameters

An effective implementation of reliability methods for Bayesian model updating of structural dynamic models with multiple uncertain parameters

D. J. Jerez[a], H. A. Jensen[b,*], M. Beer[a,c,d]

[a]*Institute for Risk and Reliability, Leibniz Universität Hannover, Callinstr. 34, 30167 Hannover, Germany*

[b]*Departamento de Obras Civiles, Universidad Técnica Federico Santa María, Avda. España 1680, Valparaíso 2390123, Chile*

[c]*International Joint Research Center for Engineering Reliability and Stochastic Mechanics, Tongji University, 200092 Shanghai, China*

[d]*Institute for Risk and Uncertainty and School of Engineering, University of Liverpool, Liverpool L69 7ZF, United Kingdom*

Abstract: The use of reliability methods in the framework of Bayesian model updating of structural dynamic models using measured responses is explored for high-dimensional model parameter spaces. This formulation relies on a recently established analogy between Bayesian updating problems and reliability problems. Under this framework, samples following the posterior distribution of the Bayesian model updating problem can be obtained as failure samples in an especially devised reliability problem. An approach that requires only minimal modifications to the standard subset simulation algorithm is proposed and implemented. The scheme uses an adaptive strategy to select the threshold value that determines the last subset level. Due to the basis of the formulation, the approach does not make use of any problem-specific information and, therefore, any type of structural model can be considered. Furthermore, no prior knowledge on the maximum likelihood function value is required by the proposed scheme. The approach is combined with an efficient parametric model reduction technique for an effective numerical implementation. The

*Corresponding author
E-mail addresses: danko.jerez@irz.uni-hannover.de (D. J. Jerez), hector.jensen@usm.cl (H. A. Jensen), beer@irz.uni-hannover.de (M. Beer).

performance of the proposed method is assessed numerically for a linear building model and a nonlinear three-dimensional bridge structural model. The results indicate that the proposed scheme represents an effective numerical technique to address high-dimensional Bayesian model updating problems involving complex structural dynamic models.

Keywords: Bayesian analysis; Identification; Markov chain Monte Carlo; Model updating; Reliability analysis; Structural dynamics; Subset simulation.

7.1 Introduction

Model updating of structural dynamic models using measured responses has a significant number of applications in robust structural response prediction, reliability and sensitivity analyses, structural control, structural health monitoring, etc. Moreover, the appropriate evaluation of the state of structures over their lifetime based on measurements is an important and challenging task in structural engineering applications [214, 259, 260, 386–388]. For a proper assessment of updated models all uncertainties involved in the problem need to be considered. In this regard, a fully probabilistic Bayesian model updating approach provides a robust and rigorous framework for model updating due to its ability to characterize uncertainties associated with the underlying structural dynamic system and update the corresponding distribution based on available data about the structural behavior [24, 261, 262].

For problems of practical interest, the Bayesian approach requires the evaluation of multidimensional integrals which cannot be done analytically. One way to address this difficulty is to use a Gaussian approximation to the posterior probability density function by means of the Laplace method of asymptotic approximation [53]. This type of methods requires to identify the point in the uncertain parameter space which yields the maximum likelihood value and to evaluate the corresponding Hessian matrix of the likelihood function [215, 273]. Such approach has been used in the past and it is usually valid when there is a large amount of data and the model is globally identifiable. However, the application of this approximation faces some problems in practical cases when

the amount of data is not sufficient or when the problem is unidentifiable based on the available information [54]. A more general approach is to use stochastic simulation methods in which samples consistent with the posterior probability density function are generated. Some potential difficulties related to this approach are associated with the evaluation of the so-called evidence, which requires a high-dimensional integration over the uncertain parameter space. Moreover, the high probability content of the posterior probability density function frequently occupies a very small volume compared with that of the prior probability density function. Therefore, the required samples cannot be generated efficiently by sampling from the prior probability density function using direct Monte Carlo simulation. To tackle the previous difficulties, Markov chain Monte Carlo (MCMC) methods have been proposed to solve Bayesian model updating problems more efficiently [81, 389]. In this framework, the most well-known MCMC method is the Metropolis-Hastings (MH) algorithm [88, 89]. The method creates samples from a Markov chain whose stationary state is a specified target probability density function, which corresponds to the posterior distribution. Though this algorithm is quite general, its direct implementation is usually inefficient since the high probability content tends to concentrate in a small volume of the parameter space, as indicated before. To improve the effectiveness of the method, an approach based on the MH algorithm and simulated annealing concepts was proposed in [282]. The main idea is to simulate from a sequence of target probability density functions which converges to the posterior distribution. For each level, a kernel sampling density based on results from the previous level is used as global proposal distribution to simulate samples efficiently. However, this strategy requires a prohibitively large number of samples for higher dimensions. An effective method that adopts the idea as in [282] of using a sequence of intermediate distributions, called the transitional Markov chain Monte Carlo (TMCMC) method, was proposed in [178]. Instead of using kernel sampling densities, the method relies on a combination of reweighting, resampling and random walk strategies to obtain samples during each level. The approach is more efficient and, in addition, it allows the estimation of the evidence as a byproduct of the simulation process. However, the TMCMC method has potential problems in higher dimensions since, in such cases, the convergence to the target probability density function

can be very slow and the corresponding statistical estimates can be biased [263].

To handle high-dimensional Bayesian model updating problems of structural dynamic models using measured responses, sampling schemes based on fictitious dynamic systems have been implemented [263, 264]. These methods rely on the introduction of an auxiliary dynamic system whose potential energy function is defined in terms of the posterior distribution of the model parameters, which allows to exploit the structure of the identification problem. The implementation of this class of algorithms involves the calibration of a number of parameters associated with the characterization and numerical solution of the fictitious dynamic system [263, 264, 266] and, in addition, they unavoidably require taking derivatives of the likelihood function with respect to the identification parameters. Additional methods that have been suggested for this type of identification problems include subspace identification techniques [268] and Kalman-filtering-based approaches [269, 390]. Finally, another approach that in principle can handle problems involving a large number of uncertain parameters is based on structural reliability methods [298]. In this case, the idea is to build an analogy between Bayesian updating problems and reliability problems. In this context, samples following the posterior distribution in the Bayesian updating problem can be obtained as failure samples in an equivalent reliability problem. This approach, referred to as BUS (Bayesian updating with structural reliability methods), has been considered in [298] where the posterior samples are obtained as the conditional samples in subset simulation [133, 134] at the highest simulation level. One of the difficulties of this approach is the proper choice of the so-called likelihood multiplier connected with the rejection principle [276] involved in its formulation. In this regard, several approaches have been suggested to address this issue. They include an approach based on a postprocessing step to correct the distribution of failure samples [303], an inner-outer subset simulation approach [304], and an approach that adaptively modifies the limit-state function during subset simulation [305]. The previous procedures have been applied to a variety of problems, including analytical problems with high-dimensional parameter spaces, nonlinear static systems, reliability-based monitoring sensitivity analysis for reinforced slopes, and structural dynamic models with relatively few parameters [47, 300, 301]. However, studies on the effectiveness of BUS

approaches to handle structural dynamic systems have been limited to academic-type of problems. Furthermore, high-dimensional Bayesian model updating of complex structural dynamic systems remains a significantly important challenge in the assessment and life-cycle management of existing structures. Thus, there is a necessity for developing not only sound theoretical algorithms to address this class of problems, but also the appropriate techniques for implementing such procedures in engineering practice.

Given that dimension sustainability is efficiently handled by advanced simulation techniques, it is the objective of this work to evaluate the use of structural reliability methods in the context of Bayesian model updating of complex structural dynamic models involving measured response data and multiple uncertain parameters. As previously pointed out, this type of problems has not been addressed by previous contributions in the framework of BUS. Subset simulation, a well established sampling technique, is implemented in this work by combining some of the ideas introduced in [304, 305]. The resulting algorithm uses an adaptive strategy to select the threshold value that determines the last subset level, where samples beyond such threshold follow the posterior distribution of the original Bayesian updating problem. In this setting, only minimal modifications to the standard subset simulation algorithm are required. At the same time, the approach effectively avoids the necessity of prior knowledge on the maximum value of the likelihood function, the need to redefine the limit-state function during each level of subset simulation, and the iterative solution of an inner reliability problem during the sampling process. Overall, the proposed method represents an effective numerical technique for the treatment of Bayesian identification problems involving complex, realistic and practical structural models and multiple uncertain parameters.

The structure of the paper is as follows. In Section 7.2, the use of structural reliability methods in the framework of Bayesian model updating is reviewed. The solution of the corresponding reliability problem is discussed in Section 7.3. Implementation aspects of the proposed scheme are addressed in Section 7.4. In Section 7.5, example problems involving structural dynamic models with multiple uncertain parameters are presented to demonstrate the applicability of the proposed

method. Conclusions are presented in Section 7.6.

7.2 Background

7.2.1 Bayesian model updating problem

Let $\boldsymbol{\theta} \in \boldsymbol{\Theta} \subset R^{n_{\boldsymbol{\theta}}}$ be the set of parameters of a model class M. The objective of model updating is to compute the posterior probability density function of the model parameters $p(\boldsymbol{\theta}|M, D)$ using available data D [24, 53]. According to Bayes' Theorem, the posterior probability density function of $\boldsymbol{\theta}$ is given by

$$p(\boldsymbol{\theta}|M, D) = \frac{L(D|M, \boldsymbol{\theta})\ p(\boldsymbol{\theta}|M)}{P(D|M)} \tag{7.1}$$

where $L(D|M, \boldsymbol{\theta})$ is the likelihood function, $p(\boldsymbol{\theta}|M)$ is the prior probability density function of $\boldsymbol{\theta}$, and $P(D|M)$ is the evidence of model class M. The likelihood function expresses the plausibility of observing the data D given a certain value of $\boldsymbol{\theta}$, while the prior probability density function represents the prior or initial belief about the distribution of $\boldsymbol{\theta}$. Moreover, the evidence of the model class is written as

$$P(D|M) = \int_{\Theta} L(D|M, \boldsymbol{\theta})\ p(\boldsymbol{\theta}|M) d\boldsymbol{\theta} \tag{7.2}$$

which can be used for Bayesian model class selection [271] and model averaging [272]. To simplify the notation, Eq. (7.1) is rewritten as

$$p(\boldsymbol{\theta}|D) = P(D)^{-1} L(\boldsymbol{\theta})\ p(\boldsymbol{\theta}) \tag{7.3}$$

where $p(\boldsymbol{\theta}|D)$ denotes the posterior probability density function, $L(\boldsymbol{\theta})$ denotes the likelihood function, $p(\boldsymbol{\theta})$ denotes the prior probability density function, and $P(D)$ denotes the evidence. It is noted that the posterior distribution cannot be derived analytically for general cases and, therefore, posterior samples are usually generated by means of stochastic simulation techniques. Finally, in the context of the present work it is assumed that D contains input dynamic data and output responses

from measurements on the structural system.

7.2.2 Mechanical modeling

The class of structural systems under consideration is characterized by a multi-degree of freedom model satisfying the equation of motion

$$\mathbf{M}\ddot{\mathbf{x}}(t) \; + \; \mathbf{C}\dot{\mathbf{x}}(t) \; + \; \mathbf{K}\mathbf{x}(t) + \mathbf{f}_{NL}(\mathbf{x}(t), \dot{\mathbf{x}}(t), \boldsymbol{\tau}(t)) \; = \; \mathbf{f}(t) \tag{7.4}$$

where $\mathbf{x}(t)$ denotes the displacement vector of dimension n_x, $\mathbf{f}_{NL}(\mathbf{x}(t), \dot{\mathbf{x}}(t), \boldsymbol{\tau}(t))$ the vector of nonlinear restoring forces, $\boldsymbol{\tau}(t)$ the set of variables which describe the state of the nonlinear components, and $\mathbf{f}(t)$ the external force vector. The matrices $\mathbf{M}$, $\mathbf{C}$, and $\mathbf{K}$ describe the mass, damping, and stiffness, respectively. The evolution of the set of variables $\boldsymbol{\tau}(t)$ is described by an appropriate nonlinear model which depends on the nature of the nonlinearity. Note that the previous equation of motion constitutes a dynamic system with localized nonlinearities, which can also be extended to other cases such as the consideration of nonlinear models for the structure.

7.2.3 Likelihood function

Let $r_n(t_j, \boldsymbol{\theta})$ denote the response of interest at time t_j at the n^{th} observed degree of freedom predicted by the structural model corresponding to the parameters $\boldsymbol{\theta}$, and $r_n^*(t_j)$ denotes the corresponding measured output. The prediction and measurement errors $e_n(t_j, \boldsymbol{\theta}) = r_n^*(t_j) - r_n(t_j, \boldsymbol{\theta})$ for $n = 1, \ldots, n_o$, and $j = 1, \ldots, n_t$, where n_o denotes the number of observed degrees of freedom and n_t denotes the length of the discrete time history data, are modeled as independent and identically distributed Gaussian variables with zero mean and variance σ^2 [271]. This assumption implies stochastic independence of the errors for different channels of measurements and for different time instants. In this regard, it is noted that alternative prediction error model classes can be used as well [55]. Using the above probability model for the prediction and measurement errors,

the likelihood function $L(\boldsymbol{\theta})$ can be expressed as [53, 54, 271]

$$L(\boldsymbol{\theta}) = \frac{1}{(2\pi\sigma^2)^{n_o n_t/2}} \exp\left[-\frac{1}{2\sigma^2} J(\boldsymbol{\theta})\right] \tag{7.5}$$

where

$$J(\boldsymbol{\theta}) = \sum_{n=1}^{n_o} \sum_{j=1}^{n_t} \left(r_n^*(t_j) - r_n(t_j, \boldsymbol{\theta})\right)^2 \tag{7.6}$$

is a measure-of-fit function between the measured response and the model prediction at the measured degrees of freedom. In the context of the previous equation it is noted that different types of response quantities can be used to define the measure-of-fit function.

7.2.4 Equivalent reliability problem

As previously pointed out, simulation-based Bayesian model updating techniques such as Markov chain Monte Carlo methods provide a powerful computational tool for generating posterior samples. In particular, the TMCMC method has proved to be efficient in generating samples asymptotically distributed as the posterior probability density function for low/intermediate-dimensional Bayesian model updating problems [95, 178, 288]. However, MCMC methods may encounter difficulties in connection with their efficiency and stability as the dimension of the problem increases. To handle these potential difficulties, a framework that converts the generation of posterior samples into the task of obtaining failure samples associated with an equivalent reliability problem has been suggested and explored in [298, 303–305].

The basic idea of Bayesian updating with structural reliability methods, as suggested in [298], is to transform the identification problem into a reliability problem. To this end, define a failure event F in the form

$$F = \{u < cL(\boldsymbol{\theta})\} = \{cL(\boldsymbol{\theta}) - u > 0\} \tag{7.7}$$

where u is an auxiliary random variable uniformly distributed on $[0, 1]$ with probability density function $I_{[0,1]}(u)$, and $\boldsymbol{\theta}$ is the set of uncertain model parameters with probability density function

$p(\boldsymbol{\theta})$. Note that the distribution of the model parameters associated with the failure event stated in Eq. (7.7) is actually the prior distribution of the Bayesian model updating problem defined in Eq. (7.1), i.e., $p(\boldsymbol{\theta})$. The constant $c > 0$ corresponds to the so-called likelihood multiplier, which must satisfy the inequality [276]

$$cL(\boldsymbol{\theta}) \leq 1 \;\text{ or }\; c^{-1} \geq L(\boldsymbol{\theta}), \text{ for all } \boldsymbol{\theta} \in \boldsymbol{\Theta} \tag{7.8}$$

If failure samples distributed as $p(\boldsymbol{\theta})I_{[0,1]}(u)$, conditional on the failure event F can be generated by means of any simulation technique, then such samples follow the posterior distribution $p(\boldsymbol{\theta}|D)$. In addition, the evidence of the model class, $P(D)$, can be also computed in this framework as

$$P(D) = c^{-1}P_F \tag{7.9}$$

where P_F is the probability of failure event F and c^{-1} satisfies Eq. (7.8). More details on the derivation of the previous results can be found, e.g., in [298, 304].

7.2.5 Likelihood multiplier

From Eq. (7.8) it is clear that the smallest admissible value of c^{-1}, i.e., c_{adm}^{-1}, is given by

$$c_{adm}^{-1} = \max_{\boldsymbol{\theta} \in \boldsymbol{\Theta}} L(\boldsymbol{\theta}) \tag{7.10}$$

Generally, this value is not known in advance and it is numerically challenging to choose a likelihood multiplier that guarantees the inequality $cL(\boldsymbol{\theta}) \leq 1$ for all $\boldsymbol{\theta}$. On the one hand, using a value larger than c_{adm}^{-1} will give the correct posterior distribution at the expense of decreasing the efficiency of the sample generation process. On the other hand, using a value smaller than c_{adm}^{-1} will lead to bias in the distribution of the samples. Thus, an appropriate choice of this parameter is crucial as it affects the definition of the failure event F in Eq. (7.7). In this regard, several approaches have been suggested for addressing the proper selection of the multiplier. They include

an approach based on a postprocessing step to correct the sampling results [303], an inner-outer subset simulation approach [304], and an approach that adaptively modifies the limit-state function during subset simulation [305]. An additional discussion about these approaches is provided in Section 7.3.6. Finally, it is noted that in some cases it is possible to study the structure of $L(\boldsymbol{\theta})$ and derive a value of the likelihood multiplier that guarantees $cL(\boldsymbol{\theta}) \leq 1$ [298], although it is not necessarily the optimal value. Clearly, the use of these approximations can be computationally advantageous in such particular situations. Nonetheless, the optimal value of the likelihood multiplier, which is associated with the maximum likelihood value, is difficult to determine for general cases of practical interest, as already pointed out. In this regard, an alternative approach that effectively avoids the a priori definition of this quantity is described in the next section.

7.3 Solution of equivalent reliability problem

As indicated in the previous section, any structural reliability method can be used to solve the equivalent reliability problem. In particular, subset simulation is of special interest since it is efficient and effective for handling problems involving small failure probabilities. In addition, its performance does not depend on the number of uncertain parameters involved in the problem, it is not restricted to specific types of structural systems, and its robustness and efficiency have been demonstrated in a wide variety of applications. This advanced simulation technique generates samples conditional on a sequence of intermediate failure events. Such samples are generated by MCMC and they gradually populate the target failure region, while the intermediate failure events are adaptively defined during the sampling process. In this contribution, subset simulation is implemented to generate failure samples associated with the equivalent reliability problem. The proposed technique effectively avoids a priori definitions of the likelihood multiplier, the need to redefine the driving variable during each simulation level, and the solution of inner reliability problems during the sampling process. Finally, the reader is referred to [133, 134] for a detailed description, from the theoretical and implementation viewpoints, of subset simulation for reliability analysis.

7.3.1 Preliminary observations

As previously pointed out, subset simulation is adopted to obtain samples following the posterior distribution $p(\boldsymbol{\theta}|D)$. To this end, and following some of the ideas presented in [304, 305], the failure event defined in Eq. (7.7) is first rewritten as

$$F = \{v(\boldsymbol{\theta}, u) > v^{th}\} \tag{7.11}$$

with

$$v(\boldsymbol{\theta}, u) = \ln\left(\frac{L(\boldsymbol{\theta})}{u}\right) \quad , \quad v^{th} = \ln(c^{-1}) \tag{7.12}$$

where $\ln(\cdot)$ denotes natural logarithm. Note that in the previous formulation, the driving variable v does not depend on the value of the multiplier c. Moreover, the multiplier only affects the threshold level v^{th} and, therefore, subset simulation can be performed without the necessity of specifying the value of the multiplier beforehand. In principle, as long as the multiplier satisfies the inequality in Eq. (7.8), the marginal distribution of $\boldsymbol{\theta}$ conditional on the failure event $F = \{v > v^{th}\}$ is equal to the posterior distribution $p(\boldsymbol{\theta}|D)$ [298, 304, 305]. Thus, the minimum value of v^{th} beyond which the samples theoretically follow the posterior probability density function is

$$v^{th}_{min} = \ln\left(\max_{\boldsymbol{\theta}\in\boldsymbol{\Theta}} L(\boldsymbol{\theta})\right) \tag{7.13}$$

This value, which is generally unknown, does not affect the subset simulation procedure. In fact, subset simulation can be performed until the intermediate threshold of the highest level has passed v^{th}_{min}. This is possible since the intermediate failure events in subset simulation are defined in terms of the driving variable values obtained during the sampling process, that is, their definition does not require information on the target threshold level v^{th}. An approach that adaptively estimates v^{th}_{min} based on the samples obtained during the different levels of subset simulation is described in what follows.

7.3.2 Synopsis of proposed scheme

Following the ideas of subset simulation, the first step (level 0) consists in drawing N samples $\{\boldsymbol{\theta}_i^0, u_i^0\}, i = 1, \ldots, N$ from the joint distribution $p(\boldsymbol{\theta})I_{[0,1]}(u)$. The likelihood function $L(\cdot)$ is evaluated at each sample and the initial threshold level of the reliability problem in Eq. (7.11) is selected as the logarithm of the maximum likelihood value, i.e., $v^{th} = \ln(\max_{i=1,\ldots,N} L(\boldsymbol{\theta}_i^0))$. Thereafter, each step is performed in accordance with the standard formulation of subset simulation with only a minor modification. At the end of each simulation level, say level k, the threshold level is updated based on the samples $\{\boldsymbol{\theta}_i^k, u_i^k\}, i = 1, \ldots, N$, obtained during such a level as $v^{th} \leftarrow \max\{v^{th}, \ln(\max_{i=1,\ldots,N} L(\boldsymbol{\theta}_i^k))\}$. Based on this updating scheme, it is clear that the threshold v^{th} can only increase after each iteration, providing better estimates of the optimum threshold level as the simulation continues. The iteration over the subset levels is performed until the standard stopping criterion of subset simulation is verified, that is, until the threshold associated with the current intermediate failure event surpasses the current threshold value. It is noted that a similar strategy is adopted in [305], but at the limit-state function level. In such approach, all limit-state function values are updated at the end of each subset level.

In the previous framework it is noted that the final value of $c^{-1} = \exp(v^{th})$, which is a stochastic quantity, corresponds to the largest likelihood value observed during the entire simulation. For large N, the value of c^{-1} asymptotically approaches to c_{adm}^{-1}, but for finite N, this parameter is very likely smaller than c_{adm}^{-1}. However, this fact does not impede the proposed scheme to produce samples that follow the posterior distribution from a practical viewpoint. In this regard, the number of samples employed in each level of subset simulation must be selected large enough to allow an effective exploration of the entire failure domain. Note that these samples will not necessarily identify the uncertain parameter values that maximize the likelihood function. Therefore, it is likely that the final value of c^{-1}, which corresponds to the maximum likelihood value observed during the entire sampling process, is such that $c^{-1} \leq c_{adm}^{-1}$, as previously pointed out. However, the important region of the likelihood function can be effectively explored by the proposed approach,

as illustrated in the numerical examples presented in this contribution (see Section 7.5).

7.3.3 Underlying normal space

Regarding the numerical implementation of the proposed scheme, the reliability problem is first set in terms of an underlying normal space $\mathbf{Z} \subset R^{n_\theta+1}$ of independent standard normal variables following the standard formulation of subset simulation [133]. The mapping between the spaces $\mathbf{Z}$ and $\mathbf{\Theta} \times [0,1]$ can be obtained by means of several techniques [22, 391]. In fact, without loss of generality, the transformation between the first n_θ components of $\mathbf{z}$, denoted by $(\mathbf{z})_{1:n_\theta}$, and $\boldsymbol{\theta}$ can be written in terms of a transformation as $\boldsymbol{\theta} = \boldsymbol{\theta}((\mathbf{z})_{1:n_\theta})$. On the other hand, the uniformly distributed random variable u can be written in terms of the last component of $\mathbf{z}$, i.e., $(\mathbf{z})_{n_\theta+1}$, as $u = \Phi((\mathbf{z})_{n_\theta+1})$, where $\Phi(\cdot)$ is the cumulative distribution function of the standard normal distribution. Note that, however, an implementation of the reliability problem directly in the original space $\mathbf{\Theta} \times [0,1]$ is also possible.

7.3.4 Basic procedure

In the following, a procedure that illustrates the basic implementation of subset simulation, in the context of the present formulation, is provided.

1. Define the conditional probability of the intermediate failure events p_0 and the number of samples N. These parameters are chosen such that $p_0 N$ is an integer number.

2. Generate N samples $\{(\mathbf{z}_{0,i}), i = 1, \ldots, N\}$ by direct Monte Carlo according to the standard multivariate normal distribution (the subscript 0 denotes that the samples correspond to the unconditional level, i.e., level 0).

3. Set $k = 1$ and $v^{th} = \max_{i=1,\ldots,N} \ln(L(\boldsymbol{\theta}_{0,i}))$, where $\boldsymbol{\theta}_{0,i} = \boldsymbol{\theta}((\mathbf{z}_{0,i})_{1:n_\theta})$.

4. Evaluate the driving variable v to obtain $\{v(\mathbf{z}_{k-1,i}), i = 1, \ldots, N\}$. Arrange these values in ascending order, where $v(\mathbf{z}_{k-1,i}) = \ln(L(\boldsymbol{\theta}_{k-1,i})/u_{k-1,i})$, $\boldsymbol{\theta}_{k-1,i} = \boldsymbol{\theta}((\mathbf{z}_{k-1,i})_{1:n_\theta})$, and

$u_{k-1,i} = \Phi((\mathbf{z}_{k-1,i})_{n_\theta+1})$.

5. Identify the $[(1-p_0)N]$th largest value of the set $\{v(\mathbf{z}_{k-1,i}), i = 1,\ldots,N\}$. In case this value is equal or larger than v^{th}, set $m = k$, $v_m = v^{th}$ and go to step 9. Otherwise, set the intermediate threshold value v_k equal to the aforementioned $[(1-p_0)N]$th largest value of the set $\{v(\mathbf{z}_{k-1,i}), i = 1,\ldots,N\}$.

6. The kth intermediate failure domain is defined as $F_k = \{\mathbf{z} \in \mathbf{Z} | v(\mathbf{z}) > v_k\}$. The estimate for $P(F_k)$ (if $k = 1$) or $P(F_k/F_{k-1})$ (if $k > 1$) is equal to p_0 by construction.

7. By construction there are $p_0 N$ samples among $\{(\mathbf{z}_{k-1,i}), i = 1,\ldots,N\}$ whose driving variable values are larger than v_k. Starting from each of these conditional samples, the modified Metropolis-Hastings algorithm [133] is used to generate additional $(1-p_0)N$ conditional samples that lie in F_k making a total of N conditional samples $\{(\mathbf{z}_{k,i}), i = 1,\ldots,N\}$ at level k.

8. Set $v^{\text{aux}} = \max_{i=1,\ldots,N} \ln(L(\boldsymbol{\theta}_{k,i}))$, where $\boldsymbol{\theta}_{k,i} = \boldsymbol{\theta}((\mathbf{z}_{k,i})_{1:n_\theta})$. Update the threshold level as $v^{th} \leftarrow \max\{v^{th}, v^{\text{aux}}\}$. Return to step 4 with $k \leftarrow k+1$.

9. The failure probability is estimated as

$$P_F \approx p_0^{m-1} \frac{1}{N} \sum_{i=1}^{N} I_{F_m}(\mathbf{z}_{m-1,i}) \tag{7.14}$$

where $\{\mathbf{z}_{m-1,i}, i = 1,\ldots,N\}$ is the set of samples generated at the last stage of subset simulation (conditional level $m-1$), and $I_{F_m}(\mathbf{z}_{m-1,i})$ is the indicator function of F_m, with $I_{F_m}(\mathbf{z}_{m-1,i}) = 1$ if $\mathbf{z}_{m-1,i} \in F_m$ and $I_{F_m}(\mathbf{z}_{m-1,i}) = 0$ otherwise. The samples that lie in the target failure domain F_m follow the posterior distribution $p(\boldsymbol{\theta}|D)$.

10. The evidence is estimated as

$$P(\boldsymbol{D}) \approx \exp(v^m) P_F \tag{7.15}$$

As indicated in step 7 of the above procedure, the modified Metropolis-Hastings algorithm [133]

is implemented to generate conditional samples during each simulation level. In this regard, each component of the candidate sample is generated independently. A uniform distribution centered at the lead value is selected as the proposal distribution for each component. This choice, which is commonly adopted in the implementation of subset simulation for reliability assessment of structural dynamic systems, has proven effective to handle the numerical examples presented in this contribution. Based on the above procedure, it is clear that the proposed approach requires only minimal modifications to the standard formulation of subset simulation.

7.3.5 Potential enhancements

Several additional enhancements can be implemented to improve the performance and computational efficiency of the proposed method. For example, the acceptance rate of the sampling process, in the framework of the modified Metropolis-Hastings algorithm, can be controlled by using adaptive proposal distributions [392]. Similarly, to decrease the dependency of the generated samples and, consequently, increase the overall performance of the scheme, resampling strategies for the auxiliary variable associated with the rejection sampling scheme can be considered [305]. Actually, the previous techniques have been implemented in the present formulation. Additionally, alternative definitions of the proposal distribution, in the context of the modified Metropolis-Hastings algorithm, can improve the performance of the sampling procedure for certain applications. Finally, variants of the basic formulation of subset simulation have also been proposed to improve its efficiency, e.g., [134, 135]. Certainly, such variants can also be considered in the framework of the present contribution.

7.3.6 Remarks on proposed and alternative BUS implementations

Several approaches in the framework of BUS have been proposed. A direct implementation [298] and a postprocessing step to correct the final results [303] have been previously reported. Both methods require an initial choice of the likelihood multiplier, c, which can significantly affect their

performance [303]. Alternatively, the approach presented in [304] iteratively updates the value of c in terms of the intermediate thresholds of subset simulation. The sampling process continues until the probability of the likelihood function exceeding the current value of c^{-1} is smaller than a user-defined tolerance. In practice, then, this approach indirectly defines the likelihood multiplier in terms of a certain quantile of the likelihood function. Besides, its formulation requires to solve an inner reliability problem in each stage of subset simulation. Finally, the approach presented in [305] iteratively updates the driving variable function, in the context of subset simulation, using the maximum observed likelihood value. The process continues until sufficient failure samples are obtained. Hence, the final value of c is defined using the effective support of the likelihood function instead of specifying it beforehand.

To avoid an a priori characterization of the likelihood multiplier, this work follows the strategy presented in [305]. That is, the final value of c^{-1} is equal to the maximum likelihood value observed throughout all subset simulation stages. However, to circumvent the iterative definition of the driving variable, the failure event is explicitly defined as in [304]. As previously pointed out, only minimal modifications to the standard subset simulation algorithm are needed and the iterative solution of inner reliability problems is avoided. Overall, the resulting method represents an alternative BUS approach which provides an effective treatment of the likelihood multiplier while maintaining simplicity in its formulation and implementation. This feature is particularly attractive from a practical viewpoint, especially in the context of Bayesian model updating problems involving structural dynamic systems with multiple uncertain parameters.

7.4 Implementation aspects

7.4.1 Initial remarks

The solution of the equivalent reliability problem involves a large number of model evaluations associated with the repeated evaluation of the likelihood function. In fact, this process is com-

putationally very demanding due to the large number of dynamic analyses (in the order of thousands) required for populating the failure region. This is especially important when the computational time for performing a single dynamic analysis is significant. To cope with this difficulty, a number of strategies based on meta-modeling techniques have been considered [393, 394]. In the context of Bayesian updating using structural reliability methods, strategies based on surrogate models [395, 396] have been proposed at the limit state function level. It is noted that the previous approaches have been demonstrated in applications involving structural dynamic systems with relatively few model parameters. In general, the effective integration of surrogate models for higher-dimensional parameter spaces remains one of the main challenges in Bayesian model updating applications.

7.4.2 Parametric model reduction technique

Considering that the focus of this work is on Bayesian model updating of structural dynamic models with multiple uncertain parameters and measured responses, an effective numerical implementation of the proposed method is essential. In the present formulation, a very efficient parametric model reduction technique is considered. In particular, a model reduction technique based on substructure coupling for dynamic analysis is adopted [163, 164]. The method involves dividing the structure into a number of linear and nonlinear substructures, obtaining reduced-order models of the linear substructures and then assembling a reduced-order model of the entire structure. The dynamic behavior of the linear substructures is described by a set of dominant fixed-interface normal modes along with a set of interface constraint modes that account for the coupling at each interface where the substructures are connected [164]. Based on these modes, the corresponding reduced-order matrices can be derived.

While the use of reduced-order models alleviates part of the computational effort, their repetitive generation during the solution of the reliability problem can be computationally expensive due to the substantial computational overhead that arises at the substructure level. In this regard, an effi-

cient model parametrization scheme is implemented. To this end, the division of the original model is guided by a parametrization scheme which assumes that the substructure matrices for each of the introduced linear substructures depend on only one of the model parameters. Based on this assumption, a direct parametrization of the reduced-order matrices associated with the linear substructures is obtained and, consequently, a drastic reduction in computational effort is achieved [163, 397]. In other words, the different quantities involved in the reduced-order model can be directly updated for different values of the model parameters $\boldsymbol{\theta}$. Thus, the potentially time-consuming step of computing the reduced-order matrices for different values of the model parameters is completely avoided. Moreover, the above formulation guarantees that the reduced-order model is based on the exact substructure modes for all values of the model parameters $\boldsymbol{\theta}$. The equation of motion of the reduced-order model together with the equation for the evolution of the set of variables $\boldsymbol{\tau}(t)$ can be integrated efficiently by any appropriate step-by-step integration scheme. A detailed derivation and formulation of the parametric model reduction technique can be found in [163].

Finally, it is noted that the use of parametric reduced-order models has also important implications from a practical viewpoint. In fact, the use of this technique opens the door to applications involving real structural dynamic systems and, therefore, the proposed implementation can contribute to the enhancement of the safety and reliability of practical engineering systems. Moreover, the consideration of surrogate models at the likelihood function level [287, 288] combined with the previous parametric model reduction technique can also be implemented to improve further the efficiency of the proposed scheme for solving the reliability problem. Such approach is currently under development and it will be reported in a future contribution (see Conclusions).

7.5 Examples

It is noted that validation calculations have shown that the different available BUS techniques and the proposed approach provide very similar results for the academic-type of problems presented in previous contributions. In this work, two examples comprising involved structural dynamic sys-

tems are presented. The first example comprises a benchmark system introduced in [263], which involves a linear ten-story shear building model subject to ground excitation. In this regard, this example allows to demonstrate the effectiveness of the proposed approach in predicting different types of responses as well as in identifying the spectral properties of the structural model. Additionally, a statistical performance analysis of alternative BUS approaches is provided for this example. On the other hand, the second example considers a realistic finite element model of a nonlinear three-dimensional bridge structure to demonstrate the applicability of the identification method in a complex structural system. In both examples, a large number of model parameters are considered. Additionally, it is assumed that noisy simulated acceleration data are available for updating purposes.

7.5.1 Example 1: Illustrative problem

Identification problem

The ten-story linear shear-building model shown in Figure 7.1, which has been borrowed from [263], is considered in this first example problem. The corresponding model class is characterized by the mass m_i, damping coefficient c_i, and stiffness parameter k_i for each story $i = 1, \ldots, 10$. The identification process is based on simulated acceleration data. In particular, the input ground acceleration history to generate the measurements, shown in Figure 7.2, corresponds to the El Centro ground-motion record. The input acceleration values have been scaled so that the peak ground acceleration is equal to 0.6 m/s^2. The measured response is simulated by first calculating the absolute acceleration response of the actual structure at the first and tenth floors. Thus, the number of observed degrees of freedom is $n_o = 2$. Then, a Gaussian discrete white noise sequence with standard deviation σ equal to 10% of the root-mean-square value of the corresponding acceleration time histories is added. Ten seconds of data with sampling interval $\Delta t = 0.01$ s are used, giving a total of $n_t = 1000$ time steps. The corresponding measurements are shown in Figure 7.2. The nominal model used to generate the measured data is defined in Table 7.1. This system may be

interpreted as the actual or target structural system in a Bayesian model updating framework.

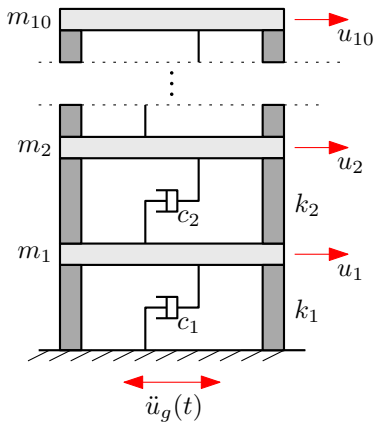

Fig. 7.1: Ten-story linear shear building model.

Table 7.1: Target values of the model parameters. Example 1.

Parameter	Value	Parameter	Value	Parameter	Value
m_{1n}	1.92×10^4 kg	c_{1n}	7.70×10^4 Ns/m	k_{1n}	2.16×10^7 N/m
m_{2n}	1.97×10^4 kg	c_{2n}	7.78×10^4 Ns/m	k_{2n}	1.74×10^7 N/m
m_{3n}	1.95×10^4 kg	c_{3n}	7.86×10^4 Ns/m	k_{3n}	2.04×10^7 N/m
m_{4n}	2.06×10^4 kg	c_{4n}	7.28×10^4 Ns/m	k_{4n}	1.99×10^7 N/m
m_{5n}	2.05×10^4 kg	c_{5n}	7.19×10^4 Ns/m	k_{5n}	1.74×10^7 N/m
m_{6n}	1.98×10^4 kg	c_{6n}	7.37×10^4 Ns/m	k_{6n}	1.68×10^7 N/m
m_{7n}	1.94×10^4 kg	c_{7n}	7.10×10^4 Ns/m	k_{7n}	1.87×10^7 N/m
m_{8n}	2.06×10^4 kg	c_{8n}	7.11×10^4 Ns/m	k_{8n}	1.77×10^7 N/m
m_{9n}	1.90×10^4 kg	c_{9n}	6.90×10^4 Ns/m	k_{9n}	1.84×10^7 N/m
m_{10n}	2.01×10^4 kg	c_{10n}	7.57×10^4 Ns/m	k_{10n}	1.72×10^7 N/m
σ_n	3.74×10^{-2} m/s^2				

For identification purposes, 31 model parameters are selected. They correspond to the masses $m_i, i = 1, \ldots, 10$, damping coefficients $c_i, i = 1, \ldots, 10$, stiffness parameters $k_i, i = 1, \ldots, 10$, and the standard deviation of the prediction and measurement errors σ. It is noted that this problem can be regarded as high-dimensional from a Bayesian model updating point of view. Moreover, the mass, damping, and stiffness parameters can be uniformly scaled without changing the acceleration response of the structural model. For reference and comparison purposes, the properties of the actual structural system as well as the prior distribution of the uncertain parameters are defined as in [263]. The prior probability density functions of the model parameters m_i, c_i, and k_i, $i = 1, \ldots, 10$,

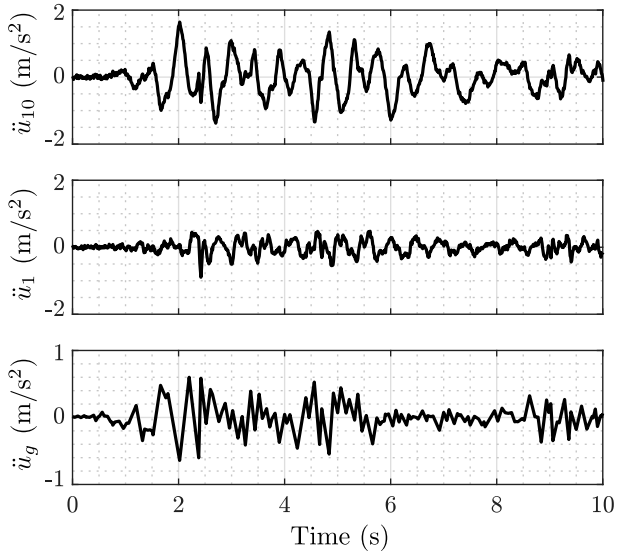

Fig. 7.2: Input ground motion and measurement data. Example 1.

correspond to Gaussian distributions with means equal to $\bar{m} = 2 \times 10^4$ kg, $\bar{c} = 6 \times 10^4$ Ns/m, $\bar{k} = 2 \times 10^7$ N/m, and coefficients of variation of 10%, 30%, and 30%, respectively. On the other hand, σ follows a lognormal distribution with median equal to 0.1 m/s^2 and a logarithmic standard deviation of 0.3, which leads to a coefficient of variation of approximately 30%. It is seen that the mean values of the uncertain parameters do not match the corresponding target or nominal values (exact values) of the model parameters (see Table 7.1).

For illustration purposes, the following user-defined parameters are considered for the numerical implementation of the proposed approach: number of samples per stage $N = 10000$, and conditional probability $p_0 = 0.1$. Note that a relatively large sample size is considered in order to focus on the effectiveness of the proposed scheme in a high-dimensional case and not on the effect of the number of samples per stage. In any case, additional validation calculations show that the number of samples per stage can be significantly reduced without affecting the performance of the identification process. Actually, around 2000 samples per stage are sufficient for the problem under consideration. Finally, due to the simplicity of the structural system, a reduced-order model is not considered in this example problem. Therefore, all analyses are performed using the original unreduced model.

Results

Figures 7.3, 7.4, 7.5 and 7.6 show the posterior marginal histograms associated with the mass, damping, stiffness and standard deviation parameters, respectively. For presentation purposes, the model parameters have been normalized with respect to their target values (see Table 7.1) as $\hat{\theta}_i = m_i/m_{in}, i = 1, ..., 10$, $\hat{\theta}_i = c_{i-10}/c_{(i-10)n}, i = 11, ..., 20$, $\hat{\theta}_i = k_{i-20}/k_{(i-20)n}, i = 21, ..., 30$, and $\hat{\theta}_{31} = \sigma/\sigma_n$. It is seen that the posterior samples tend to be concentrated relatively close to the target values, i.e., $\hat{\theta}_i = 1$, $i = 1, \ldots, 31$. Compared with the prior uncertainty in the structural model parameters, the posterior uncertainty is significantly reduced since the data provide relevant information about these parameters. The same result is obtained for the parameter associated with the standard deviation of the prediction and measurement errors, σ, as shown in Figure 7.6.

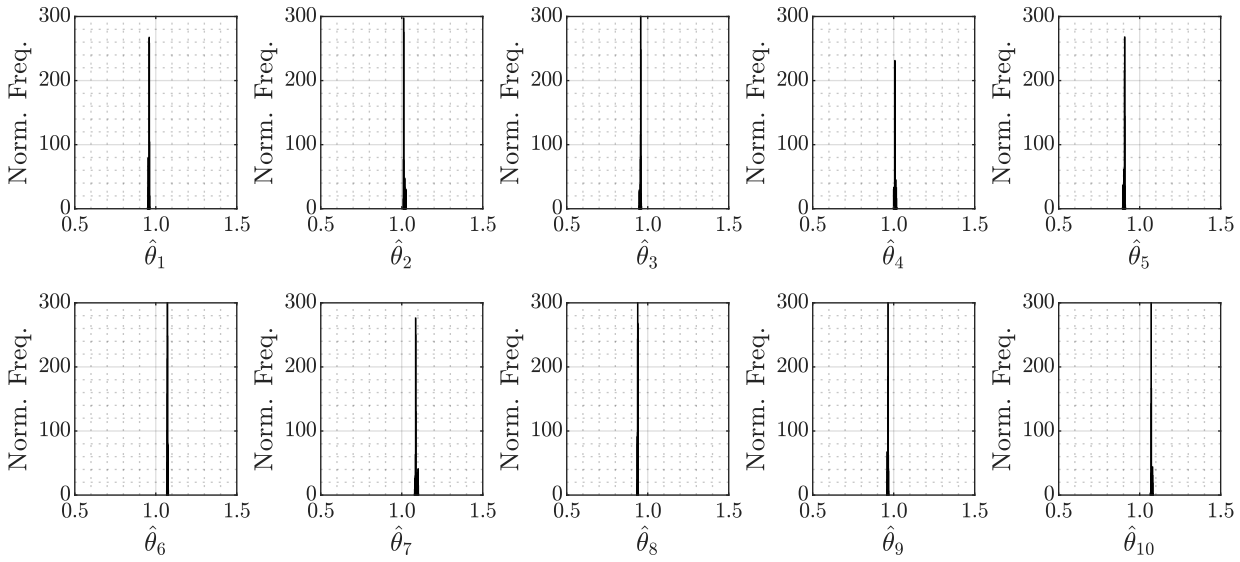

Fig. 7.3: Posterior marginal histograms corresponding to the normalized mass parameters.

The posterior mean values of the normalized variables are shown in Table 7.2. It is observed that there are larger deviations between the target and posterior mean values of the damping parameters than of the mass and stiffness parameters. In fact, this is expected from a structural viewpoint since the modal contributions to the response are more sensitive to the mass and stiffness than to the damping. The corresponding estimation error is less than 10% for the mass and stiffness parameters and less than 20% for the damping parameters. These deviations from the target values are

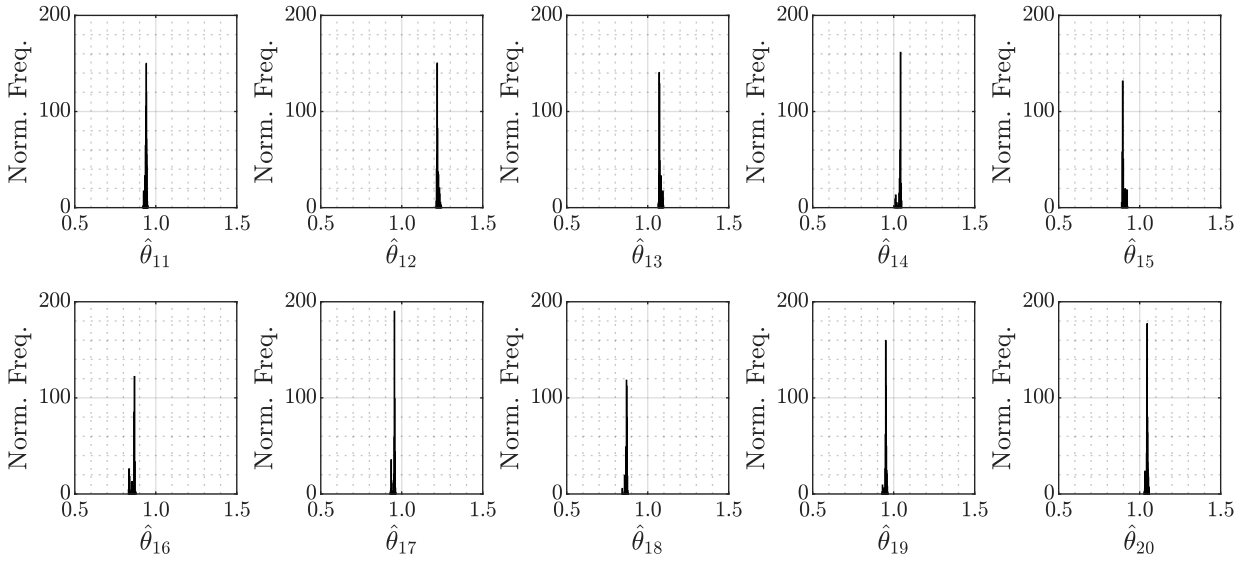

Fig. 7.4: Posterior marginal histograms corresponding to the normalized damping parameters.

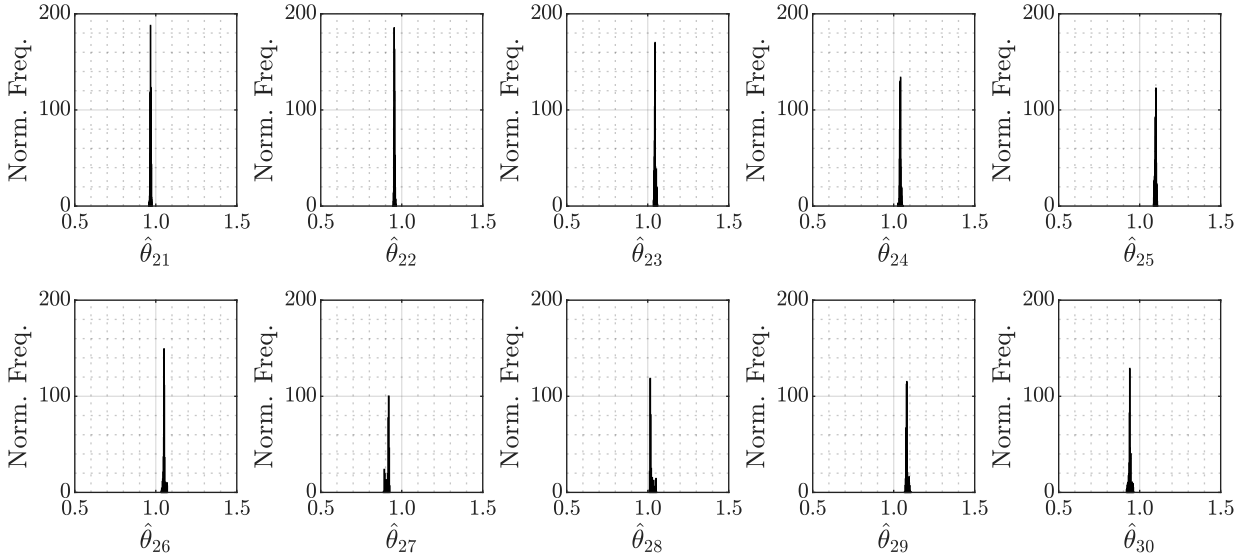

Fig. 7.5: Posterior marginal histograms corresponding to the normalized stiffness parameters.

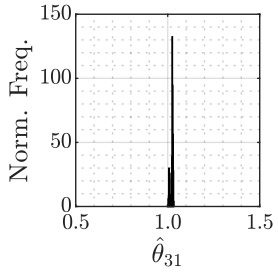

Fig. 7.6: Posterior marginal histogram corresponding to the normalized standard deviation of the prediction and measurement errors.

reasonably small and, as shown in what follows, they marginally affect the quality of the identification results in terms of the updated spectral properties of the structural system and of the updated response prediction.

Table 7.2: Posterior mean values of the normalized parameters. Example 1.

Parameter	Value	Parameter	Value	Parameter	Value
$\hat{\theta}_1$	0.958	$\hat{\theta}_{11}$	0.940	$\hat{\theta}_{21}$	0.968
$\hat{\theta}_2$	1.014	$\hat{\theta}_{12}$	1.192	$\hat{\theta}_{22}$	0.955
$\hat{\theta}_3$	0.956	$\hat{\theta}_{13}$	1.076	$\hat{\theta}_{23}$	1.045
$\hat{\theta}_4$	1.008	$\hat{\theta}_{14}$	1.038	$\hat{\theta}_{24}$	1.041
$\hat{\theta}_5$	0.906	$\hat{\theta}_{15}$	0.900	$\hat{\theta}_{25}$	1.098
$\hat{\theta}_6$	1.072	$\hat{\theta}_{16}$	0.862	$\hat{\theta}_{26}$	1.052
$\hat{\theta}_7$	1.088	$\hat{\theta}_{17}$	0.953	$\hat{\theta}_{27}$	0.914
$\hat{\theta}_8$	0.938	$\hat{\theta}_{18}$	0.868	$\hat{\theta}_{28}$	1.022
$\hat{\theta}_9$	0.965	$\hat{\theta}_{19}$	0.951	$\hat{\theta}_{29}$	1.081
$\hat{\theta}_{10}$	1.073	$\hat{\theta}_{20}$	1.046	$\hat{\theta}_{30}$	0.939
				$\hat{\theta}_{31}$	1.022

Based on the information from the posterior samples of the model parameters, the corresponding spectral properties of the structural model can be computed and compared with the exact values. In Table 7.3, the sample mean (with sample c.o.v. inside the parenthesis) of the natural frequency and damping ratio for each mode along with the target values of the natural frequency and damping ratio are shown. Note that the model has nonclassical damping and, therefore, it has complex modes. It is observed that the relative errors are quite small. Actually, the maximum relative error is around 3%, which is observed for the higher-order modes. Moreover, the estimates of the first modes are much better than those of the higher-order modes. In fact, the maximum relative error for the five first modes is below 0.5%. This is because only the first complex modes of the model are excited significantly by the ground acceleration, so it is this information from the first modes that is utilized in estimating the model parameters.

To illustrate the predictive power of the previous identification scheme, the exact time histories of the displacement, drift response, and total acceleration of some unobserved floors are compared

Table 7.3: Natural frequencies and damping ratios associated with the target parameter values and with the posterior distribution of the model parameters.

	Target model		Bayesian updating			
Complex mode	Natural frequency (Hz)	Damping ratio (%)	Natural frequency (Hz)		Damping ratio (%)	
1	0.7343	0.92	0.7345	(0.04%)	0.94	(0.21%)
2	2.1568	2.71	2.1562	(0.01%)	2.67	(0.32%)
3	3.5585	4.45	3.5603	(0.05%)	4.20	(0.33%)
4	4.8896	6.03	4.9027	(0.09%)	6.05	(0.44%)
5	6.0470	7.65	6.0526	(0.11%)	7.43	(0.42%)
6	7.1032	9.11	7.2022	(0.11%)	9.06	(0.22%)
7	8.0466	10.14	7.9530	(0.07%)	10.52	(0.28%)
8	8.6097	11.12	8.8519	(0.08%)	11.05	(0.22%)
9	9.2989	11.58	9.3704	(0.15%)	10.77	(0.55%)
10	9.6355	11.92	9.8938	(0.10%)	12.11	(0.31%)

with the corresponding posterior predictions in Figures 7.7, 7.8, and 7.9, respectively. The solid-black line shows the exact values of the response and the dashed-red line shows the corresponding posterior mean prediction. In addition, the posterior 95%-confidence interval, denoted by dotted-blue lines, is also presented in the figures. The curves for the exact and the mean responses are indistinguishable. Likewise, the 95%-confidence interval is almost indistinguishable from the other two curves. Thus, the Bayesian analysis is able to provide a high-quality updated prediction of the response even at unobserved degrees of freedom.

Performance of proposed and alternative BUS approaches

To study the performance of available BUS approaches, a statistical analysis of the log-evidence estimates is carried out. This quantity is selected since its computation involves the likelihood multiplier and the failure event of the equivalent reliability problem, two key aspects of BUS formulations. Along with the proposed approach, the following methods have been considered: adaptive driving variable-based BUS (A-BUS) [305], inner reliability problem-based BUS (I-BUS) [304], standard BUS with a priori definition of the likelihood multiplier (S-BUS) [298], and postprocessing-based BUS (P-BUS) [303]. Rejection sampling has been implemented in P-BUS with a target

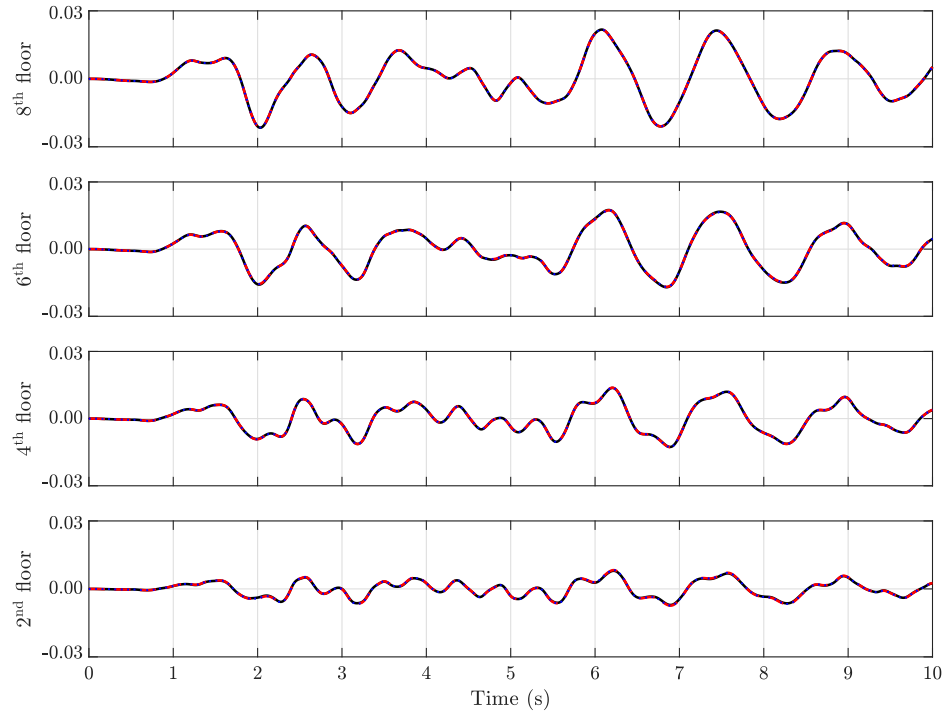

Fig. 7.7: Exact value (solid-black), posterior mean prediction (dashed-red), and posterior 95%-confidence interval (dotted-blue) of the displacement (in m) at floors 2, 4, 6 and 8.

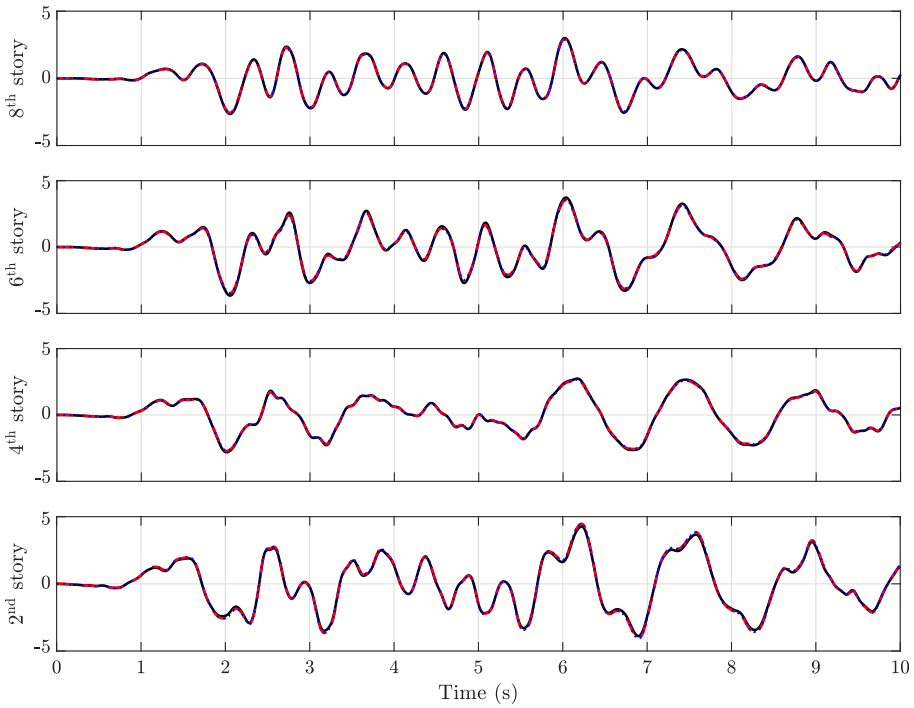

Fig. 7.8: Exact value (solid-black), posterior mean prediction (dashed-red), and posterior 95%-confidence interval (dotted-blue) of the drift response (in mm) at floors 2, 4, 6 and 8.

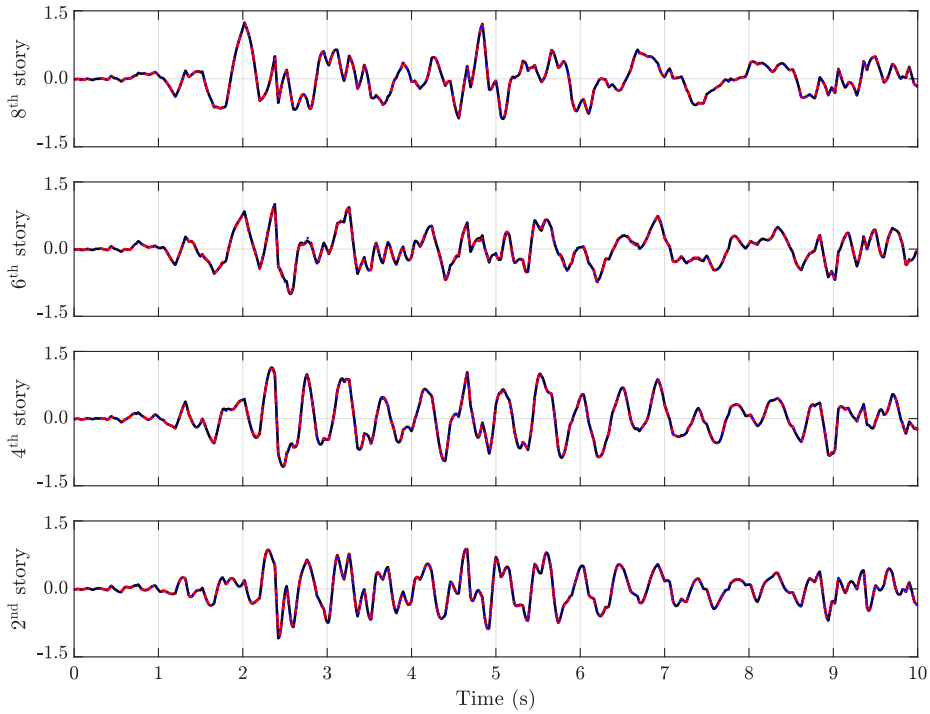

Fig. 7.9: Exact value (solid-black), posterior mean prediction (dashed-red), and posterior 95%-confidence interval (dotted-blue) of the total acceleration (in m/s^2) at floors 2, 4, 6 and 8.

number of failure samples equal to 1000. The rest of the methods consider subset simulation with $N = 10000$ samples per stage and conditional probability $p_0 = 0.1$. For each method, 30 independent runs are performed. Two cases for the tolerance value associated with the stopping criterion of I-BUS are implemented, i.e., $P_{\text{tol}} = 10^{-8}$ and $P_{\text{tol}} = 10^{-3}$. For comparison and reference purposes, the maximum values for $\ln(c^{-1})$ obtained in these two cases are considered in S-BUS. Additionally, P-BUS considers the maximum value of $\ln(c^{-1})$ obtained for I-BUS with $P_{\text{tol}} = 10^{-3}$ in order to illustrate the effect of the postprocessing step on the quality of the results.

Table 7.4 presents the average number of function calls, average log-evidence and maximum values for $\ln(c^{-1})$ obtained by the different methods across 30 independent runs. Note that the maximum values for $\ln(c^{-1})$ are not given for S-BUS and P-BUS, since the likelihood multiplier is defined a priori in these methods. In addition, the user-defined parameters required by the different methods are also presented in the table. Several observations can be made from these results. First, the evidence tends to be more underestimated for smaller values of $\ln(c^{-1})$. Such a behavior is consistent

Table 7.4: Statistical performance across 30 independent runs of different BUS methods. Example 1.

Method	User-defined parameter	Number of function calls	Average log-evidence	Maximum $\ln(c^{-1})$
This work	–	4.2×10^5	3.58×10^3	3.78×10^3
A-BUS [305]	–	4.4×10^5	3.59×10^3	3.78×10^3
I-BUS [304]	$P_{\text{tol}} = 10^{-8}$	5.1×10^5	3.22×10^3	3.38×10^3
I-BUS [304]	$P_{\text{tol}} = 10^{-3}$	1.5×10^5	2.34×10^3	2.38×10^3
S-BUS [298]	$\ln(c^{-1}) = 3.38 \times 10^3$	1.1×10^5	3.36×10^3	–
S-BUS [298]	$\ln(c^{-1}) = 2.38 \times 10^3$	4.0×10^4	2.37×10^3	–
P-BUS [303]	$\ln(c^{-1}) = 2.38 \times 10^3$	1.2×10^6	3.03×10^3	–

with the relationship between the evidence estimate and the likelihood multiplier, as discussed in previous contributions [303, 304]. Further, it illustrates the significant effect that this parameter can have on the performance of BUS formulations. Second, the maximum values for $\ln(c^{-1})$ obtained by I-BUS are smaller than those computed by A-BUS and the proposed approach. Third, the evidence estimates obtained by S-BUS ($\ln(c^{-1}) = 2.38 \times 10^3$) and I-BUS ($P_{tol} = 10^{-3}$) are similar, as expected. Analogous results are observed in the cases of S-BUS ($\ln(c^{-1}) = 3.38 \times 10^3$) and I-BUS ($P_{tol} = 10^{-8}$). At the same time, the computational efforts are higher in I-BUS due to the iterative solution of the inner reliability problem. Fourth, the average log-evidence estimates of P-BUS are higher than of S-BUS for $\ln(c^{-1}) = 2.38 \times 10^3$. Thus, the postprocessing strategy proposed in [303] appears to be effective in improving the quality of the evidence estimates for this example. Fifth, the computational efforts of P-BUS, which involves the use of rejection sampling, are around two orders of magnitude higher than of S-BUS for $\ln(c^{-1}) = 2.38 \times 10^3$. This shows an additional strength of adopting subset simulation as reliability analysis technique, since it can efficiently handle small failure probabilities. In this regard, the adaptation and evaluation of alternative structural reliability methods for Bayesian model updating represents an interesting research venue. Finally, the performances of the proposed approach and A-BUS are very similar, which is reasonable since both methods select the final likelihood multiplier based on the maximum observed likelihood value. Nonetheless, as already pointed out, the formulation presented in this work is simpler since there is no need to redefine the driving variable function at each iteration.

As a result, only minimal modifications to the standard subset simulation algorithm are required by the proposed approach. Overall, the proposed updating technique can be regarded as a viable alternative BUS approach which is attractive for practical applications due to the simplicity of both its formulation and implementation.

7.5.2 Example 2: Application problem

The objective of this application is to evaluate the performance of the proposed approach in an identification problem involving a realistic nonlinear structural model with multiple uncertain parameters and noisy seismic response data.

Description of structural model

A three-dimensional bridge finite element model with more than 10000 degrees of freedom is considered as application problem. The bridge model, which has been taken from [398], is shown in Figure 7.10. It is curved in plan and has a total length of 119.0 m with five spans of lengths equal to 24.0 m, 20.0 m, 23.0 m, 25.0 m, and 27.0 m. Four piers of 8.0 m height support the girder monolithically, where each pier is founded on an array of four piles of 35.0 m height. The piers and piles are modeled as column elements of circular cross-section with diameters of 1.6 m and 0.6 m, respectively. In addition, the deck cross section is a box girder modeled by beam and shell elements. The deck girder rests on each abutment through two sliding bearings which are composed of an upper steel plate with a housing cap for the slider, a bottom plate with a concave semi-spherical stainless steel surface, and a steel slider.

An experimentally validated model that takes into account the main sources of performance degradation that friction-based devices experience during seismic events is implemented in the structural model [256]. The major effects related to the frictional performance of these devices include: the load effect related to the reduction of the friction coefficient as the vertical load increases, the velocity effect that takes into account the variation of the friction coefficient with the velocity of motion,

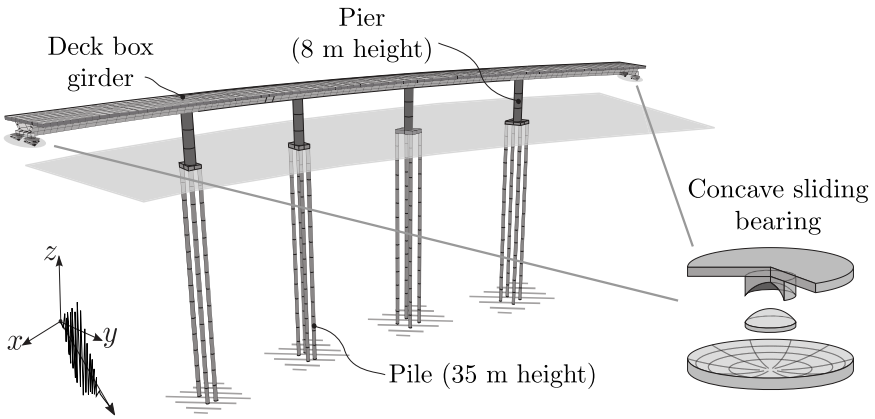

Fig. 7.10: Isometric view of the finite element model of the bridge structure with friction-based devices at the abutments.

and the cycling effect which is responsible for the degradation of friction characteristics due to temperature rise. The reader is referred to [256, 349, 399] for a detailed description and implementation of the experimentally validated model. For illustration purposes, a typical displacement-restoring force curve of these devices is shown in Figure 7.11.

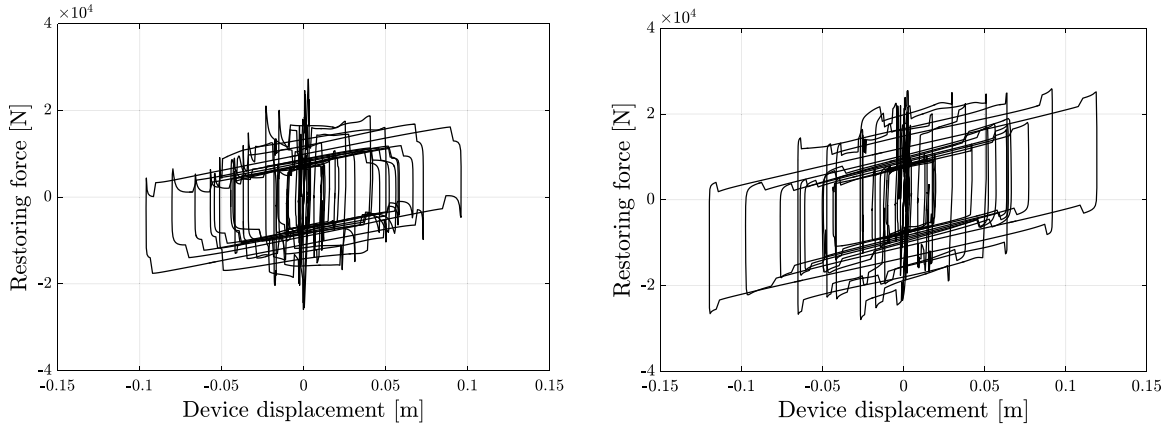

Fig. 7.11: Typical displacement-restoring force curve of the sliding bearing. Left: x direction. Right: y direction.

The interaction between the piles and the soil is modeled by a series of translational springs along the height of the piles with a nominal linear stiffness profile varying from 11200 T/m at the bottom of the piles to 560 T/m at the surface. The net effect of these springs is to increase the translational stiffness in the x and y direction of the column elements that model the piles. Nominal material properties of the structural model have been assumed as follows: Young's modulus $E = 2.0 \times 10^{10}$

N/m^2, Poisson ratio $\nu = 0.2$, and mass density $\rho = 2500$ kg/m^3. A 3% of critical damping is added to the model. It is assumed that the structural components such as the piers, piles and the deck girder remain linear during the analysis while the nonlinearities are localized in the sliding bearings response.

Parametric reduced-order model

In order to improve the numerical efficiency of the updating procedure, a parametric reduced-order model of the bridge structure is implemented. In particular, the structural model is subdivided into sixteen linear substructures and two nonlinear substructures as shown in Figure 7.12. Substructures $S_i, i = 1, \ldots, 5$ are related to the five spans of the bridge deck, substructures $S_i, i = 6, \ldots, 9$ are associated with the four piers, while substructures $S_i, i = 10, \ldots, 13$ comprise the four arrays of piles and the corresponding pile footings. In addition, the translational springs that model the interaction between the piles and the soil are included in three substructures, i.e, $S_i, i = 14, \ldots, 16$ as shown in the figure. Finally, the sliding bearings at each abutment are considered in substructures $S_i, i = 17, 18$. Thus, substructures $S_i, i = 1, \ldots, 16$ are linear while S_{17} and S_{18} are nonlinear.

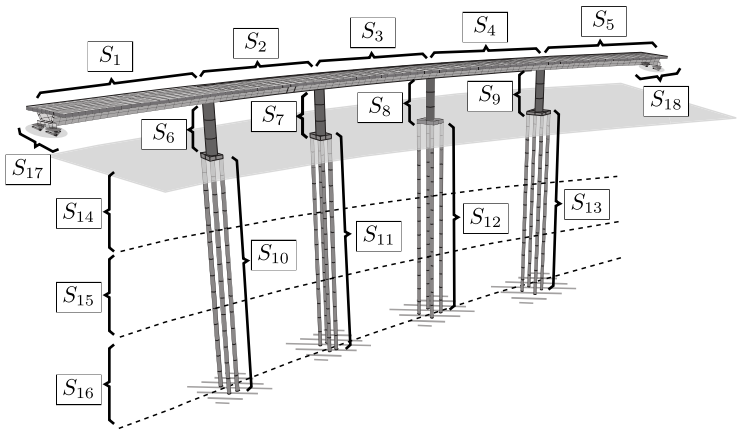

Fig. 7.12: Linear and nonlinear substructures of the finite element model.

The reduced-order model is characterized in terms of interface constraint modes and a set of dominant fixed-interface normal modes (see Section 7.4.2). In this regard, 400 interface degrees of freedom are present at the interfaces of the finite element model. Additionally, five fixed-

interface normal modes are kept for each substructure $S_i, i = 1, \ldots, 5$, three for each substructure $S_i, i = 6, \ldots, 9$, and three for each substructure $S_i, i = 10, \ldots, 13$. Note that substructures $S_i, i = 14, 15, 16$ compress interface degrees of freedom only. As a result, the number of generalized coordinates is equal to 449, which corresponds to a reduction of more than 95% with respect to the total number of degrees of freedom. Thus, the reduced-order model provides a significant dimension reduction with respect to the original unreduced finite element model. Validation calculations show that the selected reduced-order model is able to capture the dynamics of the unreduced model with great accuracy. In this regard, Figure 7.13 shows a 3-D representation of the matrix of modal assurance criterion (MAC) values [400] between the 10 first modal vectors computed from the full finite element model and the reduced-order model. For comparison purposes, only the linear components of the undamped structural model are considered in the computation of mode shapes and natural frequencies. It is seen that the off-diagonal terms are almost zero and, hence, both models are consistent in terms of their mode shapes. Moreover, additional computations show that the errors for the ten lowest natural frequencies fall bellow 0.5%. The comparison in terms of the ten lowest-order modes seems reasonable since the contribution of higher-order modes in the dynamic response of the model is negligible in this case. From the practical point of view it is important to note that the selection of the fixed-interface modes per substructure, necessary to achieve a prescribed accuracy, is done offline, before the updating process takes place [163].

Eighteen parameters associated with structural properties of different sections of the structure are considered to characterize the finite element model, which are denoted as $\zeta_i, i = 1, \ldots, 18$. They are related to the modulus of elasticity of each span of the bridge deck ($\zeta_i, i = 1, \ldots, 5$), the modulus of elasticity of each pier ($\zeta_i, i = 6, \ldots, 9$), the modulus of elasticity of each pile ($\zeta_i, i = 10, \ldots, 13$), the stiffness constants of the springs along the height of the piles ($\zeta_i, i = 14, 15, 16$), and the friction coefficients of the sliding bearings at the abutments ($\zeta_i, i = 17, 18$). Thus, based on the subdivision of the finite element model, it is seen that each substructure is associated with a single parameter. Furthermore, the parameters are defined such that $\zeta_i = 1, i = 1, \ldots, 18$, corresponds to the nominal or reference values for the different structural properties. Using this

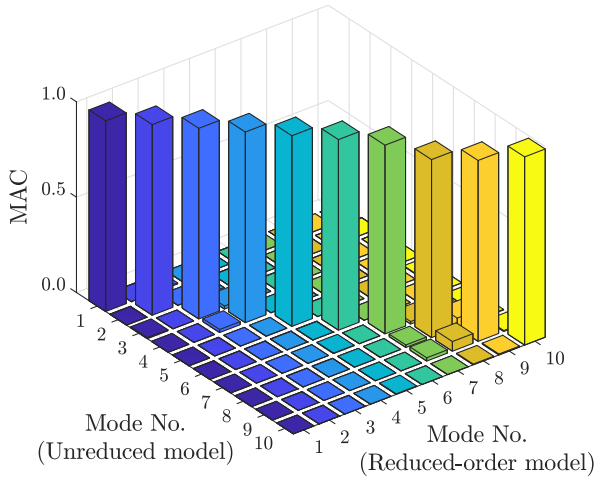

Fig. 7.13: Modal assurance criterion (MAC) values between the mode shapes associated with the full and reduced-order models.

information, the reduced-order matrices associated with the linear substructures can be efficiently parametrized as indicated in Section 7.4.2.

Numerical validations indicate that the implementation of the parametric reduced-order model allows to obtain a speedup factor of more than 10 for the computation of the structural response in this case. In this context, the speedup factor corresponds to the ratio between the execution time by considering the full finite element model and the proposed parametric reduced-order model. Since most of the computational efforts involved in the updating procedure are associated with the solution of the equation of motion for different values of the uncertain parameters, the parametrization scheme under consideration provides significant computational savings for the overall identification process.

Simulated data

Synthetically generated measurements are considered for identification purposes. The corresponding ground excitation is the El Centro ground-motion record, which is applied at 50° with respect to the x axis (see Figure 7.10) and has been scaled to a peak ground acceleration of 5 m/s^2. Acceleration responses along the x and y directions at the midpoints of the five spans of the deck are considered for identification purposes. In addition, 20 s of response with a sampling interval

of $\Delta t = 0.01$ s are considered. Thus, the identification data comprise $n_o = 10$ observed degrees of freedom and $n_t = 2000$ time steps. As in the previous example, the measurements are generated by contaminating the actual acceleration responses with a Gaussian discrete white noise sequence whose standard deviation is equal to 10% of the root-mean-square value of the responses. Table 7.5 shows the actual values of the parameters that are used to generate the measured data, where $\zeta_{in}, i = 1, \ldots, 18$ are the actual parameter values associated with the different substructures and σ_n is the actual standard deviation (in m/s^2) of the prediction and measurement errors. For illustration purposes, the input ground motion as well as the measurements at the midpoint of the bridge's deck along the x and y directions are presented in Figure 7.14.

Table 7.5: Actual values of the model parameters. Example 2.

Parameter	Value	Parameter	Value	Parameter	Value
ζ_{1n}	0.87	ζ_{7n}	0.98	ζ_{13n}	1.06
ζ_{2n}	1.07	ζ_{8n}	1.14	ζ_{14n}	1.05
ζ_{3n}	0.93	ζ_{9n}	0.94	ζ_{15n}	0.90
ζ_{4n}	0.98	ζ_{10n}	1.06	ζ_{16n}	0.89
ζ_{5n}	1.01	ζ_{11n}	0.95	ζ_{17n}	1.12
ζ_{6n}	1.13	ζ_{12n}	1.04	ζ_{18n}	0.90
				σ_n	8.01×10^{-2}

Results

For identification purposes, all structural parameters are considered as uncertain, i.e., $\theta_i = \zeta_i$, $i = 1, \ldots, 18$. In addition, the standard deviation of the prediction and measurement errors is also considered in the set of uncertain parameters as $\theta_{19} = \sigma$. Thus, the Bayesian model updating problem comprises a total of $n_\theta = 19$ parameters to be identified. Note that this is a high-dimensional problem from the identification point of view. The prior probability density function of each structural parameter $\theta_i, i = 1, \ldots, 18$, is taken as uniform over the interval $[0.5, 1.5]$, while the prior distribution of θ_{19} is lognormal with median equal to 0.1 m/s^2 and a logarithmic standard deviation of 0.3. According to this definition, the prior means of the uncertain parameters differ from their corresponding target values.

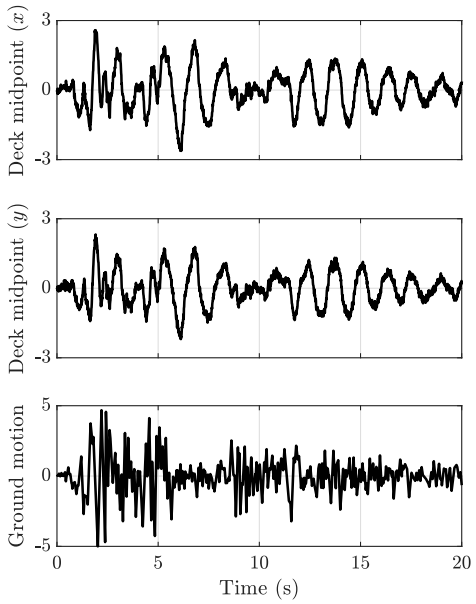

Fig. 7.14: Input ground motion and acceleration measurements (in m/s^2) at the midpoint of the deck's central span. Example 2.

In the context of the proposed identification scheme, a sample size equal to $N = 2000$ and a conditional probability of $p_0 = 0.1$ are considered. Table 7.6 shows the posterior mean values of the uncertain parameters obtained at the end of the sampling process. For presentation purposes, the parameters haven been normalized by their target values (see Table 7.5) as $\hat{\theta}_i = \theta_i/\zeta_{in}, i = 1, \ldots, 18$ and $\hat{\theta}_{19} = \theta_{19}/\sigma_n$. Relatively small differences with respect to the target values are obtained for the parameters associated with the deck (θ_i, $i = 1, \ldots, 5$), bearings (θ_{17} and θ_{18}), and standard deviation of the prediction errors (θ_{19}). Validation calculations suggest that these parameters have a significant effect on the system response. On the other hand, deviations with respect to the target values are observed for the parameters associated with the piers ($\theta_i, i = 6, \ldots, 9$) and piles ($\theta_i, i = 10, \ldots, 13$). This can be attributed to the interaction between these parameters. In terms of the substructures associated with the soil springs, it is seen that the posterior mean of the parameter associated with the superficial soil layer (θ_{14}) matches its target value, whereas the posterior mean estimates corresponding to the lower soil layers (θ_{15} and θ_{16}) present larger deviations with respect to their target values. This is reasonable from the engineering viewpoint and can be presumably attributed to a higher sensitivity of the deck acceleration response with respect to the stiffness of

the superficial soil layer (θ_{14}), as it affects the horizontal stiffness of the entire foundation system to a greater extent. It is noted that similar results are obtained when considering different runs of the proposed approach.

Table 7.6: Posterior mean values of the normalized model parameters. Example 2.

Parameter	Value	Parameter	Value
$\hat{\theta}_1$	0.956	$\hat{\theta}_{11}$	1.247
$\hat{\theta}_2$	1.011	$\hat{\theta}_{12}$	0.751
$\hat{\theta}_3$	0.982	$\hat{\theta}_{13}$	1.192
$\hat{\theta}_4$	1.029	$\hat{\theta}_{14}$	1.003
$\hat{\theta}_5$	1.043	$\hat{\theta}_{15}$	1.322
$\hat{\theta}_6$	1.146	$\hat{\theta}_{16}$	0.894
$\hat{\theta}_7$	1.149	$\hat{\theta}_{17}$	1.003
$\hat{\theta}_8$	0.811	$\hat{\theta}_{18}$	0.996
$\hat{\theta}_9$	0.843	$\hat{\theta}_{19}$	1.008
$\hat{\theta}_{10}$	0.891		

The predictive capabilities of the proposed method in terms of the system response are shown in Figure 7.15. This figure presents the target responses (solid-black line) of the horizontal displacements at the abutments, as well as the mean predictions (dotted-red line) and the 95%-confidence intervals (grey area) associated with the prior (left plots) and posterior (right plots) distributions. Note that the prior mean predictions present some deviations with respect to the target responses and, in addition, the uncertainty in such predictions is considerable. However, the incorporation of available measurement data allows to improve the predictive capabilities of the model class. Recall that, according to Eq. (7.5), the likelihood function is defined in terms of a measure-of-fit function between the measured responses and the model prediction. Hence, the objective and goal of the proposed method is to find a set of parameters that provides high-quality updated predictions of the response. In this regard, the different lines in the right plots, which are associated with the posterior distribution, are indistinguishable between each other. That is, the target and expected responses agree very well and, moreover, the uncertainty in the response prediction is significantly reduced. Thus, the results indicate that the proposed approach is able to update the information on

the system response in an effective manner for this case.

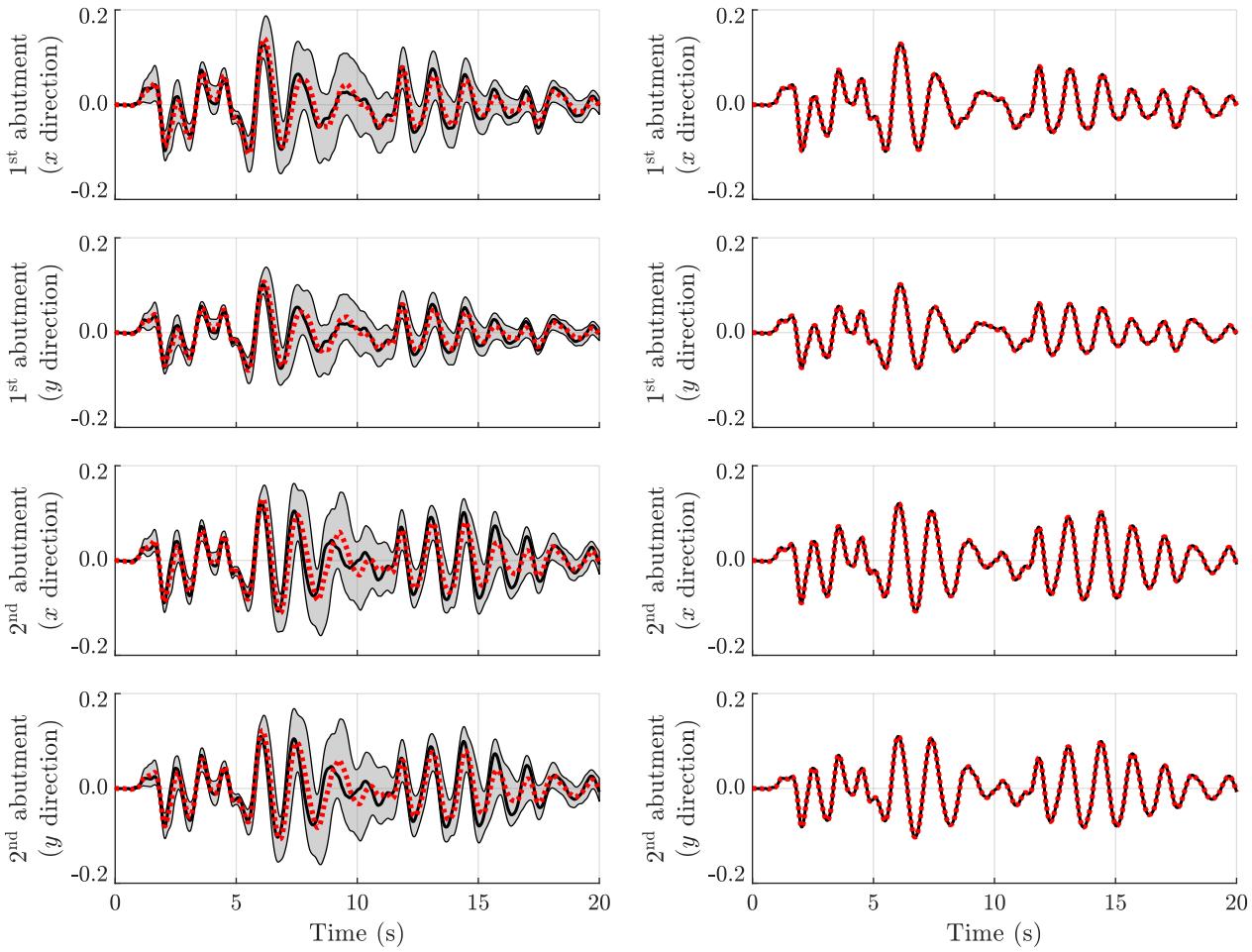

Fig. 7.15: Target response (solid-black line), mean predictions (dotted-red line), and 95%-confidence intervals (grey area) of the horizontal displacements at the abutments. Left: Prior distribution. Right: Posterior distribution. Example 2.

Figure 7.16 shows the evolution of the threshold level, v^{th}, during the different stages of subset simulation. Recall that this variable corresponds to the maximum log-likelihood value observed until the current stage. The results show that the method requires 20 stages to meet the stopping criterion. Nonetheless, the threshold level is stabilized roughly after 15 stages and it marginally increases during the final simulation levels. In this regard, the simulation process can be potentially stopped during an intermediate stage to retrieve samples that follow a truncated version of the posterior distribution [303]. However, the validity of such approach is problem-dependent and, therefore, the accuracy of the corresponding results must be assessed for each application. Finally,

Table 7.7 shows the log-evidence estimates obtained across ten independent runs of the proposed simulation scheme. Rather stable estimates are observed in this case. Thus, the method is able to provide robust evidence estimates for this high-dimensional model updating problem involving a complex structural model equipped with nonlinear devices.

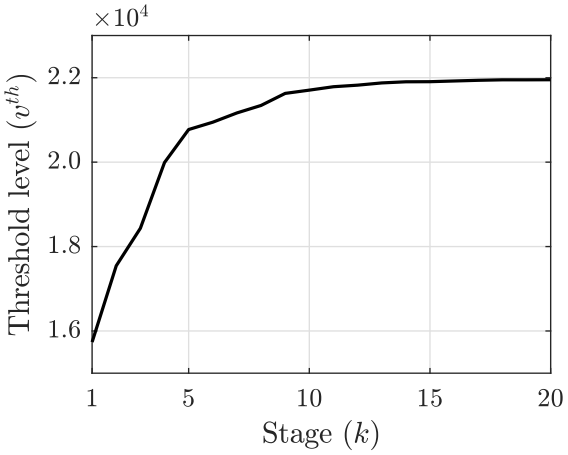

Fig. 7.16: Evolution of threshold level. Example 2.

Table 7.7: Log-evidence estimates obtained in ten independent runs of the proposed scheme. Example 2.

Run No.	Log-evidence	Run No.	Log-evidence
1	2.19×10^4	6	2.19×10^4
2	2.18×10^4	7	2.19×10^4
3	2.19×10^4	8	2.20×10^4
4	2.18×10^4	9	2.19×10^4
5	2.19×10^4	10	2.19×10^4

7.6 Conclusions

An approach for Bayesian model updating of structural dynamic systems involving multiple uncertain parameters and measured responses has been presented in this contribution. The proposed scheme is based on the use of structural reliability methods, where samples following the posterior distribution are obtained as failure samples corresponding to an equivalent reliability problem. In this framework, an estimate of the evidence is obtained as a byproduct of the sampling process.

Subset simulation, a well known and widely applied stochastic simulation technique, is adopted to generate the required failure samples. A strategy that adaptively determines the threshold level beyond which the corresponding failure samples follow the posterior distribution is implemented. Furthermore, only minimum modifications to the standard subset simulation algorithm are needed and no prior knowledge about the maximum likelihood value is required. These features are beneficial from a practical viewpoint. For an efficient numerical implementation of the proposed approach, an effective parametric reduced-order model formulation based on substructure coupling for dynamic analysis is considered. The resulting approach represents an alternative Bayesian identification technique based on structural reliability methods which provides an effective treatment of the maximum likelihood value while maintaining simplicity in its formulation and implementation.

Two examples have been studied to demonstrate the effectiveness and robustness of the proposed scheme, including a realistic model of a bridge structure equipped with nonlinear devices. Noisy acceleration measurements are synthetically generated for identification purposes. The important modal properties and the system response prediction are properly updated in both cases. In general, relatively few stages in the framework of subset simulation are required to stabilize the threshold level. This indicates the validity of the proposed method, since it is able to explore effectively the important region of the likelihood function. Similarly, the evidence estimates obtained across independent runs of the approach are rather stable for the problems analyzed in this contribution. Finally, the parametric reduced-order model strategy allows substantial computational savings without compromising the quality of the identification results. Overall, the results suggest that the proposed approach is an effective tool to address Bayesian model updating problems involving complex structural dynamic models, measured response data and high-dimensional parameter spaces. Furthermore, these developments open the door to applications involving real structural dynamic systems, which can in turn contribute to enhance the safety, reliability and life-cycle management of existing structures.

Future research efforts involve the integration of surrogate models at the likelihood function level,

which can allow additional computational savings by reducing the number of calls to the parametric reduced-order model. Another research direction corresponds to the assessment of alternative techniques for generating the conditional samples at each simulation level, such as the implementation of different proposal distributions or methods based on auxiliary dynamic systems. Further, a thorough comparison between alternative BUS formulations as well as between different structural reliability methods, in the framework of complex structural dynamic systems, is an interesting and important topic for future work. Also, the characterization of complex posterior distributions associated with the identification of involved structural dynamic systems with multiple uncertain parameters as well as the consideration of measured response data, i.e., field data, are additional aspects of practical relevance. Finally, the assessment of the proposed scheme for Bayesian model class selection and model averaging problems, i.e., updated prediction of response quantities based on different model classes, in the context of high-dimensional parameter spaces is an additional subject for future research. Some of these topics are currently under consideration.

Acknowledgments

The research reported here was partially supported by ANID (National Agency for Research and Development, Chile) under its program FONDECYT, grant number 1200087. Also, this research has been supported by ANID and DAAD (German Academic Exchange Service) under CONICYT-PFCHA/Doctorado Acuerdo Bilateral DAAD Becas Chile/2018-62180007. These supports are gratefully acknowledged by the authors.

Chapter 8

Concluding remarks and outlook

This thesis comprises several contributions pertaining to the topics of reliability-based design optimization (RBDO) of structural dynamical systems under stochastic excitation, contaminant source detection in water distribution networks (WDNs), and model updating of structural dynamical systems involving multiple uncertain parameters. Probability theory concepts and tools are adopted to devise the reported developments. Specifically, stochastic simulation techniques are instrumental in the formulation and implementation of the proposed approaches.

In Chapters 2, 3 and 4, a stochastic search-based technique is developed for the RBDO of structural dynamical systems under stochastic excitation. The RBDO problem is stated as an equivalent Bayesian model updating problem, which is solved by means of a two-phase sampling strategy. Specifically, an exploration phase is first carried out to retrieve uniformly distributed feasible designs, which are then used in an exploitation phase to obtain a set of nearly optimal designs. To this end, the transitional Markov chain Monte Carlo (TMCMC) method is implemented with adaptive surrogate models and suitable proposal distributions. Several application examples involving realistic structural models are presented, which illustrate the method effectiveness in treating constrained and unconstrained cases, as well as mixed discrete-continuous design spaces. Some valuable features of the approach comprise its high theoretical chances to reach a vicinity of the optimum solution set and its ability to obtain non-trivial insight about the problem functions as a byproduct of the sampling process. Future research efforts include, e.g., the consideration of multiobjective optimization formulations and of alternative civil engineering systems.

The contribution reported in Chapter 5 focuses on the RBDO of linear structural systems under Gaussian excitation. Directional importance sampling is implemented as a general framework to

estimate first-order derivatives of the first-passage probability. Hence, gradient-based methods are enabled to identify optimal solutions and to assess their sensitivity with respect to model parameter perturbations. Numerical results involving a realistic finite element model suggest that the approach constitutes a flexible tool to treat a practical-type of problems in civil engineering. Future research directions include, indicatively, the integration of reduced-order models and the extension to cases with random structural parameters.

A Bayesian model class selection approach for contaminant source detection in WDNs is formulated in Chapter 6. Each possible contaminant location is represented by a probabilistic model class whose parameters define the intensity and starting time of the event. The TMCMC method is adopted to perform the required calculations. Ultimately, the most probable class represents the most plausible contaminant location, and its posterior distribution allows assessing the actual system state. Two examples involving simulated measurements suggest that valuable information can be obtained by the approach, even for relatively scarce and noisy data. Potential future extensions consider the treatment of stochastic demands and of more complex contamination events.

Chapter 7 proposes, in the framework of Bayesian model updating with structural reliability methods (BUS), an effective implementation of subset simulation to treat problems involving structural dynamical systems, measured response data, and multiple identification parameters. By adaptively defining the target threshold value, the need for prior information about the maximum of the likelihood function is circumvented. For improved efficiency, a parametric model reduction technique is integrated. Two model updating problems, including the finite element model of a bridge equipped with sliding bearings, illustrate the capabilities of the approach. Future developments include the use of alternative sampling strategies and the treatment of hierarchical Bayesian model updating problems.

In conclusion, the arguments and results discussed in the preceding chapters indicate that computational aspects constitute a crucial component in the implementation of probability-based methodologies for the analysis of civil engineering structures and systems. In this regard, the different ap-

proaches reported in this thesis can be potentially adopted as functional tools to address a number of practical problems, and their extensions can further improve the overall applicability of RBDO and model updating procedures. Nonetheless, it is believed that additional research in these subjects is needed to propel their adoption in customary engineering practice. Examples of possible future improvements include, indicatively, the formulation of robust RBDO methods for high-dimensional design spaces, the efficient identification of high-fidelity models, and the treatment of uncertain operational conditions for general model updating problems. Following the previous presentation, future efforts in these areas should focus on devising not only theoretically sound methodologies, but also the appropriate implementation strategies for applying them. Ultimately, such developments can contribute to obtain valuable insight for decision making under uncertainty, which can in turn enhance the overall performance, safety and robustness of civil engineering structures and systems over their lifetime.

List of publications

Book chapter

- D. J. Jerez, H. A. Jensen, M. Beer, A two-phase sampling approach for reliability-based optimization in structural engineering, in: Y. Liu, D. Wang, J. Mi, H. Li (Eds.), *Advances in Reliability and Maintainability Methods and Engineering Applications*, Springer Series in Reliability Engineering, Springer Nature Switzerland, 2023, pp. 21–48.

Peer-reviewed international journals

- H. Jensen, D. Jerez, M. Beer, A general two-phase Markov chain Monte Carlo approach for constrained design optimization: Application to stochastic structural optimization, *Computer Methods in Applied Mechanics and Engineering* 373 (2021) 113487.
- D. J. Jerez, H. A. Jensen, M. Beer, J. Chen, Asymptotic Bayesian Optimization: A Markov sampling-based framework for design optimization, *Probabilistic Engineering Mechanics* 67 (2022) 103178.
- D. J. Jerez, H. A. Jensen, M. A. Valdebenito, M. A. Misraji, F. Mayorga, M. Beer, On the use of Directional Importance Sampling for reliability-based design and optimum design sensitivity of linear stochastic structures, *Probabilistic Engineering Mechanics* 70 (2022) 103368.
- D. J. Jerez, H. A. Jensen, M. Beer, M. Broggi, Contaminant source identification in water distribution networks: A Bayesian framework, *Mechanical Systems and Signal Processing* 159 (2021) 107834.
- D. J. Jerez, H. A. Jensen, M. Beer, An effective implementation of reliability methods for Bayesian model updating of structural dynamic models with multiple uncertain parameters, *Reliability Engineering & System Safety* 225 (2022) 108634.

References

[1] E. Simiu, Design of buildings for wind: A guide for ASCE 7-10 standard users and designers of special structures, Wiley, 2011.

[2] A. Elghazouli, Seismic design of buildings to Eurocode 8, Spon Press, London New York, 2009.

[3] S. Chandrasekaran, Dynamic analysis and design of offshore structures, Springer India, 2015. doi:10.1007/978-81-322-2277-4.

[4] M.-C. Besner, M. Prévost, S. Regli, Assessing the public health risk of microbial intrusion events in distribution systems: Conceptual model, available data, and challenges, Water Research 45 (3) (2011) 961–979. doi:10.1016/j.watres.2010.10.035.

[5] R. A. Deininger, P. G. Meier, Sabotage of public water supply systems, in: Security of Public Water Supplies, Springer Netherlands, 2000, pp. 241–248. doi:10.1007/978-94-011-4241-0_20.

[6] J. B. Roberts, P. D. Spanos, Random vibration and statistical linearization, Dover Publications, 2003.

[7] G. I. Schuëller, H. A. Jensen, Computational methods in optimization considering uncertainties – An overview, Computer Methods in Applied Mechanics and Engineering 198 (1) (2008) 2–13. doi:10.1016/j.cma.2008.05.004.

[8] C. A. Schenk, G. I. Schuëller, Uncertainty assessment of large finite element systems, Springer-Verlag, 2005. doi:10.1007/11673941.

[9] C. R. Farrar, K. Worden, An introduction to structural health monitoring, Philosophical Transactions of the Royal Society A: Mathematical, Physical and Engineering Sciences 365 (1851) (2006) 303–315. doi:10.1098/rsta.2006.1928.

[10] K. E. Lansey, N. Duan, L. W. Mays, Y.-K. Tung, Water distribution system design under uncertainties, Journal of Water Resources Planning and Management 115 (5) (1989) 630–645. doi:10.1061/(ASCE)0733-9496(1989)115:5(630).

[11] C. Alcaraz, S. Zeadally, Critical infrastructure protection: Requirements and challenges for the 21st century, International Journal of Critical Infrastructure Protection 8 (2015) 53–66. doi:10.1016/j.ijcip.2014.12.002.

[12] A. Braham, S. Casillas, Fundamentals of sustainability in civil engineering, CRC Press, 2020. doi:10.1201/9780367817442.

[13] A. Latham, J. Layton, Social infrastructure and the public life of cities: Studying urban

sociality and public spaces, Geography Compass 13 (7) (2019) e12444. doi:10.1111/gec3.12444.

[14] H. W. J. Rittel, M. M. Webber, Dilemmas in a general theory of planning, Policy Sciences 4 (2) (1973) 155–169. doi:10.1007/bf01405730.

[15] R. B. Jansen (Ed.), Advanced dam engineering for design, construction, and rehabilitation, Springer US, 1988. doi:10.1007/978-1-4613-0857-7.

[16] Critical Infrastructure Guidance Task Committee, Guiding principles for the nation's critical infrastructure, American Society of Civil Engineers, 2009. doi:10.1061/9780784410639.

[17] C. M. Chang, S. Nazarian, M. Vavrova, M. T. Yapp, L. M. Pierce, W. Robert, R. E. Smith, Consequences of delayed maintenance of highway assets, Transportation Research Board, 2017. doi:10.17226/24933.

[18] R. B. Peck, Advantages and limitations of the observational method in applied soil mechanics, Géotechnique 19 (2) (1969) 171–187. doi:10.1680/geot.1969.19.2.171.

[19] A. J. Keith, D. K. Ahner, A survey of decision making and optimization under uncertainty, Annals of Operations Research 300 (2) (2019) 319–353. doi:10.1007/s10479-019-03431-8.

[20] D. Moens, D. Vandepitte, A survey of non-probabilistic uncertainty treatment in finite element analysis, Computer Methods in Applied Mechanics and Engineering 194 (12-16) (2005) 1527–1555. doi:10.1016/j.cma.2004.03.019.

[21] B. Möller, M. Beer, Engineering computation under uncertainty – Capabilities of non-traditional models, Computers & Structures 86 (10) (2008) 1024–1041. doi:10.1016/j.compstruc.2007.05.041.

[22] O. D. Ditlevsen, H. O. Madsen, Structural reliability methods, John Wiley & Sons Ltd., 1996.

[23] E. T. Jaynes, Probability theory: The logic of science, Cambridge University Press, Cambridge, 2003.

[24] K. V. Yuen, Bayesian methods for structural dynamics and civil engineering, John Wiley & Sons, 2010.

[25] E. Chatzi, C. Papadimitriou (Eds.), Identification Methods for Structural Health Monitoring, Springer International Publishing, 2016. doi:10.1007/978-3-319-32077-9.

[26] R. E. Melchers, A. T. Beck (Eds.), Structural reliability analysis and prediction, Wiley, 2017. doi:10.1002/9781119266105.

[27] E. H. Vanmarcke, Probabilistic modeling of soil profiles, Journal of the Geotechnical Engineering Division 103 (11) (1977) 1227–1246. doi:10.1061/ajgeb6.0000517.

[28] S. Okazawa, K. Oide, K. Ikeda, K. Terada, Imperfection sensitivity and probabilistic variation of tensile strength of steel members, International Journal of Solids and Structures 39 (6) (2002) 1651–1671. doi:10.1016/s0020-7683(01)00258-x.

[29] S. Seifollahi-Aghmiuni, O. B. Haddad, M. H. Omid, M. A. Mariño, Effects of pipe roughness uncertainty on water distribution network performance during its operational period, Water Resources Management 27 (5) (2013) 1581–1599. doi:10.1007/s11269-013-0259-6.

[30] N. Duan, L. W. Mays, Reliability analysis of pumping systems, Journal of Hydraulic Engineering 116 (2) (1990) 230–248. doi:10.1061/(ASCE)0733-9429(1990)116:2(230).

[31] K. M. Zuev, S. Wu, J. L. Beck, General network reliability problem and its efficient solution by subset simulation, Probabilistic Engineering Mechanics 40 (2015) 25–35. doi:10.1016/j.probengmech.2015.02.002.

[32] E. J. M. Blokker, J. H. G. Vreeburg, J. C. van Dijk, Simulating residential water demand with a stochastic end-use model, Journal of Water Resources Planning and Management 136 (1) (2010) 19–26. doi:10.1061/(asce)wr.1943-5452.0000002.

[33] E. J. M. Blokker, E. J. Pieterse-Quirijins, J. H. G. Vreeburg, J. C. van Dijk, Simulating nonresidential water demand with a stochastic end-use model, Journal of Water Resources Planning and Management 136 (1) (2011) 19–26.

[34] G. M. Atkinson, W. Silva, Stochastic modeling of California ground motions, Bulletin of the Seismological Society of America 90 (2) (2000) 255–274. doi:10.1785/0119990064.

[35] K. S. Kumar, T. Stathopoulos, Wind loads on low building roofs: A stochastic perspective, Journal of Structural Engineering 126 (8) (2000) 944–956. doi:10.1061/(asce)0733-9445(2000)126:8(944).

[36] O. Ditlevsen, Stochastic model for joint wave and wind loads on offshore structures, Structural Safety 24 (2-4) (2002) 139–163. doi:10.1016/s0167-4730(02)00022-x.

[37] S. Rezaeian, A. Der Kiureghian, A stochastic ground motion model with separable temporal and spectral nonstationarities, Earthquake Engineering & Structural Dynamics 37 (13) (2008) 1565–1584. doi:10.1002/eqe.831.

[38] G. Lindgren, D. Bolin, F. Lindgren, Non-traditional stochastic models for ocean waves, The European Physical Journal Special Topics 185 (1) (2010) 209–224. doi:10.1140/epjst/e2010-01250-y.

[39] G. D. Pasparakis, K. R. M. dos Santos, I. A. Kougioumtzoglou, M. Beer, Wind data extrapolation and stochastic field statistics estimation via compressive sampling and low rank matrix recovery methods, Mechanical Systems and Signal Processing 162 (2022) 107975. doi:10.1016/j.ymssp.2021.107975.

[40] H. A. Jensen, A. Marillanca, O. Peñaloza, A computational procedure for response statistics-based optimization of stochastic non-linear FE-models, Computer Methods in Applied Me-

chanics and Engineering 198 (1) (2008) 125–137. doi:10.1016/j.cma.2008.02.034.

[41] D. S. Kang, M. F. K. Pasha, K. Lansey, Approximate methods for uncertainty analysis of water distribution systems, Urban Water Journal 6 (3) (2009) 233–249. doi:10.1080/15730620802566844.

[42] P. Castaldo, B. Palazzo, P. D. Vecchia, Seismic reliability of base-isolated structures with friction pendulum bearings, Engineering Structures 95 (2015) 80–93. doi:10.1016/j.engstruct.2015.03.053.

[43] M. Chwała, Undrained bearing capacity of spatially random soil for rectangular footings, Soils and Foundations 59 (5) (2019) 1508–1521. doi:10.1016/j.sandf.2019.07.005.

[44] A. Deb, A. L. Zha, Z. A. Caamaño-Withall, J. P. Conte, J. I. Restrepo, Updated probabilistic seismic performance assessment framework for ordinary standard bridges in California, Earthquake Engineering & Structural Dynamics 50 (9) (2021) 2551–2570. doi:10.1002/eqe.3459.

[45] P. Christensen, Structural reliability theory and its applications, Springer Berlin Heidelberg, Berlin, Heidelberg, 1982.

[46] H. A. Jensen, D. J. Jerez, A stochastic framework for reliability and sensitivity analysis of large scale water distribution networks, Reliability Engineering & System Safety 176 (2018) 80–92. doi:10.1016/j.ress.2018.04.001.

[47] S.-H. Jiang, J. Huang, X.-H. Qi, C.-B. Zhou, Efficient probabilistic back analysis of spatially varying soil parameters for slope reliability assessment, Engineering Geology 271 (2020) 105597. doi:10.1016/j.enggeo.2020.105597.

[48] Z. Wan, J. Chen, J. Li, A. H.-S. Ang, An efficient new PDEM-COM based approach for time-variant reliability assessment of structures with monotonically deteriorating materials, Structural Safety 82 (2020) 101878. doi:10.1016/j.strusafe.2019.101878.

[49] I. A. Kougioumtzoglou, V. C. Fragkoulis, A. A. Pantelous, A. Pirrotta, Random vibration of linear and nonlinear structural systems with singular matrices: A frequency domain approach, Journal of Sound and Vibration 404 (2017) 84–101. doi:10.1016/j.jsv.2017.05.038.

[50] V. C. Fragkoulis, I. A. Kougioumtzoglou, A. A. Pantelous, M. Beer, Non-stationary response statistics of nonlinear oscillators with fractional derivative elements under evolutionary stochastic excitation, Nonlinear Dynamics 97 (4) (2019) 2291–2303. doi:10.1007/s11071-019-05124-0.

[51] G. D. Pasparakis, I. A. Kougioumtzoglou, V. C. Fragkoulis, F. Kong, M. Beer, Excitation–response relationships for linear structural systems with singular parameter matrices: A periodized harmonic wavelet perspective, Mechanical Systems and Signal Processing 169 (2022) 108701. doi:10.1016/j.ymssp.2021.108701.

[52] S. K. Au, Probabilistic failure analysis by importance sampling Markov chain simulation, Journal of Engineering Mechanics 130 (3) (2004) 303–311. doi:10.1061/(asce)0733-9399(2004)130:3(303).

[53] J. L. Beck, L. S. Katafygiotis, Updating models and their uncertainties. I: Bayesian statistical framework, Journal of Engineering Mechanics 124 (4) (1998) 455–461. doi:10.1061/(ASCE)0733-9399(1998)124:4(455).

[54] L. S. Katafygiotis, J. L. Beck, Updating models and their uncertainties. II: Model identifiability, Journal of Engineering Mechanics 124 (4) (1998) 463–467. doi:10.1061/(ASCE)0733-9399(1998)124:4(463).

[55] E. Simoen, C. Papadimitriou, G. Lombaert, On prediction error correlation in Bayesian model updating, Journal of Sound and Vibration 332 (18) (2013) 4136–4152. doi:10.1016/j.jsv.2013.03.019.

[56] H. A. Jensen, D. J. Jerez, A Bayesian model updating approach for detection-related problems in water distribution networks, Reliability Engineering & System Safety 185 (2019) 100–112.

[57] H. A. Jensen, D. J. Jerez, A stochastic framework for hydraulic performance assessment of complex water distribution networks: Application to connectivity detection problems, Probabilistic Engineering Mechanics 60 (2020) 103029. doi:10.1016/j.probengmech.2020.103029.

[58] C. Papadimitriou, J. L. Beck, S.-K. Au, Entropy-based optimal sensor location for structural model updating, Journal of Vibration and Control 6 (5) (2000) 781–800. doi:10.1177/107754630000600508.

[59] M. Chwała, Soil sounding location optimisation for spatially variable soil, Géotechnique Letters 10 (3) (2020) 409–418. doi:10.1680/jgele.20.00012.

[60] S. S. Rao, Multiobjective optimization in structural design with uncertain parameters and stochastic processes, AIAA Journal 22 (11) (1984) 1670–1678. doi:10.2514/3.8834.

[61] Y. K. Wen, Reliability and performance-based design, Structural Safety 23 (4) (2001) 407–428. doi:10.1016/s0167-4730(02)00011-5.

[62] Y. Tsompanakis, N. D. Lagaros, M. Papadrakakis (Eds.), Structural design optimization considering uncertainties, CRC Press, 2008. doi:10.1201/b10995.

[63] M. J. Tait, Modelling and preliminary design of a structure-TLD system, Engineering Structures 30 (10) (2008) 2644–2655. doi:10.1016/j.engstruct.2008.02.017.

[64] D. Jung, D. Kang, J. H. Kim, K. Lansey, Robustness-based design of water distribution systems, Journal of Water Resources Planning and Management 140 (11) (2014) 04014033. doi:10.1061/(ASCE)WR.1943-5452.0000421.

[65] S. Song, Z. Lu, H. Qiao, Subset simulation for structural reliability sensitivity analysis, Reliability Engineering & System Safety 94 (2) (2009) 658–665. doi:10.1016/j.ress.2008.07.006.

[66] H. A. Jensen, Design and sensitivity analysis of dynamical systems subjected to stochastic loading, Computers & Structures 83 (14) (2005) 1062–1075. doi:10.1016/j.compstruc.2004.11.016.

[67] S. K. Au, Reliability-based design sensitivity by efficient simulation, Computers & Structures 83 (14) (2005) 1048–1061. doi:10.1016/j.compstruc.2004.11.015.

[68] H. A. Jensen, F. Mayorga, C. Papadimitriou, Reliability sensitivity analysis of stochastic finite element models, Computer Methods in Applied Mechanics and Engineering 296 (Supplement C) (2015) 327–351. doi:10.1016/j.cma.2015.08.007.

[69] S. Engelund, J. D. Sørensen, A probabilistic model for chloride-ingress and initiation of corrosion in reinforced concrete structures, Structural Safety 20 (1) (1998) 69–89. doi:10.1016/s0167-4730(97)00022-2.

[70] M. P. Enright, D. M. Frangopol, Condition prediction of deteriorating concrete bridges using Bayesian updating, Journal of Structural Engineering 125 (10) (1999) 1118–1125. doi:10.1061/(asce)0733-9445(1999)125:10(1118).

[71] A. Der Kiureghian, The geometry of random vibrations and solutions by FORM and SORM, Probabilistic Engineering Mechanics 15 (1) (2000) 81–90. doi:10.1016/s0266-8920(99)00011-9.

[72] J. Li, S. Wei, W. Liu, Seismic reliability analysis of urban water distribution network, Earthquake Engineering and Engineering Vibration 5 (1) (2006) 71–77. doi:10.1007/s11803-006-0628-8.

[73] R. M. Neupauer, M. K. Records, W. H. Ashwood, Backward probabilistic modeling to identify contaminant sources in water distribution systems, Journal of Water Resources Planning and Management 136 (5) (2010) 587–591. doi:10.1061/(asce)wr.1943-5452.0000057.

[74] A. J. Torii, R. H. Lopez, Reliability analysis of water distribution networks using the adaptive response surface approach, Journal of Hydraulic Engineering 138 (3) (2012) 227–236. doi:10.1061/(ASCE)HY.1943-7900.0000504.

[75] X. Yang, D. L. Boccelli, Bayesian approach for real-time probabilistic contamination source identification, Journal of Water Resources Planning and Management 140 (8) (2014) 04014019. doi:10.1061/(asce)wr.1943-5452.0000381.

[76] V. C. Fragkoulis, I. A. Kougioumtzoglou, A. A. Pantelous, Statistical linearization of nonlinear structural systems with singular matrices, Journal of Engineering Mechanics 142 (9) (2016). doi:10.1061/(asce)em.1943-7889.0001119.

[77] P. Ni, D. J. Jerez, V. C. Fragkoulis, M. G. R. Faes, M. A. Valdebenito, M. Beer, Operator norm-based statistical linearization to bound the first excursion probability of nonlinear structures subjected to imprecise stochastic loading, ASCE-ASME Journal of Risk and Uncertainty in Engineering Systems, Part A: Civil Engineering 8 (1) (2022) 04021086. doi:10.1061/ajrua6.0001217.

[78] V. C. Fragkoulis, I. A. Kougioumtzoglou, A. A. Pantelous, M. Beer, Joint statistics of natural frequencies corresponding to structural systems with singular random parameter matrices, Journal of Engineering Mechanics 148 (3) (2022). doi:10.1061/(asce)em.1943-7889.0002081.

[79] V. C. Fragkoulis, I. A. Kougioumtzoglou, Survival probability determination of nonlinear oscillators with fractional derivative elements under evolutionary stochastic excitation, Probabilistic Engineering Mechanics 71 (2023) 103411. doi:10.1016/j.probengmech.2022.103411.

[80] G. S. Fishman, Monte Carlo, Springer New York, 1996. doi:10.1007/978-1-4757-2553-7.

[81] C. Robert, G. Casella, Monte Carlo Statistical Methods, Springer New York, 2010.

[82] G. I. Schuëller, H. J. Pradlwarter, P. S. Koutsourelakis, A critical appraisal of reliability estimation procedures for high dimensions, Probabilistic Engineering Mechanics 19 (4) (2004) 463–474. doi:10.1016/j.probengmech.2004.05.004.

[83] R. Y. Rubinstein, D. P. Kroese, Simulation and the Monte Carlo method, John Wiley & Sons, Inc., 2016. doi:10.1002/9781118631980.

[84] G. I. Schuëller, H. J. Pradlwarter, Benchmark study on reliability estimation in higher dimensions of structural systems - An overview, Structural Safety 29 (3) (2007) 167–182. doi:10.1016/j.strusafe.2006.07.010.

[85] B. Goller, H. J. Pradlwarter, G. I. Schuëller, Reliability assessment in structural dynamics, Journal of Sound and Vibration 332 (10) (2013) 2488–2499. doi:10.1016/j.jsv.2012.11.021.

[86] E. Simoen, G. D. Roeck, G. Lombaert, Dealing with uncertainty in model updating for damage assessment: A review, Mechanical Systems and Signal Processing 56-57 (2015) 123–149. doi:10.1016/j.ymssp.2014.11.001.

[87] S. Brooks, A. Gelman, G. L. Jones, X.-L. Meng (Eds.), Handbook of Markov chain Monte Carlo, CRC Press, Boca Raton London, 2011.

[88] N. Metropolis, A. W. Rosenbluth, M. N. Rosenbluth, A. H. Teller, E. Teller, Equation of state calculations by fast computing machines, The Journal of Chemical Physics 21 (6) (1953) 1087–1092. doi:10.1063/1.1699114.

[89] W. K. Hastings, Monte Carlo sampling methods using Markov chains and their applications, Biometrika 57 (1) (1970) 97–109. doi:10.2307/2334940.

[90] J. Ching, W.-C. Hsu, An efficient method for evaluating origin-destination connectivity reliability of real-world lifeline networks, Computer-Aided Civil and Infrastructure Engineering 22 (8) (2007) 584–596. doi:10.1111/j.1467-8667.2007.00501.x.

[91] G. Stefanou, The stochastic finite element method: Past, present and future, Computer Methods in Applied Mechanics and Engineering 198 (9-12) (2009) 1031–1051. doi:10.1016/j.cma.2008.11.007.

[92] K. F. Tee, L. R. Khan, H. Li, Application of subset simulation in reliability estimation of underground pipelines, Reliability Engineering & System Safety 130 (2014) 125–131. doi:10.1016/j.ress.2014.05.006.

[93] G. A. Ortiz, D. A. Alvarez, D. Bedoya-Ruíz, Identification of Bouc–Wen type models using the transitional Markov chain Monte Carlo method, Computers & Structures 146 (2015) 252–269. doi:10.1016/j.compstruc.2014.10.012.

[94] J. B. Nagel, B. Sudret, Hamiltonian Monte Carlo and borrowing strength in hierarchical inverse problems, ASCE-ASME Journal of Risk and Uncertainty in Engineering Systems, Part A: Civil Engineering 2 (3) (sep 2016). doi:10.1061/ajrua6.0000847.

[95] J. Ching, J.-S. Wang, Application of the transitional Markov chain Monte Carlo algorithm to probabilistic site characterization, Engineering Geology 203 (2016) 151–167. doi:10.1016/j.enggeo.2015.10.015.

[96] Y.-F. Jin, Z.-Y. Yin, W.-H. Zhou, S. Horpibulsuk, Identifying parameters of advanced soil models using an enhanced transitional Markov chain Monte Carlo method, Acta Geotechnica 14 (6) (2019) 1925–1947. doi:10.1007/s11440-019-00847-1.

[97] S. Geyer, I. Papaioannou, C. Kunz, D. Straub, Reliability assessment of large hydraulic structures with spatially distributed measurements, Structure and Infrastructure Engineering 16 (4) (2019) 599–612. doi:10.1080/15732479.2019.1652331.

[98] Z. Wang, G. Jia, Non-parametric stochastic subset optimization for reliability-based importance ranking of bridges in transportation networks, Applied Mathematical Modelling 76 (2019) 348–361. doi:10.1016/j.apm.2019.06.010.

[99] R. D. O. Teloli, S. da Silva, T. G. Ritto, G. Chevallier, Bayesian model identification of higher-order frequency response functions for structures assembled by bolted joints, Mechanical Systems and Signal Processing 151 (2021) 107333. doi:10.1016/j.ymssp.2020.107333.

[100] Y.-J. Yang, D.-Q. Li, Z.-J. Cao, G.-H. Gao, K.-K. Phoon, Geotechnical reliability-based design using generalized subset simulation with a design response vector, Computers and Geotechnics 139 (2021) 104392. doi:10.1016/j.compgeo.2021.104392.

[101] M. Gasser, G. I. Schuëller, Reliability-based optimization of structural systems, Mathematical Methods of Operations Research 46 (3) (1997) 287–307. doi:10.1007/bf01194858.

[102] Y.-C. Su, L. W. Mays, N. Duan, K. E. Lansey, Reliability-based optimization model for water distribution systems, Journal of Hydraulic Engineering 113 (12) (1987) 1539–1556. doi:10.1061/(asce)0733-9429(1987)113:12(1539).

[103] B. F. Spencer, D. C. Kaspari, M. K. Sain, Structural control design: a reliability-based approach, in: Proceedings of 1994 American Control Conference - ACC '94, IEEE, 1994, pp. 1062–1066. doi:10.1109/acc.1994.751910.

[104] I. Enevoldsen, J. D. Sørensen, Reliability-based optimization in structural engineering, Structural Safety 15 (3) (1994) 169–196. doi:10.1016/0167-4730(94)90039-6.

[105] B. A. Tolson, H. R. Maier, A. R. Simpson, B. J. Lence, Genetic algorithms for reliability-based optimization of water distribution systems, Journal of Water Resources Planning and Management 130 (1) (2004) 63–72. doi:10.1061/(ASCE)0733-9496(2004)130:1(63).

[106] N. Lamaddalena, R. Khadra, Y. Tlili, Reliability-based pipe size computation of on-demand irrigation systems, Water Resources Management 26 (2) (2012) 307–328. doi:10.1007/s11269-011-9919-6.

[107] D. G. Yoo, D. Jung, D. Kang, J. H. Kim, Seismic reliability-based multiobjective design of water distribution system: Sensitivity analysis, Journal of Water Resources Planning and Management 143 (2) (2017). doi:10.1061/(ASCE)WR.1943-5452.0000727.

[108] L. Palizzolo, P. Tabbuso, Reliability-based design optimization of trusses under dynamic shakedown constraints, Structural and Multidisciplinary Optimization 60 (3) (2019) 1097–1108. doi:10.1007/s00158-019-02259-x.

[109] L. F. F. Miguel, R. H. Lopez, A. J. Torii, A. T. Beck, Reliability-based optimization of multiple Folded Pendulum TMDs through Efficient Global Optimization, Engineering Structures 266 (2022) 114524. doi:10.1016/j.engstruct.2022.114524.

[110] Y. Peng, Y. Ma, T. Huang, D. D. Domenico, Reliability-based design optimization of adaptive sliding base isolation system for improving seismic performance of structures, Reliability Engineering & System Safety 205 (2021) 107167. doi:10.1016/j.ress.2020.107167.

[111] D. J. Jerez, H. A. Jensen, M. Beer, Reliability-based design optimization of structural systems under stochastic excitation: An overview, Mechanical Systems and Signal Processing 166 (2022) 108397. doi:10.1016/j.ymssp.2021.108397.

[112] M. Shinozuka, Y. Sato, Simulation of nonstationary random process, Journal of the Engineering Mechanics Division 93 (1) (1967) 11–40. doi:10.1061/JMCEA3.000082.

[113] G. A. Athanassoulis, C. N. Stefanakos, A nonstationary stochastic model for long-term time series of significant wave height, Journal of Geophysical Research 100 (C8) (1995) 16149. doi:10.1029/94jc01022.

[114] D. M. Boore, Simulation of ground motion using the stochastic method, Pure and Applied Geophysics 160 (3) (2003) 635–676. doi:10.1007/PL00012553.

[115] J. L. Beck, Bayesian system identification based on probability logic, Structural Control and Health Monitoring 17 (7) (2010) 825–847. doi:10.1002/stc.424.

[116] D. W. Coit, E. Zio, The evolution of system reliability optimization, Reliability Engineering & System Safety 192 (2019) 106259. doi:10.1016/j.ress.2018.09.008.

[117] R. T. Haftka, Z. Gürdal, Elements of structural optimization, Springer Netherlands, 1992. doi:10.1007/978-94-011-2550-5.

[118] H. O. Madsen, N. C. Lind, S. Krenk, Methods of Structural Safety, Dover Publications, 2006.

[119] Q. S. Ding, L. D. Zhu, H. F. Xiang, Simulation of stationary Gaussian stochastic wind velocity field, Wind and Structures 9 (3) (2006) 231–243. doi:10.12989/was.2006.9.3.231.

[120] J. Chen, Y. Song, Y. Peng, P. D. Spanos, Simulation of homogeneous fluctuating wind field in two spatial dimensions via a joint wave number-frequency power spectrum, Journal of Engineering Mechanics 144 (11) (nov 2018). doi:10.1061/(asce)em.1943-7889.0001525.

[121] M. Barbato, E. Tubaldi, A probabilistic performance-based approach for mitigating the seismic pounding risk between adjacent buildings, Earthquake Engineering & Structural Dynamics 42 (8) (2012) 1203–1219. doi:10.1002/eqe.2267.

[122] C. Theodosiou, P. Aichouh, S. Natsiavas, C. Papadimitriou, Reliability-based optimal design of fluid filled tanks under seismic excitation, in: Volume 5: 19th Biennial Conference on Mechanical Vibration and Noise, Parts A, B, and C, ASMEDC, 2003, pp. 1–8. doi:10.1115/detc2003/vib-48454.

[123] I. Venanzi, A. L. Materazzi, L. Ierimonti, Robust and reliable optimization of wind-excited cable-stayed masts, Journal of Wind Engineering and Industrial Aerodynamics 147 (2015) 368–379. doi:10.1016/j.jweia.2015.07.011.

[124] X. Zeng, Y. Peng, J. Chen, Serviceability-based damping optimization of randomly wind-excited high-rise buildings, The Structural Design of Tall and Special Buildings 26 (11) (2017) e1371. doi:10.1002/tal.1371.

[125] S. M. J. Spence, M. Gioffrè, Large scale reliability-based design optimization of wind excited tall buildings, Probabilistic Engineering Mechanics 28 (2012) 206–215. doi:10.1016/j.probengmech.2011.08.001.

[126] S. M. J. Spence, A. Kareem, Performance-based design and optimization of uncertain wind-excited dynamic building systems, Engineering Structures 78 (2014) 133–144. doi:10.1016/j.engstruct.2014.07.026.

[127] S. M. J. Spence, M. Gioffrè, A. Kareem, An efficient framework for the reliability-based design optimization of large-scale uncertain and stochastic linear systems, Probabilistic Engineering Mechanics 44 (2016) 174–182. doi:10.1016/j.probengmech.2015.09.014.

[128] S. M. J. Spence, M. Gioffrè, Efficient algorithms for the reliability optimization of tall buildings, Journal of Wind Engineering and Industrial Aerodynamics 99 (6) (2011) 691–699. doi:10.1016/j.jweia.2011.01.017.

[129] V. Pareto, Manual of political economy, A.M. Kelley, New York, 1971.

[130] R. T. Marler, J. S. Arora, Survey of multi-objective optimization methods for engineering,

Structural and Multidisciplinary Optimization 26 (6) (2004) 369–395. doi:10.1007/s00158-003-0368-6.

[131] L. D. Lutes, S. Sarkani, Random vibrations: Analysis of structural and mechanical systems, Elsevier Butterworth-Heinemann, Burlintong, MA, USA, 2004.

[132] N. C. Nigam, Structural optimization in random vibration environment, AIAA Journal 10 (4) (1972) 551–553. doi:10.2514/3.50151.

[133] S.-K. Au, J. L. Beck, Estimation of small failure probabilities in high dimensions by subset simulation, Probabilistic Engineering Mechanics 16 (4) (2001) 263–277. doi:10.1016/S0266-8920(01)00019-4.

[134] Y. W. Siu-Kui Au, Engineering risk assessment with Subset Simulation, John Wiley & Sons Inc., 2014.

[135] S.-K. Au, E. Patelli, Rare event simulation in finite-infinite dimensional space, Reliability Engineering & System Safety 148 (Supplement C) (2016) 67–77. doi:10.1016/j.ress.2015.11.012.

[136] I. Papaioannou, W. Betz, K. Zwirglmaier, D. Straub, MCMC algorithms for subset simulation, Probabilistic Engineering Mechanics 41 (Supplement C) (2015) 89–103. doi:10.1016/j.probengmech.2015.06.006.

[137] S. K. Au, J. L. Beck, First excursion probabilities for linear systems by very efficient importance sampling, Probabilistic Engineering Mechanics 16 (3) (2001) 193–207. doi:10.1016/S0266-8920(01)00002-9.

[138] P. S. Koutsourelakis, H. J. Pradlwarter, G. I. Schuëller, Reliability of structures in high dimensions, part I: algorithms and applications, Probabilistic Engineering Mechanics 19 (4) (2004) 409–417. doi:10.1016/j.probengmech.2004.05.001.

[139] L. Katafygiotis, S. H. Cheung, Domain Decomposition Method for calculating the failure probability of linear dynamic systems subjected to Gaussian stochastic loads, Journal of Engineering Mechanics 132 (5) (2006) 475–486. doi:10.1061/(ASCE)0733-9399(2006)132:5(475).

[140] M. A. Misraji, M. A. Valdebenito, H. A. Jensen, C. F. Mayorga, Application of directional importance sampling for estimation of first excursion probabilities of linear structural systems subject to stochastic Gaussian loading, Mechanical Systems and Signal Processing 139 (2020) 106621. doi:10.1016/j.ymssp.2020.106621.

[141] J. Li, J. B. Chen, Probability density evolution method for dynamic response analysis of structures with uncertain parameters, Computational Mechanics 34 (5) (2004) 400–409. doi:10.1007/s00466-004-0583-8.

[142] J. Li, J. Chen, Stochastic dynamics of structures, John Wiley & Sons, Ltd, 2009. doi:10.1002/9780470824269.

[143] J. Nocedal, S. J. Wright, Numerical optimization, Springer New York, 2006. doi:10.1007/978-0-387-40065-5.

[144] R. E. Melchers, M. Ahammed, A fast approximate method for parameter sensitivity estimation in Monte Carlo structural reliability, Computers & Structures 82 (1) (2004) 55–61. doi:10.1016/j.compstruc.2003.08.003.

[145] H. A. Jensen, Structural optimization of linear dynamical systems under stochastic excitation: a moving reliability database approach, Computer Methods in Applied Mechanics and Engineering 194 (12-16) (2005) 1757–1778. doi:10.1016/j.cma.2003.10.022.

[146] C. Fleury, V. Braibant, Structural optimization: A new dual method using mixed variables, International Journal for Numerical Methods in Engineering 23 (3) (1986) 409–428. doi:10.1002/nme.1620230307.

[147] R. B. Nelson, Simplified calculation of eigenvector derivatives, AIAA Journal 14 (9) (1976) 1201–1205. doi:10.2514/3.7211.

[148] H. A. Jensen, M. A. Valdebenito, G. I. Schuëller, An efficient reliability-based optimization scheme for uncertain linear systems subject to general Gaussian excitation, Computer Methods in Applied Mechanics and Engineering 198 (1) (2008) 72–87. doi:10.1016/j.cma.2008.01.003.

[149] H. Yu, F. Gillot, M. Ichchou, Reliability based robust design optimization for tuned mass damper in passive vibration control of deterministic/uncertain structures, Journal of Sound and Vibration 332 (9) (2013) 2222–2238. doi:10.1016/j.jsv.2012.12.014.

[150] H. A. Jensen, M. S. Ferre, D. S. Kusanovic, Reliability-based synthesis of non-linear stochastic dynamical systems: a global approximation approach, International Journal of Reliability and Safety 4 (2/3) (2010) 139–165. doi:10.1504/ijrs.2010.032443.

[151] H. A. Jensen, J. G. Sepulveda, Structural optimization of uncertain dynamical systems considering mixed-design variables, Probabilistic Engineering Mechanics 26 (2) (2011) 269–280. doi:10.1016/j.probengmech.2010.08.005.

[152] H. A. Jensen, M. Beer, Discrete-continuous variable structural optimization of systems under stochastic loading, Structural Safety 32 (5) (2010) 293–304. doi:10.1016/j.strusafe.2010.03.007.

[153] H. A. Jensen, M. A. Valdebenito, G. I. Schuëller, D. S. Kusanovic, Reliability-based optimization of stochastic systems using line search, Computer Methods in Applied Mechanics and Engineering 198 (49) (2009) 3915–3924. doi:10.1016/j.cma.2009.08.016.

[154] M. A. Valdebenito, G. I. Schuëller, Efficient strategies for reliability-based optimization involving non-linear, dynamical structures, Computers & Structures 89 (19) (2011) 1797–1811. doi:10.1016/j.compstruc.2010.10.014.

[155] H. A. Jensen, J. G. Sepulveda, On the reliability-based design of structures including passive energy dissipation systems, Structural Safety 34 (1) (2012) 390–400. doi:10.1016/j.strusafe.2011.09.005.

[156] H. Jensen, J. Sepulveda, L. Becerra, Robust stochastic design of base-isolated structural

systems, International Journal for Uncertainty Quantification 2 (2) (2012) 95–110. doi:10.1615/Int.J.UncertaintyQuantification.v2.i2.20.

[157] J. Chen, J. Yang, H. Jensen, Structural optimization considering dynamic reliability constraints via probability density evolution method and change of probability measure, Structural and Multidisciplinary Optimization 62 (5) (2020) 2499–2516. doi:10.1007/s00158-020-02621-4.

[158] M. A. Valdebenito, G. I. Schuëller, Reliability-based optimization considering design variables of discrete size, Engineering Structures 32 (9) (2010) 2919–2930. doi:10.1016/j.engstruct.2010.05.011.

[159] H. A. Jensen, L. G. Becerra, M. A. Valdebenito, On the use of a class of interior point algorithms in stochastic structural optimization, Computers & Structures 126 (2013) 69–85. doi:10.1016/j.compstruc.2013.01.008.

[160] F. van Keulen, K. Vervenne, Gradient-enhanced response surface building, Structural and Multidisciplinary Optimization 27 (5) (2004) 337–351. doi:10.1007/s00158-004-0392-1.

[161] H. A. Jensen, D. S. Kusanovic, M. A. Valdebenito, Compromise design of stochastic dynamical systems: A reliability-based approach, Probabilistic Engineering Mechanics 29 (2012) 40–52. doi:10.1016/j.probengmech.2012.02.001.

[162] H. A. Jensen, A. Muñoz, C. Papadimitriou, E. Millas, Model-reduction techniques for reliability-based design problems of complex structural systems, Reliability Engineering & System Safety 149 (2016) 204–217. doi:10.1016/j.ress.2016.01.003.

[163] H. Jensen, C. Papadimitriou, Sub-structure coupling for dynamic analysis, Springer International Publishing, 2019. doi:10.1007/978-3-030-12819-7.

[164] R. Craig, Structural dynamics: An introduction to computer methods, Wiley, New York, 1981.

[165] H. A. Jensen, D. S. Kusanovic, M. A. Valdebenito, G. I. Schuëller, Reliability-based design optimization of uncertain stochastic systems: Gradient-based scheme, Journal of Engineering Mechanics 138 (1) (2012) 60–70. doi:10.1061/(ASCE)EM.1943-7889.0000304.

[166] J. Yang, H. Jensen, J. Chen, Structural optimization under dynamic reliability constraints utilizing probability density evolution method and metamodels in augmented input space, Structural and Multidisciplinary Optimization 65 (4) (mar 2022). doi:10.1007/s00158-022-03188-y.

[167] M. A. Valdebenito, M. A. Misraji, H. A. Jensen, C. F. Mayorga, Sensitivity estimation of first excursion probabilities of linear structures subject to stochastic Gaussian loading, Computers & Structures 248 (2021) 106482. doi:10.1016/j.compstruc.2021.106482.

[168] D. J. Jerez, H. A. Jensen, M. A. Valdebenito, M. A. Misraji, F. Mayorga, M. Beer, On the use of Directional Importance Sampling for reliability-based design and optimum design

sensitivity of linear stochastic structures, Probabilistic Engineering Mechanics 70 (2022) 103368. doi:10.1016/j.probengmech.2022.103368.

[169] S. M. J. Spence, Optimization of uncertain and dynamic high-rise structures for occupant comfort: An adaptive kriging approach, Structural Safety 75 (2018) 57–66. doi:10.1016/j.strusafe.2018.05.008.

[170] A. Suksuwan, S. M. J. Spence, Efficient approach to system-level reliability-based design optimization of large-scale uncertain and dynamic wind-excited systems, ASCE-ASME Journal of Risk and Uncertainty in Engineering Systems, Part A: Civil Engineering 4 (2) (2018) 04018013. doi:10.1061/AJRUA6.0000960.

[171] M. G. R. Faes, M. A. Valdebenito, Fully decoupled reliability-based design optimization of structural systems subject to uncertain loads, Computer Methods in Applied Mechanics and Engineering 371 (2020) 113313. doi:10.1016/j.cma.2020.113313.

[172] M. G. R. Faes, M. A. Valdebenito, Fully decoupled reliability-based optimization of linear structures subject to Gaussian dynamic loading considering discrete design variables, Mechanical Systems and Signal Processing 156 (2021) 107616. doi:10.1016/j.ymssp.2021.107616.

[173] J. C. Spall, Introduction to Stochastic Search and Optimization, John Wiley & Sons, Inc., 2003. doi:10.1002/0471722138.

[174] S. Kirkpatrick, C. D. Gelatt, M. P. Vecchi, Optimization by simulated annealing, Science 220 (4598) (1983) 671–680. doi:10.1126/science.220.4598.671.

[175] K. M. Zuev, J. L. Beck, Global optimization using the asymptotically independent Markov sampling method, Computers & Structures 126 (2013) 107–119. doi:10.1016/j.compstruc.2013.04.005.

[176] J. L. Beck, K. M. Zuev, Asymptotically independent Markov sampling: A new Markov chain Monte Carlo scheme for Bayesian inference, International Journal for Uncertainty Quantification 3 (5) (2013) 445–474. doi:10.1061/9780784413609.20.

[177] J. Wang, L. S. Katafygiotis, Reliability-based optimal design of linear structures subjected to stochastic excitations, Structural Safety 47 (2014) 29–38. doi:10.1016/j.strusafe.2013.11.002.

[178] J. Ching, Y.-C. Chen, Transitional Markov chain Monte Carlo method for Bayesian model updating, model class selection, and model averaging, Journal of Engineering Mechanics 133 (7) (2007) 816–832. doi:10.1061/(ASCE)0733-9399(2007)133:7(816).

[179] W. Betz, I. Papaioannou, D. Straub, Transitional Markov chain Monte Carlo: Observations and improvements, Journal of Engineering Mechanics 142 (5) (2016) 04016016. doi:10.1061/(ASCE)EM.1943-7889.0001066.

[180] H. A. Jensen, D. J. Jerez, M. Valdebenito, An adaptive scheme for reliability-based global design optimization: A Markov chain Monte Carlo approach, Mechanical Systems and Signal Processing 143 (2020) 106836. doi:10.1016/j.ymssp.2020.106836.

[181] H. Jensen, D. Jerez, M. Beer, A general two-phase Markov chain Monte Carlo approach for constrained design optimization: Application to stochastic structural optimization, Computer Methods in Applied Mechanics and Engineering 373 (2021) 113487. doi:10.1016/j.cma.2020.113487.

[182] H. A. Jensen, D. J. Jerez, M. Beer, Structural synthesis considering mixed discrete–continuous design variables: A Bayesian framework, Mechanical Systems and Signal Processing 162 (2022) 108042. doi:10.1016/j.ymssp.2021.108042.

[183] D. J. Jerez, H. A. Jensen, M. Beer, J. Chen, Asymptotic Bayesian Optimization: A Markov sampling-based framework for design optimization, Probabilistic Engineering Mechanics 67 (2022) 103178. doi:10.1016/j.probengmech.2021.103178.

[184] D. J. Jerez, H. A. Jensen, M. Beer, A two-phase sampling approach for reliability-based optimization in structural engineering, in: Y. Liu, D. Wang, J. Mi, H. Li (Eds.), Advances in Reliability and Maintainability Methods and Engineering Applications, Springer Series in Reliability Engineering, Springer Nature Switzerland, 2023, pp. 21–48. doi:10.1007/978-3-031-28859-3_2.

[185] P. S. Koutsourelakis, Design of complex systems in the presence of large uncertainties: A statistical approach, Computer Methods in Applied Mechanics and Engineering 197 (49-50) (2008) 4092–4103. doi:10.1016/j.cma.2008.04.012.

[186] A. A. Taflanidis, J. L. Beck, Stochastic Subset Optimization for optimal reliability problems, Probabilistic Engineering Mechanics 23 (2) (2008) 324–338. doi:10.1016/j.probengmech.2007.12.011.

[187] A. A. Taflanidis, J. L. Beck, An efficient framework for optimal robust stochastic system design using stochastic simulation, Computer Methods in Applied Mechanics and Engineering 198 (1) (2008) 88–101. doi:10.1016/j.cma.2008.03.029.

[188] P. M. Pardalos, M. G. C. Resende, Handbook of applied optimization, OXFORD UNIV PR, 2002.

[189] A. A. Taflanidis, J. L. Beck, Stochastic Subset Optimization for reliability optimization and sensitivity analysis in system design, Computers & Structures 87 (5) (2009) 318–331. doi:10.1016/j.compstruc.2008.12.015.

[190] A. A. Taflanidis, J. L. Beck, Reliability-based design using two-stage stochastic optimization with a treatment of model prediction errors, Journal of Engineering Mechanics 136 (12) (2010) 1460–1473. doi:10.1061/(ASCE)EM.1943-7889.0000189.

[191] P.-R. Wagner, V. K. Dertimanis, E. N. Chatzi, J. L. Beck, Robust-to-uncertainties optimal design of seismic metamaterials, Journal of Engineering Mechanics 144 (3) (2018) 04017181. doi:10.1061/(ASCE)EM.1943-7889.0001404.

[192] G. Jia, A. A. Taflanidis, Non-parametric stochastic subset optimization for optimal-reliability design problems, Computers & Structures 126 (2013) 86–99. doi:10.1016/j.compstruc.2012.12.009.

[193] G. Jia, A. A. Taflanidis, Non-parametric stochastic subset optimization utilizing multivariate boundary kernels and adaptive stochastic sampling, Advances in Engineering Software 89 (2015) 3–16. doi:10.1016/j.advengsoft.2015.06.014.

[194] G. Jia, A. A. Taflanidis, J. L. Beck, Non-parametric stochastic subset optimization for design problems with reliability constraints, Structural and Multidisciplinary Optimization 52 (6) (2015) 1185–1204. doi:10.1007/s00158-015-1300-6.

[195] J. Beirlant, E. J. Dudewicz, L. Györfi, E. C. Van Der Meulen, Nonparametric entropy estimation: An overview, International Journal of Mathematical and Statistical Sciences 6 (1) (1997) 17–39.

[196] D. W. Scott, S. R. Sain, Multidimensional density estimation, in: Handbook of Statistics, Elsevier, 2005, pp. 229–261. doi:10.1016/s0169-7161(04)24009-3.

[197] R. Karunamuni, T. Alberts, On boundary correction in kernel density estimation, Statistical Methodology 2 (3) (2005) 191–212. doi:10.1016/j.stamet.2005.04.001.

[198] R. Karunamuni, S. Zhang, Some improvements on a boundary corrected kernel density estimator, Statistics & Probability Letters 78 (5) (2008) 499–507. doi:10.1016/j.spl.2007.09.002.

[199] R. Tibshirani, G. Walther, T. Hastie, Estimating the number of clusters in a data set via the gap statistic, Journal of the Royal Statistical Society: Series B (Statistical Methodology) 63 (2) (2001) 411–423. doi:10.1111/1467-9868.00293.

[200] J. A. Hartigan, M. A. Wong, Algorithm AS 136: A K-Means Clustering Algorithm, Applied Statistics 28 (1) (1979) 100–108. doi:10.2307/2346830.

[201] J. P. Neilsen, Multivariate boundary kernels from local linear estimation, Scandinavian Actuarial Journal 1999 (1) (1999) 93–95. doi:10.1080/03461230050131902.

[202] B. Schölkopf, A. J. Smola, Learning with Kernels: Support Vector Machines, Regularization, Optimization, and Beyond, MIT Press Ltd, 2018.

[203] D. W. Scott, Multivariate Density Estimation, Wiley, 1992. doi:10.1002/9780470316849.

[204] W.-S. Liu, S. H. Cheung, Reliability based design optimization with approximate failure probability function in partitioned design space, Reliability Engineering & System Safety 167 (2017) 602–611. doi:10.1016/j.ress.2017.07.007.

[205] J. N. Yang, S. Lin, Identification of parametric variations of structures based on least squares estimation and adaptive tracking technique, Journal of Engineering Mechanics 131 (3) (2005) 290–298. doi:10.1061/(asce)0733-9399(2005)131:3(290).

[206] S.-C. Kang, H.-M. Koh, J. F. Choo, An efficient response surface method using moving least squares approximation for structural reliability analysis, Probabilistic Engineering Mechanics 25 (4) (2010) 365–371. doi:10.1016/j.probengmech.2010.04.002.

[207] D. Ormoneit, H. White, An efficient algorithm to compute maximum entropy densities, Econometric Reviews 18 (2) (1999) 127–140. doi:10.1080/07474939908800436.

[208] A. Zellner, R. A. Highfield, Calculation of maximum entropy distributions and approximation of marginalposterior distributions, Journal of Econometrics 37 (2) (1988) 195–209. doi:10.1016/0304-4076(88)90002-4.

[209] J. Ching, Y.-H. Hsieh, Approximate reliability-based optimization using a three-step approach based on subset simulation, Journal of Engineering Mechanics 133 (4) (2007) 481–493. doi:10.1061/(ASCE)0733-9399(2007)133:4(481).

[210] J. Ching, Y.-H. Hsieh, Local estimation of failure probability function and its confidence interval with maximum entropy principle, Probabilistic Engineering Mechanics 22 (1) (2007) 39–49. doi:10.1016/j.probengmech.2006.05.002.

[211] E. T. Jaynes, Information theory and statistical mechanics, Physical Review 106 (4) (1957) 620–630. doi:10.1103/physrev.106.620.

[212] J. Ching, W.-C. Hsu, Approximate optimization of systems with high-dimensional uncertainties and multiple reliability constraints, Computer Methods in Applied Mechanics and Engineering 198 (1) (2008) 52–71. doi:10.1016/j.cma.2008.01.004.

[213] W.-C. Hsu, J. Ching, Evaluating small failure probabilities of multiple limit states by parallel subset simulation, Probabilistic Engineering Mechanics 25 (3) (2010) 291–304. doi:10.1016/j.probengmech.2010.01.003.

[214] N. M. Okasha, D. M. Frangopol, A. D. Orcesi, Automated finite element updating using strain data for the lifetime reliability assessment of bridges, Reliability Engineering & System Safety 99 (2012) 139–150. doi:10.1016/j.ress.2011.11.007.

[215] C. Papadimitriou, J. L. Beck, L. S. Katafygiotis, Updating robust reliability using structural test data, Probabilistic Engineering Mechanics 16 (2) (2001) 103–113. doi:10.1016/s0266-8920(00)00012-6.

[216] Z. Hu, B. Chen, W. Chen, D. Tan, D. Shen, Review of model-based and data-driven approaches for leak detection and location in water distribution systems, Water Supply 21 (7) (2021) 3282–3306. doi:10.2166/ws.2021.101.

[217] D. Kang, Real-time optimal control of water distribution systems, Procedia Engineering 70 (2014) 917–923. doi:10.1016/j.proeng.2014.02.102.

[218] D. G. Jamieson, U. Shamir, F. Martinez, M. Franchini, Conceptual design of a generic, real-time, near-optimal control system for water-distribution networks, Journal of Hydroinformatics 9 (1) (2007) 3–14. doi:10.2166/hydro.2006.013.

[219] S. Ereiz, I. Duvnjak, J. F. Jiménez-Alonso, Review of finite element model updating methods for structural applications, Structures 41 (2022) 684–723. doi:10.1016/j.istruc.2022.05.041.

[220] E. Kyriakides, M. Polycarpou (Eds.), Intelligent monitoring, control, and security of crit-

ical infrastructure systems, Springer-Verlag Berlin Heidelberg, 2015. doi:10.1007/978-3-662-44160-2.

[221] B. Goller, G. I. Schuëller, Investigation of model uncertainties in Bayesian structural model updating, Journal of Sound and Vibration 330 (25) (2011) 6122–6136. doi:10.1016/j.jsv.2011.07.036.

[222] S.-K. Au, F.-L. Zhang, Fundamental two-stage formulation for Bayesian system identification, Part I: General theory, Mechanical Systems and Signal Processing 66-67 (2016) 31–42. doi:10.1016/j.ymssp.2015.04.025.

[223] D. Malakoff, Bayes offers a 'new' way to make sense of numbers, Science 286 (5444) (1999) 1460–1464. doi:10.1126/science.286.5444.1460.

[224] R. Puust, Z. Kapelan, D. A. Savic, T. Koppel, A review of methods for leakage management in pipe networks, Urban Water Journal 7 (1) (2010) 25–45. doi:10.1080/15730621003610878.

[225] R. Li, H. Huang, K. Xin, T. Tao, A review of methods for burst/leakage detection and location in water distribution systems, Water Science and Technology: Water Supply 15 (3) (2015) 429–441. doi:10.2166/ws.2014.131.

[226] Y. Wu, S. Liu, A review of data-driven approaches for burst detection in water distribution systems, Urban Water Journal 14 (9) (2017) 972–983. doi:10.1080/1573062X.2017.1279191.

[227] L. Berardi, R. Ugarelli, J. Røstum, O. Giustolisi, Assessing mechanical vulnerability in water distribution networks under multiple failures, Water Resources Research 50 (3) (2014) 2586–2599. doi:10.1002/2013WR014770.

[228] A. O. Lambert, T. G. Brown, M. Takizawa, D. Weimer, A review of performance indicators for real losses from water supply systems, Journal of Water Supply: Research and Technology—AQUA 48 (6) (1999) 227–237. doi:10.2166/aqua.1999.0025.

[229] A. Kessler, A. Ostfeld, G. Sinai, Detecting accidental contaminations in municipal water networks, Journal of Water Resources Planning and Management 124 (4) (1998) 192–198. doi:10.1061/(asce)0733-9496(1998)124:4(192).

[230] R. Janke, M. E. Tryby, R. M. Clark, Protecting water supply critical infrastructure: An overview, in: Securing Water and Wastewater Systems, Springer International Publishing, 2013, pp. 29–85. doi:10.1007/978-3-319-01092-2_2.

[231] World Health Organization, Guidelines for drinking-water quality, 4th Edition (2017).

[232] D. B. Field, B. Ratcliffe, Location of leaks in pressurised pipelines using sulphur hexafluoride as a tracer, Tech. Rep. 80, Water Research Centre (1978).

[233] J. M. Muggleton, M. J. Brennan, R. J. Pinnington, Y. Gao, A novel sensor for measuring the acoustic pressure in buried plastic water pipes, Journal of Sound and Vibration 295 (3-5) (2006) 1085–1098. doi:10.1016/j.jsv.2006.01.032.

[234] S. Demirci, E. Yigit, I. H. Eskidemir, C. Ozdemir, Ground penetrating radar imaging of water leaks from buried pipes based on back-projection method, NDT & E International 47 (2012) 35–42. doi:10.1016/j.ndteint.2011.12.008.

[235] S. Sophocleous, D. Savić, Z. Kapelan, Leak localization in a real water distribution network based on search-space reduction, Journal of Water Resources Planning and Management 145 (7) (2019) 04019024. doi:10.1061/(asce)wr.1943-5452.0001079.

[236] K. B. Adedeji, Y. Hamam, B. T. Abe, A. M. Abu-Mahfouz, Towards achieving a reliable leakage detection and localization algorithm for application in water piping networks: An overview, IEEE Access 5 (2017) 20272–20285. doi:10.1109/access.2017.2752802.

[237] O. S. Adedoja, Y. Hamam, B. Khalaf, R. Sadiku, A state-of-the-art review of an optimal sensor placement for contaminant warning system in a water distribution network, Urban Water Journal 15 (10) (2018) 985–1000. doi:10.1080/1573062x.2019.1597378.

[238] A. E. De Sanctis, F. Shang, J. G. Uber, Real-time identification of possible contamination sources using network backtracking methods, Journal of Water Resources Planning and Management 136 (4) (2010) 444–453. doi:10.1061/(asce)wr.1943-5452.0000050.

[239] C. D. Laird, L. T. Biegler, B. G. van Bloemen Waanders, R. A. Bartlett, Contamination source determination for water networks, Journal of Water Resources Planning and Management 131 (2) (2005) 125–134. doi:10.1061/(asce)0733-9496(2005)131:2(125).

[240] A. Preis, A. Ostfeld, Genetic algorithm for contaminant source characterization using imperfect sensors, Civil Engineering and Environmental Systems 25 (1) (2008) 29–39. doi:10.1080/10286600701695471.

[241] J. Guan, M. M. Aral, M. L. Maslia, W. M. Grayman, Identification of contaminant sources in water distribution systems using simulation-optimization method: Case study, Journal of Water Resources Planning and Management 132 (4) (2006) 252–262. doi:10.1061/(ASCE)0733-9496(2006)132:4(252).

[242] A. Preis, A. Ostfeld, A contamination source identification model for water distribution system security, Engineering Optimization 39 (8) (2007) 941–947. doi:10.1080/03052150701540670.

[243] L. Liu, S. R. Ranjithan, G. Mahinthakumar, Contamination source identification in water distribution systems using an adaptive dynamic optimization procedure, Journal of Water Resources Planning and Management 137 (2) (2011) 183–192. doi:10.1061/(asce)wr.1943-5452.0000104.

[244] J. Kumar, E. D. Brill, G. Mahinthakumar, S. R. Ranjithan, Contaminant source characterization in water distribution systems using binary signals, Journal of Hydroinformatics 14 (3) (2012) 585–602. doi:10.2166/hydro.2012.073.

[245] Z. Poulakis, D. Valougeorgis, C. Papadimitriou, Leakage detection in water pipe networks using a bayesian probabilistic framework, Probabilistic Engineering Mechanics 18 (4) (2003) 315–327. doi:10.1016/S0266-8920(03)00045-6.

[246] O. Giustolisi, D. Laucelli, A. F. Colombo, Deterministic versus stochastic design of water distribution networks, Journal of Water Resources Planning and Management 135 (2) (2009) 117–127. doi:10.1061/(ASCE)0733-9496(2009)135:2(117).

[247] E. Ortega, A. Braunstein, A. Lage-Castellanos, Contamination source detection in water distribution networks using belief propagation, Stochastic Environmental Research and Risk Assessment 34 (3-4) (2020) 493–511. doi:10.1007/s00477-020-01788-y.

[248] N. Sankary, A. Ostfeld, Bayesian localization of water distribution system contamination intrusion events using inline mobile sensor data, Journal of Water Resources Planning and Management 145 (8) (2019) 04019029. doi:10.1061/(asce)wr.1943-5452.0001086.

[249] L. Perelman, A. Ostfeld, Bayesian networks for source intrusion detection, Journal of Water Resources Planning and Management 139 (4) (2013) 426–432. doi:10.1061/(asce)wr.1943-5452.0000288.

[250] W. J. Dawsey, B. S. Minsker, V. L. VanBlaricum, Bayesian belief networks to integrate monitoring evidence of water distribution system contamination, Journal of Water Resources Planning and Management 132 (4) (2006) 234–241. doi:10.1061/(asce)0733-9496(2006)132:4(234).

[251] H. Wang, K. W. Harrison, Bayesian update method for contaminant source characterization in water distribution systems, Journal of Water Resources Planning and Management 139 (1) (2013) 13–22. doi:10.1061/(ASCE)WR.1943-5452.0000221.

[252] H. Wang, K. W. Harrison, Bayesian approach to contaminant source characterization in water distribution systems: adaptive sampling framework, Stochastic Environmental Research and Risk Assessment 27 (8) (2013) 1921–1928. doi:10.1007/s00477-013-0727-9.

[253] H. Wang, K. W. Harrison, Improving efficiency of the Bayesian approach to water distribution contaminant source characterization with support vector regression, Journal of Water Resources Planning and Management 140 (1) (2014) 3–11. doi:10.1061/(asce)wr.1943-5452.0000323.

[254] D. J. Jerez, H. A. Jensen, M. Beer, M. Broggi, Contaminant source identification in water distribution networks: A Bayesian framework, Mechanical Systems and Signal Processing 159 (2021) 107834. doi:10.1016/j.ymssp.2021.107834.

[255] G. Tsampras, R. Sause, D. Zhang, R. B. Fleischman, J. I. Restrepo, D. Mar, J. Maffei, Development of deformable connection for earthquake-resistant buildings to reduce floor accelerations and force responses, Earthquake Engineering & Structural Dynamics 45 (9) (2016) 1473–1494. doi:10.1002/eqe.2718.

[256] G. Lomiento, N. Bonessio, G. Benzoni, Friction model for sliding bearings under seismic excitation, Journal of Earthquake Engineering 17 (8) (2013) 1162–1191. doi:10.1080/13632469.2013.814611.

[257] Y. Peng, T. Huang, Sliding implant-magnetic bearing for adaptive seismic mitigation of base-isolated structures, Structural Control and Health Monitoring 26 (10) (jul 2019). doi:10.1002/stc.2431.

[258] K. T. Nguyen, D. S. Kusanovic, D. Asimaki, Three-dimensional nonlinear soil-structure interaction for Rayleigh wave incidence in layered soils, Earthquake Engineering & Structural Dynamics (jun 2022). doi:10.1002/eqe.3700.

[259] Q. Huang, P. Gardoni, S. Hurlebaus, A probabilistic damage detection approach using vibration-based nondestructive testing, Structural Safety 38 (2012) 11–21. doi:10.1016/j.strusafe.2012.01.004.

[260] Q. Huang, P. Gardoni, S. Hurlebaus, Adaptive reliability analysis of reinforced concrete bridges subject to seismic loading using nondestructive testing, ASCE-ASME Journal of Risk and Uncertainty in Engineering Systems, Part A: Civil Engineering 1 (4) (2015) 04015014. doi:10.1061/ajrua6.0000835.

[261] H. Xu, P. Gardoni, Conditional formulation for the calibration of multi-level random fields with incomplete data, Reliability Engineering & System Safety 204 (2020) 107121. doi:10.1016/j.ress.2020.107121.

[262] Z. Pang, X. Si, C. Hu, D. Du, H. Pei, A Bayesian inference for remaining useful life estimation by fusing accelerated degradation data and condition monitoring data, Reliability Engineering & System Safety 208 (2021) 107341. doi:10.1016/j.ress.2020.107341.

[263] S. H. Cheung, J. L. Beck, Bayesian model updating using hybrid Monte Carlo simulation with application to structural dynamic models with many uncertain parameters, Journal of Engineering Mechanics 135 (4) (2009) 243–255. doi:10.1061/(asce)0733-9399(2009)135:4(243).

[264] T. A. Catanach, J. L. Beck, Bayesian system identification using auxiliary stochastic dynamical systems, International Journal of Non-Linear Mechanics 94 (2017) 72–83. doi:10.1016/j.ijnonlinmec.2017.03.012.

[265] R. Neal, MCMC using Hamiltonian dynamics, in: S. Brooks, A. Gelman, G. Jones, X.-L. Meng (Eds.), Handbook of Markov chain Monte Carlo, Chapman & Hall/CRC Handbooks of Modern Statistical Methods, Chapman and Hall/CRC, 2011, pp. 1–46. doi:10.1201/b10905-6.

[266] M. Betancourt, S. Byrne, S. Livingstone, M. Girolami, The geometric foundations of Hamiltonian Monte Carlo, Bernoulli 23 (4A) (nov 2017). doi:10.3150/16-bej810.

[267] D. J. Jerez, H. A. Jensen, M. Beer, An effective implementation of reliability methods for Bayesian model updating of structural dynamic models with multiple uncertain parameters, Reliability Engineering & System Safety 225 (2022) 108634. doi:10.1016/j.ress.2022.108634.

[268] J.-H. Weng, C.-H. Loh, J. N. Yang, Experimental study of damage detection by data-driven subspace identification and finite-element model updating, Journal of Structural Engineering 135 (12) (2009) 1533–1544. doi:10.1061/(asce)st.1943-541x.0000079.

[269] E. Ghorbani, Y.-J. Cha, An iterated cubature unscented Kalman filter for large-DoF systems identification with noisy data, Journal of Sound and Vibration 420 (2018) 21–34. doi:10.1016/j.jsv.2018.01.035.

[270] H. A. Jensen, C. Vergara, C. Papadimitriou, E. Millas, The use of updated robust reliability measures in stochastic dynamical systems, Computer Methods in Applied Mechanics and Engineering 267 (Supplement C) (2013) 293–317. doi:10.1016/j.cma.2013.08.015.

[271] J. L. Beck, K.-V. Yuen, Model selection using response measurements: Bayesian probabilistic approach, Journal of Engineering Mechanics 130 (2) (2004) 192–203. doi:10.1061/(asce)0733-9399(2004)130:2(192).

[272] J. A. Hoeting, D. Madigan, A. E. Raftery, C. T. Volinsky, Bayesian model averaging: A tutorial, Statistical Science 14 (4) (1999) 382–401.

[273] X. Guan, J. He, R. Jha, Y. Liu, An efficient analytical Bayesian method for reliability and system response updating based on Laplace and inverse first-order reliability computations, Reliability Engineering & System Safety 97 (1) (2012) 1–13. doi:10.1016/j.ress.2011.09.008.

[274] G. C. Ballesteros, P. Angelikopoulos, C. Papadimitriou, P. Koumoutsakos, Bayesian hierarchical models for uncertainty quantification in structural dynamics, in: Vulnerability, Uncertainty, and Risk, American Society of Civil Engineers, 2014, pp. 1615–1624. doi:10.1061/9780784413609.162.

[275] R. Bellman, K. J. Åström, On structural identifiability, Mathematical Biosciences 7 (3-4) (1970) 329–339. doi:10.1016/0025-5564(70)90132-x.

[276] B. D. Flury, Acceptance–rejection sampling made easy, SIAM Review 32 (3) (1990) 474–476. doi:10.1137/1032082.

[277] L. Tierney, Markov chains for exploring posterior distributions, The Annals of Statistics 22 (4) (dec 1994). doi:10.1214/aos/1176325750.

[278] P. L. Green, E. J. Cross, K. Worden, Bayesian system identification of dynamical systems using highly informative training data, Mechanical Systems and Signal Processing 56-57 (2015) 109–122. doi:10.1016/j.ymssp.2014.10.003.

[279] S. Biswal, A. Ramaswamy, Finite element model updating of concrete structures based on imprecise probability, Mechanical Systems and Signal Processing 94 (2017) 165–179. doi:10.1016/j.ymssp.2017.02.042.

[280] H. Jalali, H. H. Khodaparast, H. Madinei, M. I. Friswell, Stochastic modelling and updating of a joint contact interface, Mechanical Systems and Signal Processing 129 (2019) 645–658. doi:10.1016/j.ymssp.2019.04.003.

[281] T. J. Rogers, K. Worden, E. J. Cross, On the application of Gaussian process latent force models for joint input-state-parameter estimation: With a view to Bayesian operational identification, Mechanical Systems and Signal Processing 140 (2020) 106580. doi:10.1016/j.ymssp.2019.106580.

[282] J. L. Beck, S.-K. Au, Bayesian updating of structural models and reliability using Markov chain Monte Carlo simulation, Journal of Engineering Mechanics 128 (4) (2002) 380–391. doi:10.1061/(asce)0733-9399(2002)128:4(380).

[283] S. He, C.-T. Ng, Guided wave-based identification of multiple cracks in beams using a Bayesian approach, Mechanical Systems and Signal Processing 84 (2017) 324–345. doi:10.1016/j.ymssp.2016.07.013.

[284] W.-H. Zhou, F. Tan, K.-V. Yuen, Model updating and uncertainty analysis for creep behavior of soft soil, Computers and Geotechnics 100 (2018) 135–143. doi:10.1016/j.compgeo.2018.04.006.

[285] O. Sedehi, C. Papadimitriou, L. S. Katafygiotis, Probabilistic hierarchical Bayesian framework for time-domain model updating and robust predictions, Mechanical Systems and Signal Processing 123 (2019) 648–673. doi:10.1016/j.ymssp.2018.09.041.

[286] P. Angelikopoulos, C. Papadimitriou, P. Koumoutsakos, Bayesian uncertainty quantification and propagation in molecular dynamics simulations: A high performance computing framework, The Journal of Chemical Physics 137 (14) (2012) 144103. doi:10.1063/1.4757266.

[287] P. Angelikopoulos, C. Papadimitriou, P. Koumoutsakos, X-TMCMC: Adaptive kriging for Bayesian inverse modeling, Computer Methods in Applied Mechanics and Engineering 289 (2015) 409–428. doi:10.1016/j.cma.2015.01.015.

[288] H. A. Jensen, C. Esse, V. Araya, C. Papadimitriou, Implementation of an adaptive metamodel for Bayesian finite element model updating in time domain, Reliability Engineering & System Safety 160 (2017) 174–190. doi:10.1016/j.ress.2016.12.005.

[289] S. Duane, A. D. Kennedy, B. J. Pendleton, D. Roweth, Hybrid Monte Carlo, Physics Letters B 195 (2) (1987) 216–222. doi:10.1016/0370-2693(87)91197-x.

[290] V. I. Arnold, Mathematical methods of classical mechanics, Springer New York, 1978. doi:10.1007/978-1-4757-1693-1.

[291] W. Chen, Z. Wang, M. Broccardo, J. Song, Riemannian manifold Hamiltonian Monte Carlo based subset simulation for reliability analysis in non-Gaussian space, Structural Safety 94 (2022) 102134. doi:10.1016/j.strusafe.2021.102134.

[292] T. S. Kleppe, Modified Cholesky Riemann manifold Hamiltonian Monte Carlo: exploiting sparsity for fast sampling of high-dimensional targets, Statistics and Computing 28 (4) (2017) 795–817. doi:10.1007/s11222-017-9763-5.

[293] M. Girolami, B. Calderhead, Riemann manifold Langevin and Hamiltonian Monte Carlo

methods, Journal of the Royal Statistical Society: Series B (Statistical Methodology) 73 (2) (2011) 123–214. doi:10.1111/j.1467-9868.2010.00765.x.

[294] V. Černý, Thermodynamical approach to the traveling salesman problem: An efficient simulation algorithm, Journal of Optimization Theory and Applications 45 (1) (1985) 41–51. doi:10.1007/bf00940812.

[295] L. Verlet, Computer "experiments" on classical fluids. I. Thermodynamical properties of Lennard-Jones molecules, Physical Review 159 (1) (1967) 98–103. doi:10.1103/physrev.159.98.

[296] I. Boulkaibet, L. Mthembu, T. Marwala, M. I. Friswell, S. Adhikari, Finite element model updating using the shadow hybrid Monte Carlo technique, Mechanical Systems and Signal Processing 52-53 (2015) 115–132. doi:10.1016/j.ymssp.2014.06.005.

[297] Z. Wang, M. Broccardo, J. Song, Hamiltonian Monte Carlo methods for subset simulation in reliability analysis, Structural Safety 76 (2019) 51–67. doi:10.1016/j.strusafe.2018.05.005.

[298] D. Straub, I. Papaioannou, Bayesian updating with structural reliability methods, Journal of Engineering Mechanics 141 (3) (2015) 04014134. doi:10.1061/(ASCE)EM.1943-7889.0000839.

[299] S.-H. Jiang, I. Papaioannou, D. Straub, Bayesian updating of slope reliability in spatially variable soils with in-situ measurements, Engineering Geology 239 (2018) 310–320. doi:10.1016/j.enggeo.2018.03.021.

[300] P. Liu, S. Huang, M. Song, W. Yang, Bayesian model updating of a twin-tower masonry structure through subset simulation optimization using ambient vibration data, Journal of Civil Structural Health Monitoring 11 (1) (2020) 129–148. doi:10.1007/s13349-020-00443-y.

[301] H.-M. Tian, D.-Q. Li, Z.-J. Cao, D.-S. Xu, X.-Y. Fu, Reliability-based monitoring sensitivity analysis for reinforced slopes using BUS and subset simulation methods, Engineering Geology 293 (2021) 106331. doi:10.1016/j.enggeo.2021.106331.

[302] F. Uribe, I. Papaioannou, J. Latz, W. Betz, E. Ullmann, D. Straub, Bayesian inference with subset simulation in varying dimensions applied to the Karhunen–Loève expansion, International Journal for Numerical Methods in Engineering 122 (18) (2021) 5100–5127. doi:10.1002/nme.6758.

[303] W. Betz, J. L. Beck, I. Papaioannou, D. Straub, Bayesian inference with reliability methods without knowing the maximum of the likelihood function, Probabilistic Engineering Mechanics 53 (2018) 14–22. doi:10.1016/j.probengmech.2018.03.004.

[304] F. A. DiazDelaO, A. Garbuno-Inigo, S.-K. Au, I. Yoshida, Bayesian updating and model class selection with Subset Simulation, Computer Methods in Applied Mechanics and Engineering 317 (2017) 1102–1121. doi:10.1016/j.cma.2017.01.006.

[305] W. Betz, I. Papaioannou, J. L. Beck, D. Straub, Bayesian inference with Subset Simulation:

Strategies and improvements, Computer Methods in Applied Mechanics and Engineering 331 (2018) 72–93. doi:10.1016/j.cma.2017.11.021.

[306] J. S. Arora, Introduction to optimum design, Elsevier, 2017. doi:10.1016/c2013-0-15344-5.

[307] J. H. Holland, Adaptation in natural and artificial systems: An introductory analysis with applications to biology, control and artificial intelligence, MIT Press, Cambridge, MA, USA, 1992.

[308] J. Kennedy, R. Eberhart, Particle swarm optimization, in: Proceedings of ICNN'95 - International Conference on Neural Networks, Vol. 4, 1995, pp. 1942–1948. doi:10.1109/ICNN.1995.488968.

[309] M. Dorigo, V. Maniezzo, A. Colorni, Ant system: optimization by a colony of cooperating agents, IEEE Transactions on Systems, Man, and Cybernetics, Part B (Cybernetics) 26 (1) (1996) 29–41. doi:10.1109/3477.484436.

[310] F. Liang, Annealing evolutionary stochastic approximation monte carlo for global optimization, Statistics and Computing 21 (3) (2011) 375–393. doi:10.1007/s11222-010-9176-1.

[311] C. A. C. Coello, E. M. Montes, Constraint-handling in genetic algorithms through the use of dominance-based tournament selection, Advanced Engineering Informatics 16 (3) (2002) 193–203. doi:10.1016/s1474-0346(02)00011-3.

[312] Y. Dong, J. Tang, B. Xu, D. Wang, An application of swarm optimization to nonlinear programming, Computers & Mathematics with Applications 49 (11-12) (2005) 1655–1668. doi:10.1016/j.camwa.2005.02.006.

[313] E. Mezura-Montes, C. A. C. Coello, Use of multiobjective optimization concepts to handle constraints in Genetic Algorithms, in: A. Abraham, L. Jain, R. Goldberg (Eds.), Advanced Information and Knowledge Processing, Springer-Verlag, 2005, pp. 229–254. doi:10.1007/1-84628-137-7_10.

[314] Z. Michalewicz, M. Schoenauer, Evolutionary algorithms for constrained parameter optimization problems, Evolutionary Computation 4 (1) (1996) 1–32. doi:10.1162/evco.1996.4.1.1.

[315] A.-R. Hedar, M. Fukushima, Derivative-free filter simulated annealing method for constrained continuous global optimization, Journal of Global Optimization 35 (4) (2006) 521–549. doi:10.1007/s10898-005-3693-z.

[316] L. Li, Z. Huang, F. Liu, Q. Wu, A heuristic particle swarm optimizer for optimization of pin connected structures, Computers & Structures 85 (7-8) (2007) 340–349. doi:10.1016/j.compstruc.2006.11.020.

[317] H.-S. Li, S.-K. Au, Design optimization using Subset Simulation algorithm, Structural Safety 32 (6) (2010) 384–392. doi:10.1016/j.strusafe.2010.03.001.

[318] A. Kong, J. S. Liu, W. H. Wong, Sequential imputations and Bayesian missing data problems, Journal of the American Statistical Association 89 (425) (1994) 278–288. doi:10.2307/2291224.

[319] J. S. Liu, Metropolized independent sampling with comparisons to rejection sampling and importance sampling, Statistics and Computing 6 (2) (1996) 113–119. doi:10.1007/bf00162521.

[320] M. Pellissetti, Parallel processing in structural reliability, Structural Engineering and Mechanics 32 (1) (2009) 95–126. doi:10.12989/sem.2009.32.1.095.

[321] G. P. Mavroeidis, A mathematical representation of near-fault ground motions, Bulletin of the Seismological Society of America 93 (3) (2003) 1099–1131. doi:10.1785/0120020100.

[322] Q. He, L. Wang, An effective co-evolutionary particle swarm optimization for constrained engineering design problems, Engineering Applications of Artificial Intelligence 20 (1) (2007) 89–99. doi:10.1016/j.engappai.2006.03.003.

[323] Q. He, L. Wang, A hybrid particle swarm optimization with a feasibility-based rule for constrained optimization, Applied Mathematics and Computation 186 (2) (2007) 1407–1422. doi:10.1016/j.amc.2006.07.134.

[324] C. A. Coello Coello, Use of a self-adaptive penalty approach for engineering optimization problems, Computers in Industry 41 (2) (2000) 113–127. doi:10.1016/s0166-3615(99)00046-9.

[325] K. S. Lee, Z. W. Geem, A new structural optimization method based on the harmony search algorithm, Computers & Structures 82 (9-10) (2004) 781–798. doi:10.1016/j.compstruc.2004.01.002.

[326] H. J. Pradlwarter, G. I. Schuëller, Equivalent linearization—a suitable tool for analyzing MDOF-systems, Probabilistic Engineering Mechanics 8 (2) (1993) 115–126. doi:10.1016/0266-8920(93)90005-g.

[327] T. J. Santner, B. J. Williams, W. I. Notz, The design and analysis of computer experiments, Springer-Verlag GmbH, 2018. doi:10.1007/978-1-4757-3799-8.

[328] H. B. Nielsen, S. N. Lophaven, J. Søndergaard, DACE - A Matlab kriging toolbox, Tech. rep., Technical University of Denmark (DTU) (2002).

[329] M.-W. Huang, J. S. Arora, Optimal design with discrete variables: Some numerical experiments, International Journal for Numerical Methods in Engineering 40 (1) (1997) 165–188. doi:10.1002/(SICI)1097-0207(19970115)40:1<165::AID-NME60>3.0.CO;2-I.

[330] A. D. Belegundu, T. R. Chandrupatla, Optimization concepts and applications in engineering, Cambridge University Press, 2011. doi:10.1017/cbo9780511975905.

[331] H.-G. Beyer, The Theory of Evolution Strategies, Springer Berlin Heidelberg, Berlin, Heidelberg, 2001.

[332] W. Banzhaf, P. Nordin, R. E. Keller, Genetic Programming: An Introduction, Morgan Kaufmann Publ. Inc., 1997.

[333] E. Rashedi, H. Nezamabadi-pour, S. Saryazdi, GSA: A Gravitational Search Algorithm, Information Sciences 179 (13) (2009) 2232–2248. doi:10.1016/j.ins.2009.03.004.

[334] A. Kaveh, M. Khayatazad, A new meta-heuristic method: Ray Optimization, Computers & Structures 112-113 (2012) 283–294. doi:10.1016/j.compstruc.2012.09.003.

[335] Z. W. Geem, J. H. Kim, G. V. Loganathan, A new heuristic optimization algorithm: Harmony search, SIMULATION 76 (2) (2001) 60–68. doi:10.1177/003754970107600201.

[336] D. Karaboga, An idea based on honey bee swarm for numerical optimization, Tech. Rep. Technical report TR06, Computer Engineering Department, Erciyes University, Turkey (2005).

[337] J. Golinski, An adaptive optimization system applied to machine synthesis, Mechanism and Machine Theory 8 (4) (1973) 419–436. doi:10.1016/0094-114x(73)90018-9.

[338] T. Ray, K. M. Liew, Society and civilization: an optimization algorithm based on the simulation of social behavior, IEEE Transactions on Evolutionary Computation 7 (4) (2003) 386–396. doi:10.1109/tevc.2003.814902.

[339] H. Liu, Z. Cai, Y. Wang, Hybridizing particle swarm optimization with differential evolution for constrained numerical and engineering optimization, Applied Soft Computing 10 (2) (2010) 629–640. doi:10.1016/j.asoc.2009.08.031.

[340] L. Wang, L. po Li, An effective differential evolution with level comparison for constrained engineering design, Structural and Multidisciplinary Optimization 41 (6) (2009) 947–963. doi:10.1007/s00158-009-0454-5.

[341] A. Sadollah, A. Bahreininejad, H. Eskandar, M. Hamdi, Mine blast algorithm: A new population based algorithm for solving constrained engineering optimization problems, Applied Soft Computing 13 (5) (2013) 2592–2612. doi:10.1016/j.asoc.2012.11.026.

[342] A. M. Committee, AISC Manual of Steel Construction, American Institute of Steel Construction (2001).

[343] J. G. Anderson, S. E. Hough, A model for the shape of the Fourier amplitude spectrum of acceleration at high frequencies, Bulletin of the Seismological Society of America 74 (5) (1984) 1969–1993. doi:10.1785/BSSA0740051969.

[344] H. J. Pradlwarter, G. I. Schuëller, U. Dorka, Reliability of MDOF-systems with hysteretic devices, Engineering Structures 20 (8) (1998) 685–691. doi:10.1016/s0141-0296(97)00105-3.

[345] X. Yuan, S. Liu, M. A. Valdebenito, M. G. R. Faes, D. J. Jerez, H. A. Jensen, M. Beer, Decoupled reliability-based optimization using Markov chain Monte Carlo in augmented space, Advances in Engineering Software 157-158 (2021) 103020. doi:10.1016/j.advengsoft.2021.103020.

[346] S. Bobby, A. Suksuwan, S. M. J. Spence, A. Kareem, Reliability-based topology optimization of uncertain building systems subject to stochastic excitation, Structural Safety 66 (2017) 1–16. doi:10.1016/j.strusafe.2017.01.005.

[347] I. Petromichelakis, A. F. Psaros, I. A. Kougioumtzoglou, Stochastic response analysis and reliability-based design optimization of nonlinear electromechanical energy harvesters with fractional derivative elements, ASCE-ASME J Risk and Uncert in Engrg Sys Part B Mech Engrg 7 (1) (jan 2021).

[348] O. Kanjilal, I. Papaioannou, D. Straub, Cross entropy-based importance sampling for first-passage probability estimation of randomly excited linear structures with parameter uncertainty, Structural Safety 91 (2021) 102090. doi:10.1016/j.strusafe.2021.102090.

[349] G. Mosqueda, A. S. Whittaker, G. L. Fenves, Characterization and modeling of friction pendulum bearings subjected to multiple components of excitation, Journal of Structural Engineering 130 (3) (2004) 433–442. doi:10.1061/(asce)0733-9445(2004)130:3(433).

[350] Y. Ding, Y. Peng, J. Li, A stochastic semi-physical model of seismic ground motions in time domain, Journal of Earthquake and Tsunami 12 (03) (2018) 1850006. doi:10.1142/s1793431118500069.

[351] B. A. Benowitz, G. Deodatis, Simulation of wind velocities on long span structures: A novel stochastic wave based model, Journal of Wind Engineering and Industrial Aerodynamics 147 (2015) 154–163. doi:10.1016/j.jweia.2015.10.004.

[352] A. G. Carlon, R. H. Lopez, L. F. R. Espath, L. F. F. Miguel, A. T. Beck, A stochastic gradient approach for the reliability maximization of passively controlled structures, Engineering Structures 186 (2019) 1–12. doi:10.1016/j.engstruct.2019.01.121.

[353] M. F. Huang, C. M. Chan, W. J. Lou, Optimal performance-based design of wind sensitive tall buildings considering uncertainties, Computers & Structures 98-99 (2012) 7–16. doi:10.1016/j.compstruc.2012.01.012.

[354] D. Honfi, A. Mårtensson, S. Thelandersson, Reliability of beams according to Eurocodes in serviceability limit state, Engineering Structures 35 (2012) 48–54. doi:10.1016/j.engstruct.2011.11.003.

[355] M. A. Valdebenito, P. Wei, J. Song, M. Beer, M. Broggi, Failure probability estimation of a class of series systems by multidomain Line Sampling, Reliability Engineering & System Safety 213 (2021) 107673. doi:10.1016/j.ress.2021.107673.

[356] J. Herskovits, G. Santos, On the computer implementation of feasible direction interior point algorithms for nonlinear optimization, Structural optimization 14 (2) (1997) 165–172. doi:10.1007/BF01812519.

[357] G. N. Vanderplaats, N. Yoshida, Efficient calculation of optimum design sensitivity, AIAA Journal 23 (11) (1985) 1798–1803. doi:10.2514/3.9168.

[358] N. Hoang, Y. Fujino, P. Warnitchai, Optimal tuned mass damper for seismic applications and practical design formulas, Engineering Structures 30 (3) (2008) 707–715. doi:10.1016/j.engstruct.2007.05.007.

[359] R. O. Ruiz, D. Lopez-Garcia, A. A. Taflanidis, Modeling and experimental validation of a new type of tuned liquid damper, Acta Mechanica 227 (11) (2016) 3275–3294. doi:10.1007/s00707-015-1536-7.

[360] F. Gomez, B. F. Spencer, Topology optimization framework for structures subjected to stationary stochastic dynamic loads, Structural and Multidisciplinary Optimization 59 (3) (2018) 813–833. doi:10.1007/s00158-018-2103-3.

[361] C. Su, B. Li, T. Chen, X. Dai, Stochastic optimal design of nonlinear viscous dampers for large-scale structures subjected to non-stationary seismic excitations based on dimension-reduced explicit method, Engineering Structures 175 (2018) 217–230. doi:10.1016/j.engstruct.2018.08.028.

[362] A. Chopra, Dynamics of structures: Theory and applications to earthquake engineering, Pearson, Hoboken, NJ, 2017.

[363] W. Gautschi, Numerical analysis, Birkhäuser, Boston, 2012.

[364] O. Ditlevsen, R. Olesen, G. Mohr, Solution of a class of load combination problems by directional simulation, Structural Safety 4 (2) (1986) 95–109. doi:10.1016/0167-4730(86)90025-1.

[365] P. Bjerager, Probability integration by Directional Simulation, Journal of Engineering Mechanics 114 (8) (1988) 1285–1302. doi:10.1061/(asce)0733-9399(1988)114:8(1285).

[366] J. Nie, B. R. Ellingwood, Directional methods for structural reliability analysis, Structural Safety 22 (3) (2000) 233–249. doi:10.1016/s0167-4730(00)00014-x.

[367] I.-W. Lee, G.-H. Jung, An efficient algebraic method for the computation of natural frequency and mode shape sensitivities—Part I Distinct natural frequencies, Computers & Structures 62 (3) (1997) 429–435. doi:10.1016/s0045-7949(96)00206-4.

[368] G. N. Vanderplaats, An efficient feasible directions algorithm for design synthesis, AIAA Journal 22 (11) (1984) 1633–1640. doi:10.2514/3.8829.

[369] G. Vanderplaats, Numerical optimization techniques for engineering design: with applications, McGraw-Hill, New York, 1984.

[370] A. Zerva, Spatial variation of seismic ground motions: modeling and engineering applications, CRC Press, Boca Raton, FL, 2009.

[371] P. A. Hidalgo, C. A. Ledezma, R. M. Jordan, Seismic behavior of squat reinforced concrete shear walls, Earthquake Spectra 18 (2) (2002) 287–308. doi:10.1193/1.1490353.

[372] R. M. Lin, J. E. Mottershead, T. Y. Ng, A state-of-the-art review on theory and engineer-

ing applications of eigenvalue and eigenvector derivatives, Mechanical Systems and Signal Processing 138 (2020) 106536. doi:10.1016/j.ymssp.2019.106536.

[373] E. Z. Berglund, J. E. Pesantez, A. Rasekh, M. E. Shafiee, L. Sela, T. Haxton, Review of modeling methodologies for managing water distribution security, Journal of Water Resources Planning and Management 146 (8) (2020) 03120001. doi:10.1061/(asce)wr.1943-5452.0001265.

[374] D. M. Costa, L. F. Melo, F. G. Martins, Localization of contamination sources in drinking water distribution systems: A method based on successive positive readings of sensors, Water Resources Management 27 (13) (2013) 4623–4635. doi:10.1007/s11269-013-0431-z.

[375] H. Shen, E. McBean, False negative/positive issues in contaminant source identification for water-distribution systems, Journal of Water Resources Planning and Management 138 (3) (2012) 230–236. doi:10.1061/(asce)wr.1943-5452.0000162.

[376] L. Grbčić, I. Lučin, L. Kranjčević, S. Družeta, A Machine Learning-based algorithm for water network contamination source localization, Sensors 20 (9) (2020) 2613. doi:10.3390/s20092613.

[377] Y. Bao, L. W. Mays, Model for water distribution system reliability, Journal of Hydraulic Engineering 116 (9) (1990) 1119–1137. doi:10.1061/(ASCE)0733-9429(1990)116:9(1119).

[378] CNIP'06, Proceedings of the International Workshop on Complex Network and Infrastructure Protection.

[379] L. Rossman, H. Woo, M. Tryby, F. Shang, R. Janke, T. Haxton, EPANET 2.2 User Manual, U.S. Environmental Protection Agency, Washington, DC (2020).

[380] D. G. Eliades, M. Kyriakou, S. Vrachimis, M. M. Polycarpou, EPANET-MATLAB Toolkit: An open-source software for interfacing EPANET with MATLAB, in: Proceedings of Critical Information Infrastructures Security: Computing & Control for the Water Industry (CCWI), Amsterdam, The Netherlands, 2017. doi:10.5281/ZENODO.831493.

[381] L. Liu, A. Sankarasubramanian, S. R. Ranjithan, Logistic regression analysis to estimate contaminant sources in water distribution systems, Journal of Hydroinformatics 13 (3) (2010) 545–557. doi:10.2166/hydro.2010.106.

[382] C. Di Cristo, A. Leopardi, Pollution source identification of accidental contamination in water distribution networks, Journal of Water Resources Planning and Management 134 (2) (2008) 197–202. doi:10.1061/(asce)0733-9496(2008)134:2(197).

[383] D. Goldberg, Genetic algorithms in search, optimization, and machine learning, Addison-Wesley Publishing Company, Reading, Mass, 1989.

[384] L. S. Katafygiotis, O. Sedehi, F. R. Rofooei, Bayesian time-domain model updating considering correlation of prediction errors, in: 12th International Conference on Structural Safety and Reliability, Vienna, Austria, 2017, pp. 2500–2509.

[385] J. Berry, E. Boman, L. A. Riesen, W. E. Hart, C. A. Phillips, J.-P. Watson, User's Manual: TEVA-SPOT toolkit 2.4, U.S. Environmental Protection Agency (sep 2012).

[386] H. Qin, M. G. Stewart, Construction defects and wind fragility assessment for metal roof failure: A Bayesian approach, Reliability Engineering & System Safety 197 (2020) 106777. doi:10.1016/j.ress.2019.106777.

[387] A. H. de Andrade Melani, M. A. de Carvalho Michalski, R. F. da Silva, G. F. M. de Souza, A framework to automate fault detection and diagnosis based on moving window principal component analysis and Bayesian network, Reliability Engineering & System Safety 215 (2021) 107837. doi:10.1016/j.ress.2021.107837.

[388] M. A. Vega, Z. Hu, T. B. Fillmore, M. D. Smith, M. D. Todd, A novel framework for integration of abstracted inspection data and structural health monitoring for damage prognosis of miter gates, Reliability Engineering & System Safety 211 (2021) 107561. doi:10.1016/j.ress.2021.107561.

[389] J. Ching, M. Muto, J. L. Beck, Structural model updating and health monitoring with incomplete modal data using Gibbs sampler, Computer-Aided Civil and Infrastructure Engineering 21 (4) (2006) 242–257. doi:10.1111/j.1467-8667.2006.00432.x.

[390] R. Astroza, N. Barrientos, Y. Li, E. I. S. Flores, Z. Liu, Bayesian updating of complex nonlinear FE models with high-dimensional parameter space using heterogeneous measurements and a batch-recursive approach, Engineering Structures 201 (2019) 109724. doi:10.1016/j.engstruct.2019.109724.

[391] P.-L. Liu, A. D. Kiureghian, Multivariate distribution models with prescribed marginals and covariances, Probabilistic Engineering Mechanics 1 (2) (1986) 105–112. doi:10.1016/0266-8920(86)90033-0.

[392] K. M. Zuev, J. L. Beck, S.-K. Au, L. S. Katafygiotis, Bayesian post-processor and other enhancements of Subset Simulation for estimating failure probabilities in high dimensions, Computers & Structures 92 (2012) 283–296. doi:10.1016/j.compstruc.2011.10.017.

[393] V. Papadopoulos, D. G. Giovanis, N. D. Lagaros, M. Papadrakakis, Accelerated subset simulation with neural networks for reliability analysis, Computer Methods in Applied Mechanics and Engineering 223-224 (2012) 70–80. doi:10.1016/j.cma.2012.02.013.

[394] J.-M. Bourinet, F. Deheeger, M. Lemaire, Assessing small failure probabilities by combined subset simulation and Support Vector Machines, Structural Safety 33 (6) (2011) 343–353. doi:10.1016/j.strusafe.2011.06.001.

[395] Z. Wang, A. Shafieezadeh, Highly efficient Bayesian updating using metamodels: An adaptive Kriging-based approach, Structural Safety 84 (2020) 101915. doi:10.1016/j.strusafe.2019.101915.

[396] M. Kitahara, S. Bi, M. Broggi, M. Beer, Bayesian model updating in time domain with metamodel-based reliability method, ASCE-ASME Journal of Risk and Uncertainty in En-

gineering Systems, Part A: Civil Engineering 7 (3) (2021) 04021030. doi:10.1061/ajrua6.0001149.

[397] H. A. Jensen, V. A. Araya, A. D. Muñoz, M. A. Valdebenito, A physical domain-based substructuring as a framework for dynamic modeling and reanalysis of systems, Computer Methods in Applied Mechanics and Engineering 326 (2017) 656–678. doi:10.1016/j.cma.2017.08.044.

[398] H. A. Jensen, F. Mayorga, M. A. Valdebenito, On the reliability of structures equipped with a class of friction-based devices under stochastic excitation, Computer Methods in Applied Mechanics and Engineering 364 (2020) 112965. doi:10.1016/j.cma.2020.112965.

[399] C. S. Tsai, Finite element formulations for friction pendulum seismic isolation bearings, International Journal for Numerical Methods in Engineering 40 (1) (1997) 29–49. doi:10.1002/(sici)1097-0207(19970115)40:1<29::aid-nme47>3.0.co;2-a.

[400] M. Pastor, M. Binda, T. Harčarik, Modal Assurance Criterion, Procedia Engineering 48 (2012) 543–548. doi:10.1016/j.proeng.2012.09.551.